

Selective Interference Cancellation and Frame Synchronization for Packet Radio Communications

M. Mostofa. K. Howlader

Dissertation submitted to the Faculty of the
Virginia Polytechnic Institute and State University
in partial fulfillment of the requirements for the degree of

Doctor of Philosophy
in
Electrical Engineering

Brian D. Woerner, Chair
Jeffrey H. Reed
William H. Tranter
Ira Jacobs
William R. Saunders

July 7, 2000
Blacksburg, Virginia

Keywords: Interference Cancellation, Packet Radio, Frame Synchronization
Copyright 1999, M. Mostofa. K. Howlader

Selective Interference Cancellation and Frame Synchronization for Packet Radio Communications

M. Mostofa. K. Howlader

(ABSTRACT)

This research investigates the application of multiuser interference suppression to direct-sequence code-division multiple-access (DS-CDMA) for peer-to-peer packet radio networks. The emphasis of this work is to develop and validate efficient interference suppression techniques through selective cancellation of interference; next, the combination of interference suppression with error correction coding is studied. A decoder-assisted frame synchronization technique is proposed for future packet radio system.

The performance of DS-CDMA in packet radio networks suffers from the near-far problem. This near-far problem can be alleviated by using either a multiuser receiver or a single-user adaptive receiver along with centralized or distributed power control. The first part of this dissertation compares the use of these receivers in a peer-to-peer environment. Next, we investigate how interference cancellation can be combined with forward error correction coding for throughput enhancement of the system. Although receivers using interference suppression are simple in structure, the performance degrades due to the lack of exact knowledge of the interfering signal in cancellation and also due to biased decision statistics for the parallel cancellation case. We consider a system that employs both partial parallel interference cancellation and convolutional coding. Information is shared between the operations of interference cancellation and decoding in an iterative manner, using log-likelihood ratios of the estimated coded symbols. We investigate the performance of this system for both synchronous and asynchronous CDMA systems, and for both equal and unequal signal powers.

Finally, a new code-assisted frame synchronization scheme, which uses the soft-information of the decoder, is proposed and evaluated. The sync bits are placed in the mid-amble, and encoded as a part of the data sequence using the error correction encoder to resolve time ambiguities. This technique is applied for turbo decoder-assisted frame synchronization. The performance improvement of these proposed techniques over conventional synchronization techniques is explored via simulation.

Acknowledgments

I want to thank my advisor, Dr. Brian Woerner for his guidance, encouragement and support. I am forever in debt for the profound education he contributed; it has been an honor and a pleasure to studied with him these last three years. I also thank the other members of my committee for their time and valuable comments. I am grateful to the MPRG faculty as well, for their inspiration. Next, I would like to thank the students and staff at MPRG. One of the greatest benefits of being involved with MPRG is the quality of students and level of student interaction. Because I have worked in the company of so many bright students at MPRG, it is impossible to name them all. However, I would like to give special thanks to Neiyer Correal and Matt Valenti; I learned a lot from informal discussions with them. I would also like to thank Rennie Givens, Hilda Reynolds and Shelby Smith for their invaluable assistance and support.

A special thank to those I love: my wife Laiju, my father Abdur Rob and my siblings. Finally, I dedicate this thesis to the memory of my mother.

The work was made possible by the support of the Office of Naval Research (ONR), the Defense Advanced Research Projects Agency (DARPA) and the MPRG Industrial Partners program.

Contents

1	Introduction	1
1.1	Spread Spectrum and Multiple Access Techniques	2
1.2	Aim and Organization of the Document	3
2	Spread Spectrum Techniques for Packet Transmission in Peer-to-Peer Wireless Networks	5
2.1	Spread Spectrum Schemes	5
2.2	Direct Sequence versus Frequency Hopping	8
2.3	Peer-to-Peer Packet Transmission and Protocol	11
2.3.1	Wireless Transmission Techniques	11
2.3.2	Peer-to-Peer Communications	12
2.3.3	Receiver Design for Peer-to-Peer Communications	13
2.3.4	Protocols for DS-CDMA Systems	14
2.4	Signal Propagation Through Wireless Channel	15
2.4.1	Amplitude Characteristics	16
2.4.2	Doppler Effect	18
2.4.3	Multipath	18
2.5	Chapter Summary	20
3	Multiuser Receivers for Wireless Systems	21
3.1	Background of Interference Cancellation Receivers	21
3.2	Classes of Multiuser Receivers	24
3.2.1	Optimum Receivers	25
3.2.2	Suboptimal Receivers	26

3.2.3	Decorrelators	27
3.2.4	Linear Minimum Mean-Square Error (MMSE) Receivers	29
3.2.5	Subtractive Interference Cancellation Receivers	31
3.2.6	Successive Interference Cancellation Receivers	31
3.2.7	Parallel Interference Cancellation Receivers	33
3.3	Computational Complexity	36
3.4	Chapter Summary	38
4	CDMA Detection for Peer-to-Peer Packet Radio	39
4.1	CDMA Multiuser Detection for Peer-to-Peer Packet Radio	40
4.1.1	Model of Packet Radio Networks	41
4.1.2	Interference Cancellation Models	44
4.1.3	Path-loss Model	48
4.1.4	Results and Comparison	49
4.1.5	Results from Simulations	54
4.1.6	Comparison between PIC and SIC	60
4.1.7	A Realistic Implementation of the PIC Receiver	63
4.1.8	Summary of Multiuser Detection in a Peer-to-Peer Environment	67
4.2	Single-User Adaptive and Multiuser Receivers for DS-CDMA in Peer-to-Peer Packet Radio Networks	69
4.2.1	Single-User Adaptive Receiver	69
4.2.2	Simulation Results	72
4.2.3	Conclusions	77
4.3	Chapter Summary	78
5	Iterative Interference Cancellation and Decoding Using a Soft Cancellation Factor for DS-CDMA	79
5.1	Coding in DS-CDMA	80
5.1.1	Block Codes	81
5.1.2	Convolutional Codes	82
5.2	Iterative Interference Cancellation and Decoding for DS-CDMA	83
5.2.1	System Description	85
5.2.2	Iterative Decoding	86
5.2.3	Simulation Results	92
5.2.4	Section Summary	95

5.3	Optimization of Soft-Cancellation Factor in Parallel Interference Cancellation.	96
5.3.1	The Soft Cancellation Factor in Parallel IC	97
5.3.2	Derivation of the SCF from Iterative Decoding	98
5.3.3	A Pragmatic Approach for Optimization of the SCF	101
5.3.4	Simulation Results	105
5.3.5	Section Summary	110
6	Decoder-Assisted Frame Synchronization for Coded Systems	112
6.1	Motivation and Problem Definition	112
6.2	State-of-the-Art	114
6.3	Standard Frame Synchronization Techniques	116
6.3.1	Basics of Frame Synchronization	116
6.3.2	Single-Frame Synchronization	118
6.3.3	Multiple-Frame Synchronization	120
6.3.4	The Choice of the Sync Word	121
6.3.5	Frame Synchronization of Coded Packet	121
6.3.6	Preamble-less Packet Communication	123
6.4	Proposed Scheme	124
6.4.1	Motivation of the Coded SW	126
6.5	Simulation Results	127
6.6	Soft-Synchronization of Frame	131
6.7	Concatenated Synchronizers	134
6.7.1	Scheme for Estimating Longer Packet Delays	135
6.7.2	Scheme for Estimating Shorter Packet Delays	138
6.7.3	Scheme for Estimating Shorter or Longer Packet Delays	139
6.7.4	Derivation of the Likelihood Function in a Coded System	140
6.7.5	Section Summary	143
6.8	Turbo Synchronization	143
6.9	Packet Synchronization for TDMA	152
6.10	Chapter Summary	153
7	Summary and Future Work	154
7.1	Summary	154
7.2	Recommendation for Future Work	156

A	Abbreviation	159
B	A Postdetection Approach for Interference Cancellation and Soft Cancellation Factor	162
B.1	Interference Cancellation Based on the Joint Observation of the Re- ceived Signal and the Tentative Decision Statistics in the Previous Stage	165
	Bibliography	168
	Vita	178

List of Tables

4.1	Selected receiver-transmitter sets shown in Figs. 4.1 and 4.2, and their corresponding parameters.	50
-----	--	----

List of Figures

2.1	BPSK DS-SS Transmitter.	6
2.2	BPSK DS-SS Receiver.	7
2.3	Block diagram of a frequency hopping spread spectrum (FH-SS) system.	9
2.4	Typical path loss vs. transmitter-receiver separation distance. The lines are obtained using a linear regression model. The carrier frequency is 5.85 GHz.	17
2.5	Typical received power as the terminal moves.	19
3.1	Block diagram of an optimum multiuser receiver.	26
3.2	Block diagram of a decorrelating receiver.	28
3.3	Block diagram of a MMSE detector.	30
3.4	Block diagram of a successive interference cancellation receiver. . . .	32
3.5	Block diagram of a multistage parallel interference cancellation receiver.	34
4.1	Spatial distributions of users at an instant in the packet radio networks represented by the rectangular coordinate system. The symbol “*” denotes that the user’s mobile is ON (54 users), whereas the symbol “o” presents that user’s mobile is OFF. Dashed line is the desired transmitter end and solid line is the designated receiver end for one of the T-R sets active in the network.	43
4.2	Spatial distributions of users at an instant in the packet radio networks represented by the rectangular coordinate system. The symbol “*” denotes that the user’s mobile is ON (15 users), whereas “o” shows that user’s mobile is OFF. Dashed line is the desired transmitter end and solid line is the designated receiver end for one of the T-R sets active in the network.	45

4.3	BER of the desired user as a function of E_b/N_0 for AWGN channel using parallel interference cancellation and successive interference cancellation, respectively. The exponential PL model is used ; the system is heavily loaded with 54 users are ON.	51
4.4	BER of the desired user vs. E_b/N_0 for AWGN channel using parallel interference cancellation and successive interference cancellation, respectively. The PL model is exponential; the system is heavily loaded where 54 users are ON. The Receiver $(0.90, 0.57) \in C$ shown in Fig. 4.1 and the transmitter is the farthest among all 53 candidate transmitters.	53
4.5	BER of the desired user vs. E_b/N_0 for AWGN channel using parallel interference cancellation and successive interference cancellation, respectively. The PL model is exponential; the system is lightly loaded where 15 users out of 100 are ON.	55
4.6	BER of the desired user vs. E_b/N_0 for AWGN channel using parallel interference cancellation and successive interference cancellation, respectively. The PL model is exponential; the system is lightly loaded where 15 users are ON. The plots are for user Set Q [Rx(0.68,0.88), Tx(0.94,0.83)] shown in Fig. 4.2.	56
4.7	BER of the desired user vs. E_b/N_0 . Different simulation result sets are obtained from different amplitude estimations, namely, perfect amplitude estimation, single-bit amplitude estimation and bit-averaging amplitude estimation; (a) for user Set P [Rx(0.55,0.56), Tx(0.27,0.41)] shown in Fig. 4.2. (b) for the Receiver $(0.55, 0.56) \in P$ shown in Fig. 4.2 and the transmitter is located farthest among all the active 14 candidate users.	59
4.8	BER of the desired user obtained analytically and Monte-Carlo simulation, respectively, against its E_b/N_0 . Different simulation result sets are obtained from different amplitude estimations, namely, perfect amplitude estimation, single-bit amplitude estimation and bit-averaging amplitude estimation; (a) for user Set Q [Rx(0.68,0.88), Tx(0.94,0.83)] shown in Fig. 4.2 (b) for user Set R [Rx(0.67,0.75), Tx(0.94,0.83)] shown in Fig. 4.2.	61
4.9	Simulated BER of the desired user (Set P) against its E_b/N_0 for fading channel.	62

4.10	Simulated BER of the desired user (Set Q) as a function of its E_b/N_0 for fading channel.	63
4.11	Simulated BER of the desired user (Set R) vs. its E_b/N_0 for fading channel.	64
4.12	Average BER of the entire system (all pairs of users) versus E_b/N_0 for AWGN channel using parallel cancellation and successive cancellation, respectively. The PL model is exponential; (a) for 54 user-pairs shown in Fig. 4.1, (b) for 15 user-pairs shown in Fig. 4.2.	65
4.13	BER of the desired user vs. its E_b/N_0 for the T-R Set P ; one set of plots consider only 3 significant interferers, and the other set of plots consider significant interferers determined by a threshold value (plots of Fig. 4.7(a))	66
4.14	BER of the desired user vs. its E_b/N_0 for the T-R Set Q ; one set of plots consider only 3 significant interferers, and the other set of plots consider significant interferers determined by a threshold value (plots of Fig. 4.8(a)).	67
4.15	BER of the desired user against its E_b/N_0 for the T-R Set R ; one set of plots consider only 3 significant interferers, and the other set of plots consider significant interferers determined by a threshold value (plots of Fig. 4.8(b)).	68
4.16	Model of a CHRT-LAR.	71
4.17	MSE as a function of training symbols.	73
4.18	BER of the desired user vs. number of users in the system for matched filter and CHRT-LAR, respectively, in synchronous and asynchronous environments.	75
4.19	BER of the desired user vs. number of users in the system by considering MF, PIC receiver, SIC receiver and CHRT-LAR, respectively.	76
4.20	Computational complexity of various receivers.	78
5.1	An RSC encoder for rate 1/2 recursive convolutional code.	83
5.2	Block diagram of iterative MUD (PIC) and decoding for DS-CDMA system.	87
5.3	Block diagram of a soft-input soft-output (SISO) decoder.	88
5.4	Various Decoding Algorithms.	89
5.5	The trellis diagram for the decoding of a RSC code using MAP algorithm.	91

5.6	System model of a iterative parallel interference cancellation receiver for a coded system.	92
5.7	BER of the desired user as a function of its E_b/N_0 considering 10 users in the system and 2 stages of IC.	94
5.8	BER of the desired user vs. its E_b/N_0 for second stage of IC considering 10 users in the system.	95
5.9	System model of a multistage parallel IC receiver for CDMA based on the approach described in [67].	99
5.10	System model of a multistage PIC receiver for CDMA considering a SCF, where the complexity of the receiver is linear with the number of users.	106
5.11	Desired user's BER as a function of its E_b/N_0 considering 10 users in the system.	107
5.12	Desired user's BER as a function of its E_b/N_0 with 10, 20 or 30 users in the system, respectively.	108
5.13	Desired user's BER versus its E_b/N_0 considering 10 users in the coded system.	109
5.14	Desired user's BER versus E_b/N_0 considering 10 users in the coded system for hard and soft estimation of the signal amplitude.	111
6.1	Synchronization window for carrier and frame synchronization.	120
6.2	List synchronizer to compensate for the dependency of the coded data bits.	123
6.3	Trellis diagram of the proposed synchronization scheme; Packet arrivals at the receiver for different delays are also shown for the proposed scheme of frame synchronization.	125
6.4	Flow charts for Monte Carlo simulation method to obtain the probability of false synchronization.	128
6.5	Probability of false acquisition versus $\frac{E_b}{N_0}$ of the system using various synchronization schemes.	130
6.6	Probability of false acquisition as a function of $\frac{E_b}{N_0}$ of the system for various packet sizes using the proposed scheme.	131
6.7	Probability of false acquisition vs. $\frac{E_b}{N_0}$ for different values of Q , which is descried in the text.	132
6.8	Probability of false acquisition vs. $\frac{E_b}{N_0}$ of the system for flat fading channel.	133

6.9	Block diagram of a concatenated frame synchronizer.	134
6.10	Synchronization failure rate vs. $\frac{E_b}{N_0}$ of the system using convolutional encoding, where soft synchronization is employed.	135
6.11	List synchronizer for resolving any time ambiguity of the packet.	136
6.12	Schematic diagram showing the independent coded SW due to a uncoded SW in the mid-amble.	137
6.13	Synchronization failure rate vs. $\frac{E_b}{N_0}$ of the system using the standard ML schemes and the list-synchronization scheme, respectively.	139
6.14	List synchronizer for resolving shorter packet delays.	140
6.15	Synchronization failure rate against $\frac{E_b}{N_0}$ of the system using various schemes for resolving up to 8 coded bit delay	141
6.16	Frame synchronizer for estimating shorter packet delay, which is capable of resolving any packet delay.	142
6.17	Block diagram of a turbo-decoder assisted list-synchronizer	144
6.18	Comparison of the turbo synchronization performance considering hard and soft estimation of the synchronizer.	145
6.19	Block diagram of a turbo-decoder assisted list-synchronizer; the first module is a standard synchronizer, which resolves uncoded SW (Barker code) embedded in the pre-amble of the packet, and is followed by the turbo decoder and CRC error detection code word, which accepts an error free packet starting position from the list supplied by the first module.	147
6.20	Block diagram of a turbo-decoder assisted list-synchronizer; the first module is a standard synchronizer, which resolves coded SW embedded in the pre-amble of the packet (due to uncoded Barker code), and is followed by the turbo decoder, which calculates the best probable packet starting position from the list supplied by the first module.	148
6.21	Block diagram of a turbo-decoder assisted list-synchronizer; the first module is a standard synchronizer, which resolves the coded SW embedded in a mid-amble, and is followed by the proposed synchronizer described in Section 6.4.	149
6.22	Schematic diagram showing the independent coded SW due to uncoded SW in the mid-amble.	150
6.23	Simulated frame failure rate against the E_b/N_0 of the system for the turbo-decoder assisted list-synchronizer shown in Fig. 6.21	151

6.24	Block diagram of a turbo-decoder assisted list-synchronizer; the first module is a standard synchronizer, which resolves the coded SW embedded in a mid-amble, and is followed by the proposed synchronizer described in Section 6.4. The final module is an extrapolator, which verifies the synchronization output: for example, a source coder, a decoder, CRC decoder or the last module of Fig. 6.20.	152
7.1	Illustration of the main contributions of the work.	157

Chapter 1

Introduction

Humankind has long dreamed of communicating with each other anytime, anywhere. Today's information technology brings that dream closer to reality than ever before. Many technical challenges must be solved to provide such capability with reliable and affordable communication systems. A large gap remains between public expectations for wireless systems and available technologies. One type of wireless technology which has been widely used to meet these challenges is direct sequence code division multiple access (DS-CDMA), a technology inherently robust to jamming and interference. In the development of third generation wireless, attention has been focused on the use of an efficient DS-CDMA system. The search for improved performance and increased capacity has motivated the evolution of receiver structures for wireless systems.

The purpose of this dissertation is to analyze and improve upon alternative demodulation techniques for DS-CDMA. Multiuser demodulation (MUD) jointly estimates multiple users' signals in a communication system, thereby increasing the capacity of the communication system. Multiuser receivers have the potential to significantly improve the performance and capacity of a DS-CDMA system. Interference cancellation is one approach for MUD, which is followed in this dissertation. As an introduction to the topic, a brief discussion on spread spectrum and the multiple access techniques is presented in Section 1.1. Section 1.2 describes the aim and organization of the document.

1.1 Spread Spectrum and Multiple Access Techniques

The field of information theory was born 1948, when Claude Shannon published his famous treatise [1]. Shannon showed that if the source information rate is less than the channel capacity, there exists a scheme for transmitting an information source over a communication channel that achieves error-free communication. Shannon's equation for capacity of the band-limited additive Gaussian noise channel is [1]

$$C = \int_0^B \log_2 \left(1 + \frac{P(f)}{N(f)} \right) df \quad \text{bits/sec}, \quad (1.1)$$

where $P(f)$ is the optimally chosen transmitted signal power density, B is the channel bandwidth and $N(f)$ is the noise power density at frequency f . This equation suggests that the more available bandwidth B , the larger the capacity C . The higher capacity allows faster information rate.

A spread spectrum signal *uses* a transmission bandwidth substantially greater than the information bandwidth of the signal. The information bandwidth, known as the Shannon bandwidth, is the amount of bandwidth that the signal *needs* for transmission over the channel, and the transmission bandwidth is also known as the Fourier bandwidth. So, the formal definition of a spread spectrum signal is a signal whose Fourier bandwidth W [2] is much greater than its Shannon bandwidth B [3], where Shannon bandwidth is one-half the number of dimensions of signal space required per second. There is a fundamental difference between the bandwidth expansion due to spectrum spreading and that due to coding. In fact, spectrum spreading increases the Fourier bandwidth W but not the Shannon bandwidth B where as coding increases the true Shannon bandwidth B . By bandwidth expansion, spread spectrum signaling does not increase the capacity, but provides low probability of interception of the signal and multiple access capability [3] that results in improved performance characteristics for the wireless channel.

The phrase 'multiple access' refers to sharing a common communication channel among multiple users. Types of multiple access techniques used, when designing multiuser communication systems include space, time, and frequency. This results in time division multiple access (TDMA), frequency division multiple access (FDMA), and space division multiple access (SDMA), a highly refined form of antenna diversity. Recently, polarization techniques have also been proposed where the wave

property of the transmitted signal is used to create orthogonality. The invention of spread spectrum techniques for communication systems with antijamming and low probability of interception capabilities led to the idea of code-division multiple access (CDMA) [4]. CDMA can be implemented in numerous ways including frequency-hopping (FH), direct-sequence (DS), and time-hopping (TH) as well as multicarrier techniques (MC). The next chapter presents more detailed discussion on CDMA.

1.2 Aim and Organization of the Document

Unprecedented growth in wireless communications, in conjunction with new emerging applications, has increased the demand for higher capacity multiple-access techniques. During the last 4-5 years, there have been major research efforts invested in the development of multiuser receivers to improve the capacity and robustness of CDMA systems. A large number of receiver structures have been proposed for this purpose, and some of them are considered in more detail later in this dissertation. To date, most of the analyses focused on commercial cellular systems, where the multiuser receiver will be deployed at a centralized base station. This dissertation extends these efforts to peer-to-peer systems.

Chapter 2 begins with a discussion and comparison of DS-SS and FH-SS under various environments to justify our choice of DS-CDMA in packet radio networks. Next, peer-to-peer packet radio communications are discussed briefly. Since most applications of our investigation are intended for wireless channels, a condensed discussion on wireless channel modeling is presented in this chapter.

Chapter 3 chronologically develops the emergence of interference suppression for DS-CDMA, since our main consideration is interference suppression. Several relevant receivers are presented from the literature, including the receiver structures considered later in this work.

The remaining chapters will present our original research contributions in several areas. Chapter 4 studies and validates subtractive interference cancellation technique in evolving peer-to-peer packet radio networks; next, this chapter compares the feasibility of using a multiuser receiver, based on selective parallel or successive interference cancellation techniques, with a single-user adaptive receiver in peer-to-peer packet communications environments. First, a prototype of the system is simulated to study the receiver's performance. The receivers are compared in terms of BER

improvement, considering various scenarios: spatial distributions of the interferers, channel environments and path-loss model. The performance of an N-tap chip-rate linear adaptive receiver (CHRT-LAR) with normalized least-mean square algorithm (NLMS) is analyzed as a basis for comparison. To illustrate their potential for peer-to-peer networks, the BER performance and the complexity of these two detection schemes are compared in this chapter.

Chapter 5 discusses the integration of parallel interference cancellation (PIC) with error correction coding. An integrated receiver that implements multiple stages of interference cancellation and decoding is presented and evaluated through simulation. This integrated approach is compared with a partitioned approach, where the final stage output of parallel interference cancellation is followed by decoding. The chapter shows how the soft-information can be exchanged between the PIC detection and decoding. Then, we focus on the optimization of the soft-cancellation factor in a DS-CDMA system that employs both partial parallel interference cancellation and convolutional coding. We investigate the performance of this system for both synchronous and asynchronous CDMA systems, as well as for both equal and unequal signal powers. These include both uncoded and coded systems. A pragmatic approach is adopted to examine the best choice of the soft-cancellation factor for optimizing the combined performance of interference cancellation and coding, while keeping the receiver complexity linear with the number of users.

In Chapter 6, a decoder-assisted synchronization scheme is proposed for convolutionally encoded data packets, where synchronization is fully integrated with the decoding operation. Rather than employing a traditional header, synchronization bits are placed in the mid-amble of the information packet. In this case, the packet delay can be inferred from the state of the encoder at specific points in the packet. Next, the proposed synchronization scheme is extended to list-synchronization and turbo synchronization techniques.

Chapter 7 concludes the dissertation. The main results and contributions are summarized. Open problems are listed for future research.

Chapter 2

Spread Spectrum Techniques for Packet Transmission in Peer-to-Peer Wireless Networks

There are two primary methods of generating spread-spectrum signals, each with its own particular advantages [5]. A basis for comparison among them is the Processing Gain (PG), the ratio of the spread signal bandwidth to the data signal bandwidth, which reflects the degree of spectral spreading. This chapter briefly describes the characteristics of two widely used spread spectrum techniques: direct sequence spread spectrum (DS-SS) and frequency hopping spread spectrum (FH-SS). We will find that while DS-SS has predominated in commercial CDMA systems for cellular environments, FH-SS has usually been preferred for packet radio environments. We believe that the processing techniques developed in this dissertation hold the potential to tip the balance in favor of DS-SS for peer-to-peer environments. Some basics about the peer-to-peer packet radio network are presented next. Since we are interested in the wireless channel, a brief description of signal propagation through the wireless channel is provided.

2.1 Spread Spectrum Schemes

There are two principal types of spread spectrum techniques.

1. **Direct Sequence Spread Spectrum (DS-SS):**

DS-SS has been used in cellular systems. Desirable properties of this technique include low power spectral density, multipath resistance, and relatively high capacity. In DS-SS, each user's data signal is multiplied by its unique high rate signature sequence waveform, thus the title *direct sequence*. The spreading operation is a layer of phase modulation on top of the digital modulation format used for transmission (usually BPSK or QPSK). The additional modulation permits users to be distinguished from one another at the receiver. The PG in DS-SS can be measured as the ratio of the spreading code rate to the data rate.

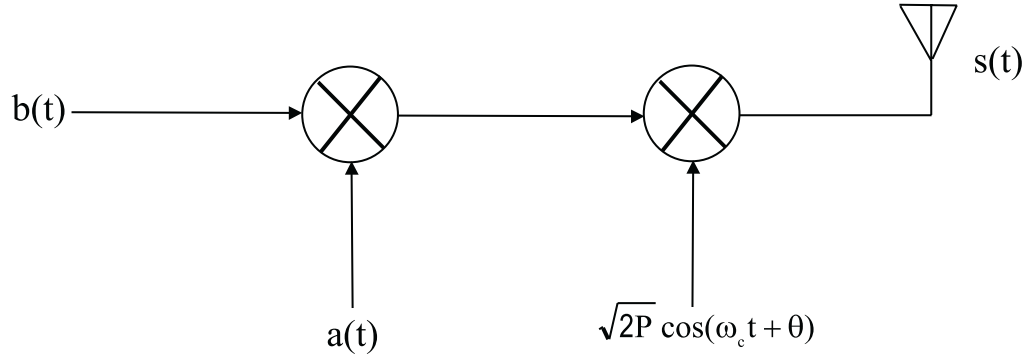


Figure 2.1: BPSK DS-SS Transmitter.

The transmitter of a BPSK DS-SS system for a single user is shown in Fig. 2.1. The transmitted signal $s(t)$ is given by the expression

$$s(t) = \sqrt{2P}b(t)a(t)\cos(\omega_c t + \theta), \quad (2.1)$$

where $b(t)$ is a binary data signal and can be expressed as

$$b(t) = \sum_{i=-\infty}^{\infty} b_i p_T(t - iT). \quad (2.2)$$

Here, $b_i \in \{\pm 1\}$ represents the i th data bit, which is independent and identically distributed (i.i.d.) random variable, and $p_T(t)$ is a unit rectangular pulse with duration T . The PN sequence $a(t)$ is given by

$$a(t) = \sum_{j=-\infty}^{\infty} a_j p_{T_c}(t - jT_c), \quad (2.3)$$

where $a_j \in \{\pm 1\}$ is the j th chip in the PN sequence, and $p_{T_c}(t)$ is a unit rectangular pulse with duration T_c . The terms ' ω_c ', ' θ ', and ' P ' refer to the

carrier frequency, the phase offset of the carrier frequency, and the transmitted power of the signal, respectively.

The transmitted power is delayed and corrupted when it reaches the receiver. The received signal $r(t)$ at the receiver is the summation of the transmitted signal with propagation delay τ and noise, and is given by

$$r(t) = \sqrt{2P}b(t - \tau)a(t - \tau)\cos(\omega_c t + \phi) + n(t), \quad (2.4)$$

where $n(t)$ is an AWGN process with two-sided power spectral density $N_0/2$; the term τ is the random delay of the user that accounts for the propagation delay and synchronization offset of the received signal and is uniformly distributed on $[0, T]$, and $\phi = [\theta - \omega_c \tau] \bmod 2\pi$. If θ is uniformly distributed on $[0, 2\pi]$, then for large frequencies ($\omega_c T \gg 1$), ϕ is a random variable with uniform distribution on $[0, 2\pi]$. The received signal, $r(t)$ is correlated with a synchronous copy of the spreading signal. Let $y[i]$ be the decision statistic for the i th bit and is given by

$$y[i] = \int_{iT+\tau}^{(i+1)T+\tau} r(t)a(t - \tau)\cos(\omega_c t + \phi)dt. \quad (2.5)$$

Then the data bit is recovered using a threshold device. This receiver of the BPSK DS-SS system is shown in Fig. 2.2 where $\hat{b}[i]$ is the estimation of i th transmitted data bit.

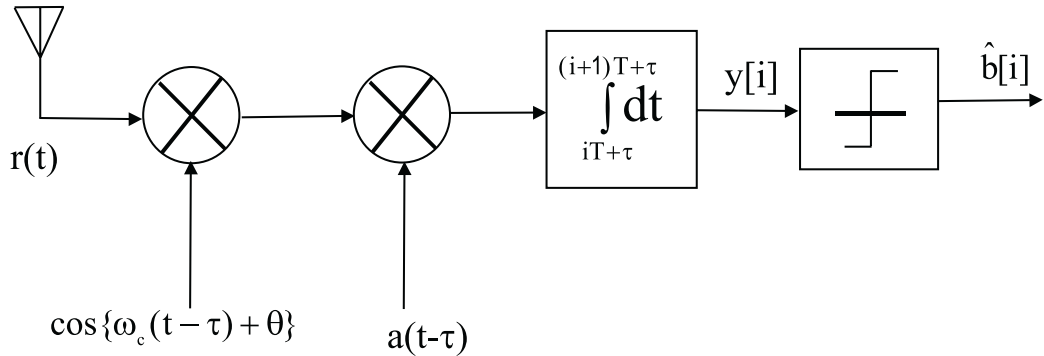


Figure 2.2: BPSK DS-SS Receiver.

2. Frequency Hopped Spread Spectrum (FH-SS):

FH-SS achieves spectral spreading by transmitting the narrowband message signal at successively different carrier frequencies. This process results in inherent frequency diversity, improving the resistance of FH-SS systems to both

frequency selective fading and narrowband jamming. The block diagrams of the transmitter and the receiver for a FH-SS are shown in Fig. 2.3 [6]. The FH-SS signal is obtained by changing the carrier frequency of the narrowband modulated signal according to PN sequence. The FH-SS system must have a large number of frequencies usable on demand, and the *hopping pattern* is pseudo-random in nature, which is determined by the spreading code. The bandwidth dedicated to a FH-SS signal is much larger than the narrowband modulated signal, even though it may not use all of them at the same time. When the hopping rate is slower than the data rate, it is called slow frequency hopping and if the hopping rate is faster than the data rate, it is called fast frequency hopping. In FH-SS systems, the PG is determined by the total number of different carrier frequencies in the hopping pattern.

Less commonly discussed are chirped spread spectrum (CH-SS) and time hopping spread spectrum (TH-SS) [7]. TH-SS systems are analogous to FH-SS in that TH-SS systems use a pseudo-random code to specify the times to transmit the narrowband message signal in the form of extremely short pulses. Here, PG is the total number of different transmission times. Additionally, these techniques can be combined to develop a hybrid system which may combine the attractive features of the independent techniques.

2.2 Direct Sequence versus Frequency Hopping

The relative advantages of DS-SS versus FH-SS depend on the particular implementation scenario [7].

- **Multiple Access Interference:** DS-CDMA allows multiple simultaneous users to transmit in the same frequency band with graceful performance degradation as the number of interferers increases, provided all users have similar received powers. A model for the capacity of a DS-CDMA cellular system was presented in [8] and is given by:

$$K - 1 = \frac{W/R}{E_b/(N_0 + I_0)}, \quad (2.6)$$

where K is the number of simultaneous users having equal energy and able to coexist in a multiple access system. The transmitted power is constrained to the minimum value for maintaining a given signal-to-noise ratio for the required

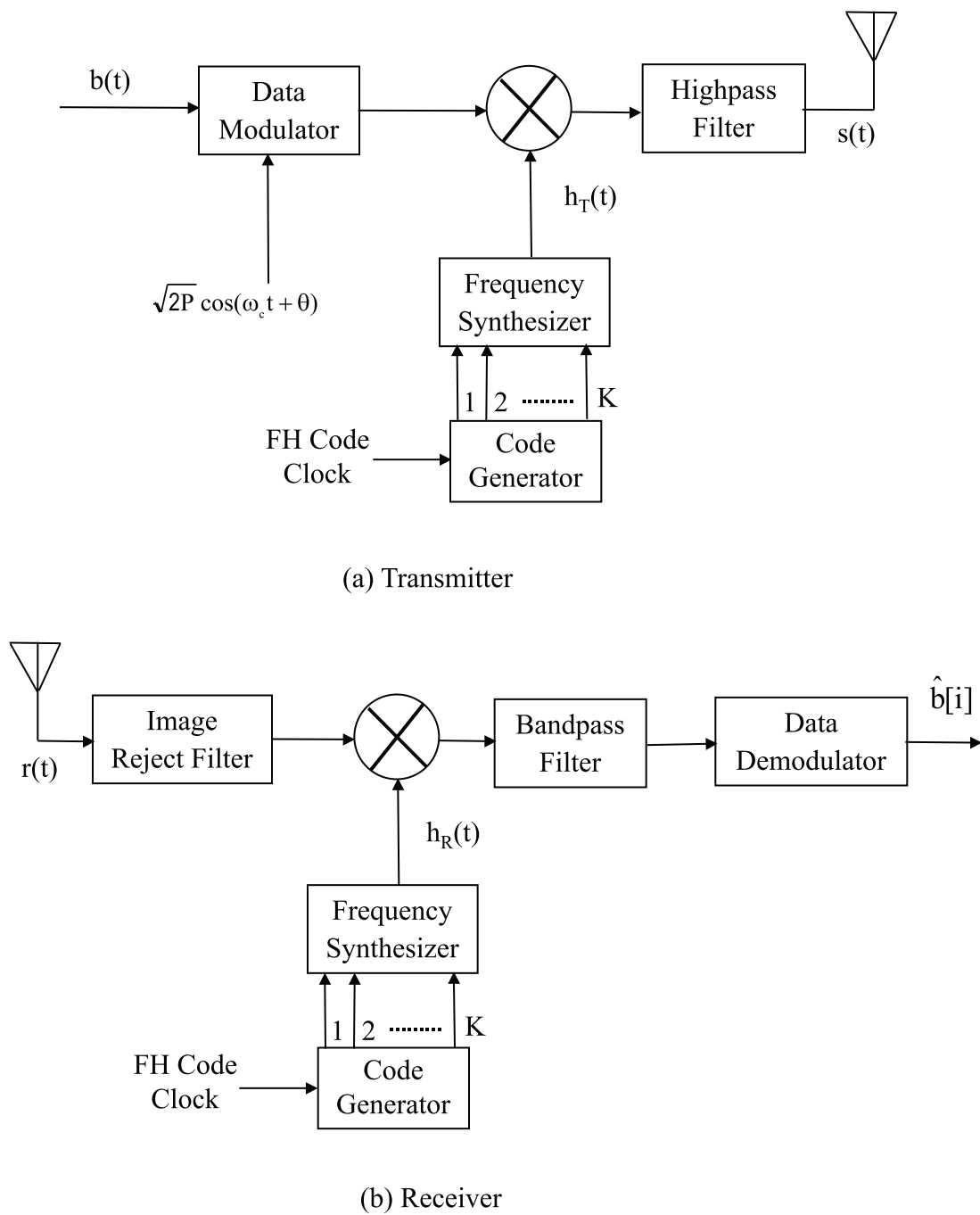


Figure 2.3: Block diagram of a frequency hopping spread spectrum (FH-SS) system.

level of performance and the received signal energy per bit is E_b for each user. All signals have the same information rate R and are spread over the same bandwidth W . The terms N_0 and I_0 refer, respectively, to the channel noise density and the interference density from other users on the desired user over the spreading bandwidth W . For this reason, DS-CDMA is a desirable transmission technique for networks with a centralized cellular architecture.

Multiple access interference will degrade the performance of a FH-SS system through ‘collisions’ which occur when two FH-SS transmitters hop simultaneously to the same narrow frequency band, resulting in a high error probability. In some cellular systems such as GSM, hopping patterns can be synchronized to avoid collisions, but this is not possible in packet radio environments that lack centralized control. For this reason, the primary protection from MAI in a FH-SS system lies in error correction codes applied across multiple hops. Provided other effects can be overcome, DS-CDMA appears to offer some advantage with respect to MAI and capacity.

- **Near-Far Effects:** The multiple access capabilities of DS-CDMA are contingent upon the assumption that all signals arrive at the receiver with approximately equal signal power. Violation of this condition results in the well-known near-far effect in which a much stronger interferer can overwhelm the desired user, resulting in severe performance degradation [9]. In cellular systems, centralized power control is employed to prevent the near-far problem, but this solution is not possible in decentralized peer-to-peer systems.

FH-SS systems are not subject to the near-far effect, since each collision is highly likely to result in errors regardless of relative signal powers. Conversely, when signals do not collide in FH-SS systems, interference is extremely unlikely, regardless of relative signal powers.

- **Intentional Jamming:** Both DS-SS and FH-SS systems provide some degree of resistance to intentional interference or jamming, which may occur in some military applications. The degree of resistance for both systems is proportional to the processing gain. A FH-SS system is particularly resistant to narrowband jamming for the same reasons that it is resistant to the near-far problem. A DS-SS system may require adaptive interference excision filters for adequate narrowband jamming resistance. Because of their noiselike power

spectral density, DS-SS systems are resistant to detection and interception in military applications.

- **Multipath And Frequency Selective Fading:** DS-SS provides natural resistance to multipath fading. If the delay of a multipath component exceeds one chip of duration, a DS-SS receiver will treat the multipath as simply another multiple access interfering component. FH-SS with coding can provide a form of frequency diversity against frequency selective fading.
- **Synchronization And Security:** DS-SS is self-synchronizing since it employs a very short code that can be searched with a time-invariant matched filter. FH-SS needs synchronization with each frequency hop. FH-SS suffers from other implementation difficulties including an easily identifiable spectrum.

Overall, the high capacity of DS-SS has led to its adoption for 3rd Generation cellular systems. However, the near-far problem has severely limited the effectiveness of DS-SS in a peer-to-peer environment. For this reason, detailed comparisons have recommended FH-SS as the technology of choice for packet radio applications [10]. The purpose of this dissertation is to investigate whether improved receiver structures may tip the balance in favor of DS-SS.

2.3 Peer-to-Peer Packet Transmission and Protocol

2.3.1 Wireless Transmission Techniques

In radio networks, there are two fundamental approaches for connecting two terminals: circuit switching and packet switching. In circuit switching, information is sent over a continuous connection which reserves dedicated resources of call set-up until these resources are released at call termination. The connection is transparent: once a connection is established, it appears to attached devices as if there were a direct connection. Circuit switching has been mainly used for voice traffic, because most of the time one party transmits information; however, circuit switching can also handle digital data, although this is often inefficient. Circuit switching is used in public telephone networks and most of the present generation wireless systems, where voice transmission is predominant, use circuit switching.

In a packet radio network, data is grouped in packets and sent through the network that routes each individual packet to its destination. Each packet contains some portion of the user data plus control information needed for proper functioning of the network. The original messages are reassembled at the destination on a packet-by-packet basis. The main feature of a packet radio network is that each node stores the packets until the link becomes available. Thus, many competing users share a common link dynamically. There are two ways of transmitting information in a packet radio network: virtual circuit and datagram. In virtual circuits, a route is defined between two endpoints and all the packets for that virtual circuit follow the same route. In a datagram, each packet is treated independently and the packets, which are parts of the complete information intended for the same destination, can follow different routes. Packet radio was originally designed for bursty data traffic, where latency is tolerable. Examples include mobile packet radio networks, cellular digital packet data (CDPD), satellite data networks, mobile satellite networks such as Globalstar and Iridium, and CDMA networks such as IS-95.

2.3.2 Peer-to-Peer Communications

An *ad hoc* or peer-to-peer network is a network that does not require any infrastructure in order to operate. An ad hoc wireless network is a collection of wireless mobile users forming a temporary network without the aid of any established infrastructure or centralized control. Users can co-locate several terminals and expect them to communicate with each other with minimal configuration. Adding an access point allows this network to communicate with a traditional wired network. Generally, ad hoc networks use wireless links and support mobility. A more descriptive name for such a network is a wireless multi-hop network. This differentiates an ad hoc network from a traditional wireless local area network (LAN) in which stations communicate over a single wireless hop, and nodes in multiple wireless LANs are connected via a wired infrastructure. A LAN covers a limited geographical area, where every node in the network can communicate with every other node without any need of a central controller. According to IEEE 802 committee, “A local area network is a data communication system which allows a number of independent devices to communicate with each other.” In a wireless multi-hop network, each packet is routed across one or more wireless hops to the destination without using any wired infrastructure. An ad hoc network plays a limited role in today’s wireless networks. Frequently cited

applications include military, rescue workers, and disaster recovery. The primary reasons for this limited deployment are the high complexity of the required algorithms and the inefficient use of the frequency spectrum. Commercial packet radio networks have been built around single-hop base-station-oriented architectures, as in the Ardis or Mobitex systems, and multihop peer-to-peer architectures, as in the Metricom system. These networks can be constructed with fixed-location infrastructure elements (as in Metricom) or can achieve connectivity in a completely ad hoc manner. In general, ad hoc packet-radio networks can be set up, deployed, and redeployed rapidly. These characteristics are important in military operations.

A packet network is highly flexible for mobile users with changing connectivity patterns and holds the potential for efficient use of the radio spectrum. The terms ‘untethered’ and ‘peer-to-peer’ were coined in military applications, referring to the union of wireless and mobile technologies. In a peer-to-peer network architecture, transmissions flow between the users without passing through a central hub. Packet radio, *ad hoc*, peer-to-peer and untethered networks refer to self-governing, self organizing, and distributed networks. No central control is devoted to organize the communications among nodes, and mobile users can communicate with each other directly, without the involvement of an access point. Each communication flows from one node to its peer, without intervention or assistance from a central controller, which may not exist. Nodes use the radio channel in a random access manner. Some intelligence is required at the mobile to support this model. Ethernet is an example of distributed controlled communications through a wired channel, where computer terminals involved in the distributed scheme determine access to the channel. As digital signal processing (DSP) and microprocessor speed becomes faster and silicon becomes cheaper, portable radio will become more powerful and lighter. Thus, peer-to-peer packet radio networks are nearing reality.

2.3.3 Receiver Design for Peer-to-Peer Communications

The object of improved receiver design for peer-to-peer network is to develop technologies for hand-held devices, that will provide military and commercial users with the ability to reliably access and exchange multimedia information over wireless networks, while deployed in a wide variety of environments- e.g. rural, urban, & desert. The challenge is to develop techniques that ensure that users can stay connected to the network under harsh environmental conditions, while achieving the acceptable

performance with extended battery life.

Current industrial approaches are limited to point solutions that are not always suitable for the multi-faceted needs of the military; i.e. low-power, high data-rate networking products are available but only work reliably in indoor environments and do not provide support for speech and image; wireless voice communication devices can operate in indoors and outdoors, but require high transmit power resulting in short battery life and support only low data rates. There is a need for techniques that will allow the same hand-held node to adapt to the needs of different types of information in widely varying environmental conditions, while providing the best possible data rate with a low transmit power. Since there is no dedicated base station and the system needs to be deployed in a reasonable period, special attention is required to the complexity of the system. These factors will be considered for the receiver design and performance analysis.

The peer-to-peer packet radio environment presents a number of unique constraints on receiver design that are not obvious in the cellular environment. Handsets must have low complexity and require low power to maintain battery life. A variety of data rates must be supported to enable multimedia communications. Knowledge of other users' signal parameters may be more limited than at a base station.

2.3.4 Protocols for DS-CDMA Systems

The protocol for peer-to-peer packet radio networks is important. A protocol is a set of rules, including formats and procedures that allow one user to communicate with the other user. In a CDMA system, spreading codes distinguish one user from the other. Interference from an undesired user corrupts the desired user's signal due to the quasi-orthogonal nature of these codes and that results in collision in packet transmission. The spreading sequence can be assigned to active users in the CDMA network in one of the following ways.

2.3.4.1 Transmitter-Receiver-Oriented Protocol

Every pair of nodes is assigned a distinct code sequence, i.e., in a network with M nodes, $M(M - 1)$ code sequences are needed. At the transmitter end, if user k needs to communicate with user l , it will use a unique code sequence M_{kl} assigned to this pair. At the receiver end, user l must know the code sequence M_{kl} and monitor it at the right time. This protocol is suitable for point-to-point communication.

2.3.4.2 Transmitter-Oriented Protocol

Every transmitter is assigned its own code sequence; i.e., in a network with M nodes, exactly M code sequences are needed. If transmitter k wants to send a signal to any receiver, it will use its code sequence M_k . The receiver needs to generate all possible code sequences if random access schemes are used in conjunction with this protocol. As a result, the acquisition of the signal is longer and the implementation of the receiver is more complex. Since every transmitter has a different code sequence, there will not be any packet collision if the receptions of multiple packets from various users occur at the same time. Hence, the system has good capturing capabilities. This protocol is suitable for DS-CDMA cellular systems and DS-CDMA peer-to-peer networks.

2.3.4.3 Receiver-Oriented Protocol

Every receiver is assigned its own distinct code regardless of the chosen transmitter. If user k wants to send signals to receiver l , it must use user l 's code sequence. So, fast acquisition of the signal is an advantage for this protocol. On the other hand, there will be collisions of packets at the receiver if two transmitters send signals at the same time. Hence, the system has poor capturing capabilities. For broadcasting purpose another protocol is used, called common code protocol, where all users are assigned a common spreading sequence. Channel access protocols define the rules for sharing the channel. The choice of a protocol depends on the network type, channel properties, traffic patterns and spread spectrum properties. For spread-spectrum networks it is possible to use controlled access and random access schemes. Random access schemes include various types of ALOHA systems and controlled access schemes include CSMA, R-ALOHA.

2.4 Signal Propagation Through Wireless Channel

This section presents simple models for signal propagation through a wireless channel [11], [12]. The received signal is influenced by a myriad details of the physical environment of the transmitter, receiver and the space between them. Three phenomena - shadowing, Doppler effects, and multipath propagation, introduce severe impairments to wireless signals. Various countermeasures such as coding, equalization and diversity are introduced at the physical layer to overcome these impairments to the

radio signal. We begin with the amplitude characteristics of the signal received at moving terminals, followed by the temporal characteristics of the signal due to the Doppler effect. Finally, multipath propagation is described briefly. Although the deployment of commercial cellular systems has motivated extensive study of propagation between a mobile and a tall antenna tower, substantially less information is available on propagation between two hand held terminals [11].

2.4.1 Amplitude Characteristics

The received signal strength indicator from a mobile user can generate a plot like Fig. 2.4, where path loss is shown as a function of the transmitter-receiver separation distance [13]. In the plot each point represents a measurement of path loss, which corresponds to the received power from a fixed transmitter such as a base station. For a fixed transmitted power, the path loss is a translation of the measured received powers. Each power measurement is an average energy, generally expressed in *dBm*. To normalize that, the plots divide the relative measured power by 1 meter free-space path loss, which depends only on the path-loss exponent. Each power measurement is an average over a time interval on the order of one second, corresponding to about one hundred wavelengths of the transmitted carrier.

Although the signal strengths at various locations equidistant from the transmitter exhibit a wide range of values due to local differences of the environment, a general trend of decreasing signal power with increasing transmitter to receiver distance is observed. Slow log-normal fading due to shadowing may explain these variations. In the measurements, p watts taken at various points d meters from the base station, are sample values of a log-normal random variable, P . The corresponding *dBm* values, t , are sample values of a Gaussian random variable T with probability density function,

$$f_T(t) = \frac{1}{\sigma\sqrt{2\pi}} \exp\left[-\frac{[t - T_r]^2}{2\sigma^2}\right], \quad (2.7)$$

where the expected value $E[T] = T_r$ is the point on the line in Fig. 2.4. For all measurements at distance d , there is an average received power. Measured in *dB*, this power is T_r . The standard deviation, σ *dB*, in (2.7) depends on the environment and is in the range of 6 - 12 *dB*.

Power measurements taken over shorter intervals, generally on the order of milliseconds, reveal rapid signal strength fluctuations. The time variation of the signal

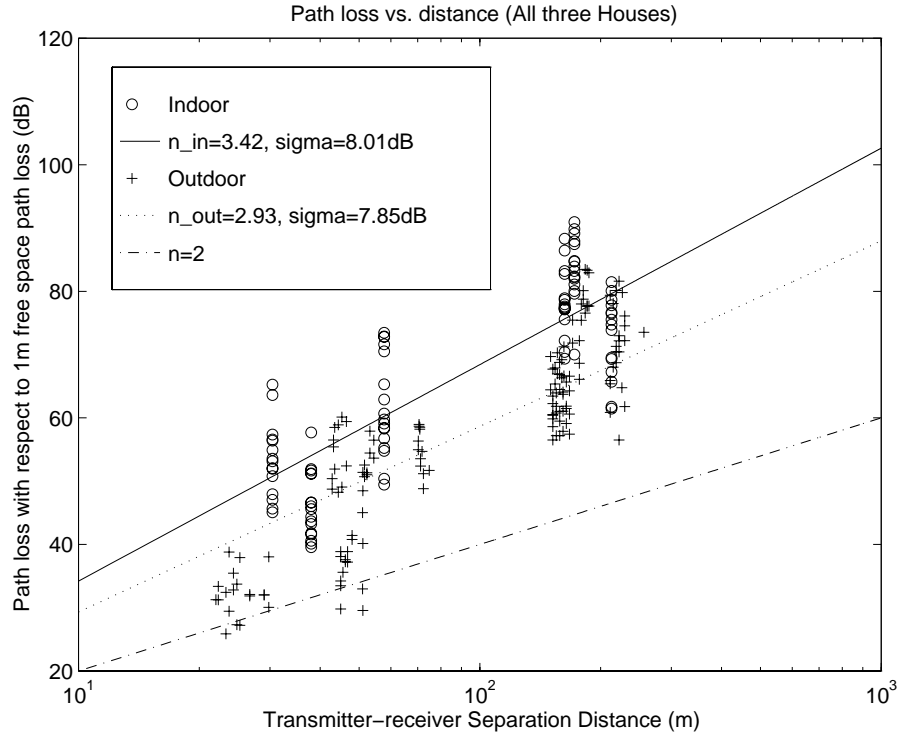


Figure 2.4: Typical path loss vs. transmitter-receiver separation distance. The lines are obtained using a linear regression model. The carrier frequency is 5.85 GHz.

envelope is due to the motion of the wireless terminal and the scattering of the transmitted signal by the environment. When there is no line-of-sight direct path, the envelope excursions conform to the Rayleigh probability density functions,

$$\begin{aligned}
 f_C(c) &= \frac{c}{p} \exp\left[-\frac{c^2}{2p}\right], & c \geq 0 \\
 &= 0, & \text{otherwise,}
 \end{aligned} \tag{2.8}$$

where p watts, corresponding to one of the points plotted in Fig. 2.4. The mean square value of $c(t)$ is $2p$.

The instantaneous phase of the received signal is uniformly distributed over the range $[0, 2\pi]$. The instantaneous power is an exponential random variable. If a line of sight path exists between the transmitter and the receiver, the envelope of this signal is a Ricean random variable with the probability density function

$$\begin{aligned}
 f_C(c) &= \frac{c}{p} \exp\left[-\frac{c^2 + D^2}{2p}\right] I_0\left[\frac{cD}{p}\right], & c \geq 0 \\
 &= 0, & \text{otherwise,}
 \end{aligned} \tag{2.9}$$

where D is a constant and indicates the amplitude of the direct path component, $I_0(\cdot)$ is the modified Bessel function of zero order. The total instantaneous received power, is a chi-square random variable. All of these probability functions apply to the case for a fixed distance, d , between the transmitter and the receiver and the average scattered power p is a sample value of a log-normal random variable, P .

2.4.2 Doppler Effect

As the wireless terminal moves through an electromagnetic field due to a transmitted signal, it encounters peaks and nulls, as the signal varies in a correlated manner. The time scale of this short-time fading effect is proportional to the maximum Doppler frequency, f_d . The structure of signal fading is characterized by $S_{rr}(f)$, the power spectral density of the received signal. Following the pioneering work of Clarke [14], we have

$$\begin{aligned} S_{rr}(f) &= \frac{1}{\pi f_d \sqrt{1 - (f - f_c)^2 / f_d^2}}, & f_c - f_d < f < f_c + f_d \\ &= 0, & \text{otherwise,} \end{aligned} \quad (2.10)$$

where f_c is the carrier frequency. This indicates that the fading signal has most of its energy concentrated near $f = f_c \pm f_d$. The observed power shown in Fig. 2.5, goes through peaks and nulls at a rate close to f_d times per second. Fig. 2.5 is typical of recordings of signal strength, measured on a decibel scale, as a function of time, as a terminal moves around in a service area and the probability distribution function of the signal is as described above. The carrier frequency is 400 MHz, and the relative velocity between the transmitter and the receiver is 100 km/h for the plot.

2.4.3 Multipath

In the model described above, there is a “bundle” of rays with propagation path lengths differing by fractions of a wavelength. Physically, the receiving antenna can have several discrete signal bundles. The differences in delays of arriving multipath reflections can be from tens to thousands of carrier wavelengths. This multipath propagation phenomenon leads to a representation of the impulse response of the radio channel as a tapped delay line filter superimposed on the amplitude model of the Doppler effect. The tap delays and tap weights correspond to path propagation

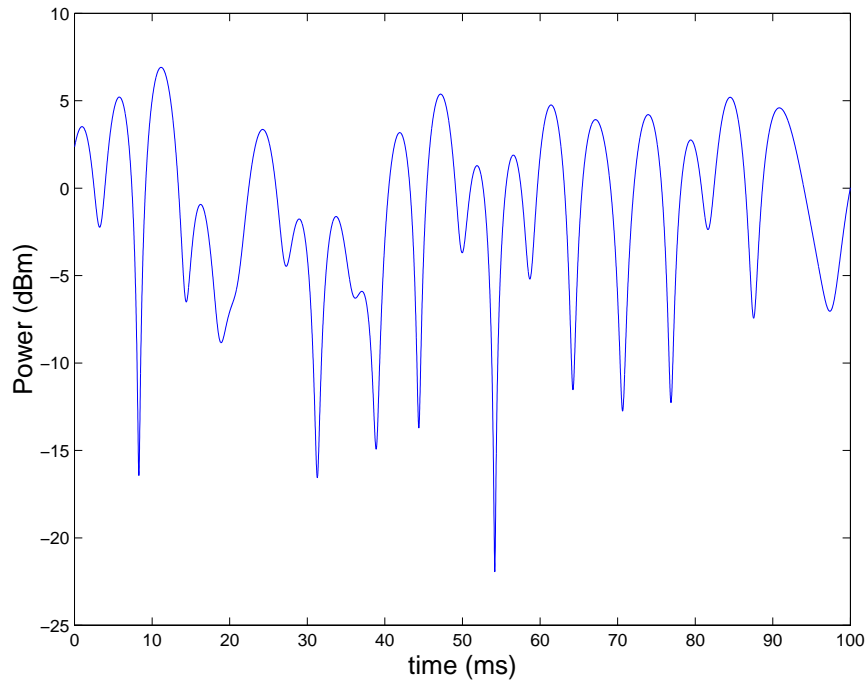


Figure 2.5: Typical received power as the terminal moves.

times and path attenuations. Thus, with a sine wave carrier transmitted, the received signal is

$$r_M(t) = \sum_{i=1}^N a_i r_S(t - t_i), \quad (2.11)$$

where $r_S(t)$ is the summation of the scattered signal at the receiver, N is the number of paths; t_i and a_i are the delay and gain respectively of path i . If we label the paths in an ascending order of delay with $t_1 < t_2 < \dots < t_N$, the maximum delay spread can be defined as

$$t_{max} = t_N - t_1. \quad (2.12)$$

While t_{max} provides an indication of the effect of multipath, it depends only on two of the N path amplitudes (a_i and a_N) and delays (t_i and t_N) in (2.11). Another quantity, t_{rms} , the root mean square delay spread, represents the average variation in delay around the mean path delay,

$$t_{mean} = \frac{\sum_{i=1}^N a_i t_i}{\sum_{i=1}^N a_i}, \quad (2.13)$$

is a good indicator of the effects of multipath propagation on communication quality.

2.5 Chapter Summary

In this chapter we reviewed the basic types of spread-spectrum systems, introduced the architecture of a packet radio network, and presented simple models for wireless propagation. These basic ideas serve to define the problem that we attack in this dissertation through improved receiver structures. We consider those improved structures in Chapter 3.

Chapter 3

Multiuser Receivers for Wireless Systems

This chapter introduces the receiver structures that will be investigated in the remainder of this dissertation. We begin with the derivation of a conventional correlation matched filter (MF) receiver and analyze the effects of interference on the performance of this receiver, which motivates the development of an optimal multiuser receiver. Several possible suboptimal linear and non-linear receivers are presented for the interest of our research.

3.1 Background of Interference Cancellation Receivers

For a DS-CDMA system, the receiver's function is to recover the transmitted bit stream with minimum BER. Its success in this endeavor depends upon its detection statistics, the spreading code properties, and the channel conditions as well. Consider a K -user CDMA channel with additive white Gaussian noise (AWGN) $n(t)$ of variance $\sigma^2 = N_0T/2$, consisting of the sum of BPSK modulated signals. The received signal can be modeled by

$$r(t) = \sum_{k=1}^K A_k b_k a_k(t) + n(t), \quad t \in [0, T], \quad (3.1)$$

where T is the bit period, $b_k \in \{-1, 1\}$ is the information bit of user k , $a_k(t)$ and A_k denotes signature waveform and signal amplitude respectively. For the single user

case the received signal becomes

$$r(t) = A b a(t) + n(t), \quad t \in [0, T]. \quad (3.2)$$

Let us consider a demodulator that outputs the sign of the correlation between the observed waveform and a deterministic signal $h(t)$ of duration T :

$$\begin{aligned} \hat{b} &= \text{sgn} [\langle r(t), h(t) \rangle] \\ &= \text{sgn} [\langle a(t), h(t) \rangle] \\ &= \text{sgn} \left[\int_0^T a(t) h(t) dt \right]. \end{aligned} \quad (3.3)$$

The optimal way to choose $h(t)$ is by maximizing the signal-to-noise ratio (SNR) of the decision statistic:

$$\max_{h(t)} \frac{A^2 (\langle a(t), h(t) \rangle)^2}{\sigma^2 \|h(t)\|^2}. \quad (3.4)$$

From the Cauchy Schwarz inequality we can write the above expression as

$$\frac{A^2 (\langle a(t), h(t) \rangle)^2}{\sigma^2 \|h(t)\|^2} \leq \frac{A^2}{\sigma^2} \|a(t)\|^2, \quad (3.5)$$

with equality if and only if $h(t)$ is a multiple of $a(t)$ and then $\hat{b} = \text{sgn} [\langle r(t), m a(t) \rangle]$, where m is an integer. This linear detector is known as an MF detector. Note that the noise need not be of any particular distribution. If the noise is Gaussian, the MF is optimal to minimize the probability of error,

$$Pr(e) = Q \left(\frac{A \langle a(t), h(t) \rangle}{\sigma \|h(t)\|} \right) \quad (3.6)$$

for a zero threshold device, where the Q function is the complementary cumulative distribution function of the unit normal random variable. Now let us consider a non-orthogonal CDMA channel that consists of two users. The probability of error of user 1 due to the above conventional MF detection is

$$\begin{aligned} Pr(e_1) &= Pr [b_1 \neq \hat{b}_1] \\ &= Pr [b_1 = +1] Pr [y_1 < 0 | b_1 = +1] + Pr [b_1 = -1] Pr [y_1 > 0 | b_1 = -1] \\ &= \frac{1}{2} Q \left(\frac{A_1 - A_2 |\rho_{1,2}|}{\sigma} \right) + \frac{1}{2} Q \left(\frac{A_1 + A_2 |\rho_{1,2}|}{\sigma} \right), \end{aligned} \quad (3.7)$$

where $\rho_{i,j}$ is the cross correlation between signature codes of user i and user j , defined as

$$\begin{aligned} \rho_{i,j} &\triangleq \langle a_i(t), a_j(t) \rangle \\ &= \int_0^T a_i(t) a_j(t) dt. \end{aligned} \quad (3.8)$$

The MF output from user 1 is equal to

$$y_1 = A_1 b_1 + A_2 b_2 \rho_{1,2} + n_1, \quad t \in [0, T], \quad (3.9)$$

where $n_1 = \int_0^T n(t) a_1(t) dt$. From the monotonic decrease in magnitude of the Q function, we can express the upperbound

$$Pr(e_1) \leq Q\left(\frac{A_1 - A_2 |\rho_{1,2}|}{\sigma}\right). \quad (3.10)$$

For the detection of user 1, if the relative amplitude of user 2 (interfering user) is such that

$$\frac{A_2}{A_1} > \frac{1}{|\rho_{1,2}|}, \quad (3.11)$$

then the MF fails to detect the signal of user 1. This is known as the near-far situation. In general, for K -user detection where user k is the user of interest, if

$$A_k > \sum_{j \neq k} A_j |\rho_{j,k}|, \quad (3.12)$$

we can make an error-free decision in the absence of noise. This is commonly referred to as the *open-eye* condition. On the other hand, the opposite condition results in near-far situation where, conventional MF detection fails to decode the information bits of user k . The MF output of user k is

$$y_k = A_k b_k + \sum_{j \neq k}^K A_j b_j \rho_{j,k} + n(t), \quad t \in [0, T]. \quad (3.13)$$

The second term in the above equation can be approximated by a Gaussian random variable, by virtue of central limit theorem. A widespread misinterpretation of the Gaussian approximation was the belief that the MF is near optimal since the interference can be modeled as a Gaussian random variable. Note that the *open-eye* condition is sufficient enough to contradict this belief and that resulted in the study of optimal multiuser receivers [15]. Here the decoding is based on the joint optimization of the decision statistics of all K users, which is described below, instead of the individual optimization of the user of interest as done above using MF detection. Now consider a 2-user CDMA synchronous channel and the received signal can be expressed as

$$r(t) = A_1 b_1 s_1(t) + A_2 b_2 s_2(t) + n(t), \quad t \in [0, T]. \quad (3.14)$$

The minimum probability of error decision for user 1 can be obtained by selecting the value of $b_1 \in \{-1, +1\}$ that maximizes the a posteriori probability

$$Pr [b_1 | \{r(t), 0 \leq t \leq T\}]. \quad (3.15)$$

The above a posteriori probability can also be considered jointly on $[b_1, b_2] \in \{-1, +1\}^2$ as

$$Pr [(b_1, b_2) | \{r(t), 0 \leq t \leq T\}]. \quad (3.16)$$

This jointly optimum decision may not result in the same decision as the individually optimum decision does. If we assume that the information bits are equiprobable and independent, the jointly optimum decisions are the maximum likelihood (ML) decisions (\hat{b}_1, \hat{b}_2) chosen such that

$$f[\{r(t), 0 \leq t \leq T\} | (b_1, b_2)] = \exp \left(-\frac{1}{2\sigma^2} \int_0^T \{r(t) - (A_1 b_1 s_1(t) + A_2 b_2 s_2(t))\}^2 dt \right) \quad (3.17)$$

is minimum in mean square sense. Since the noise statistics are Gaussian, this is optimal among all estimation criteria. The ML decision can be implemented optimally using the Viterbi algorithm [16]. The complexity of this implementation grows exponentially with the number of users, which triggered a quest for low complexity suboptimal receivers that approach the performance of the optimal receiver.

It is clear from the above expressions that the near-far problem is not inherent to CDMA systems, but is dependent upon the receivers used, which have motivated the search for receiver structures that can increase the capacity even in the presence of disparate received power levels. A popular approach is the multiuser receiver, which uses information about all received signals to improve the performance. Since multiuser receivers require information about all considered received signals, they are inappropriate for scenarios where single-user receivers are required.

3.2 Classes of Multiuser Receivers

There has been a great effort in improving DS-SS detection through the use of multiuser receivers. The purpose of all multiuser receivers is to overcome the near-far problem and offer performance close to a single-user system. The important assumption is that the spreading codes of all active users are known to the receiver a priori and timing, amplitudes and phases of all considered users must be estimated for

better detection of an individual user. The common performance measure of interest in digital communication is the BER. In MUD, another parameter called multiuser efficiency is feasible to measure the performance. The near-far resistance as defined in [17, 18] is based on the asymptotic multiuser efficiency η_k , which is the limit as $\sigma \rightarrow 0$ of the ratio of the effective SNR to the actual SNR of a multiuser system. The effective SNR is the SNR required by a single user system to achieve the same asymptotic BER as a multiuser system. The near-far resistance, then, is the minimum η_k considered over all possible interfering bit energies. The minimum allowable value of near-far resistance is zero, which implies that to achieve the BER of a single user system, the multiuser system would require an infinite SNR. The conventional correlation receiver has an efficiency of zero. The maximum allowable value of near-far resistance is one, which implies that the multiuser system is performing as well as the single-user system. Thus the optimum multiuser receiver will have a near-far resistance of one.

3.2.1 Optimum Receivers

Verdu's seminal work [17] proposed and analyzed an optimum multiuser receiver for an asynchronous Gaussian multiple-access channel based on maximum-likelihood detection. The traditional MF receiver requires no knowledge beyond the signal waveform and timing of the desired user, and there is no interaction between the single-user MF receivers [17]. The optimum single-user receiver can be modeled as a bank of single-user MF, each of which is followed by a threshold detector. Verdu's proposed receiver has a bank of single-user matched filters followed by a Viterbi algorithm, as shown in Fig. 3.1, where $r(t)$ is the received signal, K is the total number of users and \hat{b}_k is the bit estimate of user k , $1 \leq k \leq K$. In comparing the receiver structures, the optimal multiuser receiver is an extension of the traditional receiver. Using maximum-likelihood detection, the detector selects the sequence that maximizes

$$P[\{r(t), t \in R\} | \mathbf{b}] = C \exp(\Omega(\mathbf{b})/2\sigma^2), \quad (3.18)$$

where $r(t)$ is the received signal, C is a positive scalar, R is the set of real numbers, \mathbf{b} is the matrix of all K users' transmitted data bits, σ is the standard deviation of the noise, and $\Omega(\mathbf{b})$ is given by

$$\Omega(\mathbf{b}) = 2 \int_{-\infty}^{\infty} S_t(\mathbf{b})r(t)dt - \int_{-\infty}^{\infty} S_t^2(\mathbf{b})dt, \quad (3.19)$$

where $S_t(\mathbf{b})$ is the matrix of all K users' transmitted signals. This detection process chooses the sequence which minimizes the noise energy.

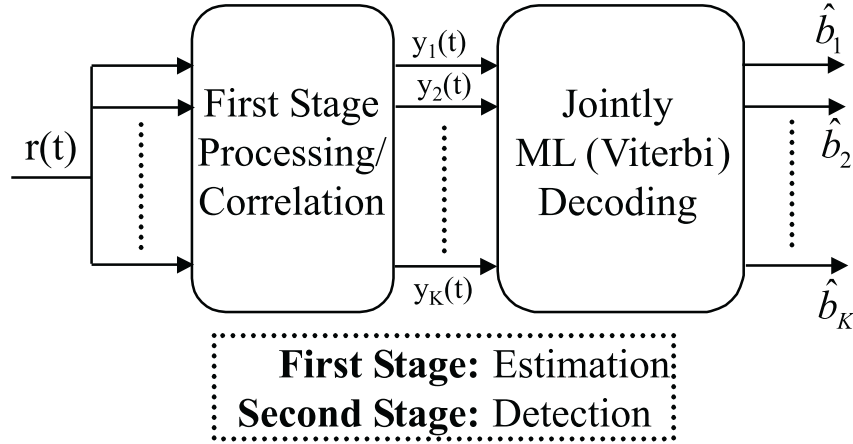


Figure 3.1: Block diagram of an optimum multiuser receiver.

For an asynchronous system, the optimal multiuser receiver is required to know not only the codes and timing of all active users, but also the estimate of the received signal amplitudes of every user and the noise level. In addition, the entire received waveform over all time must be known, since in an asynchronous system each data bit overlaps two adjacent bits from each interfering user. Any technique that only takes into account the received signal during the detection interval is inherently suboptimal. The Viterbi algorithm has 2^{K-1} states and thus a time complexity for each bit decision of $O[K^2]$. Verdu developed tight approximations to the bit error rate that, even though the complexity of the receiver structure precludes a practical implementation, demonstrated the significant performance improvements of the optimal multiuser receiver over the traditional MF receiver.

3.2.2 Suboptimal Receivers

The exponential complexity of the optimal receiver on one end and the huge performance loss in a traditional MF receiver on the other have led to the development of suboptimal multiuser receivers that exhibit balance between the two extremes. The bulk of the research has been focused on the search for suboptimal techniques that approach the performance of the optimum technique, but with a much lower computational complexity and, therefore, are suitable for practical implementation.

There are two main classes of suboptimal receivers, the linear suboptimal multiuser receivers, and the non-linear suboptimal multiuser receivers.

Linear receivers such as the decorrelating receiver were first proposed in [19, 20] and extensively analyzed by Lupas in [18, 21]. These receiver structures were extended to the linear minimum mean square error (MMSE) receiver in [22]. Nonlinear subtractive interference cancellation receivers such as successive interference cancellation receivers, parallel interference cancellation receivers, and zero-forcing decision feedback receivers are some of the widely known suboptimal receivers in the literature [23]. Recent research has focused on a search for a multiuser receiver whose complexity grows at most linearly with the number of users, without sacrificing substantial performance improvement over conventional MF detection. The parallel interference cancellation and successive interference cancellation techniques offer this kind of performance and complexity. The practical implementations of these receivers are underway. We will present more analysis about those receivers throughout the dissertation.

3.2.3 Decorrelators

The decorrelator is a linear multiuser detector and as its name implies, the receiver seeks to undo the various inter-user correlations so as to isolate users from one another. It functions by applying a linear transformation to the set of MF outputs. This decorrelation is carried out by computing the spreading code waveform cross-correlation values shown in (3.8), storing these in a $K \times K$ matrix, and multiplying the inverse of this matrix by the vector of MF outputs from the first stage. The most important advantage of this receiver is that it does not require the knowledge of signal amplitudes and is completely insensitive to the near-far effect. The decorrelator is optimal according to three criteria: near-far resistance, least-square, and ML when the received amplitudes are unknown. In general, the decorrelator provides substantial performance and capacity gains over the conventional receiver, however, it has many drawbacks (as discussed below) and as a result is not widely used. A block diagram of this receiver is shown in Fig. 3.2. Here, \mathbf{R} is the cross-correlation matrix for an equivalent synchronous problem and its elements are given in (3.8).

This matrix is time varying as users enter and leave the system, thereby making updates on such a large matrix expensive. Furthermore, this correlation matrix needs to be inverted, raising the issue of singularity. The decorrelator relies upon accurate

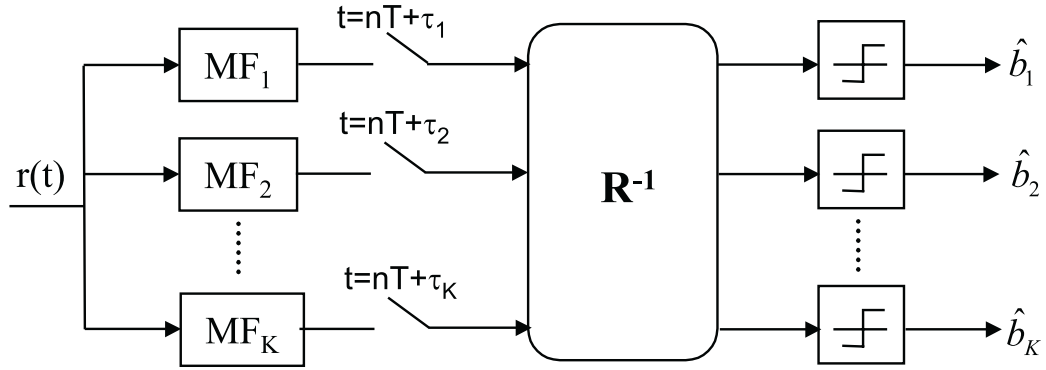


Figure 3.2: Block diagram of a decorrelating receiver.

spreading code correlation values, and if the inverse correlation matrix becomes unstable or undefined, then the detector ceases to function adequately. Of concern as well is noise enhancement produced by the decorrelation operation, rendering decision statistics more noisy.

The output of the MF is given by

$$\mathbf{y} = \mathbf{R}\mathbf{W}\mathbf{b} + \mathbf{n}, \quad (3.20)$$

where, \mathbf{W} is a diagonal matrix with the received signal energies from each user on the diagonal, \mathbf{b} is the information sequence, and \mathbf{n} is white Gaussian noise. For any linear detector, the i th bit estimate of user k can be found from

$$\hat{b}_k(i) = \text{sgn}[\mathbf{p}^T \mathbf{y}], \quad (3.21)$$

where \mathbf{p} characterizes the detector. For a decorrelating receiver, this is given by

$$\mathbf{p} = \mathbf{R}^{-1}. \quad (3.22)$$

It is shown in [18] that this detector approaches the near-far resistance of the optimum detector in an AWGN channel. As can be seen in (3.8), the cross-correlation matrix is independent of signal energies and thus the decorrelator does not need information about received signal energies, which is a significant benefit. It can be decentralized in the sense that the demodulation of each user can be implemented independently.

To improve the performance of the decorrelator when decoding weaker users, a decorrelating decision-feedback detector was introduced in [24] for a synchronous CDMA system in an AWGN channel. The receiver ranks users in descending order

of received estimated energies, but now the decisions of stronger users from previous stage are used in the decision process for the next stage. Thus, knowledge of stronger users is used to improve the performance of the weaker users. This structure is similar to the successive interference cancellation discussed next, although the emphasis is on optimizing the receiver filter structures. This structure outperforms the decorrelator, although the gains are most significant for the weakest users. A significant drawback is that the estimate of each user's power level is now strictly required by the decision-feedback process.

3.2.4 Linear Minimum Mean-Square Error (MMSE) Receivers

This receiver, originally proposed in [25], corresponds to the linear transformation of the MF outputs $\hat{\mathbf{b}} = \mathbf{M}\mathbf{y}$, where \mathbf{M} is chosen to minimize the mean-square error between the vector of the transmitted bit and the one estimated via the linear transformation $E\{\|\mathbf{b} - \mathbf{M}\mathbf{y}\|^2\}$. The decorrelator performs badly when all interfering users are very weak. The linear MMSE receiver has the knowledge of the received amplitudes of every active user in order to obtain linear multiuser detection that outperforms the decorrelator. The linear MMSE receiver replaces the inverse correlation matrix \mathbf{R}^{-1} of the decorrelator by the matrix $\mathbf{M} = [\mathbf{R} + (N_0/2)\mathbf{W}^{-2}]^{-1}$, [26]. The operation of the MMSE detector can be viewed as offering a balance between interference suppression and noise enhancement. If one interfering user or noise level dominates, then this receiver approaches the performance of the conventional MF receiver. On the other extreme, as the noise level tends to zero, this receiver approaches the decorrelator. Therefore, the asymptotic multiuser efficiency and the near-far resistance of the linear MMSE receiver are the same as those of the decorrelator. Fig. 3.3 shows a block diagram of the linear MMSE detector.

In the asynchronous case, the MMSE has a discrete time transfer function given by [26]:

$$\left[\mathbf{R}^T [1] z + \mathbf{R} [0] \frac{N_0}{2} \mathbf{W}^{-2} + \mathbf{R} [1] z^{-1} \right]^{-1}. \quad (3.23)$$

This transfer function is non-causal and has an infinite length response. It can however be realized by truncating the observation window to a length that causes minimum degradation.

An advantage of the MMSE receiver is that the linear transformation \mathbf{M} always exists even when \mathbf{R}^{-1} is singular. As long as the noise is low, there is little point in

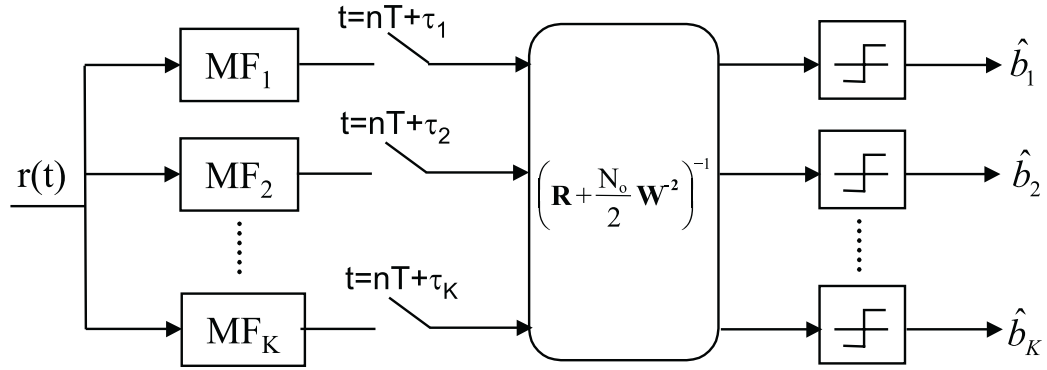


Figure 3.3: Block diagram of a MMSE detector.

incurring additional complexity over the decorrelating receiver required by the need to know received amplitudes. However, the MMSE receiver lends itself for adaptive implementation. This implementation requires information about the desired user, depending on the algorithm and the channel, but does not require the information about the interfering users. This results in the complexity reduction of the receiver with a penalty for the performance improvement. In some cases, these receivers have similar structures to the MF receivers, the only difference being that their filter weights are adaptive.

Generally, multiuser receivers can be viewed as multi-input multi-output (MIMO) structures, but the adaptive implementation of the MMSE receiver can be considered as a single-input single-output (SISO) structure. When the LMS or normalized LMS is used for adaptation, convergence speed depends on the eigenvalue spread. Convergence speed thus suffers degradation in near-far situations and the loading of the system. The adaptive MMSE receiver is limited to systems having short spreading codes, because longer spreading codes require a larger number of taps for the filter, which delays convergence and increases MSE. Blind demodulation is possible using similar principles to those used in linearly constrained minimum variance filtering [27]. In [28], a canonical representation of linear multiuser detectors consisting of a sum of two orthogonal components, one of them chosen as the signature sequence of the desired user, is used to demonstrate that MMSE demodulation is equivalent to minimum output variance detection. Since minimization of the variance at the output of the receiver does not require knowledge of the transmitted data, anchored blind adaptation becomes possible. Adaptive MMSE receiver based on stochastic

gradient techniques, using fractionally spaced structures for fading channel have been proposed in [29]. In Chapter 4, we will compare the performance and complexity of an adaptive MMSE receiver with those of the subtractive interference cancellation receivers.

3.2.5 Subtractive Interference Cancellation Receivers

These receivers are also known as decision-oriented multiuser receivers. The principal idea is to subtract the interference from the received signal, thereby creating the residual signal that is approximately free of interference. Intuitively, if all of the multiple access interference can be perfectly cancelled, the performance of the receiver will be identical to that of a conventional receiver in a single-user system and the receiver will have a near-far resistance of one. In practice, the interference cannot be cancelled perfectly and the efficiency will be somewhat less than one. A major drawback to these techniques is that the performance improvement is dependent upon being able to accurately estimate each user's received power level. There are two main approaches to subtractive interference cancellation: successive interference cancellation and parallel interference cancellation.

3.2.6 Successive Interference Cancellation Receivers

The successive interference cancellation approach was proposed by Viterbi in [30] for coded systems. This approach is based on the idea that if a decision has been made about an interfering user's bit, then that interfering signal can be regenerated at the receiver and subtracted from the received waveform. The performance of this technique depends on the reliability of these tentative decisions made internally by the demodulator. Once the subtraction is completed, the receiver takes the optimistic view that the resulting signal contains one fewer users and the process can be repeated with another interfering user until the desired user has been demodulated. In its simplest form, successive cancellation uses the decision by the correlation receiver, ignoring the presence of interference.

As we mentioned, the motivation behind this receiver is to minimize the complexity for practical implementation of a CDMA system. Since erroneous decisions about interfering signals affect the reliability of all successive decisions, the order in which users are demodulated affects performance. As a result, the system operates

by subtracting users in descending order of received power levels. However, this is not necessarily optimum since it fails to take into account the cross-correlations among users. A sensible alternative is to order users according to the average value of the correlations over n bits (the value of n must be set according to the channel to ensure that the received power ranking does not change over those n bits). A block diagram of this approach is illustrated in Fig. 3.4. The receiver outperforms the conventional receiver, but performs best when there is some degree of variance in the received power levels. The BER decreases as the variance of user powers rises from zero (perfect power control), and then begins to increase again after the powers vary to a greater degree [31]. This suggests that some variation in power levels is beneficial for this receiver architecture, as it allows the stronger users to be decoded well (because of the reduced MAI from the weaker users) and therefore allows their signals to be cancelled effectively. If the power levels become too disparate, however, the weak users cannot be estimated properly due to noise from imperfect cancellation. The following features should be noted regarding the implementation of successive cancellation.

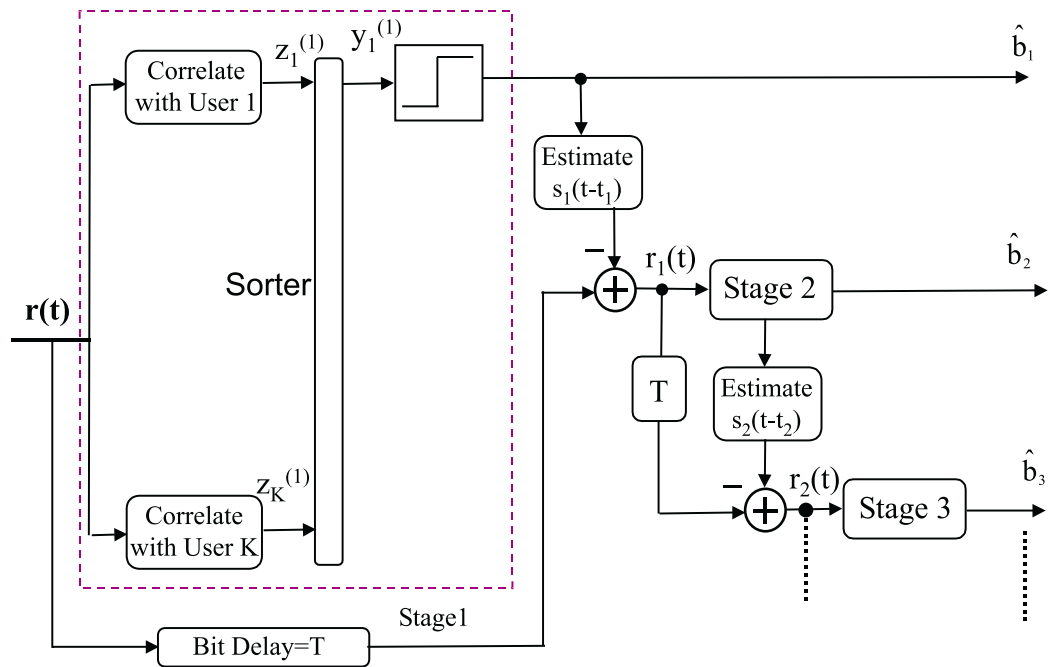


Figure 3.4: Block diagram of a successive interference cancellation receiver.

- Successive cancellation requires the knowledge of the received amplitudes. The

error in the decisions translate into noise for succeeding decisions.

- The demodulation delays grow with the number of interfering user needed to be cancelled.
- The computational complexity per bit is linear with the number of users.
- Users weaker than the user of interest are neglected.
- No arithmetic computations more complicated than correlation and addition/subtraction are required.
- Successive cancellation can be applied to any multiple access channel where the receiver observes the additive superposition of the transmitted signals.
- The BER performance due to a strong interfering user approaches that of no interfering user.
- The residuals may be approximated as independent Gaussian sources.

Patel and Holtzman developed BER expressions for uncoded systems in [31]. A modification to the successive cancellation technique is to base the cancellation process upon Walsh transforms [32, 33], such as those used in IS-95 cellular CDMA system. The idea is still to successively cancel interfering user from the strongest to the weakest, but the cancellation is now accomplished via the use of Walsh Transform. A given user is cancelled by taking the Walsh Transform, nulling out the corresponding bin in the Walsh spectrum, and then reconstructing the signal via the Inverse Walsh Transform.

3.2.7 Parallel Interference Cancellation Receivers

An alternative to the successive cancellation schemes is parallel cancellation, in which estimates are made simultaneously for all interfering users, and then subtracted from the received signal. This may be repeated for multiple stages to gain better estimates of the interference, giving rise to the term *multistage* receiver. One technique was proposed by Varanasi and Aazhang in [34] using correlation receivers, where an expression for the BER of a two-stage receiver was also obtained. An alternative approach is presented in [35] using adaptive filters, where a BER expression is obtained when the filters are in a steady state (although simulations showed that for noisy,

time-varying channels, stable convergence of the filter tap coefficients was difficult to obtain).

The receiver used for this dissertation is based upon the structure proposed in [34]. A block diagram of a two-stage receiver is shown in Fig. 3.5. The first stage is just a bank of single-user correlation receivers. The only difference is that a hard-bit decision is not made at this point. At the beginning of the second stage, an estimate is made of each user's received signal. These estimates are then subtracted from the received signal. The desired user's signal is then added back into this residual signal, and the signal is again passed to a correlator. The complexity per demodulated symbol is shown to be linear with respect to the total number of users K while maintaining an excellent performance for most practical cases.

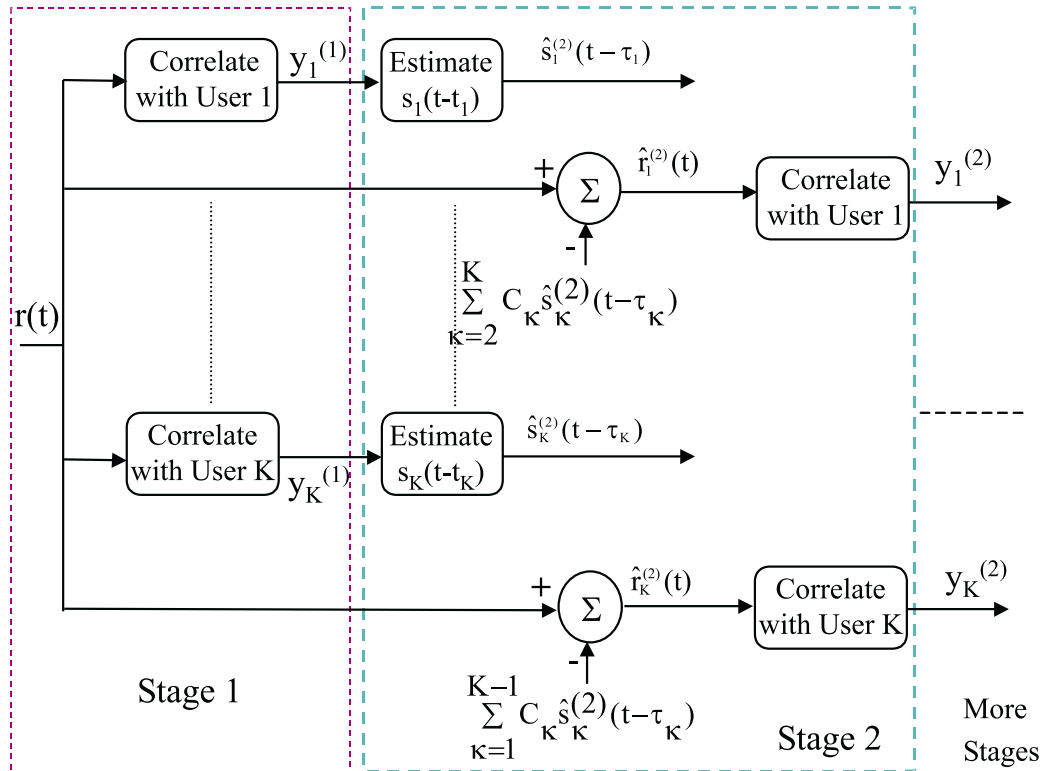


Figure 3.5: Block diagram of a multistage parallel interference cancellation receiver.

There have been significant research effort dedicated to deriving the analytical expressions for various performance criteria of this receiver [36, 37, 38]. Based on these results, some of the important expressions are presented for our interest. Closed form expressions have been derived for BER using the Gaussian approximation for

MAI in [39, 37] in the case of AWGN channel, which (assuming we are decoding user 1) is given at stage $q + 1$ by

$$P_b^{(q+1)} = Q \left\{ \left[\frac{1}{2(P_1 T / N_o)} \left(\frac{1 - \left(\frac{K-1}{3N}\right)^{q+1}}{1 - \left(\frac{K-1}{3N}\right)} \right) + \left(\frac{1}{3N}\right)^{q+1} \right. \right. \quad (3.24)$$

$$\left. \left. \left(\frac{(K-1)^{q-1} - (-1)^{q+1}}{K} \left(\frac{\sum_{k=2}^K P_k}{P_1} + 1 \right) + (-1)^{q+1} \right) \right]^{-1/2} \right\},$$

where there are K total active users in the system, P_k is the power level of the received signal from user k , the Gaussian noise has two-sided power spectral density $N_o/2$, and N is the processing gain of the CDMA system. For a receiver with infinite stages ($q = \infty$), if $(K - 1)/3N < 1$, this reduces to

$$\lim_{q \rightarrow \infty} P_b^{(q+1)} = Q \left\{ \left[2(P_1 T / N_o) \left(1 - \left(\frac{K-1}{3N}\right) \right) \right]^{1/2} \right\}. \quad (3.25)$$

The Gaussian approximation is known to be optimistic under certain conditions [40], particularly for low BER and low number of users. The Gaussian approximation also assumes that no single interfering user dominates the performance of the overall system. If one interfering user is not cancelled effectively in a multistage system, that user may dominate the interference and the Gaussian approximation may be increasingly less accurate. An improved form of the Gaussian approximation was first introduced in [40] for CDMA system without interference cancellation, and a further simplified (but still accurate) approximation in [41]. This was further modified by Liberti in [42] to allow for disparate received power levels (whether random or constant). Buehrer [36] applied this form of the improved Gaussian approximation to develop a more accurate expression for BER in a multistage receiver.

The cancellation process can actually increase the noise in the multiple access interference if a user's received power falls below a certain threshold [39, 37]. This occurs because an accurate estimate of the received signal cannot be obtained and the ineffective cancellation increases the overall noise. The technique of *selective* cancellation has been introduced to cancel only those users whose received powers are above a set threshold. For the AWGN channel, it is only beneficial to cancel the interference from user k if the received power P_k is given by [38]

$$P_k > \frac{N_o}{2T} + \frac{1}{3N} \sum_{j=1, j \neq k}^K P_j. \quad (3.26)$$

In a cellular CDMA system, a large amount of MAI comes from out-of-cell interference [43, 44]. These interfering users are often received with low powers due to the longer distances from the base station. While attempting to cancel all users improves the BER over using traditional receivers, even lower BER can be achieved by selectively canceling the interfering users. It is shown in [43] that the average received power estimate over several bit periods can improve the estimate if the power does not change significantly during that time. In Chapter 4, we will adopt selective interference cancellation and bit-averaging in IC for our peer-to-peer system.

In [45], the concepts of a Rake receiver and a multistage receiver are combined. By replacing the bank of correlation receivers with a bank of Rake receivers, the multistage architecture can be used to combat fading and MAI in a multipath environment.

3.3 Computational Complexity

The exponential complexity of the optimal multiuser receiver necessitates the use of practically implementable suboptimal receivers. One of the main factors that influence the selection of a multiuser receiver for practical implementation is complexity. In this section, we present computational complexities of several multiuser receivers in terms of the asymptotic time complexity per bit decision (TCB). TCB corresponds to the time required by the decision algorithm to select the received sequence divided by the number of transmitted bits (as the number of transmitted bits tends to infinity) [17].

The optimal receiver for asynchronous CDMA channels in AWGN is a maximum-likelihood sequence estimator. In [19], by deriving the relationship between the observation vector and the transmitted symbols in an asynchronous DS-SS-CDMA system, and noting that this relationship is analogous to the input-output relations of a linear finite-state machine corresponding to a rate 1 convolutional encoder, the author hypothesized that an optimal receiver could be implemented as a maximum-likelihood sequence estimator with 2^{2K} states and $O[8^K]$ time complexity per bit. In [17], the complexity is reduced by utilizing the fact that every user's symbol only overlaps with two symbols of every other user in the system. This fact results in the triple-diagonal structure of the matrix R , and simplifies sequential computation of the log-likelihood function. In this case, the number of states are 2^{K-1} and thus the TCB is $O[2^K]$.

Most of the linear detection techniques involve a solution of a linear system of equations. In a naive implementation of those receivers, this requires $O[n^3]$ TCB, where n is the size of the matrix to solve the linear equations. In linear multiuser detection, the main problem is to find practical algorithms. The linear receivers require some form of matrix inversion, which needs $O[n^3]$ TCB, where n is size of the code-correlation matrix. The simple MF detection requires $O[4KL]$ TCB, where KL is the number of users times number of multipath components. Implementation of a decision feedback detector involves ordering of the users according to their received energies, generation of the forward filter using a Cholesky decomposition of the matrix R , and an inversion of the resulting triangular matrix plus forward/feedback filtering. The combination of all these involved tasks translates into an $O[11(KL)^3]$ TCB [46]. In all these implementations, the computational load is huge, since it has cubic dependence on the number of users times the number of multipath components. Iterative algorithms, such as steepest descent and conjugate gradient algorithms, were proposed for decorrelating and LMMSE receiver implementations [46]. These algorithms reduce the complexity to $O[(KL)^2]$, but the performance suffers. Iterative techniques for inversion of the tri-diagonal decorrelating matrix having a complexity of $O[(KL)^2]$ per iteration have been proposed in [46].

The authors of [47] propose complexity reduction schemes of a linear suboptimal multiuser receiver in fading environments by exploiting the properties of the correlation matrix. Generally, the complexity of a linear multiuser detector is in the $O[(KL)^3]$, where KL is the size of the correlation matrix of the signature codes. By using a rotation matrix, the correlation-matrix size is reduced from KL to K . Then the properties of the correlation matrix, which is also a block-Toeplitz matrix, are used to reduce the complexity from cubic form to $O[K^2] + O[K \log N]$, where N is the number of bits considered in a block. Two algorithms are suggested: Fourier Algorithm and Kronecker Algorithm. The Fourier Algorithm has a complexity of $O[K^2] + O[K \log NK]$ and the Kronecker Algorithm has the lowest complexity of $O[K^2] + O[K \log N]$.

Direct implementation of the MMSE receiver faces the same complexity limitations encountered by the decorrelator. However, the MMSE can be more readily computed based on adaptive algorithms that avoid direct matrix inversion [48]. The complexity of the adaptive MMSE receiver is independent of the number of users in the system. A blind adaptive technique that does not require training sequences and requires as little information as the conventional receiver has been derived in

[28]. The moderate complexity of the gradient adaptation algorithm together with the advantages of blind adaptation make this approach attractive.

The computational complexity of the subtractive interference cancellation has a linear dependence on the number of users. There is no complex algorithm involved in the bit estimations. The main operations are addition, subtraction and multiplications. There are three main phases of operations involved in PIC. They are the correlation of the received signals with the locally generated spreading codes and bit estimations, regeneration of the signals, and the interference cancellation. For a q stage PIC, the TCB requirement is $O[8KLq]$, [49]. One advantage of the PIC receiver is that the computational complexity can be shared among the active users in the system. The TCB in SIC is very similar to TCB in PIC. In Chapter 4, we will compare the TCB of these subtractive interference cancellation receivers with that of the adaptive MMSE receiver.

3.4 Chapter Summary

CDMA systems are inherently interference limited, resulting in problems with capacity and the near-far problem when conventional correlation receivers are employed. Multiuser receivers allow structured interference to be modeled and removed, resulting in overall better performance. The optimal multiuser receiver treats CDMA reception as a sequence detection problem, and significantly improves performance, albeit with prohibitive complexity. A number of suboptimal multiuser receivers with excellent performance have been described in this chapter. These techniques have been applied to date primarily within the context of base station receivers. In the next chapter we focus on how interference cancellation might be applied within mobile nodes of peer-to-peer communication system.

Chapter 4

CDMA Detection for Peer-to-Peer Packet Radio

The performance of DS-SS in packet radio networks suffers from the near-far problem. This near-far problem can be alleviated by using either a multiuser receiver or a single-user adaptive receiver along with centralized or distributed power control. This chapter focuses on two issues: how interference cancellation might be applied in peer-to-peer communications systems, and the performance of single-user adaptive and multiuser receivers for DS-CDMA in peer-to-peer packet radio networks.

First, this chapter introduces a model for peer-to-peer communications using simple subtractive interference cancellation techniques which require cancellation of only a few dominant interferers. These techniques include both parallel multistage interference cancellation and successive interference cancellation. The performance of interference cancellation depends on the desired user power, the variation of interfering users' signal strength and the power of the strongest interfering signal. The system performance is evaluated for various spatial arrangements of interferers, and for different loading conditions. Simulation results are presented for these two subtractive interference cancellation techniques considering various factors such as amplitude estimation and partial cancellation factor.

Second, this chapter compares the feasibility of using a multiuser receiver based on the selective parallel or successive interference cancellation technique with a single-user adaptive receiver in a peer-to-peer packet communication environment. The

performance of an N tap chip-rate linear adaptive receiver (CHRT-LAR) with normalized least-mean square algorithm (NLMS) is analyzed. For the single-user adaptive receiver, one user's spreading code and delay is known at the receiver, whereas the multiuser detector requires knowledge of the spreading codes and delays of all the users producing significant interference. To illustrate their potential for ad hoc networks, the BER performance and complexity of these two detection schemes are compared in this chapter.

4.1 CDMA Multiuser Detection for Peer-to-Peer Packet Radio

In both military and commercial communications, robust performance of multimedia communications is required. A common challenge of military communications is to furnish personnel with communications capability in the form of data, voice and video in a secure and robust environment. Packet radio networks have been widely used for this purpose. The combination of packet radio networks and spread spectrum technology can exhibit robust performance for military applications [50]. DS-SS is often preferred to FH-SS in a cellular environment, but in a peer-to-peer network, precise power control is difficult, leading to near-far problems when DS-SS is used in conjunction with multiple access. In this section, we explore the plausibility of using a multiuser receiver to alleviate the near-far problem for DS-SS packet radio networks. Multiple access capability, capture, multipath resistance and soft capacity limit are the key features of spread spectrum in packet radio networks. Usually, FH-SS is used in packet radio networks since DS-SS suffers from the near-far problem. Gass and Pursley [51] compared the performance of FH-SS and DS-SS systems for a wideband frequency-selective fading channel. Torrieri [52] described FH-SS as a potential candidate over DS-SS for future army communications by illustrating the limitations of the near-far problem and by showing the flexibility of the FH-SS in communication networks. However, FH-SS suffers from many implementation difficulties including synchronization with each frequency hop, and an easily identifiable spectrum.

Conventional correlation receivers do not exploit the structure of CDMA because they treat multiple-access interference (MAI), which is inherent to CDMA, as if it were additive noise. Furthermore, if the combined contribution of interfering users surpass the signal magnitude due to the desired user, the interference will dominate

the performance in a correlation receiver because of the near-far problem. When the power ratio of strong to weak signals approaches or surpasses the processing gain of the DS-SS system, correct detection of the weaker signals becomes problematic for a conventional CDMA receiver. Since CDMA capacity is interference limited, any reduction in interference converts directly into an increase in the capacity. CDMA performance can be significantly improved by multiuser receivers, which compensate for MAI.

The implementation of multiuser receivers can be very complex, especially without prior knowledge of channel conditions, received signal energy and the propagation delay [17]. The implementation of multiuser receivers in these environments is referred to as adaptive multiuser detection or adaptive interference cancellation. Furthermore, the near-far situations which arise in packet radio networks may be due to only one or two significant interferers. Thus, simple multiuser techniques which cancel only one or two strong interferers may be effective. In multistage interference cancellation, interference is cancelled in stages and the decision made in any stage, can be used either to make a final decision on the data or to enhance the signal through interference cancellation, which leads to another stage of detection [34]. In packet radio networks, power control can be used to reduce the near-far problem to some extent and multiuser detection can be deployed for improved performance of the system. Systems combining these two techniques manifest the potential to achieve robust performance needed for military communication.

The purpose of this section is to present a prototype for packet radio networks and to concentrate the discussion on multiuser detection for reducing the near-far problem. In Section 4.1.1 we develop a simple model for packet radio networks; in Section 4.1.2, we present the analysis for parallel interference cancellation (PIC) and successive interference cancellation (SIC), respectively. Section 4.1.3 describes the path-loss model considered for the system. In Section 4.1.4, we present combined semi-analytical and simulation results for different loading conditions such as heavy loading and light loading and compare these two subtractive interference cancellation schemes. Concluding comments are provided in Section 4.1.8.

4.1.1 Model of Packet Radio Networks

Packet radio networks provide communication between distant users via a radio channel based on packet switching. All data are grouped in packets and launched into

the network, which routes each individual packet through to its destination. In this section, we present a simple model for characterizing the radio links within a packet radio network. A rectangular coordinate system is used to identify the position of a mobile radio (user) in the spatial domain. The position of a user is considered to lie in the first quadrant and its coordinate values (abscissa and ordinate) vary from zero to one. Every mobile radio has the capability to transmit signals to any other user and can receive signals from any other user. The only constraint for traneceiving is the minimum detectable signal power, which is directly related to the transmitter-receiver (T-R) separation of a pair of mobiles. For modeling purposes, we assume that users are distributed uniformly throughout a two-dimensional grid, with ranges from 0 to 2 kilometer (km). We consider 100 users in the system for our prototype. The ON/OFF status of a mobile is controlled by generating a uniform random variable, which varies from zero to unity, and comparing that random variable with a threshold value. By changing the threshold, the system loading status can be chosen, such as heavy loading or light loading. Now, we assume to have a defined number of users in the system.

We generated an m -by- m -by-3 dimensional (3-D) matrix that provides the information about the user position, user ON/OFF status, and the distance from a user to any other user, where m is 100 in our example. Fig. 4.1 shows the system where, out of 100 users, 54 are ON for that instant which is shown by the asterisk. The type shown by a circle is OFF. Each of the 54 transmitters has a designated receiver chosen randomly. Note that if a user needs to be connected with a desired user, but that desired user is out of range from the transmitting user, they can be connected by multiple hops via another intermediate available user. In our example, we assume that the range is 1 km in a 2 km square area. Generally, the maximum range depends on the acceptable interference level of the traneceiving users or the average interference level of the communications systems to maintain the required information quality. From Fig. 4.1, it is clear that one user can receive signals simultaneously from several transmitters but can transmit signals to only one receiver at a particular instant. In other words, the receiver selection is an independent event and by definition, does not depend on any other T-R selection. For a receiver, the specified transmitting user's signal is the desired one and the other 52 users' signals are considered as interference towards the desired user. In the plot, all the T-R pairs are shown where the solid line represents the receiver end and the dashed line denotes the transmitter end.

By setting a threshold for a desired light loading example, we presented a lightly

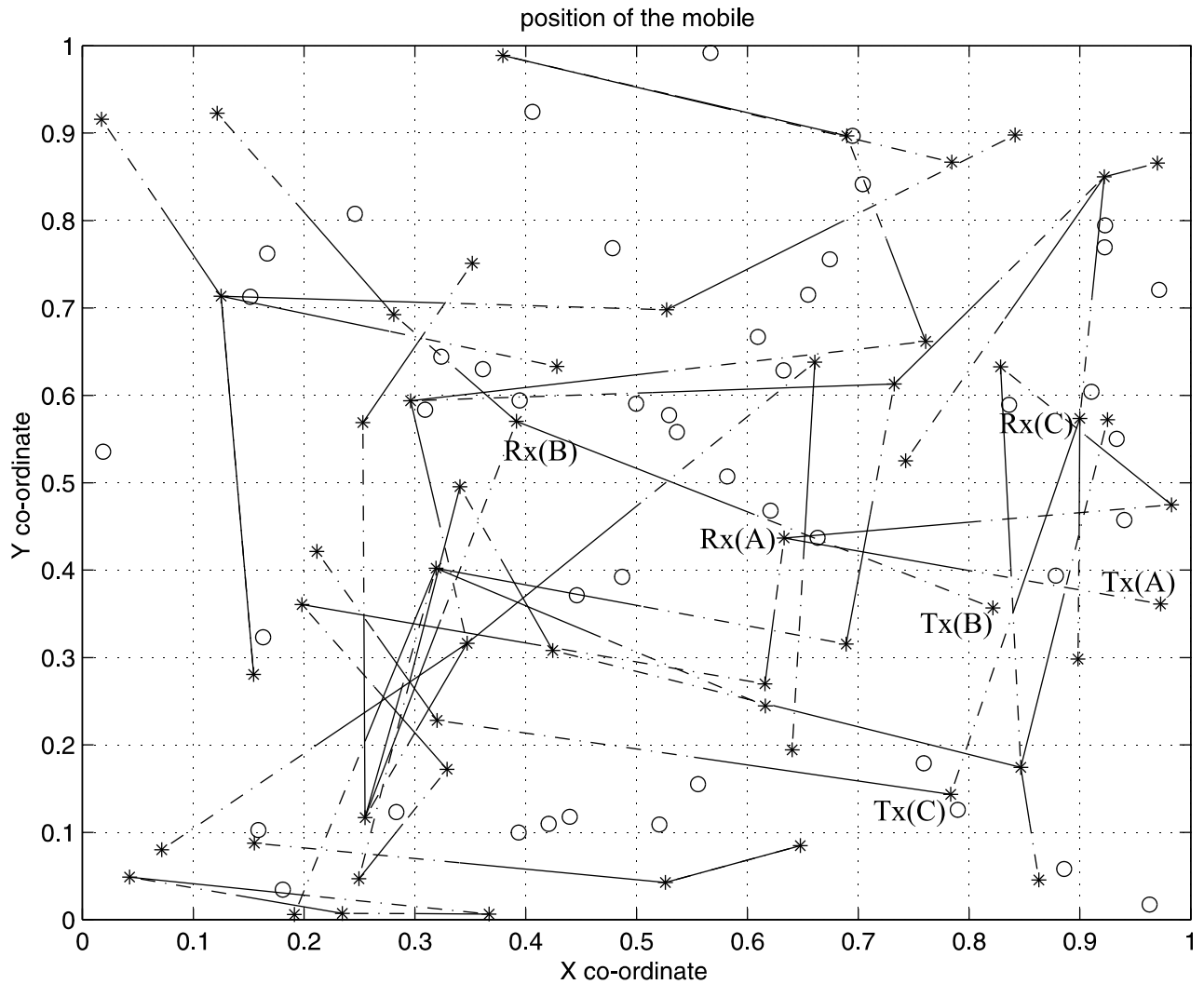


Figure 4.1: Spatial distributions of users at an instant in the packet radio networks represented by the rectangular coordinate system. The symbol “*” denotes that the user’s mobile is ON (54 users), whereas the symbol “o” presents that user’s mobile is OFF. Dashed line is the desired transmitter end and solid line is the designated receiver end for one of the T-R sets active in the network.

loaded system in Fig. 4.2 where out of a total of 100 mobile radios in the system, 15 mobile radios are ON and these are shown by the asterisk. The type shown by the circle is OFF. Each of the 15 transmitters has a designated receiver chosen randomly.

We also express the user density in terms of $users/km^2$. Since we assumed that the area of the described example is $4 km^2$, the user density is $13.5 users/km^2$ for the heavy loading condition where 54 users are ON. The user density is $3.75 users/km^2$ for the lightly loaded system because 15 users are ON in the system. We use the jargon such as *light loading* for user density less than $8 users/km^2$ and *heavy loading* for user density greater than $8 users/km^2$.

4.1.2 Interference Cancellation Models

4.1.2.1 Model for PIC

A method for interference cancellation was presented by Varanasi and Aazhang [34] in which estimates are made simultaneously for all the interferers and then subtracted from the received signal. We use a model for PIC in a DS-SS based on the approach of [37] which builds on [34]. The first stage of this receiver consists of a bank of conventional correlators that are used to generate decision statistics for every i th bit of the k th user. These decision statistics provide the estimate of the user's signal, $\hat{s}_k(t)$. In the next stage, a new estimate for the k th user is formed by taking the received signal and subtracting all $\hat{s}_j(t)$ from it such that $j = 1, \dots, N; j \neq k$. This process may be repeated for an arbitrary number of stages as needed. The key equations of parallel multistage interference cancellation are presented here. There are a total of K users in the system and the k th user transmits a binary data signal. The received signal $r(t)$ is given by

$$r(t) = n(t) + \sum_{k=1}^K \sqrt{2P_k} a_k(t - \tau_k) b(t - \tau_k) \cos(\omega_c t + \phi_k), \quad (4.1)$$

where $n(t)$ is an AWGN process with two-sided power spectral density $N_0/2$, P_k is the transmitted power of user k , τ_k is the random delay of the k th user that accounts for the propagation delay and synchronization offset between the signals and is uniformly distributed on $[0, T]$, and $\phi_k = [\theta_k - \omega_c \tau_k] \bmod 2\pi$, where θ_k is the phase offset of transmitter k . If θ_k is uniformly distributed on $[0, 2\pi]$, then for large frequencies ($\omega_c T \gg 1$), ϕ_k is a random variable with uniform distribution on $[0, 2\pi]$.

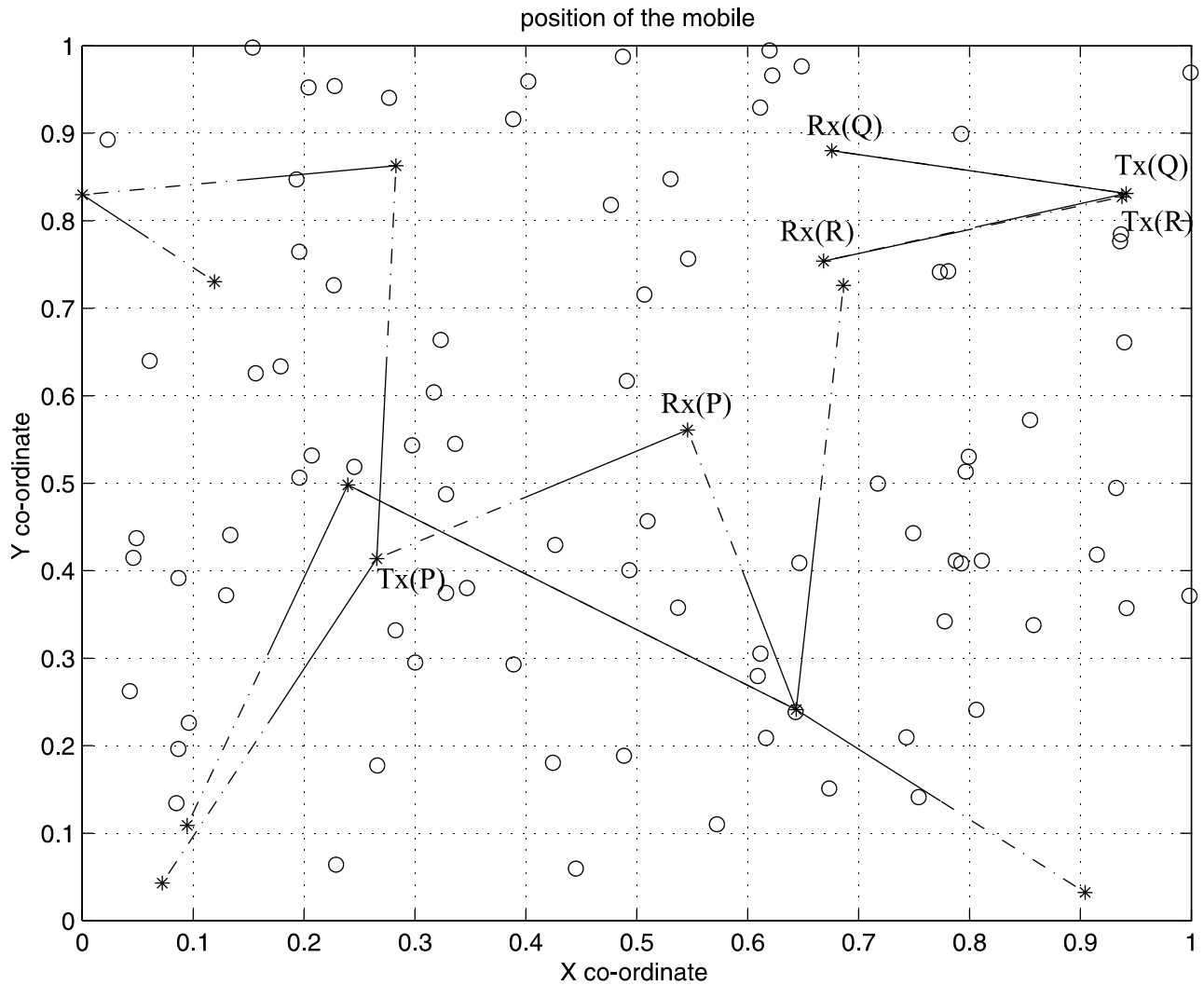


Figure 4.2: Spatial distributions of users at an instant in the packet radio networks represented by the rectangular coordinate system. The symbol “*” denotes that the user’s mobile is ON (15 users), whereas “o” shows that user’s mobile is OFF. Dashed line is the desired transmitter end and solid line is the designated receiver end for one of the T-R sets active in the network.

For channel with multipaths, all resolvable multipath components can be represented by the signal $s_k(t)$ and all unresolvable multipath components can be contained in the noise process $n(t)$. The received signal, $r(t)$ is correlated with a synchronous copy of the spreading signal. Let $y_{k,i}^{(q)}$ be the decision statistic for the i th bit of the k th user at stage q . Then the decision statistic for user k at stage 1 is given by

$$y_{k,i}^{(1)} = \int_{iT+\tau_k}^{(i+1)T+\tau_k} r(t)a_k(t-\tau_k)\cos(\omega_c t + \phi_k)dt. \quad (4.2)$$

If a Gaussian approximation is employed for MAI, then $y_{k,i}^{(1)}$ can be modeled as a Gaussian random variable with expected value

$$E[y_{k,i}^{(1)}|b_{k,i}] = b_{k,i}T\sqrt{\frac{P_k}{2}}. \quad (4.3)$$

All subsequent stages of the receiver perform interference cancellation based on the decision statistics from the previous stage. At stage q of the receiver, the decision statistic $y_{k,i}^{(q)}$ can be used to form an unbiased estimate of the product, $\hat{b}_{k,i}\sqrt{\hat{P}_k}$ where $\hat{b}_{k,i} = y_{k,i}^{(q)}/|y_{k,i}^{(q)}|$ is an estimate of the k th user's data bit. After stage q , we can estimate the k th user signal as

$$\hat{s}_k^{(q)}(t) = \frac{2}{T}a_k(t)\cos(\omega_c t + \phi_k) \sum_{i=-\infty}^{\infty} y_{k,i}^{(q)}p_T(t-iT). \quad (4.4)$$

Interference cancellation is performed by subtracting the estimated signals of the interfering users from the received signal to form a new received signal for the k th user after stage q , given by

$$\begin{aligned} r_k^{(q)}(t) &= r(t) - \sum_{j=1, j \neq k}^K \hat{s}_j^{(q)}(t - \tau_j) \\ &= n(t) + \sqrt{2P_k}a_k(t - \tau_k)b_k(t - \tau_k)\cos(\omega_c t + \phi_k) \\ &\quad + \sum_{j=1, j \neq k}^K [s_j(t - \tau_j) - \hat{s}_j^{(q)}(t - \tau_j)]. \end{aligned} \quad (4.5)$$

The decision statistic for the i th bit of the k th user at stage $q+1$ is formed by correlating $r_k^{(q)}(t)$ with the k th user's signature signal. The Gaussian approximation for MAI is used to derive a closed form expression for BER of the receiver modeled at any arbitrary stage q and the resulting probability of bit error for user k at stage q of the receiver can be computed as [39]

$$P_{b_k}^{(q)} = Q \left[\left(\frac{1}{2(E_{b_k}/N_0)} \left(\frac{1 - \left(\frac{K-1}{3N}\right)^q}{1 - \left(\frac{K-1}{3N}\right)} \right) \right) \right]$$

$$+ \frac{1}{(3N)^q} \left(\frac{(K-1)^q - (-1)^q}{K} \left(\frac{\sum_{k=1}^K P_k}{P_k} \right) + (-1)^q \right)^{-1/2}. \quad (4.6)$$

4.1.2.2 Model for SIC

The SIC scheme takes a serial approach to cancel the interferences of the users where the cancellation is performed on a user by user basis [30, 31]. The users are ranked on the basis of the received powers, which are obtained either from the outputs of the conventional MF outputs or from the separate channel estimates. The former method is known as the soft-decision SIC (SD-SIC) where the joint estimate of the amplitude and information bit of a user is considered without making an explicit data decision. The latter one is named as the hard-decision SIC (HD-SIC), where a separate estimate of the amplitude and the information bit is determined. The cancellation can be performed on a spread signal that requires the regeneration of the wideband signal and the storage of received samples, or despread signal that needs cross-correlation of spreading code. Both methods require the knowledge of the user's spreading code and channel parameters and are equivalent in term of BER performance. In our study, we consider only the cancellation on the spreading signal using SD-SIC. We also assume asynchronous detection, which is realistic for peer-to-peer communications. Since amplitude estimation can be improved by averaging over several information bits [31], amplitude is averaged over 10 bits. After ranking the users, the signal with the largest power is regenerated; then, the regenerated signal is subtracted from the buffered received signal. The remaining signals are now re-estimated and the new largest power user is selected. This process will continue until all the users' signals have been recovered or the maximum allowable number of cancellations is reached.

Since both PIC and SIC receivers are the same up to the first stage of interference cancellation, following all the notations and the Gaussian approximation in the previous section, the decision statistic for the k th user after users 1 through $k-1$ have been removed is

$$y_{k,i} = \int_{iT+\tau_k}^{(i+1)T+\tau_k} r(t) a_k(t - \tau_k) \cos(\omega_c t + \phi_k) dt, \quad (4.7)$$

which is similar to equation (4.2) and $r_k(t)$ is given by

$$r_k(t) = r(t) - \sum_{j=1}^{k-1} \hat{s}_j(t - \tau_j) \quad (4.8)$$

$$= n(t) + \sqrt{2P_k} a_k(t - \tau_k) b_k(t - \tau_k) \cos(\omega_c t + \phi_k) + \sum_{j=1}^{k-1} [s_j(t - \tau_j) - \hat{s}_j(t - \tau_j)].$$

This equation is similar to equation (4.5) in the previous section. The BER for the k th user after users 1 through $k - 1$ have been removed is

$$P_{b_k} = Q \left(\sqrt{\frac{E [y_{k,i} | b_{k,i}]^2}{\text{var} [y_{k,i} | b_{k,i}]}} \right). \quad (4.9)$$

The numerator is the expected value of the decision statistics for a given transmitted bit and is given by

$$E [y_{k,i} | b_{k,i}] = w_{k,i} b_{k,i}, \quad (4.10)$$

where $w_{k,i}$ is the energy associated with i th bit of k th user. The variance of the decision metric can be shown to be [36]

$$\text{var} [y_{k,i} | b_{k,i}] = \left[\frac{N_o T}{4} + \frac{T^2}{6N} \sum_{j=2}^K P_j \right] \left(1 + \frac{1}{3N} \right)^{k-1} - \frac{T^2}{6N} \sum_{j=2}^K \left(1 + \frac{1}{3N} \right)^{k-1} P_j. \quad (4.11)$$

SIC has been shown to be robust to imperfect power control in a DS-CDMA system [31, 53]. Signal estimations of users having higher power are more reliable; if these better estimated signals are cancelled from the received signal, desired user's performance improves significantly. SIC is considered one of the simplest forms of interference cancellation because of the single stage of cancellation. However, the processor performing the cancellation, must perform all the cancellations while maintaining the necessary data rate. Note that for parallel cancellation, the computational complexity is high but the computational burden can be distributed among all the participating users. Estimating the power of the user is fairly straightforward in a coherent DS-BPSK system. Here, we have the knowledge of the amplitudes and phases of the users' signal and can reconstruct a good estimate of the signals for cancellation. In our peer-to-peer communication model, a noncoherent reception would force the receiver to use the output of the correlators as the only statistics for regenerating the signal.

4.1.3 Path-loss Model

For our example, we assume that each transmitter sends signals of equal power. Each signal is attenuated by propagating through the channel, and the magnitude of

attenuation depends on the T-R separation; thus, the users deliver unequal powers at the receiver. We examined two path-loss models. First, we considered an exponential path-loss model. Generally, the exponent varies from two to four; we chose 3.2, which was consistent with the experimental path-loss model for outdoor environment with moderate cell size. We also considered a second path-loss model which made use of the Fresnel zone or break-point. We adopted the double-regression method described in [54] where the path loss as a function of distance d is given by

$$\alpha(d) = \begin{cases} f_1(n_1, d) + f(d_0), & d_0 < d < d_f \\ f_1(n_1, d) + f_2(n_2, d, d_f) + f(d_0), & d > d_f \end{cases} \quad (4.12)$$

where $f_1(\cdot)$, $f_2(\cdot)$ and $f(\cdot)$ are functions defined in [54] and d_f is the distance at which the first Fresnel zone becomes obstructed and is a function of antenna height and operating frequency. We assume that the transmitting and the receiving antenna had the same height of 1.7 meter, and the operating frequency was 300 MHz. The variable d_0 is the reference distance, which depends on the specific channel environment, and n_1 and n_2 are the mean path-loss exponents inside and outside of the first Fresnel zone, respectively. We chose $n_1 = 2$ and $n_2 = 4$ for our calculation. Note that this model depends on the polarization of the signal, and we assume transverse magnetic (TM) polarization. Our simulation study showed that the model incorporating a break-point offered a better system performance in terms of BER than the exponential path-loss model in every case. In that respect, the exponential path-loss model is more conservative. Also, the break-point model is not valid for transverse electric (TE) polarization component of the signal if the reflected angle goes below the Brewster angle. Thus, the plots shown in the next section were obtained using the exponential path-loss model, and comments are provided when there is a significant difference between the results using these two models.

4.1.4 Results and Comparison

4.1.4.1 Heavy Loading

We considered three receiver-transmitter sets A , B and C for the heavily loaded system shown in Fig. 4.1. Each receiver is identified by its rectangular coordinates and their corresponding values are presented in Table 4.1. We picked these three T-R sets on the basis of the receiver distance (distances) from the dominant interferer. For example, the distance of the dominant interferer from the receiver Rx(A) in Set

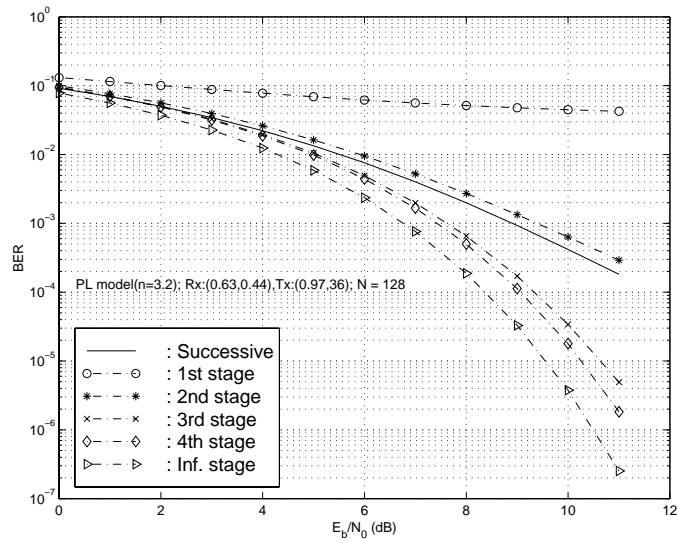
A has the largest value while that from $R_x(C)$ in Set C has the least value among the three cases. The position of the receiver was an additional factor for considering a set in the spatial domain.

Table 4.1: Selected receiver-transmitter sets shown in Figs. 4.1 and 4.2, and their corresponding parameters.

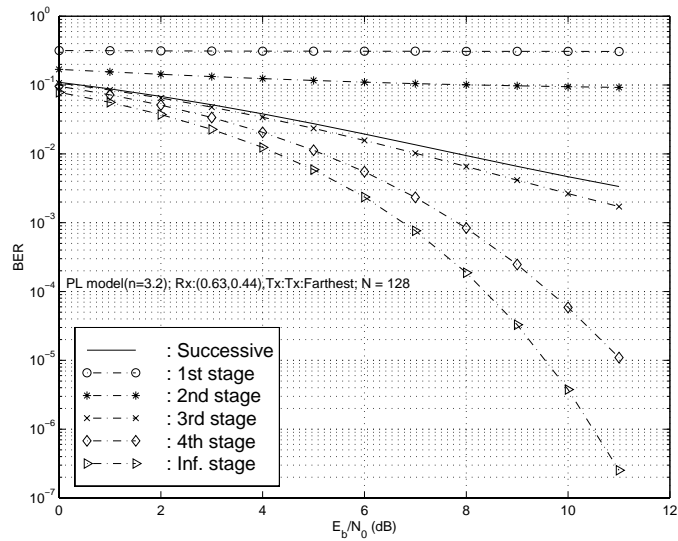
Loading	T-R Set	Coordinate Values		T-R Separation
		R_x	T_x	d
Heavy	A	(0.63,0.44)	(0.97,0.36)	0.35
	B	(0.39,0.57)	(0.82,0.36)	0.48
	C	(0.90,0.57)	(0.78,0.14)	0.45
Light	P	(0.55,0.56)	(0.27,0.41)	0.34
	Q	(0.68,0.88)	(0.94,0.83)	0.26
	R	(0.67,0.75)	(0.94,0.83)	0.28

After choosing one of these three T-R sets in a MAI environment, we evaluated the performance of the receiving user in terms of BER using semi-analytical results presented in the previous sections for parallel and successive cancellations. First, we considered the chosen transmitting user, which is the desired user of the receiver - receiving user- and randomly selected for the receiver as described previously. Next, we looked into the two extreme conjunctures, the nearest desired transmitting user and the farthest desired transmitting user. Note that the spatial distribution of the active users is unchanged for these three cases. We considered an AWGN channel and BPSK modulation; the processing gain N was 128. We assume that 10^{-4} is the maximum allowable BER at 10 dB E_b/N_0 for quality of service unless we do not specify any other value.

Fig. 4.3(a) shows the calculated BER versus E_b/N_0 of the desired user for T-R Set A , where there are 54 users in the system. From the plots, it is evident that a two-stage (one stage interference cancellation) receiver yields substantial performance improvement over the single-stage (MF) receiver. The interference cancellation from the third stage cancellation is insignificant and is close to the asymptotic value. So, more stages of interference cancellation will not pay off in significant performance improvement. By comparing the performance improvement using parallel and successive cancellation, successive cancellation achieves BER slightly better than one stage parallel cancellation.



(a) For user Set A { Rx(0.63,0.44), Tx(0.97,0.36)} shown in Fig. 4.1



(b) For the Receiver (0.63,0.44) ∈ A shown in Fig. 4.1 and the transmitter is located farthest among all the active 53 candidate users

Figure 4.3: BER of the desired user as a function of E_b/N_0 for AWGN channel using parallel interference cancellation and successive interference cancellation, respectively. The exponential PL model is used ; the system is heavily loaded with 54 users are ON.

Now, let us consider that the desired transmitting user is located farthest among all candidate 53 users from the receiver Rx(A), where $Rx(0.63, 0.44) \in A$ is shown in Fig. 4.1. Fig. 4.3(b) exhibits the BER of the desired user against E_b/N_0 for this case. Since the desired transmitter is located farthest from the selected receiver Rx(A) in the spatial domain, the desired signal is the weakest one among all signals to the receiver Rx(A). In this case, more stages of interference cancellation are required for the detection of the desired signal. We found that the path-loss model played a greater role if the desired signal was weaker than any interfering signal; for example, two stages of interference cancellation will be required if we would use the path-loss model considering the break-point. Fig. 4.3(b) shows that we need three stages of interference cancellation to get the performance using the exponential path-loss model. Successive cancellation shows better performance than one stage parallel cancellation, but the BER achievement is not sufficient for quality detection.

We also simulated the system for the receiver-transmitter Set B . Notice from Fig. 4.1 that there are three interferers situated near the receiver Rx(B) in this set and each of them has smaller distance from the receiver Rx(B) than the distance of the nearest interferer from the receiver Rx(A) in receiver-transmitter Set A . As a result, the BER performance of the desired user (Rx(B)) should degrade substantially, which we found from our simulation.

Next, we consider the worst case scenario, Set C , where the desired transmitter is located farthest from the selected receiver in the spatial domain; there is an interfering user very close to the receiver Rx(C) and the desired signal is the weakest one. Fig. 4.4 shows the BER plots for the desired user ($Rx(C) \in C$). As expected, these plots show the worst performance because the receiver faces the strongest interference if we consider all cases. In addition, the desired signal is the weakest one. Thus, it is obvious that no interfering user can be closer than a certain distance from the receiver; otherwise, no other user can transmit to that receiver. This minimum distance of the interferer depends on the loading of the system, BER requirement, desired user location and channel environment. More than three stages of PIC are required for signal detection which is almost impractical. Successive cancellation does not provide enough improvement either. We also simulated the system for the other extreme, i.e., the desired transmitter is the nearest one. From our observation, we found that one-stage of interference cancellation was enough or no interference cancellation was needed for the case of the receiver Rx(C) in Set C where transmitter is very close to it.

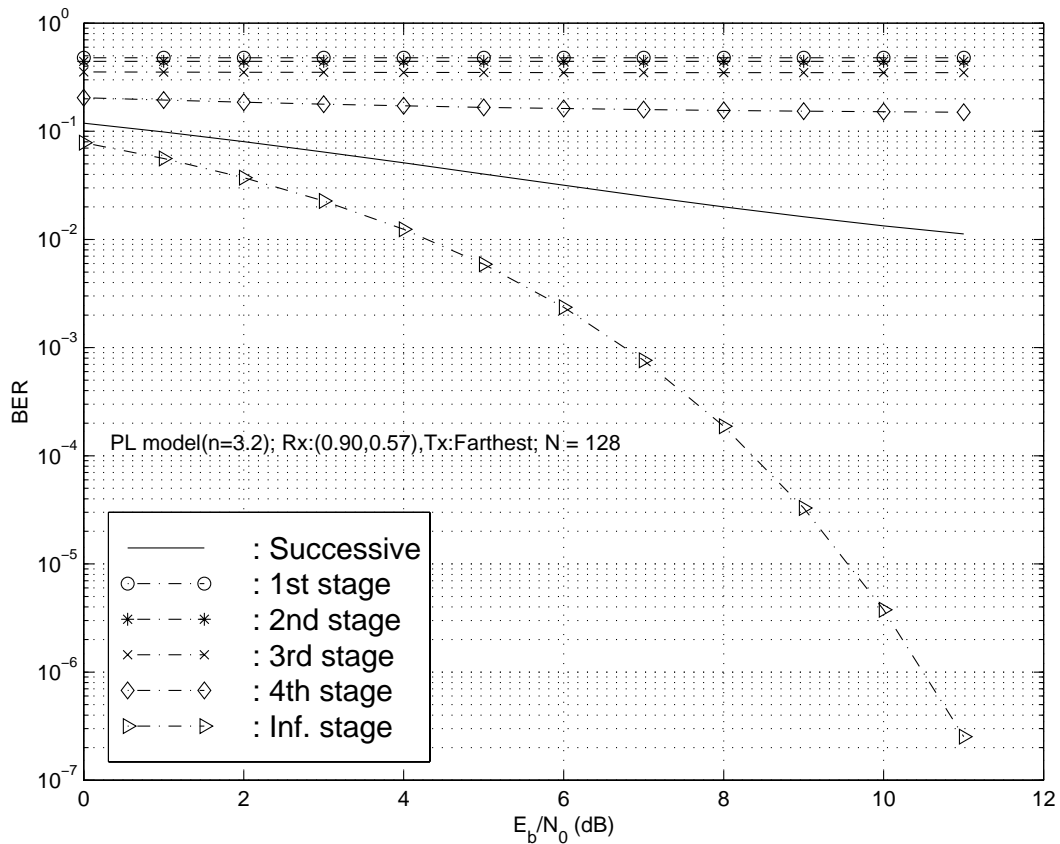


Figure 4.4: BER of the desired user vs. E_b/N_0 for AWGN channel using parallel interference cancellation and successive interference cancellation, respectively. The PL model is exponential; the system is heavily loaded where 54 users are ON. The Receiver $(0.90, 0.57) \in C$ shown in Fig. 4.1 and the transmitter is the farthest among all 53 candidate transmitters.

4.1.4.2 Light Loading

For our light loading example, 15 mobile radios are ON out of a total of 100 mobile radios in the system. These are shown by the asterisk in Fig. 4.2. Each of the 15 transmitters has a designated receiver chosen randomly and we selected three receiver-transmitter sets P , Q and R as shown in Fig. 4.2. Each receiver is identified by its rectangular coordinates, and their corresponding values are also presented in Table 4.1. Fig. 4.5(a) presents the calculated BER of the desired user versus E_b/N_0 considering 15 users in the system for T-R Set P . One stage of PIC performs better than the successive cancellation for this situation and their performances are sufficient for reliable detection. If we notice the spatial distributions of this T-R set [Rx(P) and Tx(P)] and interferers associated with this set shown in Fig. 4.2, one set of

interferers whose signals are needed to be cancelled out and the desired transmitter have the same signal level. So, parallel cancellation performs well for this kind of power distribution. Other interferers are weaker and their signal levels are almost the same in magnitude; so, their contributions are less significant.

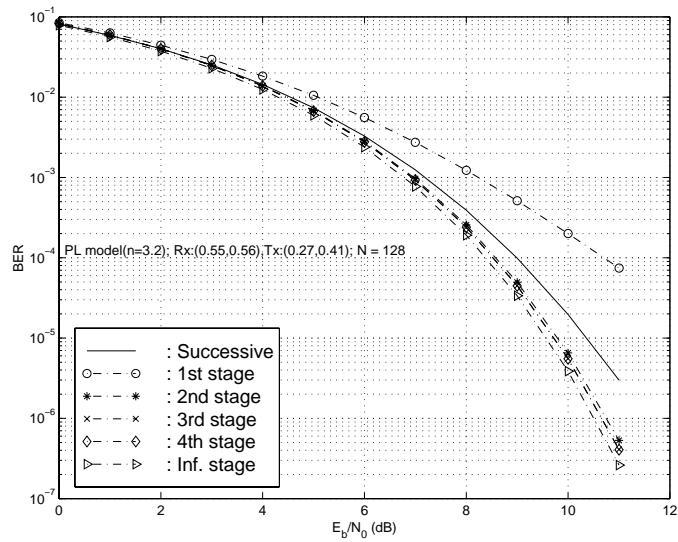
We present the BER improvements for the same receiver Rx(P) of Set P in Fig. 4.5(b) when the desired transmitter is located farthest from the selected receiver in the spatial domain, i.e, the desired signal is the weakest one. Now successive cancellation shows better performance than parallel cancellation because the contributing interferers have a broader range of signal levels when compared to the desired signal level and the desired signal level is smaller than any interferer. As a result, the weakest signal benefits the most from the successive cancellation.

Fig. 4.6 exhibits the BER performance of receiver Rx(Q) shown in Fig. 4.2, where $\{Rx(0.68, 0.88), Tx(0.94, 0.83)\} \in Q$. One stage of interference cancellation is needed to obtain reliable performance from the receiver. Note that the distance of the nearest interferer from the receiver Rx(Q) in this T-R set (Fig. 4.2) is similar to that of the nearest interferer from the receiver Rx(A) in T-R Set A (Fig. 4.1) of the heavily loaded system. These results suggest that system performance can be improved by cutting the load of the system. Now the system can afford reduced distance from the interferers if we keep the number of cancellation stages unchanged. The latter claim is observed when we evaluate the BER performance of Set R (simulated results of Fig. 4.7(b)). Here the dominant interferer is closer to the receiver Rx(R) than that to the receiver Rx(A) in Set A but the BER curves are almost identical. Successive cancellation shows excellent performance as parallel does.

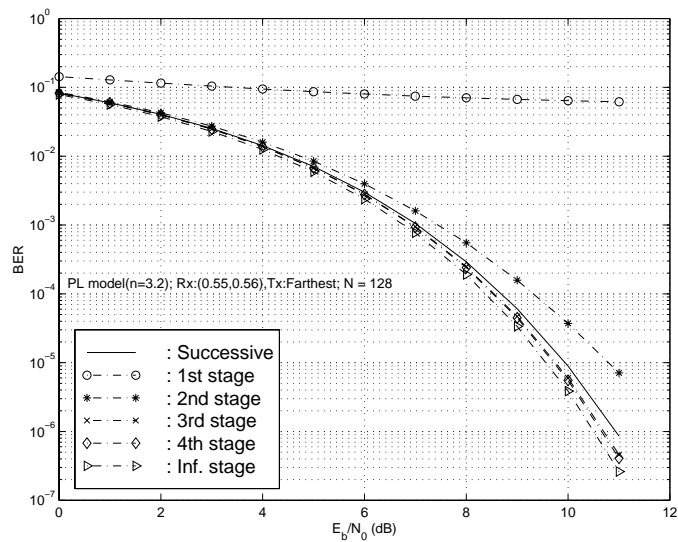
We also simulated the BER for the same Set R using the break-point path-loss model and found that one stage of interference cancellation was needed. Again, the path-loss model is also important for the lightly loaded system when interferers are very close to the desired user.

4.1.5 Results from Simulations

For our simulation, we considered only the light loading example. To avoid redundancy, we will not present simulated results for the heavily loaded model, but all remarks from the simulation in this section for light loading are also appropriate for the heavy loading example. The results from simulations and semi-analytical solutions were obtained by considering asynchronous transmission and this is a more



(a) For user Set P {Rx(0.55,0.56), Tx(0.27,0.41)} shown in Fig. 4.2.



(b) For the Receiver(0.55,0.56) ∈ P shown in Fig. 4.2 and the transmitter is located farthest among all the active 14 candidate users

Figure 4.5: BER of the desired user vs. E_b/N_0 for AWGN channel using parallel interference cancellation and successive interference cancellation, respectively. The PL model is exponential; the system is lightly loaded where 15 users out of 100 are ON.

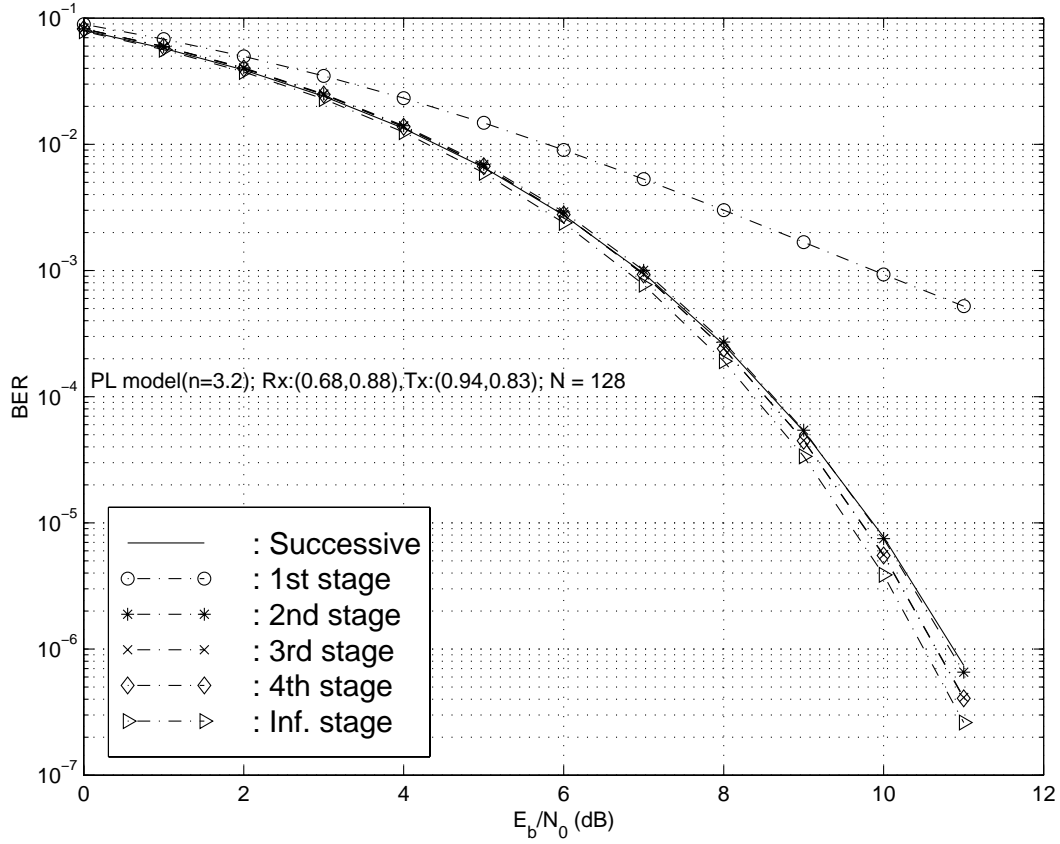


Figure 4.6: BER of the desired user vs. E_b/N_0 for AWGN channel using parallel interference cancellation and successive interference cancellation, respectively. The PL model is exponential; the system is lightly loaded where 15 users are ON. The plots are for user Set Q [Rx(0.68,0.88), Tx(0.94,0.83)] shown in Fig. 4.2.

realistic phenomenon for peer-to-peer communications. Interference cancellation performs better in an asynchronous case than it does in a synchronous case. The other factor we considered in the simulation was the received signal amplitude estimation or channel gain. Perhaps, one of the most important aspect of interference cancellation is the estimation of the received signal amplitude. The perfect amplitude, which is $A_k = \sqrt{2P_k}$ according to our model, is not realistic to determine from the receiver output, but can be estimated from the demodulated output signal or from separate channel estimation. From the receiver, the estimated amplitude can be expressed as

$$\hat{A}_{k,i} = \left| \frac{2y_{k,i}}{T} \right|. \quad (4.13)$$

We present three different amplitude estimate methods for the AWGN channel. Two of these methods depend on correlator outputs, namely single-bit amplitude

estimation and bit-averaging estimation. The third one depends on the estimated powers of the signals from separate channel estimate and we named this as perfect amplitude estimation. In averaging methods, we use a 10-bit averaging amplitude estimation for SIC as suggested by [31] and 5-bit averaging amplitude estimation for PIC for the same reason. We found that more bits taken for bit-averaging would not improve the amplitude estimate significantly in PIC for AWGN channel. The advantage of averaging is that the variance of the additive channel noise decreases linearly with the number of bits taken for averaging and eventually reaches the single user bound.

We adopted the selective interference cancellation scheme for simulation. We cancelled only those users who had higher estimated signal amplitudes than that of the desired user, in the SIC scheme. For the PIC case, we cancelled those users whose estimated signal amplitudes are higher than 3-dB (half) value of the desired signal amplitude. The motivation for choosing these two threshold levels was to observe the deviation of the simulation results due to a different threshold for selective cancellation. Generally, the deviations of simulation results from their analytical predictions decrease when we cancel more users and also depends on the received energy from those cancelled users but if the cancelled signal is weaker, it may hurt the BER performance because of poor estimation.

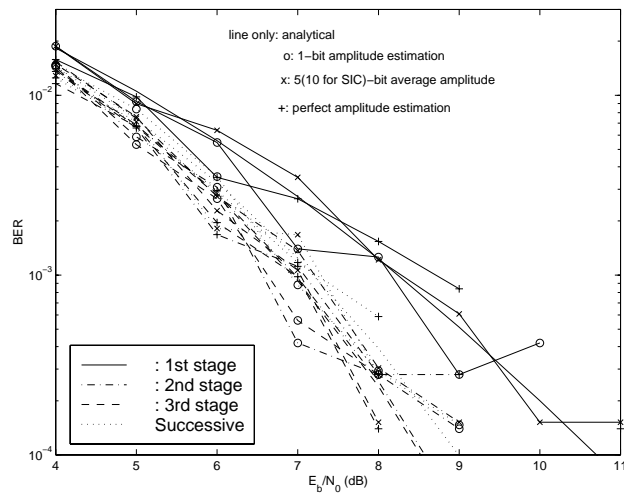
Complete cancellation of estimated interference suffers from biased estimates and soft-cancellation factors improve the BER performance towards the BER predicted from analytical solutions [55, 56]. For selective PIC, we assumed that the value of soft-cancellation factors of all users is 0.6 for the simulations. Reference [57] showed that these cancellation factors can be obtained semi-analytically for synchronous transmission and are proportional to user-signal amplitudes. This suggests that the strongest user has the largest cancellation factor and the weakest user has the smallest cancellation factor. We can set a threshold value on the cancellation factors instead of received signal amplitudes for the selectivity. Since we do not have such semi-analytical solutions for cancellation factors considering asynchronous transmission, our simulation results suffer some degradation. This factor summing with the interference of weaker users, those we do not cancel, causes deviation of our simulated results from analytical results to some degree, although this degradation is not much.

Fig. 4.7(a) compares the BER plots of Fig. 4.5(a) and the BER plots from Monte-Carlo simulation using multistage PIC and SIC, respectively, for Set P . We presented the BER value from 10^{-4} to $2(10^{-2})$. The two reasons behind this are as follows. We

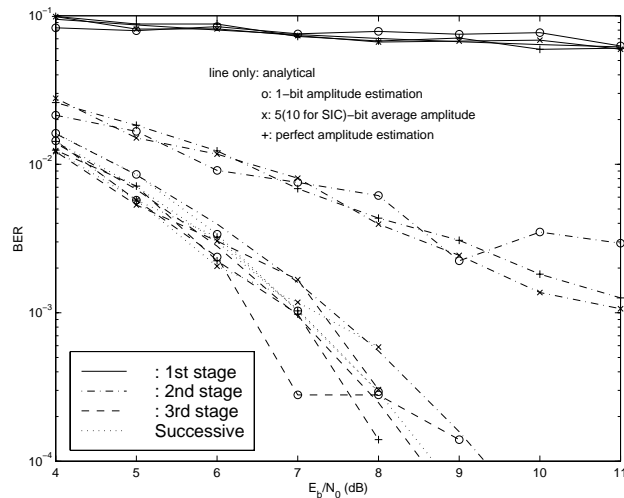
did not detect any error from Monte-Carlo simulation for lower BER, where the total number of information bits for an error event was 10^5 . Since we had 14 users in the system and we sampled every pseudonoise(PN) sequence four times where processing gain was 128, our simulation run-time was a factor for not increasing the number of trials (input information data bits). It is conceivable that more information bits (trials) would provide simulated results for lower BER to follow analytical results with the expense of more computational time. For demonstration purpose, we set the above limits. The other reason is that the simulated results perfectly matched with the semi-analytical BER for the other end of the graph using any of these amplitude estimation schemes; also, the results on this end are not interesting to consider for practical purposes.

From the plots, it is noticeable that results from three different estimations follow the analytical results closely and results from estimation with no bit-averaging are a little worse than those from the other two estimations. So bit-averaging or perfect amplitude estimation does not provide significant gain for the results in selective PIC and SIC in AWGN channel. We used the estimated signal amplitudes from the correlators for ranking the users in SIC scheme and for the selection of users for cancellation in selective PIC, respectively. Note that if we would rank the users in SIC scheme or selectively cancel the users in PIC on the basis of their perfect amplitude estimations, the results would be the lower bound (lower BER) of the BER plots presented in Fig. 4.7(a). From the simulations, we observed that the ranking of the powers in SIC scheme and the selections of the users for cancellation in PIC using the above two mentioned methods, provide similar results though the latter method of ranking provides the best results. The results from averaging depend on the channel types [36].

Fig.4.7(b) exhibits the simulated BER for the semi-analytical results presented in Fig. 4.5(b), where the above estimation techniques were applied. In addition to the similar observations of the results in Fig. 4.7(a), it is noticeable that the simulated results for the first stage of PIC differ considerably from the results from analytical expression. The power range of the interfering users varies up to 17 dB with respect to (w.r.t.) the desired user's power and the desired user signal is the weakest one. Poor estimations of the weaker signals including the desired user's signal, the choice of partial cancellation factors and stronger interfering signals cause this deviation. After one stage of cancellation, we did not observe this disagreement because considerable interference was removed with the first stage of interference cancellation.



(a) Simulated results for semi-analytical results shown in Fig. 4.5(a).



(b) Simulated results for semi-analytical results shown in Fig. 4.5(b).

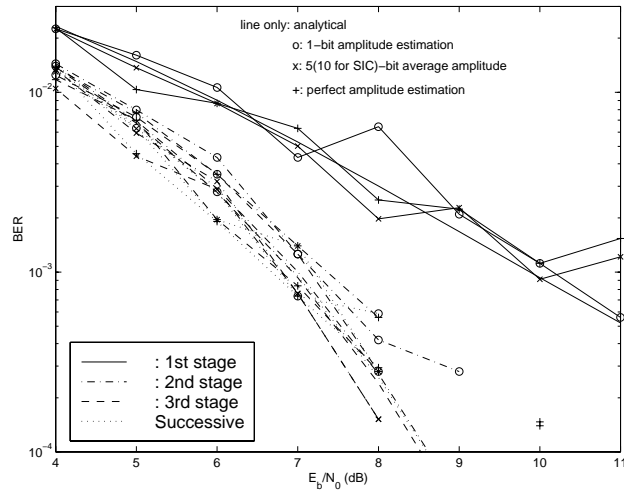
Figure 4.7: BER of the desired user vs. E_b/N_0 . Different simulation result sets are obtained from different amplitude estimations, namely, perfect amplitude estimation, single-bit amplitude estimation and bit-averaging amplitude estimation; (a) for user Set P [Rx(0.55,0.56), Tx(0.27,0.41)] shown in Fig. 4.2. (b) for the Receiver (0.55, 0.56) $\in P$ shown in Fig. 4.2 and the transmitter is located farthest among all the active 14 candidate users.

For completeness, we also present the simulated results for Q user-pair whose semi-analytical results are shown in Fig.4.6 and the simulated and semi-analytical results for R user-pair (shown in Fig. 4.2) in Fig. 4.8(a) and Fig. 4.8(b), respectively. Here, we also notice the deviation of simulated results from semi-analytical results in the first stage cancellation of Fig. 4.8(b). Here, out of 13 interfering users, the power variations of cancelled four users compared to the desired user's power are as follows: 29.5 dB, 11 dB, 2.7 dB and -0.2 dB. The rest of the users have at least 6 dB lower power than the desired user power. The strongest interfering user's power is much higher than the desired user power and, as a result, first stage PIC cancellation suffers a degradation from the predicted analytical value [37]. After first stage, much of the interfering signal is removed and the second stage cancellation does not encounter this phenomenon. The successive cancellation which benefits from diverse powers is found to be robust to strong interfering signals.

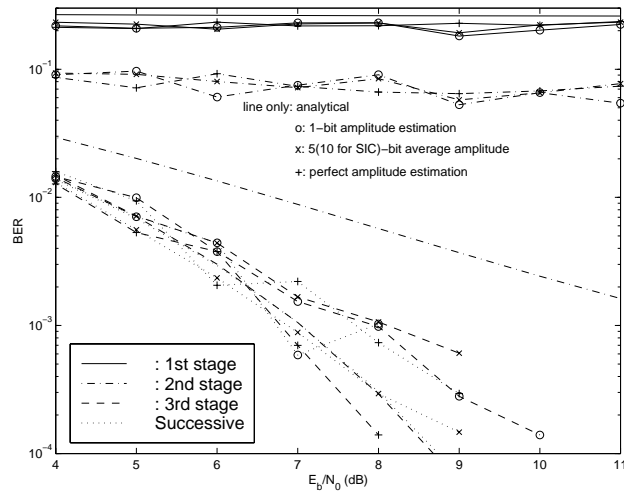
We also simulated the system for a fading channel. The mobile unit speed of 100 km/hr, a data rate of 16 kbps and a transmit frequency of 2.0 GHz were assumed. We considered Sets P , Q and R , respectively, of the lightly loaded system; we generated similar plots of Figs. 4.7(a), 4.8(a) and 4.8(b), respectively. Fig. 4.9 shows the BER performance for Set P , Fig. 4.10 shows the BER performance for Set Q , and Fig. 4.11 shows the BER performance for Set R . From the plots, it is obvious that the PIC receiver with two stages of cancellations has the best performance improvement.

4.1.6 Comparison between PIC and SIC

The delay of the system in term of bits is the number of cancellation stages for SIC and PIC. For SIC, this delay and the hardware complexity can be reduced by groupwise cancellation suggested by [58]. On the other hand, PIC has one or two bits delay because more than two stages of cancellation are not realistic. For a dynamic channel, SIC needs to rank the users before any kind of cancellation. This is a factor for which we need to study the channel behavior. We need to compare the signal processing time at the receiver with the channel fading speed. Also, if a new user enters into the system, the ranking and cancellation should be completely redone while the connection continues. This may be a problem for a heavily loaded system where users leave and enter into the system frequently. Another drawback of successive cancellation is that when there are two or three interferers, whose signal levels are



(a) Simulated results for T-R Set Q.



(b) Simulated results for T-R Set R.

Figure 4.8: BER of the desired user obtained analytically and Monte-Carlo simulation, respectively, against its E_b/N_0 . Different simulation result sets are obtained from different amplitude estimations, namely, perfect amplitude estimation, single-bit amplitude estimation and bit-averaging amplitude estimation; (a) for user Set Q [Rx(0.68,0.88), Tx(0.94,0.83)] shown in Fig. 4.2 (b) for user Set R [Rx(0.67,0.75), Tx(0.94,0.83)] shown in Fig. 4.2.

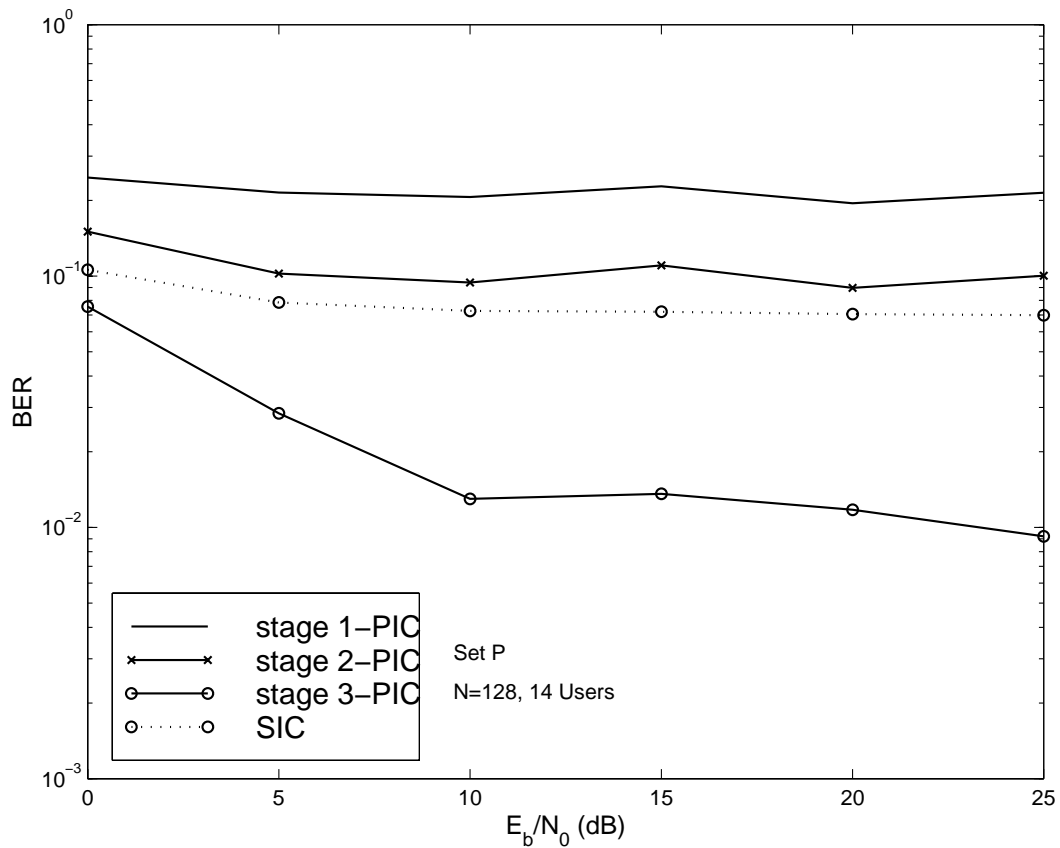


Figure 4.9: Simulated BER of the desired user (Set P) against its E_b/N_0 for fading channel.

very close to desired transmitted signal level, but not larger, SIC does not cancel those users. This may cause significant degradation of the detection performance. PIC does not suffer from this problem. In other circumstances like wide variation of signal levels, SIC performs better. Since for a light loading case very few dominant interferers need to be cancelled, both schemes perform similarly. For a weaker desired signal towards the receiver compared to interfering signals, SIC exhibits better performance with higher delays. There is no hard and fast rule for one's advantages over the other. The main drawback for SIC is delay and speed whereas the cardinal problem for PIC is the complexity. Note that a delay of a few bits is not a great concern in packet radio networks for typical data rate of 10 kbps. With the combination of distributed power control, the performance of PIC surpasses that of SIC.

We also plotted the average BER of the entire system as a function of E_b/N_0 in Fig. 4.12 for the specified T-R connections as shown in Fig. 4.1 and 4.2, respectively. In order to obtain the average BER, we first calculated the BER of each T-R set in

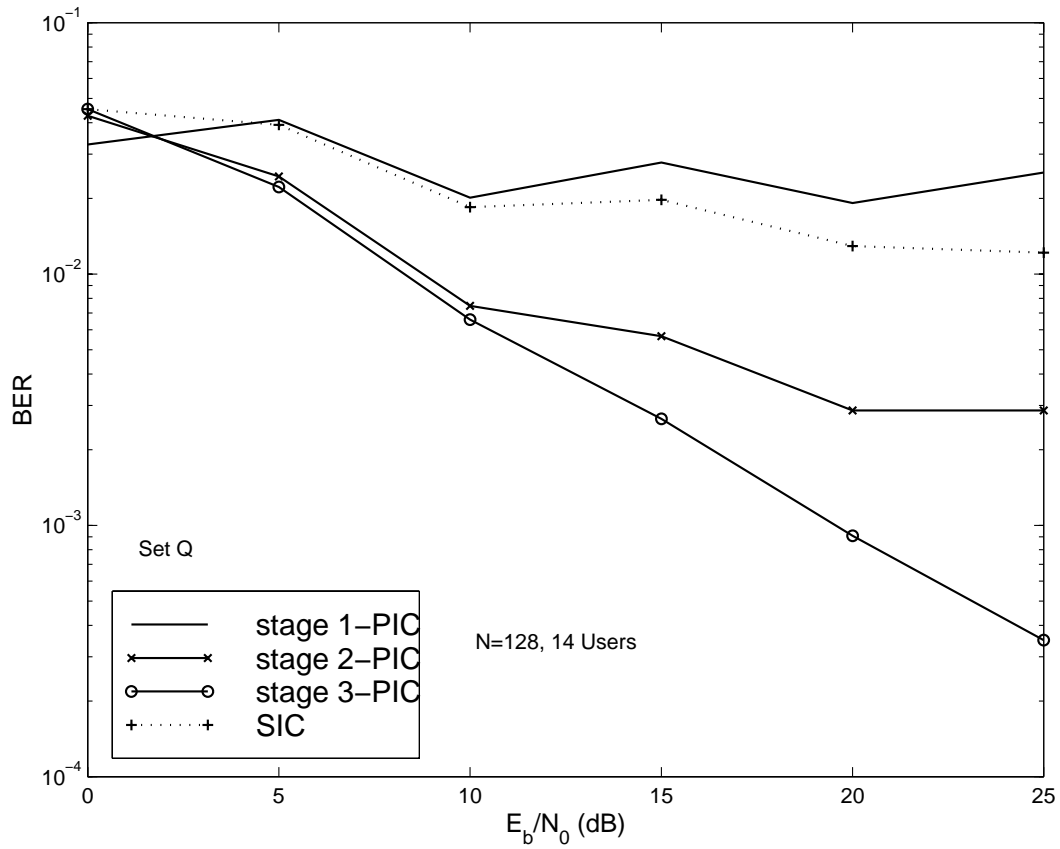


Figure 4.10: Simulated BER of the desired user (Set Q) as a function of its E_b/N_0 for fading channel.

the system as we did for T-R set *A* shown in 4.3; next, we took the average value of all the BER. The average BER is obtained from the individual Note that the average BER performance of the lightly loaded system is a bit worse than that of the heavily loaded system up to two stages of PIC. This is because there is a user very near to another user and this situation worsens the overall performance. SIC cancellation performs better in a light loading situation for this particular setup.

4.1.7 A Realistic Implementation of the PIC Receiver

By considering the above factors, we think that the PIC receiver has a performance edge over the SIC receiver for peer-to-peer communications. For a practical implementation of this PIC receiver, the receiver hardware will be fixed regardless of the channel scenarios or applications; in other words, the receiver can cancel a fixed number of interfering users. Thus, we need to evaluate the performance of the PIC receiver

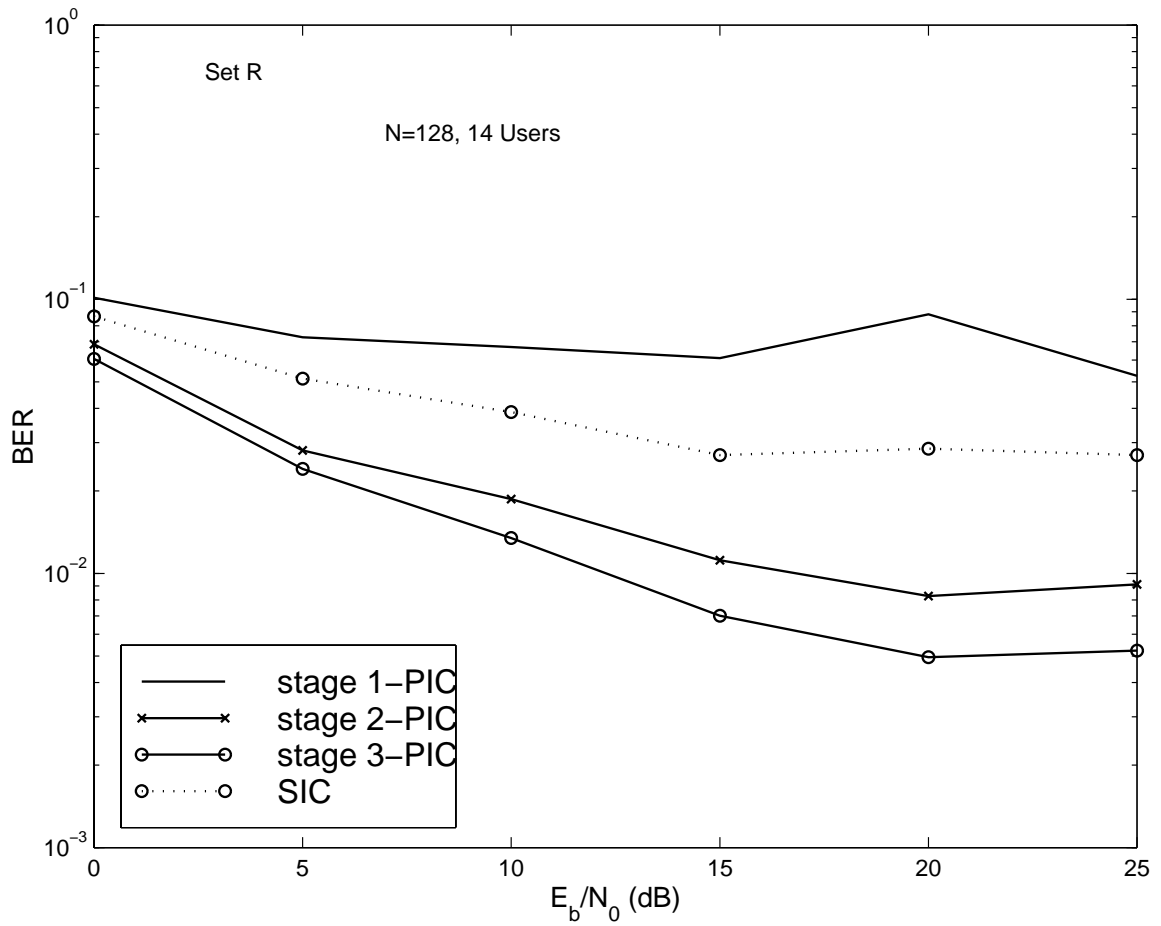
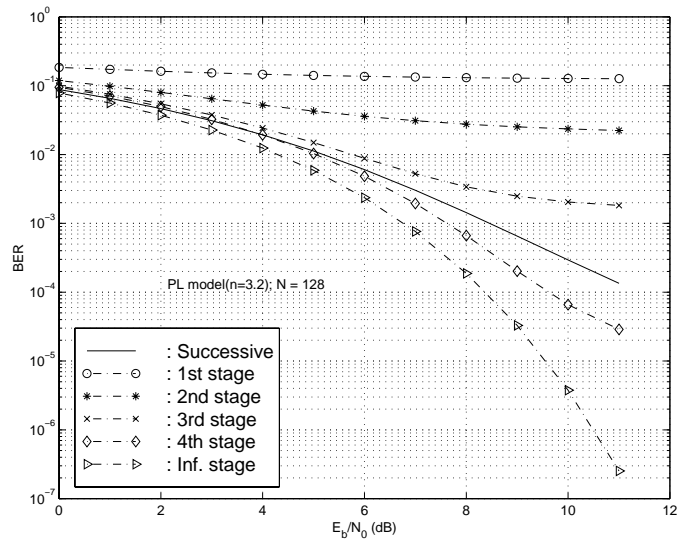
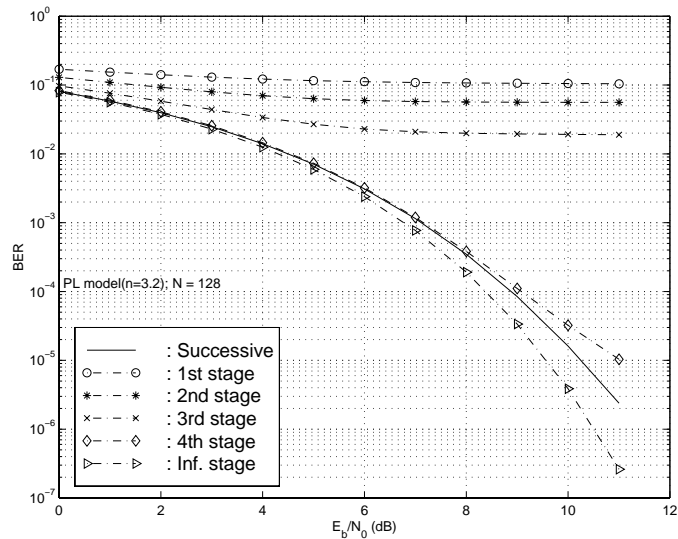


Figure 4.11: Simulated BER of the desired user (Set R) vs. its E_b/N_0 for fading channel.



(a) Heavy loading with 54 users are ON in the system.



(b) Light loading with 15 users are ON in the system.

Figure 4.12: Average BER of the entire system (all pairs of users) versus E_b/N_0 for AWGN channel using parallel cancellation and successive cancellation, respectively. The PL model is exponential; (a) for 54 user-pairs shown in Fig. 4.1, (b) for 15 user-pairs shown in Fig. 4.2.

having fixed number of branches (filter banks). We assume that the receiver has four branches; therefore, the receiver is capable of cancelling three interfering users. We simulated the system for the lightly loaded example, and again, we considered Set P , Set Q , and Set R ; we generated similar plots of Figs. 4.7(a), 4.8(a) and 4.8(b), respectively, where only 3 interfering users are cancelled. Fig. 4.13 shows the BER performance for Set P , Fig. 4.14 shows the BER performance for Set Q , and Fig. 4.15 shows the BER performance for Set R . From the plots, it is obvious that the PIC receiver having four parallel branches is as good as receivers having more than four branches. In summary, this again implies that we need to cancel only a handful significant interferers.

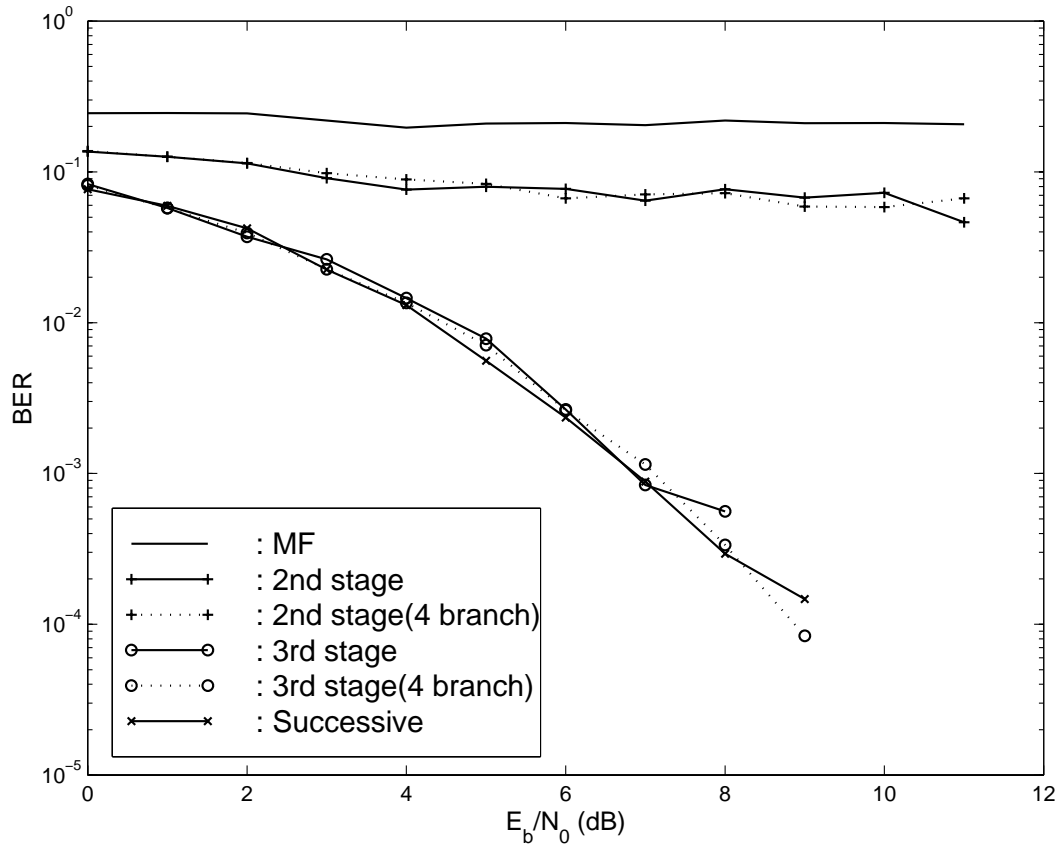


Figure 4.13: BER of the desired user vs. its E_b/N_0 for the T-R Set P ; one set of plots consider only 3 significant interferers, and the other set of plots consider significant interferers determined by a threshold value (plots of Fig. 4.7(a))

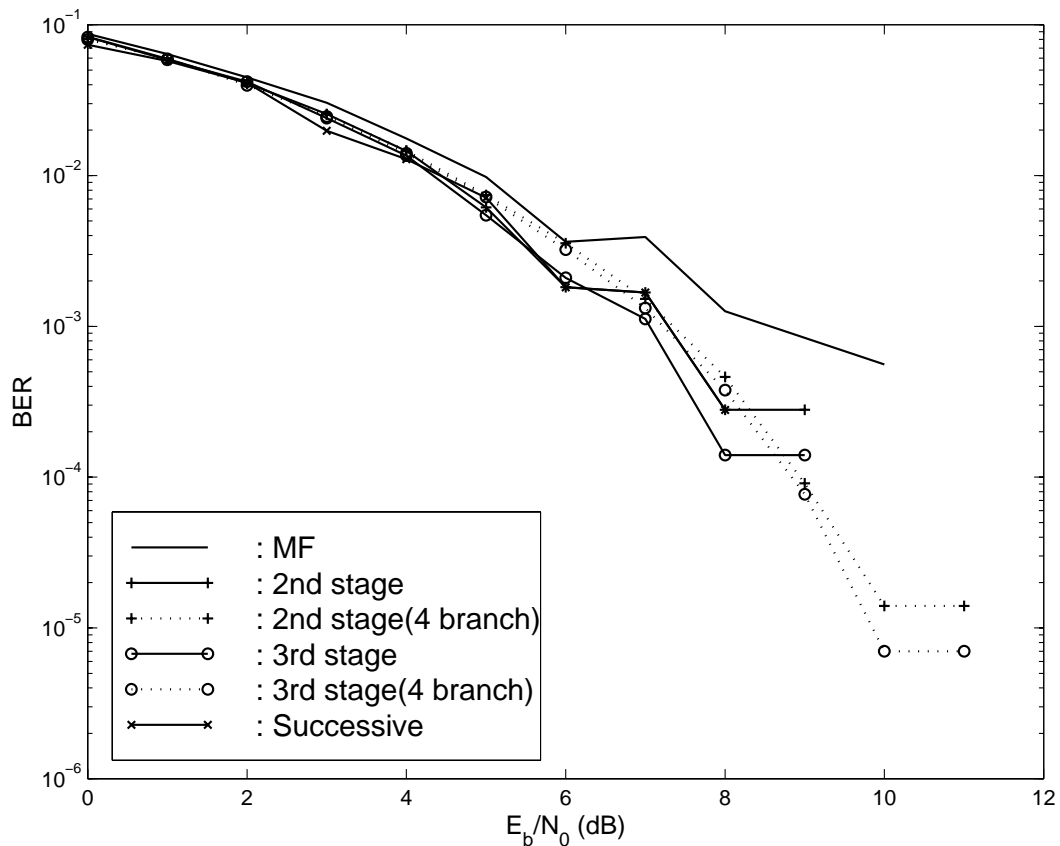


Figure 4.14: BER of the desired user vs. its E_b/N_0 for the T-R Set Q ; one set of plots consider only 3 significant interferers, and the other set of plots consider significant interferers determined by a threshold value (plots of Fig. 4.8(a)).

4.1.8 Summary of Multiuser Detection in a Peer-to-Peer Environment

The degree of BER improvement of the system for a given processing gain depends upon the desired user power, powers of the interfering signals, noise power from the channel, and system loading status. The distance of the nearest mobile from a selected receiver is the dominating factor to limit the performance of that receiver. Subtractive cancellation improves the system performance significantly. From the capacity point of view, all the BER improvement can result in improved capacity. If we compare this capacity improvement phenomenon with that for cellular systems using multiuser detection in the base station, there is no constraint for capacity improvement in peer-to-peer communications. The prime factor of the usefulness of the multiuser detection in both applications is the alleviation of near-far problem. A

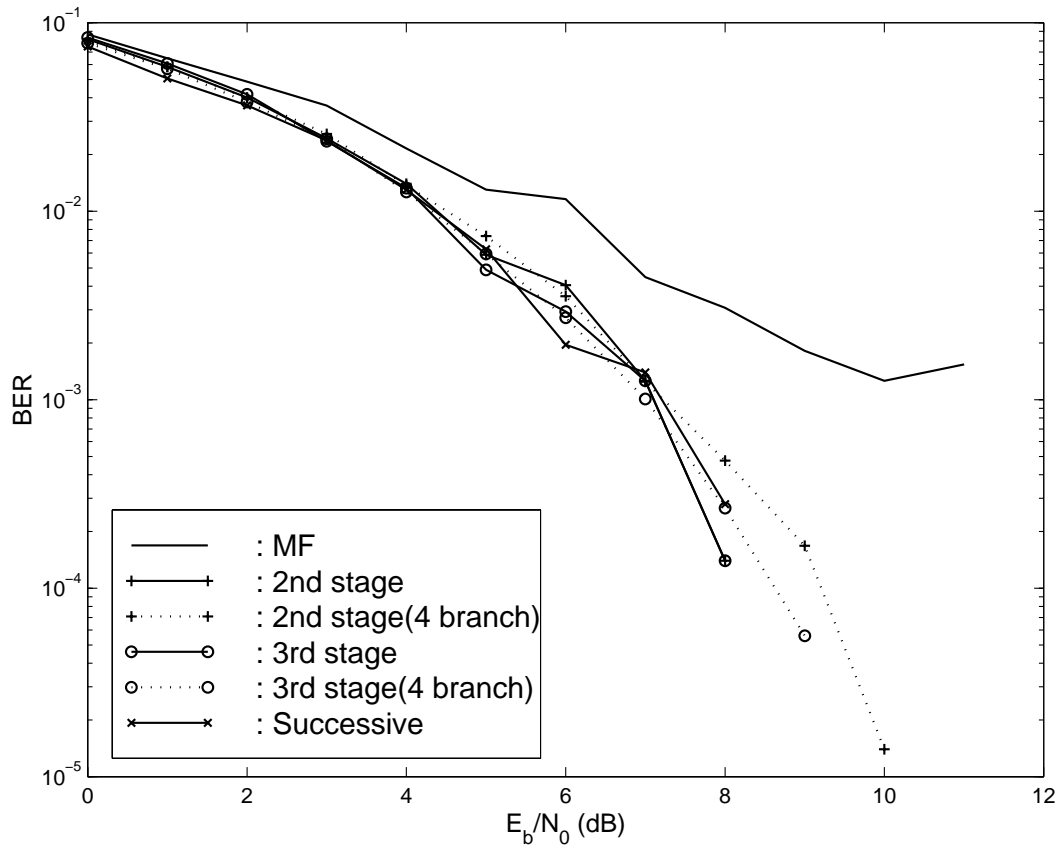


Figure 4.15: BER of the desired user against its E_b/N_0 for the T-R Set R ; one set of plots consider only 3 significant interferers, and the other set of plots consider significant interferers determined by a threshold value (plots of Fig. 4.8(b)).

consistent path-loss model is required to estimate the performance of the system when the users are connected to an obstructed transmitter located far from the receiver. Average performance of the entire peer-to-peer communication system is dominated by the users having neighbors at a closer distance. Multiple hop can be used to communicate with the remote users.

DS-SS has some implementation advantages. In the past, FH-SS has been preferred for packet radio because of the near-far problem. In this section, we have shown that simple interference cancellation can alleviate the near-far problem and significantly improve the multiple access capability. We have presented the BER performance for both light and heavy loading systems. Finally, we can infer that distributed power control coupled with interference cancellation can provide sufficient users in the system with moderate complexity.

4.2 Single-User Adaptive and Multiuser Receivers for DS-CDMA in Peer-to-Peer Packet Radio Networks

Since CDMA capacity is interference limited, any reduction in interference converts directly into an increase in the capacity. Both single-user adaptive and multiuser detection have been proposed for solutions to this problem [17], [59]. The idea of adaptive receivers performing single-user detection is suitable for ad hoc networks, where asynchronous users communicate with each other directly, without using a central hub or base station. For this application, the receivers do not have a central power control or may not have knowledge of other users' spreading codes. For cellular environments, the out-of-cell interference is unknown but the single-user adaptive receiver needs only the desired user's spreading code and delay. With multiuser detection, the spreading codes and delays of the most significant interferers are needed to be known and used at the receiver. The implementation of multiuser receivers is complex, especially without prior knowledge of channel conditions and received signal energy [17]. However, the near-far situations which arise in packet radio networks may be due to only one or two significant interferers. Thus simple multiuser techniques, which cancel only one or two strong interferers may, be effective. In packet radio networks, power control can be used to reduce the near-far problem to some extent and multiuser detection can be deployed for improved performance of this system. Systems combining these two techniques have the potential to achieve robust performance needed for military and commercial mobile communication.

The objective of this section is to compare a multiuser receiver using subtractive selective interference cancellation with a single-user adaptive receiver for the packet radio environments. In Section 4.2.1, we present a brief analysis of the single-user adaptive receiver. Section 4.2.2 shows the performance of the single-user adaptive receiver and compares the performance and complexity of the above mentioned receivers. Concluding comments are provided in Section 4.2.3.

4.2.1 Single-User Adaptive Receiver

Among several single-user adaptive receivers, we considered the N tap chip-rate linear adaptive receiver (CHRT-LAR) with a normalized least-mean square algorithm

(NLMS) where N refers to the processing gain. The N -tap CHRT-LAR performs much better than the conventional receiver in terms of BER and near-far resistance with increased complexity which results from the adaptive nature of the receiver [59]. Note that the N -tap chip-rate adaptive receiver can exploit the cyclostationary nature of the DS-SS signal, exploiting the periodicity due to the data rate. The adaptive receiver's computational requirements depend on the choice of the adaptation algorithm and the number of adaptive weights (determined by the processing gain N). A large processing gain will result in large computational requirements, a slow convergence rate, and a large filter misadjustment.

Other adaptive receivers such as fractionally-spaced linear or decision feedback and other algorithms such as RLS, blind algorithms, and prefiltering [60] have some advantages with respect to convergence time, but suffer from increased complexity. Some of the receivers are case specific. The N tap CHRT-LAR has N degrees of freedom and is, therefore, capable of rejecting up to $N-1$ synchronous or $\frac{N-1}{2}$ asynchronous interferers [59]. Data symbol oversampling LAR can reject up to $\frac{D-1}{3}$ asynchronous interferers [59], where D is the number of reduced filter weights. The optimum reduced-complexity adaptive receiver achieves the same performance as the N -tap CHRT-LAR but the knowledge of the propagation delays and spreading codes of all users is required, which defeats the purpose of introducing a single-user adaptive receiver [61].

4.2.1.1 N -tap Chip-Rate Linear Adaptive Receiver

The block diagram of a CHR-LAR is presented in Fig. 4.16, where a chip-matched filter is followed by a transversal adaptive N -tap filter, which is matched to the spreading code of the desired user. This model is based on [59]. The sampled received signal is passed through the filter matched to the chip waveform, thus performing a chip-matched filtering operation. The output of the chip-matched filter $r_c(t)$ is sampled at the chip rate $1/T_c$, to form the input to an N -tap linear transversal filter whose weights are adapted according to the MMSE criterion. The output of the transversal matched filter is sampled at the data rate $1/T$, where T is the data symbol period to obtain the estimate for the desired user's i th data symbol $y_1(i)$, and subsequently the hard decision $\hat{d}_1(i)$.

The N -tap CHRT-LAR performs symbol detection. Since code-on-pulse modulation is employed, the adaptive chip-spaced linear transversal filter contains samples

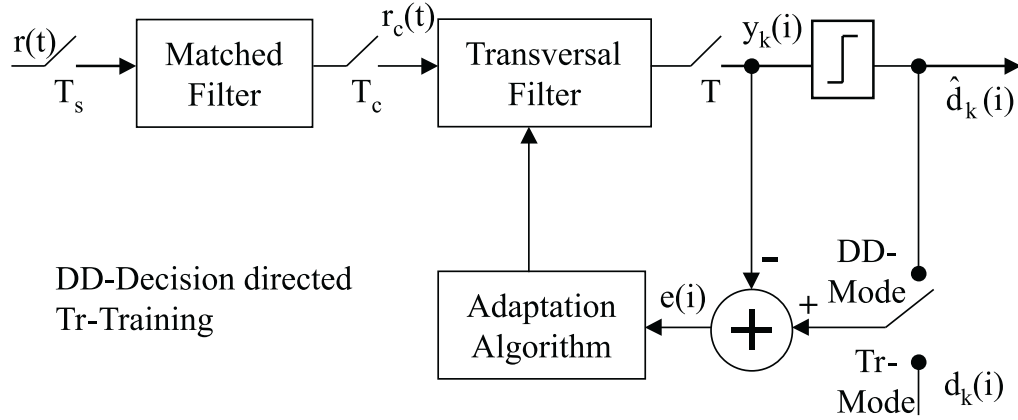


Figure 4.16: Model of a CHRT-LAR.

from one full symbol at the time when symbol detection is performed. Samples corresponding to the i th data symbol form a chip-spaced received signal vector given by,

$$\mathbf{r}_c(i) = [r_{c0}(i) \ r_{c1}(i) \ \cdots \ r_{c(N-1)}(i)]^T, \quad (4.14)$$

and the filtering operation is modeled by,

$$y_1(i) = \mathbf{w}^H \mathbf{r}_c(i), \quad (4.15)$$

where the weight vector \mathbf{w} is chosen to minimize the mean square error (MSE), given by $E[|e(i)|^2]$. The error signal $e(i)$ is formed as the difference between a reference signal and the filter estimate. During initial adaptation, a training sequence is used and the error signal is given by

$$e(i) = d_1(i) - y_1(i). \quad (4.16)$$

After the adaptation algorithm converges, decision-directed adaptation is usually employed, and the reference signal is the estimated data symbol $\hat{d}_1(i) = \text{sgn}[\text{Re}y_1(i)]$. The explanation of NLMS algorithm can be found in [27] and its filter-weights are updated according to

$$\mathbf{w}(i+1) = \mathbf{w}(i) + \mu(i) \mathbf{r}_c^*(i) e(i), \quad (4.17)$$

where the step-size $\mu(i)$ is

$$\mu(i) = \frac{\alpha}{\gamma + \mathbf{r}_c^H(i) \mathbf{r}_c^*(i)}. \quad (4.18)$$

Here, γ is a small positive constant and α is a constant which determines the amount of misadjustment, $0 \leq \alpha \leq 2$.

Adaptive filtering solves the problem of estimating a signal through an unknown or changing channel. Adaptive filters work on the basis of minimizing the mean squared value of the deviation between the filter estimate and the desired response. This minimum MSE (MMSE) criterion is the basis of Wiener filter theory and in a stationary AWGN environment leads to the optimum Wiener solution for a linear filter [27]. The optimum weight vector w_{opt} is given by

$$w_{opt} = \mathbf{R}^{-1}\mathbf{p}, \quad (4.19)$$

where \mathbf{p} is a cross-correlation vector between the desired response and the input vector $\mathbf{r}_c(i)$. The input correlation matrix \mathbf{R} is given by

$$\mathbf{R} = \mathbf{E}[\mathbf{r}_c(i)\mathbf{r}_c^H(i)]. \quad (4.20)$$

Equation (4.20) represents the *Wiener-Hopf* equation [27].

4.2.2 Simulation Results

We consider a snapshot of the system at another instant when out of the 100 users, 16 are ON. We assume that the system is asynchronous with $N = 31$, i. e., system loading is 51.6%. The relative power distribution of the users in the system is assumed as follows: $P_1 = 0 \text{ dB}, P_2 = 3 \text{ dB}, P_3 = -3 \text{ dB}, P_4 = 6 \text{ dB}, P_5 = -6 \text{ dB}, P_6 = 9 \text{ dB}, P_7 = 3 \text{ dB}, \dots, P_{16} = 9 \text{ dB}$ where P_1 is the desired user's received power. For simulations, "4 users in the system" means that the system contains four users and their power distribution follows the above series as, $P_1 = 0 \text{ dB}, P_2 = 3 \text{ dB}, P_3 = -3 \text{ dB}$ and $P_4 = 6 \text{ dB}$. These parameters are the same for various detection techniques described in this section unless any change is mentioned explicitly for a particular case. The system has a processing gain of 31 and E_b/N_0 is chosen as 8 dB.

4.2.2.1 N -tap Chip-Rate Linear Adaptive Receiver

Fig. 4.17 exhibits the convergence curves for the desired user (user 1) in the single-user system described above, where the MSE as a function of training bits is plotted. All solid lines in the plot present the corresponding synchronous case with uniform power users. The plots show that the filter convergence time lengthens with the number of

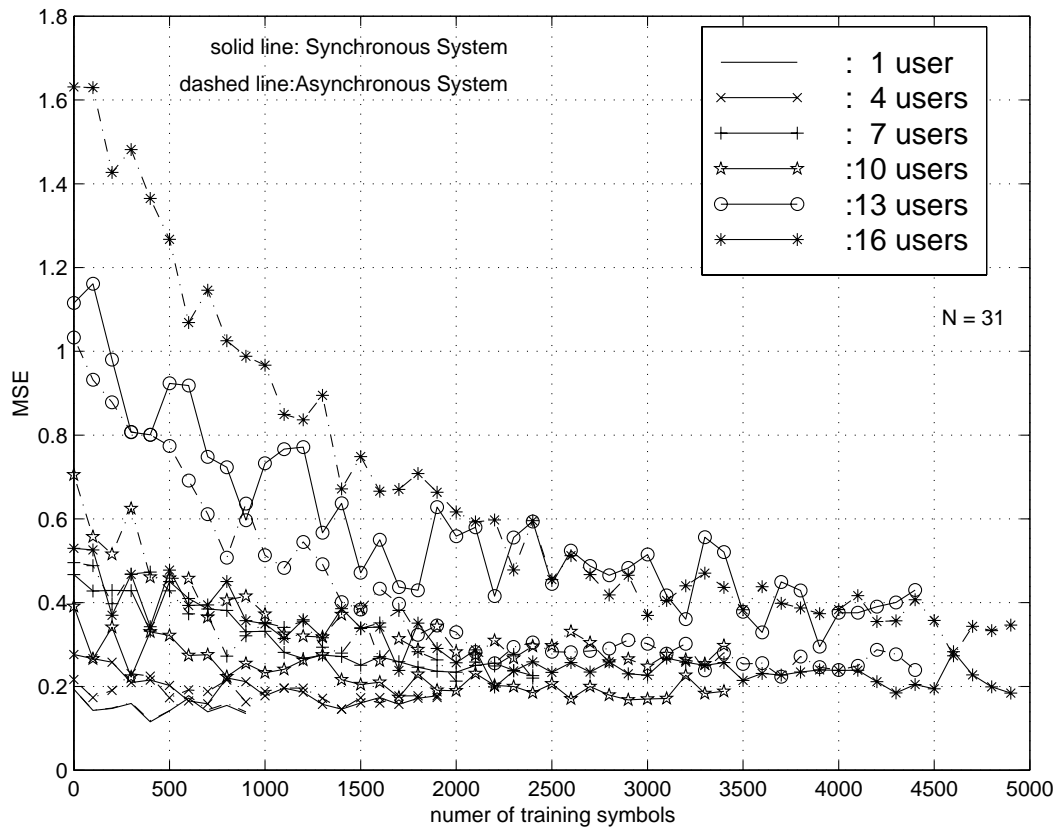


Figure 4.17: MSE as a function of training symbols.

users in the system. The convergence also depends on the ratio of the powers from interfering users to the power from desired user. For the system illustrated above, about 5000 symbols are required for a reasonable convergence. Our simulations also show that the number of training symbols required for convergence largely depends on the processing gain. While the system presented in this section exhibits slow convergence properties, it also exhibits optimal single-user performance in steady-state and thus may be considered as an example of best performance for single-user adaptive receiver. Higher processing gains mean more taps in the adaptive filter banks, which will cause more misadjustment error. As a result, higher processing gains result in a high computational time and more training symbols are required.

The BER of the desired user versus the number of users in the system are plotted in Fig. 4.18 where solid lines and dashed lines represent synchronous and asynchronous system respectively. The plots show that BER performance of both the systems using CHRT-LAR are comparable. Since this receiver can reject up to $(N - 1)/2$ interferer for asynchronous system and the load is about this upper limit, the receiver performance is not greatly affected by the synchronousness of the system as long as the load remains within the limit. Note that the MF receiver has better performance in an asynchronous system than in a synchronous system in an interfering environment because interferers have lower cross-correlation with the desired user's spreading code in an asynchronous system.

The trained adaptation algorithms require an initial adaptation involving the use of training sequence. As a result, whenever a considerable change occurs in the system (i.e., a change in the number of users, a variation in the interfering signal amplitudes, or a change in the channel), the packet transmission is interrupted for the duration of adaptation period. Decision directed adaptation algorithms suffer from 'catastrophic failure' because incorrect decisions are fed back and used by the algorithm as if they were correct. This can lead to algorithm's divergence, in which case receiver output becomes independent of transmitted data symbols. Blind adaptation algorithms can be used to overcome this problem [62]. For these type algorithms, the convergence rates should be sufficiently fast to enable successful tracking of the channel with possible minimum computational requirement. The NLMS algorithm, which is used for our simulation, can be made blind by using the knowledge of the desired user's spreading code.

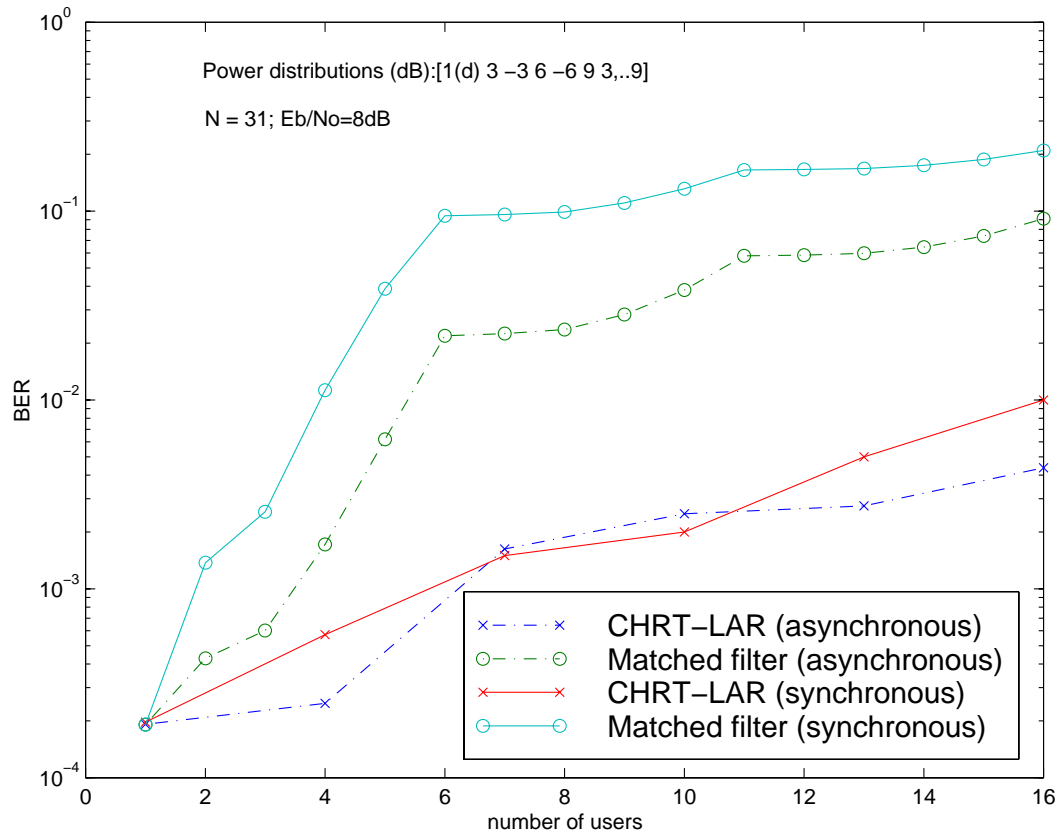


Figure 4.18: BER of the desired user vs. number of users in the system for matched filter and CHRT-LAR, respectively, in synchronous and asynchronous environments.

4.2.2.2 Combined Simulated Results

Fig. 4.19 shows the BER of the desired user as a function of the number of users in the system for various detection techniques. These are selective multistage parallel interference cancellation (PIC) and successive interference cancellation techniques (SIC) for multiuser receivers and CHRT-LAR for single-user receivers. The standard system model for PIC and SIC in multiuser receivers can be found in [39], [31], respectively, and we also presented the system model in the previous section. By selective interference cancellation, we mean that we do not cancel those users whose power is 3 dB below or less than the desired user's power. Note that for SIC, users with lower power than the desired user's power are not considered for interference cancellation.

It is shown in the plots in Fig. 4.19 that multiuser receivers outperform the single-user adaptive receiver in the BER improvement of the desired user and the multiuser

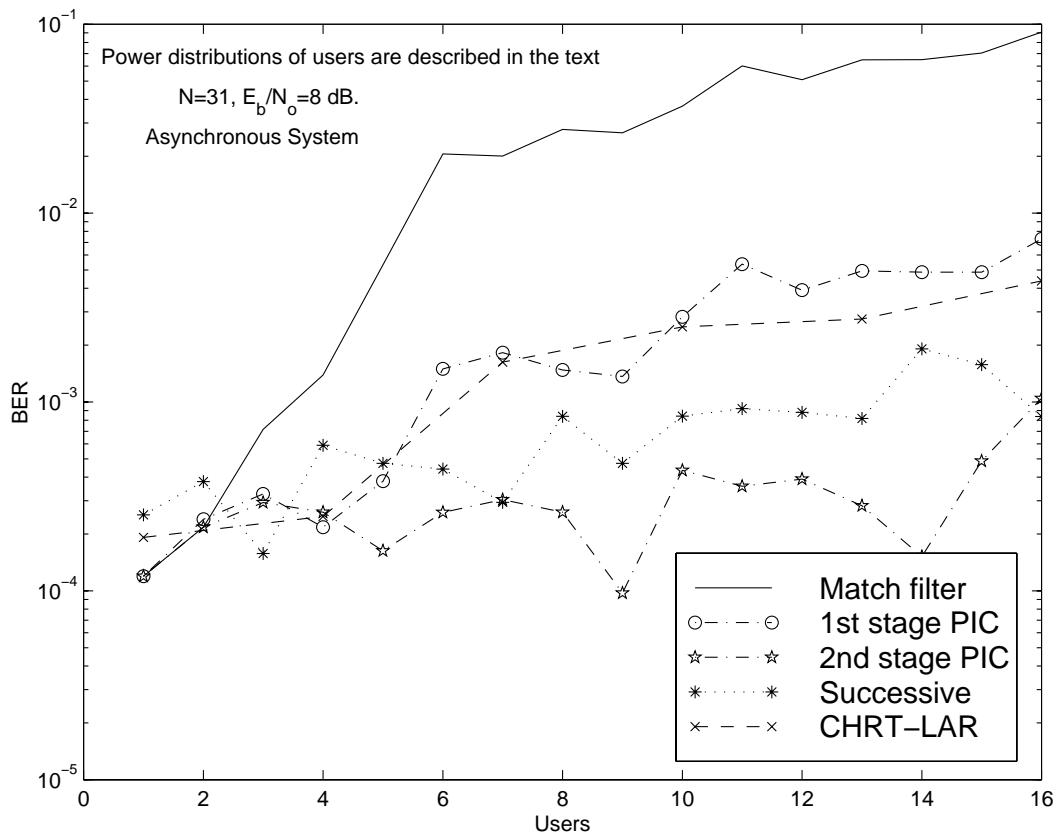


Figure 4.19: BER of the desired user vs. number of users in the system by considering MF, PIC receiver, SIC receiver and CHRT-LAR, respectively.

receiver with two stages of parallel interference cancellation has the best BER achievement among all considered receivers. For example, the system can afford up to six users by using multiuser receiver with one stage of PIC and all 16 users with two stages of PIC for typical BER requirement of 10^{-3} whereas the CHRT-LAR receiver is not acceptable for this BER requirement when the number of users in the system exceeds six. Both the single-user adaptive receiver and the multiuser receivers achieved large BER performance gain over the conventional receiver. BER performance by using a multiuser receiver with PIC and SIC respectively for various loading and spatial distributions of the users in peer-to-peer networks were presented in the previous section. It was shown that multiuser receiver using PIC technique with moderately distributed power control was more suitable in a peer-to-peer packet radio networks. Generally, PIC achieves better BER performance improvement if the desired user and the considered interferers have similar signal powers. Multiuser receivers using SIC techniques perform better when the users' power dynamic range is large. So,

we can infer from our simulations that while the CHRT-LAR may be acceptable for lightly loaded system because of its simple complexity, this receiver has limitations for moderate or heavily loaded systems.

The complexity of these receivers are plotted in Fig. 4.20 in terms of floating point operations per bit decision. This is equivalent to the TCB described in Chapter 3. One multiplication or addition was considered as one operation whereas one division was weighed as six operations. We did not consider the storage and processing complexity involved in the system. We considered two stages of cancellation for PIC. The complexity of the CHRT-LAR is independent of the number of users. This may be appealing in that one can add a very high number of users in the system by using CHRT-LAR. Previous plots showed that the computational complexity per bit decision is not the issue for the single-user receiver but the convergence of adaptive algorithms is the primary detriment for a system involving a higher number of users. Though the computational complexity per bit decision of the PIC technique is the highest, this complexity is partially compensated for by a high degree of parallelism and the development of high speed DSP and FPGAs have solved some of the computational constraints.

4.2.3 Conclusions

The use of single-user adaptive receivers is limited to short code DS-SS signals due to limitations on the size of the adaptive filters, and a training sequence is required for adapting the filter weights. The length of the training sequence as well as the adaptation period grows with factors, i.e., number of users, the processing gain and the higher amplitude of the interfering signals. For ad hoc networks, this is a drawback and blind algorithms are needed to overcome this event. The BER performance of the single-user adaptive receiver greatly depends on the orthogonality of the signature sequence, since we can not afford large processing gain. As a result, BER performance is the primary disadvantage of the single-user adaptive receiver for moderate and heavy system loading levels. The complexity of the single-user receivers does not depend on the system load but the convergence of the filter weights is the limiting factor for higher load or processing gain in the system. As a result, the single-user adaptive receiver is a possibility for lightly loaded systems with small processing gain. For more heavily loaded systems, the complexity is still lower compared with that of the multiuser receiver but the performance is unacceptable. From our simulations,

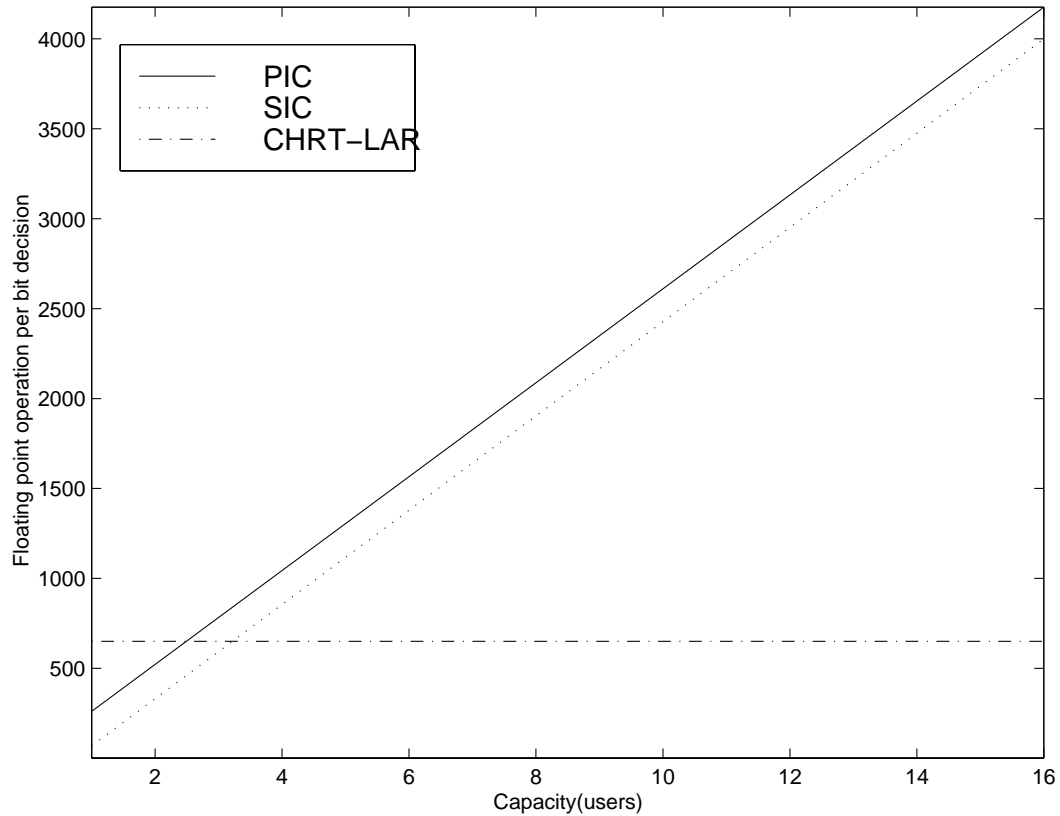


Figure 4.20: Computational complexity of various receivers.

we conclude that the multiuser receiver may be suitable for wireless ad hoc networks over the single-user adaptive receiver in moderate and heavy loaded systems.

4.3 Chapter Summary

After comparing all these receivers for the proposed peer-to-peer packet radio networks, we choose the PIC receiver; this receiver structure becomes the focus of the next chapter, where we study this receiver for possible improvements such as, optimization of the soft-cancellation factor, and integration of parallel interference cancellation with error correction coding.

Chapter 5

Iterative Interference Cancellation and Decoding Using a Soft Cancellation Factor for DS-CDMA

This chapter focuses on the integration of parallel interference cancellation with forward error correction coding, and the optimization of soft-cancellation factor in parallel interference cancellation. First, we will discuss the integration of parallel interference cancellation with forward error correction coding in a multiuser receiver for DS-CDMA systems. A soft-output PIC algorithm is followed by a log-MAP receiver for decoding of convolutional codes. An integrated receiver that implements multiple stages of interference cancellation and decoding is presented and evaluated through simulation. This integrated approach is compared with a partitioned approach, where the final stage output of PIC is followed by the decoding using a soft-input Viterbi algorithm (VA). Results presented for BER and capacity of the two systems show that both techniques represent a substantial improvement over conventional detection, but the more complex integrated approach provides only a small improvement over the decoupled approach.

Second, we will discuss the optimization of the soft cancellation factor (SCF) in a DS-CDMA system that employs both partial parallel interference cancellation and convolutional coding. Information is shared between the operations of interference cancellation and decoding in an iterative manner, using log-likelihood ratios (LLR) of the estimated coded symbols. We investigate the performance of this system for both synchronous and asynchronous CDMA systems, and for both equal and unequal

signal powers. Previous work has demonstrated the improved performance of partial parallel interference cancellation in which the interference estimates are weighted by a soft cancellation factor (SCF). We examine the best choice of the SCF for optimizing the combined performance of interference cancellation and coding. Since this chapter considers coding in a DS-CDMA system, the fundamentals of coding principle related to iterative decoding are discussed briefly in the next section.

5.1 Coding in DS-CDMA

DS-CDMA provides considerable dimensionality enhancements because of the Fourier bandwidth expansion. Forward error-correction coding (FEC) expands the Shannon bandwidth; as a result, the capacity increases due to the bandwidth expansion. In integrating multiuser detection using interference cancellation with FEC, can we achieve the performance of FEC without sacrificing the performance improvement of interference cancellation?

Coding is always beneficial and sometimes crucial for both hostile and friendly sources in spread spectrum communications [63]. From the channel coding theorem, we know that channel capacity is proportional to the transmission bandwidth and increases logarithmically with the signal-to-noise ratio (SNR). On the other hand, for a fixed capacity, the SNR requirement can be reduced by expanding the transmission bandwidth. So the increase of transmission bandwidth due to coding pays off in terms of coding gain. The coding gain is defined as the difference between the SNR requirement without coding and that with coding for a fixed error probability. Adaptive encoder-decoder technology can provide a means for efficient use of the system bandwidth. Jam-resistance and flexible data capabilities can be achieved by a variety of source coding and flow control strategies matched to voice and data traffic statistics. Also, for any given user population, there exists an optimal code rate which will maximize the system throughput. If the code rate can be varied and an exact estimate of the interference level is available, an optimal code rate can always be used resulting in optimal throughput for any user population [64]. In addition, adaptive joint source and channel coding techniques can be used to allocate bits in an optimal way between source and channel encoders as the source and channel vary [65]. In practice, exact estimate of the interference level is not often achievable. As a result, the fixed rate code is a realistic choice. The choice of the code vector length, code

rate, and the decoding algorithm influences the performance of a reliable transmission; we will concentrate on the influence of the decoding algorithm. Before that, we will present some basic terminologies used in encoding and decoding of FEC.

There are two major classes of error correction coding techniques used in practice today, block coding and convolutional coding. Recently, turbo decoding which concatenates two parallel recursive systematic convolutional (RSC) codes, achieved the performance near the Shannon limit in terms of BER [66]. Our iterative decoding in multiuser detection shares many of the concepts and terminology of the block and convolutional codes. A brief overview of the block and convolutional codes is presented as follows.

5.1.1 Block Codes

A *block* code is a set of fixed length vectors called code words or code vectors. The encoding process groups input data into blocks of k information bits, \mathbf{m} and maps them into blocks of n coded bits, \mathbf{x} . The encoding process can be realized by the matrix multiplication

$$\mathbf{x} = \mathbf{m}G, \quad (5.1)$$

where the code vector $\mathbf{x} = (x_0 \cdots x_{n-1})$, the information vector $\mathbf{m} = (m_0 \cdots m_{k-1})$ and G is the $k \times n$ generator matrix; the finite field arithmetic is employed. There are 2^k possible received code vectors, irrespective of the transmitted information bits, \mathbf{m} . The function of the decoder is to classify these 2^n possible received vectors into 2^k disjoint subsets, so the received vector will fall into one of these subsets. An important parameter for comparing codes is the minimum distance of the code, denoted d_{min} . The number of bits differing between a pair of code words is called the Hamming distance between these two code words. The minimum distance is the smallest Hamming distance between any two code words. A code with a minimum distance of d_{min} is guaranteed to correct t or fewer errors, where

$$t = \left\lfloor \frac{d_{min} - 1}{2} \right\rfloor. \quad (5.2)$$

A code is *cyclic* if cyclic permutation of the elements in a code word generates a new code word. An alternative method of representing a code word is to let the elements $(x_0 \cdots x_{n-1})$ of the code word be the coefficient of a polynomial, D . Likewise, the information can be expressed as an information polynomial $m(D)$ and

the generator matrix can be expressed by a generator polynomial $g(D)$. The encoding operation then becomes polynomial multiplication $x(D) = m(D)g(D)$.

5.1.2 Convolutional Codes

Convolutional coding is a forward error correction coding technique which is implemented by introducing controlled redundancy into the transmitted information stream allowing the receiver to detect and possibly correct errors. Unlike the block codes, a convolutional encoder converts the entire data packet into one single code word and provides the error correction capabilities for real time applications. Convolutional codes are similar to the cyclic codes in the sense that the encoder can be implemented using a linear shift register network. On the other hand, cyclic codes are block codes with fixed block size and single-input single-output codes, but convolutional codes are not restricted to those criteria.

A convolutional code is generated by passing the information sequence to be transmitted through a linear finite state shift register. The encoded outputs are obtained by modulo-2 addition of the contents of the shift register. Since the *encoding* operation involves mathematical *convolution*, these codes are *convolutional* codes. If the number of output bits for every k input bits is n , then it is called rate k/n convolutional encoder. If there are W shift registers present in the encoder then it is said that the encoder has a constraint length $W + 1$.

A code is said to be *systematic* if the information bit sequence is contained within the code word. A convolutional code can be systematic or non-systematic. Any code can be made systematic without affecting its minimum free distance by performing row reduction on the generator matrix [67]. Since the minimum free distance determines the error correcting capability of the decoding operation, the performance of the decoder does not depend on whether the code is systematic or non-systematic. The complexity of the algorithm to calculate the LLR is different for the systematic code than for non-systematic code. An example of a rate 1/2 RSC code is shown in Fig. 5.1.

The output code sequence x_i consists of the information bit m_i (also called systematic bit $x_i^{(0)}$) and the parity bit $x_i^{(1)}$. A convolutional code can be made systematic by first calculating the remainder of the polynomial division $m(D)/g^{(0)}(D)$ [67]. The parity output polynomial is then found by the polynomial multiplication $x_i^{(1)} = r(D)g^{(1)}(D)$. The remainder $r(D)$ can be found using a shift register network

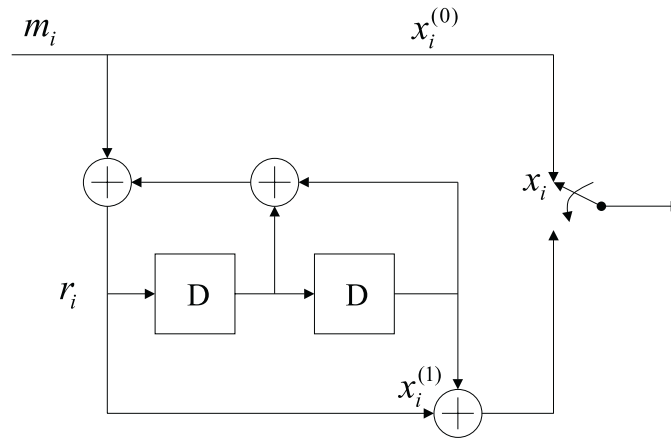


Figure 5.1: An RSC encoder for rate 1/2 recursive convolutional code.

with feedback as shown in Fig. 5.1, where the feedback polynomial is $g^{(0)}(D)$ and the forward polynomial is $g^{(1)}(D)$. Code generated in this way is called the RSC code.

5.2 Iterative Interference Cancellation and Decoding for DS-CDMA

DS-CDMA has been adopted for commercial cellular applications and due to its success in cellular systems, there is also a great deal of interest in DS-CDMA for peer-to-peer packet radio networks for military applications. Furthermore, direct sequence CDMA is emerging as the predominant technology for the next generation global wireless standard because of high spectral efficiency and robust performance in multipath [68]. For greater throughput, multiuser receivers with interference cancellation techniques have been proposed for wideband CDMA. Multiuser detection can be combined with error correction coding to achieve additional throughput enhancement. Joint detection and decoding in a multiuser receiver have been an active research area in recent years. The authors of [69] and [70] examine multistage detectors for convolutionally encoded signals, dividing multiuser receivers into two classes. One is a partitioned approach, where the multiuser detector precedes the decoder and does not utilize the decoder output. The other is an integrated approach, in which the decoder outputs of interfering signals are used for MAI cancellation in the signal of the desired user. Soft-output from the decoder of a previous stage can be used as a priori information for decoding of the following stage.

A suboptimal multiuser receiver using PIC achieves a large performance improvement over a conventional MF receiver. Error correction coding, which provides added protection against noise and interference, can be combined with PIC in this multiuser receiver. The maximum-likelihood multiuser decoding scheme proposed in [71] requires exponential complexity with respect to the number of users because it searches jointly through trellises of all users. The optimal decoding using a trellis diagram has complexity $O(2^{WK})$, where K is the total number of users in the system and W is the constraint length of the encoder. This decoding involves the joint estimation of K Markov processes, one for each user. While in theory it is possible to model this as a single Markov process, the decoding algorithm is extremely complex in practice. In [70], multiuser detection using PIC followed by a single-user decoding algorithm reduced this complexity considerably but resulted in a sub-optimal decoding technique. For this system, both the decoding complexity, and the complexity of the interference cancellation algorithms, increase linearly with the number of users, while the receiver shows a large performance improvement over the performance achieved by the noncombining techniques.

In the partitioned approach, the tentative decisions produced by the interference cancellations of each stage ignore the fact that each user's data is encoded, i.e., treating it as if it were an uncoded data sequence. Decoding is only performed after the last stage. In the integrated approach, the received data sequence for each user is considered as a coded bit sequence, and tentative decisions are made using a decoder with the resulting information bit sequence being re-encoded before the next stage of cancellation. This scheme is better from a coding point of view but needs a decoder/encoder pair for each user at each cancellation stage. One way to waive the requirement of reencoding the data is to estimate the coded bit instead of information bit using a decoder. The purpose of this section is to present a receiver which integrates PIC and decoding using the log-MAP algorithm in multiuser detection, and to compare this approach with other combining techniques. The remainder of this section is organized as follows. A description of a coded DS-CDMA system with PIC is given in Section 5.2.1. The iterative decoding principle is presented in Section 5.2.2, followed by simulation results in Section 5.2.3. Finally, a summary is given in Section 5.2.4.

5.2.1 System Description

We consider an asynchronous baseband DS-CDMA system employing BPSK modulation with K users, each transmitting a block of N_p coded bits of an information bit sequence, $\mathbf{b}_k = b_k[i]$ for $1 \leq i \leq N_p/n$, through a convolutional encoder with a rate $R = 1/n$ and constraint length W . While we assume that each user employs the same convolutional code, this model can be generalized to the case where each user employs a different code. The cumulative received signal $r(t)$ at the demodulator input can be modeled as

$$r(t) = \sum_{k=1}^K s_k(t) + n(t), \quad (5.3)$$

where $n(t)$ is a complex additive white Gaussian noise with power spectral density $N_0/2$, and $s_k(t)$ is the transmitted signal for user k , given in complex envelope form:

$$s_k(t) = \sum_{i=1}^{N_p} A_k[i] d_k[i] a_k(t - iT_d - \tau_k) e^{j\phi_k}, \quad (5.4)$$

where $d_k[i] \in \{-1, 1\}$ is the i th coded bit of user k and where T_d , $A_k[i]$, τ_k , and $\{a_k(t); 0 \leq t \leq T_d\}$ denote respectively, the coded bit interval, the received signal amplitude for i th coded bit of user k , delay of user k and the signature waveform of user k . The term coded bit refers to one of the bits in the stream of bits that constitutes a code vector of a user's encoder. It is assumed that τ_k is uniformly distributed over one coded bit period T_d , the phase offset of transmitter k is θ_k , and $\phi_k = [\theta_k - \omega_c \tau_k] \bmod 2\pi$, where ω_c is the carrier frequency. The received signal is passed through a bank of MF with output

$$y_k^{(0)}[i] = \int_{iT_d + \tau_k}^{(i+1)T_d + \tau_k} \text{Re}\{r(t) a_k(t - iT - \tau_k) e^{-j\phi_k}\} dt, \quad (5.5)$$

and the corresponding bit estimate is given by $d_k^{(0)}[i] = \text{sgn}(y_k^{(0)}[i])$. The output for the k th MF in the *zeroth* iteration stage is denoted by $\mathbf{y}_k^{(0)} = [y_k^{(0)}[1], \dots, y_k^{(0)}[N_p]]^T$ and corresponding code vector is represented by $\mathbf{d}_k^{(0)} = [d_k^{(0)}[1], \dots, d_k^{(0)}[N_p]]^T$.

We use a model for PIC based on the approach of [39] which builds on [34]. Here, the estimates of the transmitted signals are made simultaneously and in parallel for all the users. Interference cancellation is performed by subtracting the estimated signals of the interfering users from the received signal to form a new received signal for the k th user after stage q , given by

$$r_k^{(q)}(t) = r(t) - \sum_{j=1, j \neq k}^K p_{i,j}^{(q)} \hat{s}_j^{(q)}(t - \tau_j), \quad (5.6)$$

where $p_{i,j}^{(q)}$ is the optimal SCF of j th user for i th coded bit as computed in [55]. The decision statistic for the i th coded bit of the k th user at stage $q + 1$ is formed by correlating $r_k^{(q)}(t)$ with the k th user's signature signal.

5.2.2 Iterative Decoding

The problem of estimating the states of a Markov process observed through the noise has two types of solutions. One is based on the sequence estimation of the received vector where Viterbi algorithm (VA) is used [72] and the other is based on symbol-by-symbol estimation of the received signal where MAP algorithm is used [73]. The two algorithms differ in their optimality criterion. For digital communication, VA minimizes the frame or packet error probability and MAP algorithm minimizes symbol error probability. The VA searches for the most probable transmitted sequence $\hat{\mathbf{x}}$, given the received vector \mathbf{y}

$$\hat{\mathbf{x}} = \arg \left\{ \max_{\mathbf{x}} [P(\mathbf{x}|\mathbf{y})] \right\}, \quad (5.7)$$

and the MAP algorithm searches for the most probable transmitted symbol \hat{x}_i , given the received vector \mathbf{y}

$$\hat{x}_i = \arg \left\{ \max_{x_i} [P(x_i|\mathbf{y})] \right\}. \quad (5.8)$$

The complexity of optimal iterative MUD, where multiuser detection is followed by the joint ML decoding, can be reduced by combining the iterative multiuser detection using parallel interference cancellation with a single user decoding. One of the above two algorithms can be used for decoding. The decoding performance is not optimal anymore because now, we are considering all disjoint components of the set. This combination of MUD and decoding scheme, called integrated approach, is shown in Fig. 5.2. Another way, which is simpler, is the partitioned approach, where the final stage output of PIC is followed by the decoding.

Now the problem is sharing the information between MUD and decoding. While there is reason to believe that interference cancellation, which removes multiple access interference, will be at least partially complementary with error correction techniques which correct error from uncanceled interference and noise, it is also possible that the errors corrected by both techniques are at least partially overlapping.

Until now, the manner in which the error correction decoder should be combined with interference cancellation at the receiver is not entirely clear. It is obvious that the partitioned approach is less complex. Will the more complex integrated approach

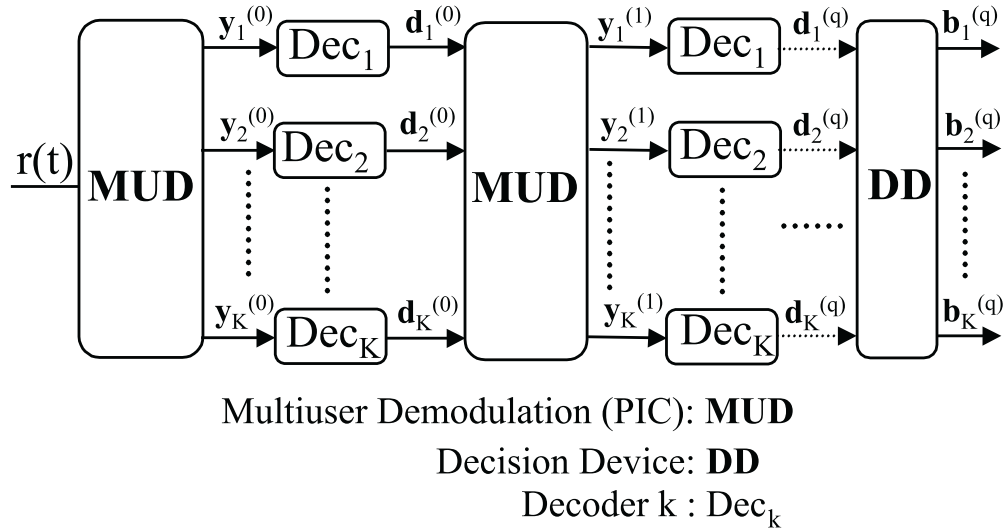


Figure 5.2: Block diagram of iterative MUD (PIC) and decoding for DS-CDMA system.

pay off in terms of performance improvement? This performance improvement also depends on the algorithm used for decoding. Obviously a soft-output algorithm provides better performance and for combination of MUD and decoding, a soft-output algorithm is desirable.

In iterative decoding, the output (a posteriori information) from one iteration is used as the input (a priori information) by the following iteration. If the outputs of the MUD are in the form of hard-bit decisions, there is little advantage of sharing the information. The soft-bit decisions inherently possess more information and perform better where those decisions contribute to later decisions. Soft-bit decisions typically take the form of log-likelihood ratios (LLR's). Let us consider a binary detection problem in which the source transmits one of two signals, where the former signal is denoted by hypothesis H_0 , and the later signal is denoted by hypothesis, H_1 . For an observation random process $Y(t)$, we know that one of the two hypotheses is true. The LLR can be defined as

$$\Lambda(\mathbf{y}) \triangleq \ln \frac{f_{Y|H_1}(\mathbf{y}|H_1)}{f_{Y|H_0}(\mathbf{y}|H_0)}. \quad (5.9)$$

For the trellis based decoding, if the observation vector is \mathbf{y} and the input information

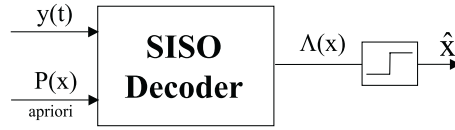


Figure 5.3: Block diagram of a soft-input soft-output (SISO) decoder.

vector is \mathbf{x} , then the LLR can be written as

$$\Lambda(x_i) \triangleq \ln \frac{P(x_i = 1|\mathbf{y})}{P(x_i = 0|\mathbf{y})}. \quad (5.10)$$

Fig. 5.3 shows the block diagram of a typical soft-input soft-output (SISO) decoder where, in addition to the observation vector $\mathbf{y}(\mathbf{t})$, the a priori information about the estimated vector \mathbf{x} is needed. The output from the SISO decoder is the a posteriori information about the estimated vector \mathbf{x} . A threshold device can be used to estimate about the vector $\hat{\mathbf{x}}$.

Fig. 5.4 depicts two classes of soft-output decoding algorithms. Algorithms based on MAP rule are more complex than the Viterbi algorithms. Since its introduction [73] in 1974, MAP algorithm got less attention due to its complexity. Recently, the revolutionary performance using iterative decoding [66] triggered the renewed interest about this algorithm. The Viterbi algorithm exploits several properties of the underlying Markov process. The conditional probability that the process is in a particular state given all previous states, depends only on the last state. The conditional probability of a particular observation y_i through the white noise, depends only on the last state transition. The MAP algorithm requires forward and backward recursions and is therefore suitable for block oriented processing. Along with the complexity, the MAP algorithm suffers from numerical sensitivity. The numerical sensitivity is alleviated by log-MAP algorithm [74] and complexity is reduced by max-log-MAP algorithm [75]. The comparison of the performances and complexities of these algorithms can be found in [74], [75] and [76].

Since we will use log-MAP and SOVA algorithms in the iterative decoding, relevant insight about the MAP algorithm is presented here through a trellis diagram. The SOVA can also be explained similarly. A convolutional code can be described through its trellis; a trellis is the representation of different states that the encoder can be in, but re-drawing all the states after each transition. A trellis diagram is used to describe and to decode the symbol sequence using the above mentioned algorithms.

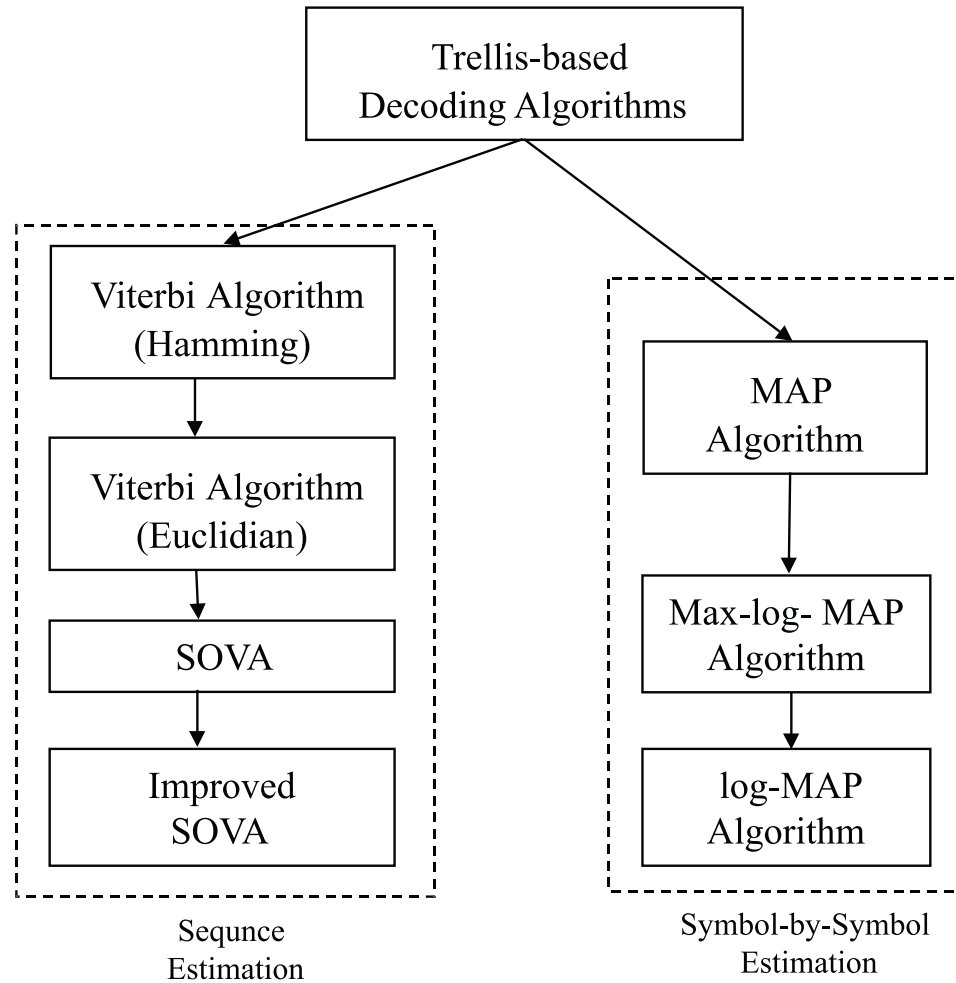


Figure 5.4: Various Decoding Algorithms.

An example of a four-state trellis of a recursive systematic convolutional (RSC) code is shown in Fig. 5.5. In the trellis, only certain transitions are allowed, and for simplicity we will restrict to two transitions per state. The number of states is equal to 2^m , where m is the memory of the encoder. The transitions are labeled with the inputs of the encoder $\in \{0, 1\}$ as well as the outputs of the encoder $\in \{0, 1\}$. The output is modulated and transmitted across the channel. In the trellis, “ $\gamma(s_i \rightarrow s_{i+1})$ ” refers to the branch metric associated with the transition from state s_i to state s_{i+1} . The terms $\alpha(s_i)$ and $\beta(s_i)$ denote the probability of the forward and backward recursion, respectively.

The MAP algorithm calculates the a posteriori probability (APP) of each state

transition, information bit, and/or coded bit, given the received signal vector \mathbf{y} . In our iterative decoding, we need to estimate the APP of the coded bit, which is the a priori information for the next iteration, and also APP of the information bit for bit decisions in the final stage of PIC, where once the APPs are calculated for all possible values of the desired quantity, a hard decision is made by taking the quantity with the highest probability. Before finding the APPs for the information bits, the MAP algorithm first finds the probability $P[s_i \rightarrow s_{i+1}|\mathbf{y}]$ of each valid state transition given the received signal vector \mathbf{y} .

The derivation of the MAP algorithm can be found in [76] and [73], but we are presenting necessary equations for our purpose as follows. From the definition of conditional probability

$$P[s_i \rightarrow s_{i+1}|\mathbf{y}] = \frac{P[s_i \rightarrow s_{i+1}, \mathbf{y}]}{P[\mathbf{y}]}.$$
 (5.11)

From the properties of the Markov process, the numerator can be expressed

$$P[s_i \rightarrow s_{i+1}, \mathbf{y}] = \alpha(s_i)\gamma(s_i \rightarrow s_{i+1})\beta(s_{i+1}),$$
 (5.12)

where the probability $\alpha(s_i)$ can be found according to the forward recursion

$$\alpha(s_i) = \sum_{s_{i-1}} \alpha(s_{i-1})\gamma(s_{i-1} \rightarrow s_i).$$
 (5.13)

Likewise, $\beta(s_i)$ can be found according to the backward recursion

$$\beta(s_i) = \sum_{s_{i+1}} \beta(s_{i+1})\gamma(s_i \rightarrow s_{i+1}).$$
 (5.14)

The log-likelihood ratio then becomes

$$\begin{aligned} \Lambda(x_i) &\triangleq \ln \frac{P(x_i = 1|\mathbf{y})}{P(x_i = 0|\mathbf{y})} \\ &= \ln \frac{\sum_{S_1} \alpha(s_i)\gamma(s_i \rightarrow s_{i+1})\beta(s_{i+1})}{\sum_{S_0} \alpha(s_i)\gamma(s_i \rightarrow s_{i+1})\beta(s_{i+1})}. \end{aligned}$$
 (5.15)

Note that x_i can be either the information bit b_i or the coded bit d_i but their LLRs are not the same, i.e., $LLR(b_i) \neq LLR(d_i)$, as shown in Fig. 5.5. We explicitly showed the transitions from stage $i = 3$ to stage $i = 4$ in Fig. 5.5 for the coded bits. Here, the transitions of two corresponding coded bits due to one information bit, are shown using two different types of nodes: filled square and a solid circle. Transitions from stage $i = 2$ to stage $i = 3$ are explicitly shown for information bits. It is

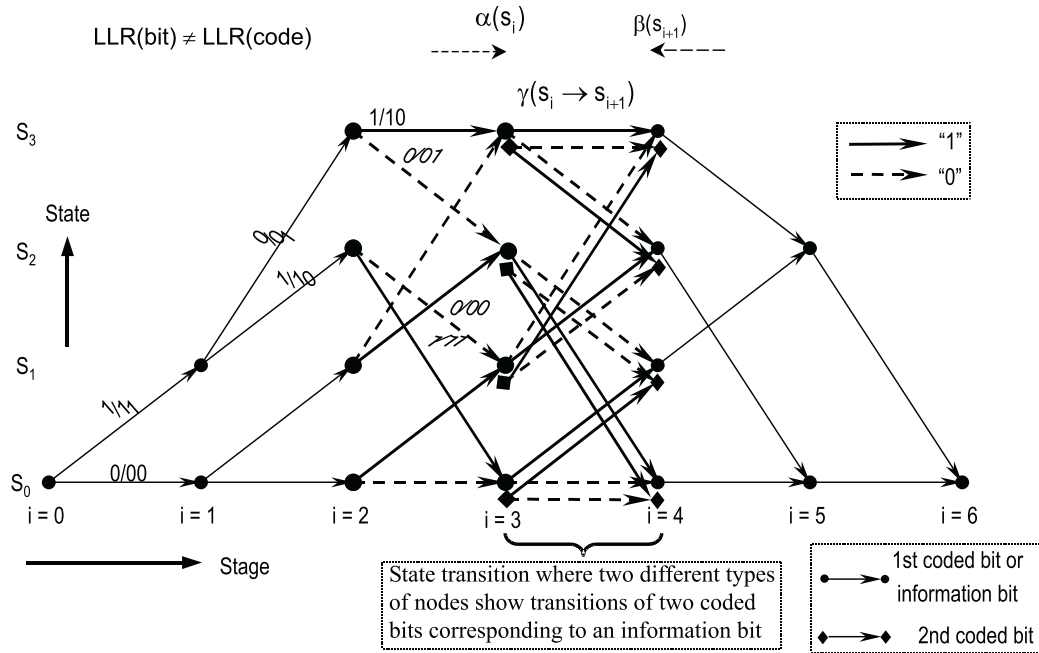


Figure 5.5: The trellis diagram for the decoding of a RSC code using MAP algorithm.

true that LLR of the first coded bit is the LLR of the information bit because of the RSC encoding. This choice of encoding for iterative decoding in a multiuser receiver reduces the computational complexity of the algorithm.

The MAP algorithm [73] minimizes the symbol error probability while obtaining precise estimates of the APP of each information bit/coded bit. The log-MAP version of this algorithm is generally used to minimize computational complexity and numerical sensitivity. The log-MAP algorithm provides better coding gain than the soft-output VA in AWGN channel [74] and performs even better in Rayleigh fading channels with greater memory requirements but similar computational complexity. The LLR $\Lambda_{kd}^{(q)}[i]$ produced by the log-MAP algorithm for the i th coded data bit of the k th user after q iterations is given by

$$\Lambda_{kd}^{(q)}[i] = \ln \frac{P(d_k^{(q)}[i] = +1 | \mathbf{y}_k^{(q)}, \Lambda_{kd}^{(q-1)})}{P(d_k^{(q)}[i] = -1 | \mathbf{y}_k^{(q)}, \Lambda_{kd}^{(q-1)})}, \quad (5.16)$$

where $d_k^{(q)}[i]$ is the value of the i th coded data bit after q iterations, $\mathbf{y}_k^{(q)}$ is the vector of decision statistics out of the q th iteration of the PIC receiver, and $\Lambda_{kd}^{(q-1)}$ is the vector of LLRs for the k th user coded data bit from the previous iteration. The a priori probability vector for the q th iteration for user k , $P(\mathbf{d}_k^{(q)})$, is equal to the APP

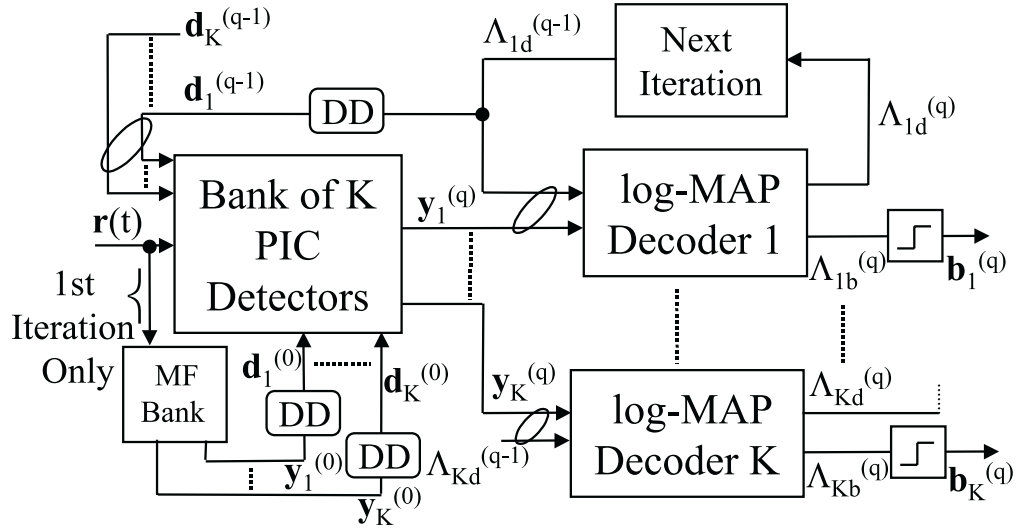


Figure 5.6: System model of an iterative parallel interference cancellation receiver for a coded system.

in $(q - 1)$ th iteration, $P(d_k^{(q-1)} | \Lambda_{kd}^{(q-1)})$, and is related to the LLR obtained during the $(q - 1)$ th iteration by :

$$P(d_k^{(q-1)}[i] | \Lambda_{kd}^{(q-1)}[i]) = \begin{cases} \frac{\exp\{\Lambda_{kd}^{(q-1)}[i]\}}{1 + \exp\{\Lambda_{kd}^{(q-1)}[i]\}}, & \text{for } d_k^{(q-1)}[i] = +1 \\ \frac{1}{1 + \exp\{\Lambda_{kd}^{(q-1)}[i]\}}, & \text{for } d_k^{(q-1)}[i] = -1. \end{cases} \quad (5.17)$$

For the first iteration $\Lambda_{kd}^{(0)}$ is initialized to be all zeros for all users. Fig. 5.6 depicts the flow diagram of the integrated approach, where PIC is used for detection and the log-MAP algorithm is used for decoding. The output of the final iteration is the estimated bit stream. If we use a recursive systematic code at the encoder, the LLR for code estimation contains LLR for information bit estimation $\Lambda_{kb}^{(q)}$. After obtaining $\Lambda_{kb}^{(q)}$, we take the sign of the vector to estimate information bits, $\mathbf{b}_k^{(q)}$.

5.2.3 Simulation Results

To provide a direct comparison between the performance of the integrated approach, the partitioned approach and the individual techniques in terms of BER at moderate to low E_b/N_0 , we present results from Monte Carlo simulations. By individual technique, we mean either PIC without coding or coding without PIC. Simulations

were performed for the AWGN channel with data packet sizes of $N_p = 50$ and random PN sequence with processing gain of $N=31$. A rate 1/2 convolutional code with constraint length 3 was used. The value of SCF was assumed to be $p_{i,j}^{(q)} = 0.6$ for all users in cancelling the interference for $q = 1$ and $p_{i,j}^{(q)} = 1$ for all subsequent stages. While there exists an optimal SCF corresponding to each user in an iteration stage, the choice of one value for all users was fixed to keep the receiver complexity linear with the number of users.

Fig. 5.7 shows BER as a function of E_b/N_0 in the case of 10 users in the system, where signal powers at the receiver due to users are as follows: $P(\text{dB}) = [0(\text{desired}) \ 3 \ 3 \ -3 \ -3 \ 3 \ 3 \ 6 \ 6 \ 0]$. The term ‘‘PIC+MAP’’ refers to the integrated approach where PIC is used for detection and the log-MAP algorithm is used for decoding. The term ‘‘PIC+SIV’’ refers to the partitioned approach when soft-input VA is used for decoding. The term ‘‘PIC’’ denotes parallel interference cancellation without coding, and in ‘‘MF output’’, there is no use of interference cancellation. The plots in Fig. 5.7 show that integrated approach outperforms the partitioned approach and both of them achieve a large performance improvement over individual techniques. Note that the performance improvement using either MAP or SIV algorithm is the same for a conventional MF receiver. Since the system is interference limited, coding alone is not sufficient.

Fig. 5.8 shows BER versus E_b/N_0 for the same CDMA system with 2 stages of PIC. This means that all plots in this figure except the ‘‘MF output’’ are obtained after second stage of PIC ($q = 2$). The term ‘‘PIC+MAP(1-bit)’’ refers to the integrated approach and PIC is used for detection, where the amplitudes of the signals for regeneration are obtained from MF output without any bit averaging. The term ‘‘PIC+MAP(perf)’’ refers to the integrated approach and PIC is used for detection, where the amplitude estimates of the signals for regeneration are assumed to be perfect. Note that the perfect amplitudes are bounds on the performance of actual amplitude estimation. In ‘‘SIV+PIC+MAP(perf)’’, we used a soft-input VA for coded bit estimation before any interference cancellation. This means that VA was used to estimate $\mathbf{d}_k^{(0)}$ from $\mathbf{y}_k^{(0)}$ of Fig. 5.9. This decoding hurts the performance considerably, because the MF output contains all the MAI and coding does not help the decision statistics since the desired signal is interference limited. The signal to interference ratio should be above a threshold value for BER improvement due to coding. We can also see the performance enhancement due to improved estimation of signal amplitudes. Our simulations also show that bit-averaging does not improve

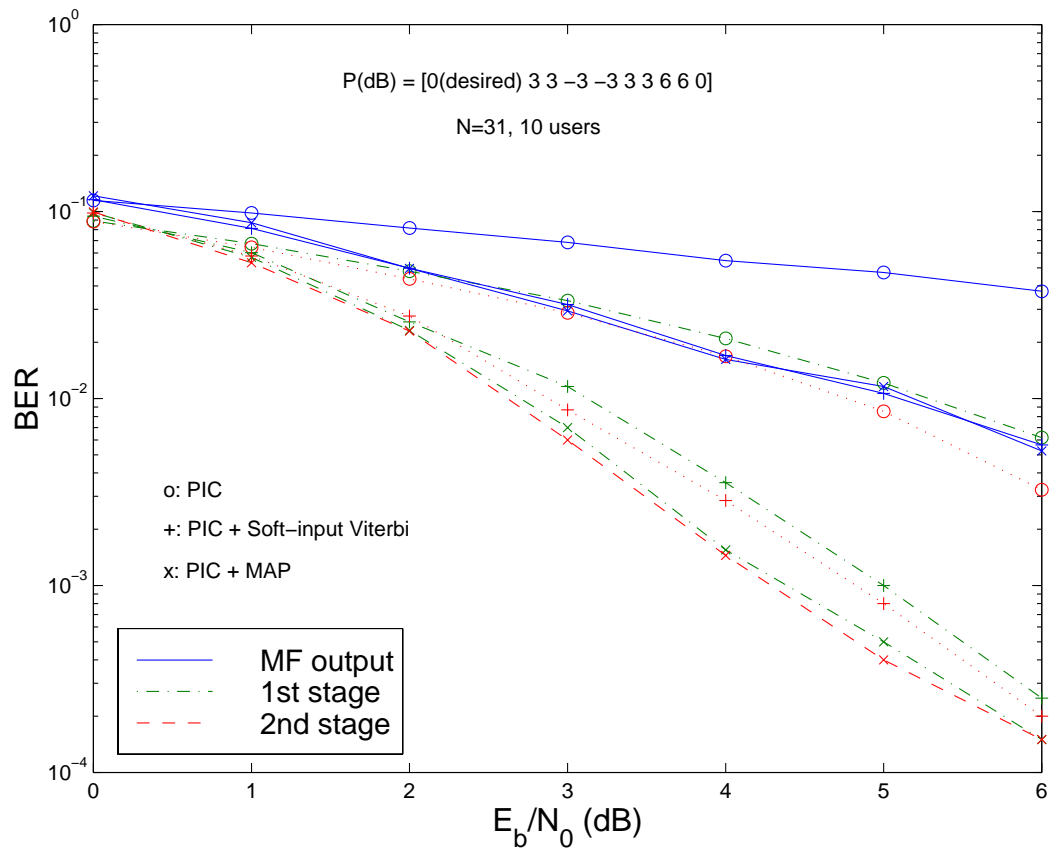


Figure 5.7: BER of the desired user as a function of its E_b/N_0 considering 10 users in the system and 2 stages of IC.

the code estimation, and even hurts the BER performance of our coded system. The term “2 stage PIC” refers to the BER performance after second stage of PIC for an uncoded system. Note that the coded system requires double the bandwidth of the uncoded system.

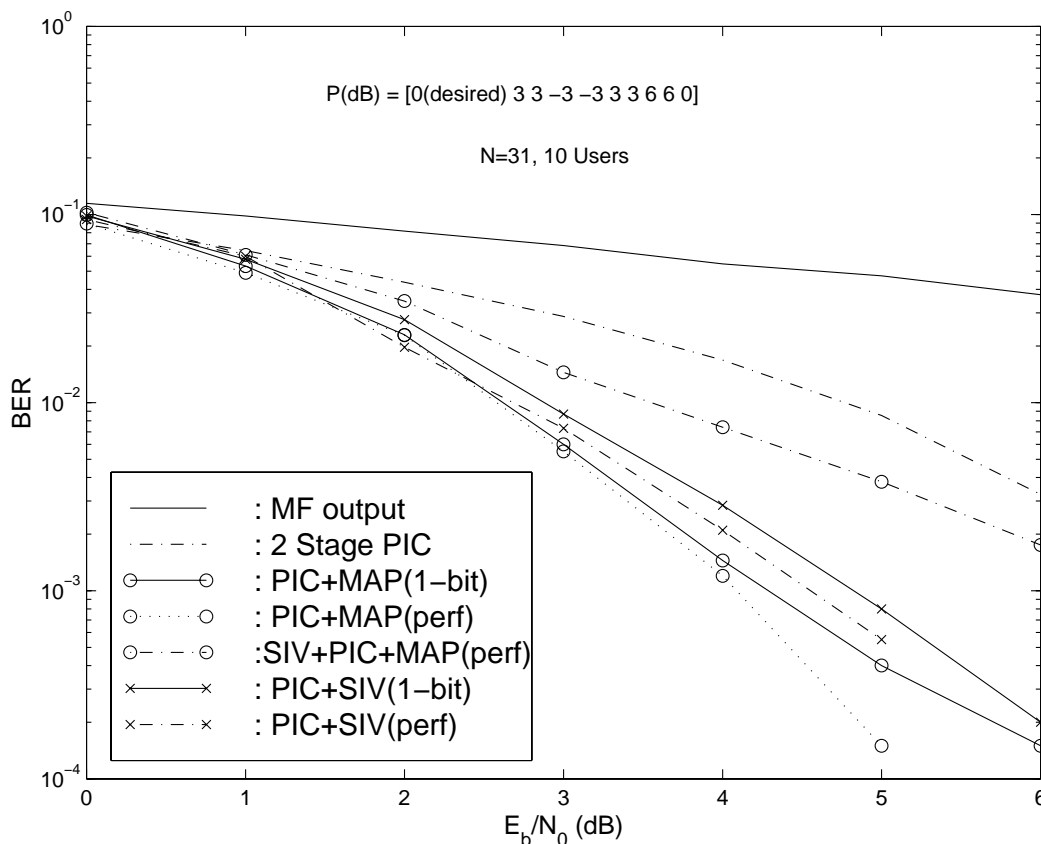


Figure 5.8: BER of the desired user vs. its E_b/N_0 for second stage of IC considering 10 users in the system.

5.2.4 Section Summary

Our simulation results show that an integrated approach to decoding and MUD outperforms the partitioned approach. It is also worth mentioning that the partitioned approach, which is easier to implement and requires less memory, achieves a large performance improvement over non-combined techniques. Note that the integrated scheme requires one more decoder per user in each iteration than the decoupled scheme. If the system has a low signal to interference ratio, most of the performance

improvement occurs due to PIC. Since we use the same code for each user, these results may be very close to the bound that can be achieved by this convolutional code. For better performance, a turbo encoder and decoder could be used by replacing our convolutional encoder and decoder, respectively. Finally, note that the optimal SCF for a partitioned approach to decoding and MUD will be different than the optimal SCF for an integrated approach.

5.3 Optimization of Soft-Cancellation Factor in Parallel Interference Cancellation.

In order to enhance capacity and near-far resistance of a DS-CDMA system, third generation systems may employ parallel interference cancellation (PIC) on the up-link. Previous work has shown that direct PIC results in a bias of the desired signal component, caused by the accumulation of small correlations between the desired signal and interference [77], [55]. One technique for mitigating this bias is weighting of the estimated interference components by a SCF, prior to cancellation. This SCF is proportional to the confidence in the reliability of the interference estimate, and decreases at higher interference levels. Because the SCF is typically less than one, the resulting cancellation technique is often termed partial PIC.

Optimization of the SCF has been previously attempted in [57] and [78]. In [57], the authors derive a semi-analytic result for the SCF that minimizes BER of the desired user as a function of signal-to-noise ratio, interference level, and processing gain. In [77], the optimal SCF for an arbitrary stage of interference cancellation is computed as a function of system parameters and the reliability of the data estimate at the previous stage. For linear (soft) estimates of the symbol, we will show that the approaches of [77] and [57] are equivalent. The linear estimate can be viewed as a joint estimate of the symbol and the channel assuming perfect channel knowledge. However, both [77] and [57] focus on derivation of the SCF for a synchronous CDMA system, because analysis of the asynchronous case is not tractable. Furthermore, both of these results assume equal power in all received signals. Most practical CDMA systems are neither synchronous nor have perfect power control available. Some simulation studies have considered optimization of the SCF for asynchronous CDMA [55], although these limited results also assume equal signal powers in all users.

We intend to study the choice of SCF in a more generalized context. We consider asynchronous systems in which near-far effects are present. It is shown in [57] that for optimal performance, unequal signal powers may lead to a choice of different SCFs for each user in the system. However, since this would result in the design of a receiver for which the complexity is no longer linearly proportional to the number of users, we consider a sub-optimal choice of SCFs which is calculated for the refined estimation of the desired user's signal. Furthermore, in practice interference cancellation will be used in conjunction with error correction coding. Though the individual performance of interference cancellation and error correction coding has been extensively studied, the performance of systems jointly employing the two techniques is less-well understood. The integration of parallel interference cancellation with forward error correction coding in a multiuser receiver for DS-CDMA systems has been presented in the previous section. The remainder of this section is organized as follows. The consideration of a SCF due to a bias in the amplitude estimation using PIC is discussed in Section 5.3.1, followed by the derivation of the SCF for general case in Section 5.3.2. Next, we take a pragmatic approach to choose an optimal SCF in Section 5.3.3. We present the simulation results in Section 5.3.4 and the summary for the optimization of SCF in Section 5.3.5, respectively.

5.3.1 The Soft Cancellation Factor in Parallel IC

By comparing the uncoded synchronous and asynchronous systems, it can be shown that the average value of signal amplitude estimation from the MF after the first stage PIC in the asynchronous system is [57]

$$E \left[y_k^{(1)}[i] | b_k[i] \right] = \underbrace{A_k[i] b_k[i]}_{\text{Des. Amp. Est}} - \underbrace{\frac{1}{3N} A_k[i] b_k[i] (K-1)}_{\text{Bias}}, \quad (5.18)$$

and the average value of the bias difference between those amplitude estimations for synchronous and asynchronous system is

$$E [Diff_{bias}] = \frac{1}{6N} A_k[i] b_k[i] (K-1), \quad (5.19)$$

where N is the processing gain. Note that the resulting bias is different for synchronous and asynchronous systems, implying that results defined for the synchronous case are not readily applicable to the asynchronous case. The analytic expression of the variance considering this bias is tedious for the asynchronous system. Since we

do not know the precise variance, and BER is a function of both the mean and the variance of the signal amplitude estimation, we use a simulation approach to evaluate BER for an asynchronous system. Since the bias difference is about 8% for a 50% ($K/N = 0.5$) loaded system, the reliability of the MAI estimate is roughly similar between the two cases for the light loaded system. Therefore, the two types of systems will have similar optimal SCFs for low loading. For a higher loading however, the bias magnitude in the synchronous system is greater than that in the asynchronous system, leading consequently to a lower SCF for the synchronous system. The bias is directly proportional to the loading of the system and partial cancellation reduces this bias, thus improving the performance. For partial cancellation, (5.18) becomes

$$E \left[y_k^{(1)}[i] \middle| b_k[i] \right] = \underbrace{A_k[i] b_k[i]}_{\text{Des. Amp. Est}} - \underbrace{\frac{P_k^{(1)}}{3N} A_k[i] b_k[i] (K-1)}_{\text{Bias}}. \quad (5.20)$$

Based on the approach in reference [77], we will study the SCF thoroughly in the following section. Appendix A, where the system model is developed from the basics of the receiver design, complements some derivation details of the next section.

5.3.2 Derivation of the SCF from Iterative Decoding

Fig. 5.9 shows a model of multistage PIC based on the approach described in [77], where two stages of partial IC for user 1 is delineated. Note that the receiver complexity is linear with the number of users. The terms $y_k^{(q)}$, $\tilde{b}_k^{(q)}$ and $c_k^{(q)}$ in Fig. 5.9 refer to matched filter output, the tentative bit decisions and a SCF respectively, of user k after q th stage of PIC. If $c_k^{(q)} = 1$ for all stages of IC, then this system model will be identical to the system model of direct PIC as shown in Chapter 3; thus, other parameters in the diagram bear the same meaning of the PIC model presented in Chapter 3.

If we follow the derivations in Section 5.2.2, from equation (5.17) the average value of the i th coded bit after $(q-1)$ th iteration, called “*soft-bit*” can be written as [79]

$$\begin{aligned} E \left(d_k^{(q-1)}[i] \right) &= P \left(d_k^{(q-1)}[i] = +1 \middle| \Lambda_{kd}^{(q-1)}[i] \right) - P \left(d_k^{(q-1)}[i] = -1 \middle| \Lambda_{kd}^{(q-1)}[i] \right) \\ &= 2P \left(d_k^{(q-1)}[i] = +1 \middle| \Lambda_{kd}^{(q-1)}[i] \right) - 1 \\ &= \tanh \left(\frac{\Lambda_{kd}^{(q-1)}[i]}{2} \right), \quad \in \{+1, -1\}. \end{aligned} \quad (5.21)$$

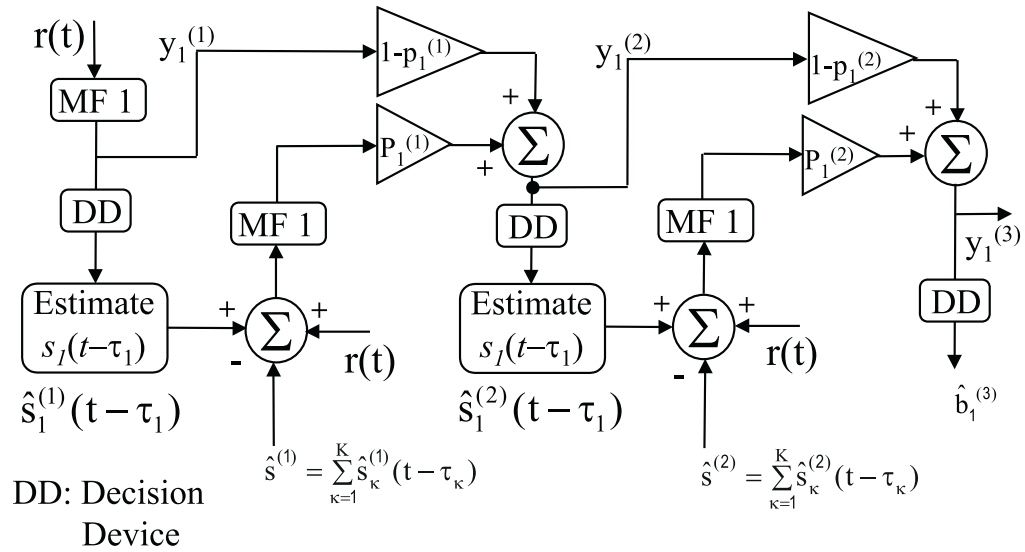


Figure 5.9: System model of a multistage parallel IC receiver for CDMA based on the approach described in [67].

Following the derivation in Appendix B, where we have the expression of the average value of the i th bit in equation (B.34), the bit estimation can be written as

$$d_k^{(q-1)}[i] = \frac{\exp(\alpha_k \beta_k) - \exp(-\alpha_k \beta_k)}{\exp(\alpha_k \beta_k) + \exp(-\alpha_k \beta_k)} = \tanh(\alpha_k \beta_k). \quad (5.22)$$

Here α_k and β_k are

$$\alpha_k \triangleq \sqrt{\frac{2E_{b1}}{N_0}} \left(\frac{\sigma_1^2 + \sigma_{2k}^2 - 2\rho_k \sigma_1 \sigma_{2k}}{\sigma_1^2 \sigma_{2k}^2 (1 - \rho_k^2)} \right) \text{ and } \beta_k \triangleq c_k (Y_1 - \hat{I}_1^{(q)}) + (1 - c_k) (\tilde{d}_{10}^{(q-1)}),$$

which is derived in Appendix B. Both of them depend on the estimation of the desired user bit and the interference in present iteration as well as on the tentative bit-estimate of the desired user from the previous iteration. From equations (5.21), (5.22) and (B.28), we can write

$$\begin{aligned} \Lambda_{kd}^{(q-1)}[i] &= 2\alpha_k \beta_k \\ &= 2\alpha_k \left(c_k^{(q)} (Y_k - \hat{I}_k^{(q-1)}) + (1 - c_k^{(q)}) (\tilde{d}_k[i]^{(q-2)}) \right). \end{aligned} \quad (5.23)$$

Now, we focus on the first stage of interference cancellation, i.e., $q = 1$ for user 1 in Fig. 5.9. For our purpose, the coded bit estimate vector $\tilde{\mathbf{d}}_1^{(q)}$ and decoder output vector $\Lambda_{1d}^{(q)}$ will replace $(\tilde{\mathbf{b}}_1^{(q)})$ and $\mathbf{y}_1^{(q)}$ respectively. The parameters α_k and

soft-cancellation factor $c_k^{(q)}$, $0 \leq c_k^{(q)} \leq 1$, are unknown and needed optimization for minimum BER of the desired user. The term “ $\Lambda_{kd}^{(q-1)}[i]$ ” is the soft-output from the decoder in LLR form and both α_k and $c_k^{(q)}$ are dependent on the biased variance and the interfering users’ power; both α_k and $c_k^{(q)}$ values for each bit of each user will be independent and may be different, and their variations depend on the estimated signal power variations and thermal noise of the receiver. In the model [77], the soft-cancellation factor for all users is assumed as c . Then the above equation can be expressed as

$$\begin{aligned}\Lambda_1^{(1)}[i] &= 2\alpha_1 \left[c(Y_1 - \hat{I}_1^{(1)}) + (1-c)(\tilde{d}_1[i]^{(0)}) \right] \\ &= 2\alpha_1 \left[c(Y_1 - \hat{I}_1^{(1)} - \tilde{d}_1[i]^{(0)}) + \tilde{d}_1[i]^{(0)} \right].\end{aligned}\quad (5.24)$$

This is the equation of a hyperbola for solving α_1 and c , where other parameters are known. Let us consider the expression of α_1 and c from their derivation.

$$\alpha_1 = \frac{\sigma_1^2 + \sigma_{21}^2 - 2\rho_1\sigma_1\sigma_{21}}{\sigma_1^2\sigma_{21}^2(1 - \rho_1^2)}, \quad (5.25)$$

and

$$c = \frac{\sigma_{21}^2 - \rho_1\sigma_1\sigma_{21}}{\sigma_1^2 + \sigma_{21}^2 - 2\rho_1\sigma_1\sigma_{21}}. \quad (5.26)$$

The multiplication of (5.25) and (5.26) can be written as

$$c\alpha_1 = \frac{1 - \frac{\rho\sigma_1}{\sigma_{21}}}{\sigma_1^2(1 - \rho_1^2)}. \quad (5.27)$$

For the first stage of estimation, the system is interference limited, i.e., $\sigma_1 \leq \sigma_{21}$ and $\rho \leq 1$. For later stages, c approaches to 1. This phenomenon can be proved from (5.26) as follows:

$$\begin{aligned}c_{later} &= \lim_{\substack{\sigma_{21} \rightarrow \sigma_1 \\ \rho \rightarrow 1}} c \\ &= \lim_{\substack{\sigma_{21} \rightarrow \sigma_1 \\ \rho \rightarrow 1}} \frac{\sigma_{21}^2 - \rho_1\sigma_1\sigma_{21}}{\sigma_1^2 + \sigma_{21}^2 - 2\rho_1\sigma_1\sigma_{21}} \\ &= \lim_{\substack{\sigma_{21} \rightarrow \sigma_1 \\ \rho \rightarrow 1}} \frac{\sigma_{21}^2 - \rho_1\sigma_1\sigma_{21}}{\sigma_1^2 + \sigma_{21}^2 - 2\rho_1\sigma_1\sigma_{21}} \\ &= \lim_{\substack{\sigma_{21} \rightarrow \sigma_1 \\ \rho \rightarrow 1}} \frac{1}{1}, \quad \text{using } l'H\hat{o}pital's \text{ rule.}\end{aligned}\quad (5.28)$$

In summary, the procedure of interference cancellation in first stage PIC for user k using the model of [77], can be described as

$$r_k^{(1)}(t) = c^{(1)} [r(t) - \hat{I}_k^{(1)}(t)] + (1 - c^{(1)})\tilde{r}_k^{(0)}(t), \quad (5.29)$$

where, $c^{(1)}$ is the common SCF for all users in the first stage of cancellation, $\hat{I}_k^{(1)}(t)$ is k th user's interference at the first stage, and $\tilde{r}_k^{(0)}(t)$ is the contribution from the soft coded-bit estimates obtained from the previous stage. In earlier stages of cancellation, the contributions of the soft coded-bit estimates are more than those in later stages of cancellation and the value of c increases monotonically to 1 in successive stages of cancellation. Soft-symbol estimation, where we use the MF output as the estimation of the product of signal amplitude and symbol and do not make any bit estimation, gives better BER performance over hard bit estimate and partial cancellation improves the BER performance significantly over brute-force cancellation. For this soft-symbol estimation, (5.24) can be written in general form as

$$\Lambda_1^{(k)}[i] = 2\alpha_k [P_k^{(q)}(Y_k - \hat{I}_k^{(k)})], \quad (5.30)$$

where $P_k^{(q)}$ is the soft-cancellation factor of user k at stage q and its value is different than $c_k^{(q)}$.

5.3.3 A Pragmatic Approach for Optimization of the SCF

In the above equation, the SCF $P_k^{(q)}$ is not analytically tractable; in this section, we present a practical way of choosing the SCF semi-analytically. Equivalently, after first stage of interference cancellation, the input of the correlator of user k can be written as

$$r(t) = r(t) - \sum_{k=1}^K P_k^{(1)} \hat{s}_k(t - \tau_k), \quad (5.31)$$

which is easier to implement and reference [57] used this model. In performing soft cancellation, our objective is to use the SCFs which minimize second stage BER. Considering user 1 as our desired user as before, we now need to optimize $\{P_l^{(1)}\}$ $l \in \{2, \dots, K\}$, such that

$$\{P_l^{(1)}\} = \arg \left\{ \min_{\substack{0 \leq P_l^{(1)} \leq 1 \\ \forall l \in \{2, \dots, K\}}} BER^{(2)}(\{P_l^{(1)}\}) \right\}, \quad (5.32)$$

where

$$BER^{(2)}(\{P_l^{(1)}\}) = Q \left(\sqrt{\frac{(E[y_{1,i}^{(2)} | b_{1,i}])^2}{Var[y_{1,i}^{(2)} | b_{1,i}]}} \right) = Q \left(\sqrt{\frac{(E[y_{1,i}^{(2)} | b_{1,i}])^2}{E[(y_{1,i}^{(2)} | b_{1,i})^2] - (E[y_{1,i}^{(2)} | b_{1,i}])^2}} \right). \quad (5.33)$$

For minimum BER, both the variance and the bias term should be optimized. Smaller values of SCFs will reduce the bias but leave more interference in the system. On the other hand, total interference cancellation will reduce the interference maximally, but leave the bias. Since variance calculation for an asynchronous system is a tedious process, we can not solve this problem analytically. Another option is to minimize the squared Euclidean distance between the received signal $r(t)$ and the weighted sum of the estimates of all users' signal, given by

$$\epsilon = \int_{iT_d + \tau_k}^{(i+1)T_d + \tau_k} \left[r(t) - \sum_{k=1}^K P_k^{(1)} \hat{s}_k(t - \tau_k) \right] dt. \quad (5.34)$$

We need a cost function to solve this problem; obviously, the minimum BER is the cost function for our purpose. For $P_l^{(1)} = 1$ and joint estimations of signals, this is the equation for optimal multiuser receiver and the symbol estimations can be obtained using a maximum likelihood sequence estimator. Here, PIC receiver is sub-optimal decision oriented receiver and the signal estimations are erroneous. As a result, the optimal choice of the partial cancellation factor $P_l^{(1)}$ will not be the solution of an optimal multiuser receiver. Secondly, the value of $P_l^{(1)}$ can be positive or negative for minimizing the cost function. For example, for a wrong estimation of the signal, the value of $P_l^{(1)}$ should be negative. This optimal cancellation factor can be solved adaptively using normalized LMS or RLS algorithm. The main drawback of the aforementioned RLS-based decorrelating method is its complexity, which is $O(NK^2)$ per bit. Since normally $N > K$ for a CDMA system, its complexity is actually $O(K^3)$, similar to that of the matrix inverse decorrelating detector. To reduce the complexity caused by the RLS algorithm, normalized LMS algorithm can be used in the adaptive multistage PIC approach. The received signal is sampled at the chip rate after chip matched filtering. The N (processing gain) samples of the received signal within one bit can be written as in complex envelope form:

$$r(j) = \sum_{k=1}^K A_k[i] d_k[i] a_k(j) e^{j\phi_k} + n(j). \quad (5.35)$$

The LMS algorithm is based on the MSE criteria, and (5.34) can be written as

$$\mathbf{c}^{(q)} = \arg \left\{ \min_{\mathbf{P}^{(q)}} E \left[(r(j) - P_k^{(q)} \hat{s}_k(j)) \right] \right\}, \quad (5.36)$$

where $\mathbf{P}^{(q)} = \{P_1^{(q)}, P_2^{(q)}, \dots, P_K^{(q)}\}^T$ is the SCF vector in q th stage of interference cancellation.

The explanation of NLMS algorithm can be found in [27] and its filter-weights are updated according to

$$\mathbf{P}^{(q)}(j+1) = \mathbf{P}^{(q)}(j) + \mu(j) \hat{\mathbf{s}}_k(j)^* e^{(q)}(j), \quad (5.37)$$

where, $e^{(q)}(j)$ is the error vector between the desired response and its estimate in the q th stage, given by

$$e^{(q)}(j) = r(j) - P_k^{(q)} \hat{s}_k(j), \quad (5.38)$$

and the step-size $\mu(i)$ is

$$\mu(j) = \frac{\alpha}{\gamma + \hat{\mathbf{s}}_k^H(j) \hat{\mathbf{s}}_k^*(j)}. \quad (5.39)$$

Let us closely look into this approach. This will increase the complexity of the PIC considerably because the complexity of the adaptive algorithm is the overhead over the standard PIC. More importantly, the optimal choice of $P_l^{(1)}$ will minimize the interference variance. This may not minimize the bias of the estimation and the BER is the function of both the variance and the bias of the estimation. Let us assume that we have perfect symbol estimation but the amplitude estimation is obtained from the correlator detector output. Then, according to (5.34), the optimal choice of $P_l^{(1)}$ is positive and will minimize the error in (5.34). Obviously, this may not optimize the bias of the estimation.

This is the approach taken by [78], which uses a normalized LMS or RLS algorithm to adaptively compute $P_k^{(1)}$. Note that when $P_k^{(1)} = 1$ and joint estimation of symbols is employed, minimization of equation (5.34) leads to the optimal MLSE receiver. However, when this criteria is applied to PIC, the resulting solution selects values of $P_k^{(1)}$ which minimize the variance of the total interference. This may not minimize the BER which is the function of both the interference variance and bias of the estimation. While the variance optimization improves the performance over standard PIC, this method does not fully capture the tradeoff between minimizing interference and reducing bias, so we do not pursue this approach here.

We follow a pragmatic approach in this section, which keeps the complexity linear with the number of users. For perfect power control, the optimal choice of SCF will be identical for all users, resulting in implementation complexity that is a linear function of K . However, if signals are received with differing power levels, each user's optimal SCF will be unique and will vary depending upon which user is the desired one, resulting in implementation complexity which is quadratic in K . In general, the choice of SCF depends on the power of the desired user and the level of interference [57]. For a cellular environment with moderately effective power control, simulations show that employing a single SCF for all users results in only slight performance degradation from optimal. We therefore make this approximation in order to maintain linear complexity. From [57], the expression of the optimal SCF is given by

$$P_{\kappa}^{(1)} = \frac{\mathcal{A}}{\mathcal{B}}, \quad (5.40)$$

where

$$\begin{aligned} \mathcal{A} = & 8N^3 \left(P_{\kappa} - \frac{N_o}{2T} \right) - \sum_{\substack{l=2 \\ l \neq \kappa}}^K \xi_l^2 \left[P_1(7N - 6) + (2N - 1) \left(\sum_{\substack{m=2 \\ m \neq \kappa, l}}^K P_m + 2NP_l \right) \right] \\ & - 2N(2N - 1) \sum_{\substack{l=2 \\ l \neq \kappa}}^K \xi_l [2P_{\kappa} - P_l] - (2N - 1) \left[\sum_{\substack{l=2 \\ l \neq \kappa}}^K \sum_{\substack{m=2 \\ m \neq \kappa, l}}^K \xi_l \xi_m (P_l - P_{\kappa}) \right] \\ & - 4N^2 \frac{N_o}{2T} \sum_{\substack{l=2 \\ l \neq \kappa}}^K \xi_l^2, \end{aligned}$$

and

$$\begin{aligned} \mathcal{B} = & 8N^3 \left(P_{\kappa} + \frac{N_o}{2T} \right) - \sum_{\substack{l=2 \\ l \neq \kappa}}^K \xi_l \left[P_1(7N - 6) + (2N - 1) \left(\sum_{\substack{m=2 \\ m \neq \kappa, l}}^K P_m + 2NP_{\kappa} \right) \right] \\ & - 2N(1 - 2N) \left[\sum_{\substack{m=2 \\ m \neq \kappa}}^K P_m + (6 - 7N)P_1 \right] - 4N^2 \frac{N_o}{2T} \sum_{\substack{l=2 \\ l \neq \kappa}}^K \xi_l. \end{aligned}$$

From the above equation, it is evident that the optimal choice of the SCF depends on the power of the user considered for estimation along with other factors. For perfect power control, all interferers bear identical value of the SCF. This in turn means that, regardless of the desired user, all users in a given system will be cancelled with a unique SCF. Given this, it is possible to implement the cancellation process by cancelling all users at once, and then for each desired user, adding in the corresponding

reconstructed signal estimate for matched-filtering. This implementation is linear in K , in contrast to the more computationally expensive quadratic in K implementation. If however, signals are received with differing power levels, each user's SCF will be different and will furthermore depend upon which user is the desired one. Therefore, for optimal soft interference cancellation, the quadratic in K complexity implementation must be used. From the above equation and our simulation, it is intuitive that this dependency is not dominant and inversely proportional to the processing gain. We discarded this dependency for our simulation study in the next section, i.e., we calculated the SCFs for all users by considering the desired user power.

The modified block diagram of the partial PIC receiver is presented in Fig. 5.10, where $p_k^{(q)}$ is the sub-optimal SCF we described above and $p_k^{(q)} \neq P_k^{(q)}$. Note that more than one stage of interference cancellation is employed and the effect of this bias is diminished by a factor of N for the second stage of interference cancellation. Generally, the value of $p_k^{(q)}$ is about 0.5 – 0.7 if the interferer power is not very low or very high compared to the desired user power. The selective interference cancellation technique can be used along with the 0.5 value of the SCF. Our simulation results in the next section will describe these in details.

5.3.4 Simulation Results

Our aim is to study the sensitivity of BER of the desired user to choose SCF for various system conditions. A semi-analytical solution for SCF exists only for the synchronous case. We optimized the SCF for a synchronous system with an AWGN channel and studied the performance of this optimal SCF in other scenarios through Monte Carlo simulation. The system has a processing gain of 31 and for the near-far event; it is assumed that half of the interfering users have 6 dB higher power than the desired user.

To provide a direct comparison of BER performance in the above scenarios, the BER of the desired user as a function of E_b/N_0 is presented in Fig. 5.11 for an uncoded system of 10 users using two stages of PIC. All of the abbreviated notations are explained in the legend of the plots in Fig. 5.11 and subsequent figures. The term ‘‘OSCF’’ refers to the optimal SCF obtained semi-analytically from the uncoded synchronous system using the model in reference [57]. For example, in the asynchronous system or coded system, we use the optimal SCF obtained from the uncoded

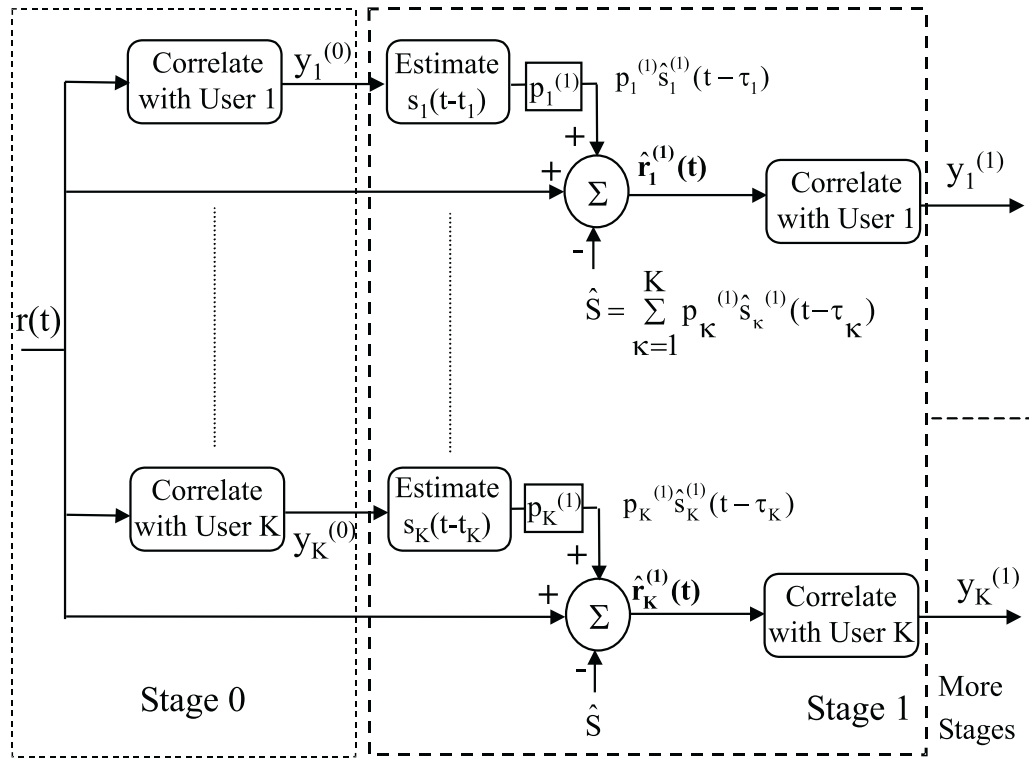


Figure 5.10: System model of a multistage PIC receiver for CDMA considering a SCF, where the complexity of the receiver is linear with the number of users.

synchronous system in all cases labeled “OSCF”. Fig. 5.11 shows that the BER performance using the optimal SCF in the asynchronous system is the best. The BER gains for the desired user using the same optimal SCF in other cases, such as near-far event and synchronous system, are very similar. Even the BER of the desired user for 0.5 value of SCF is very close to the BER using the optimal SCF. This verifies the stability of the choice of SCF. Also note that the BER performance at low E_b/N_0 is fairly robust to changes in SCF. The optimal SCF has a lower value for low E_b/N_0 . For higher E_b/N_0 , the BER performance of the desired user degrades substantially by choosing a non-optimal value of SCF.

Fig. 5.12 depicts the BER of the desired user against its E_b/N_0 for both asynchronous and synchronous uncoded systems. All the notations used for Fig. 5.11 are the same for Fig. 5.12. From the plots, it is evident that the BER improvement for the desired user in the asynchronous system obtained by using the OSCF of the synchronous system is better than that in the synchronous system. Generally, the BER improvement in the asynchronous system is more than that in the synchronous

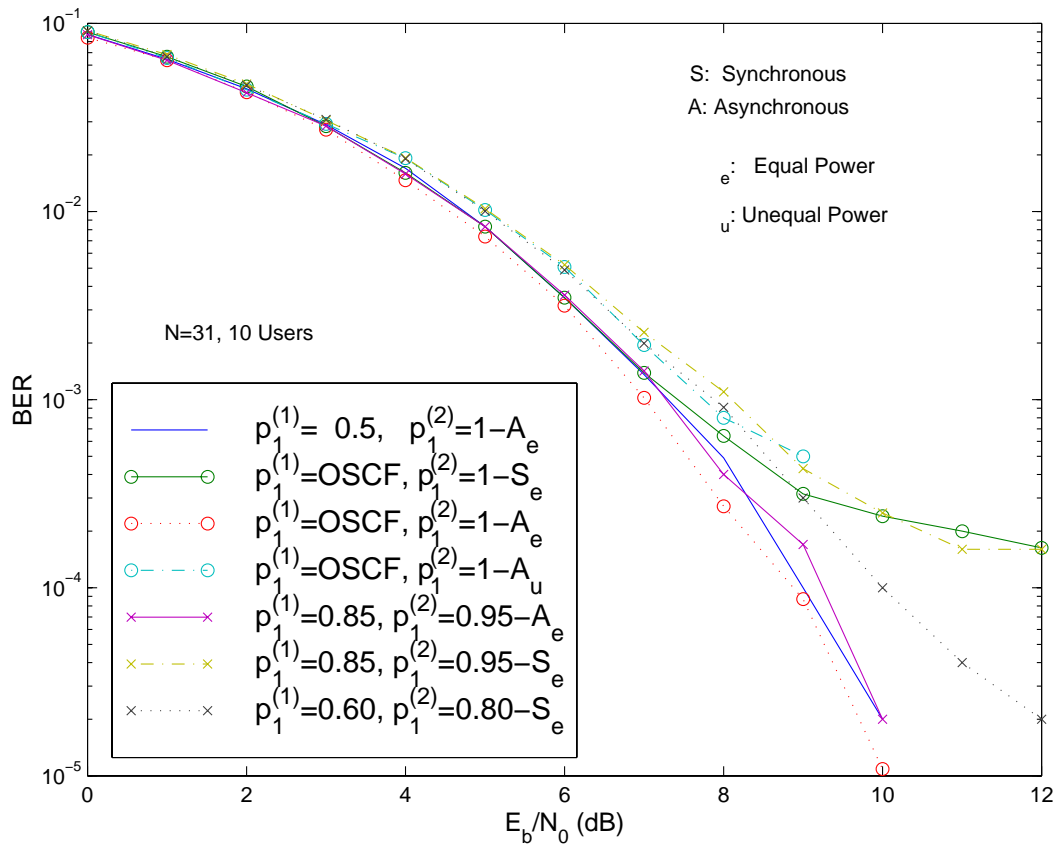


Figure 5.11: Desired user's BER as a function of its E_b/N_0 considering 10 users in the system.

system for a particular SCF because the bias is low in the former case. Note that the optimal SCF does not completely remove either the bias or the variance; rather it chooses a tradeoff between these extremes that minimizes BER. The cross-correlation between the desired user's PN sequence and the interfering user's PN sequence has a lower value in the asynchronous system. It is also noticeable that the disparity of the BER achievement is higher for a more heavily loaded system, because the bias difference is proportional to the system loading. Note that for the synchronous system, the plot associated with the notation ' $p_1^{(1)} = 0.5$ ' has similar performance compared with the corresponding plot using the optimal SCF. Hence, the optimal SCF has a value very close to 0.5 for the higher end of the E_b/N_0 . These two curves also show that BER in IC is stable for lower signal-to-noise ratio in more heavily loaded systems.

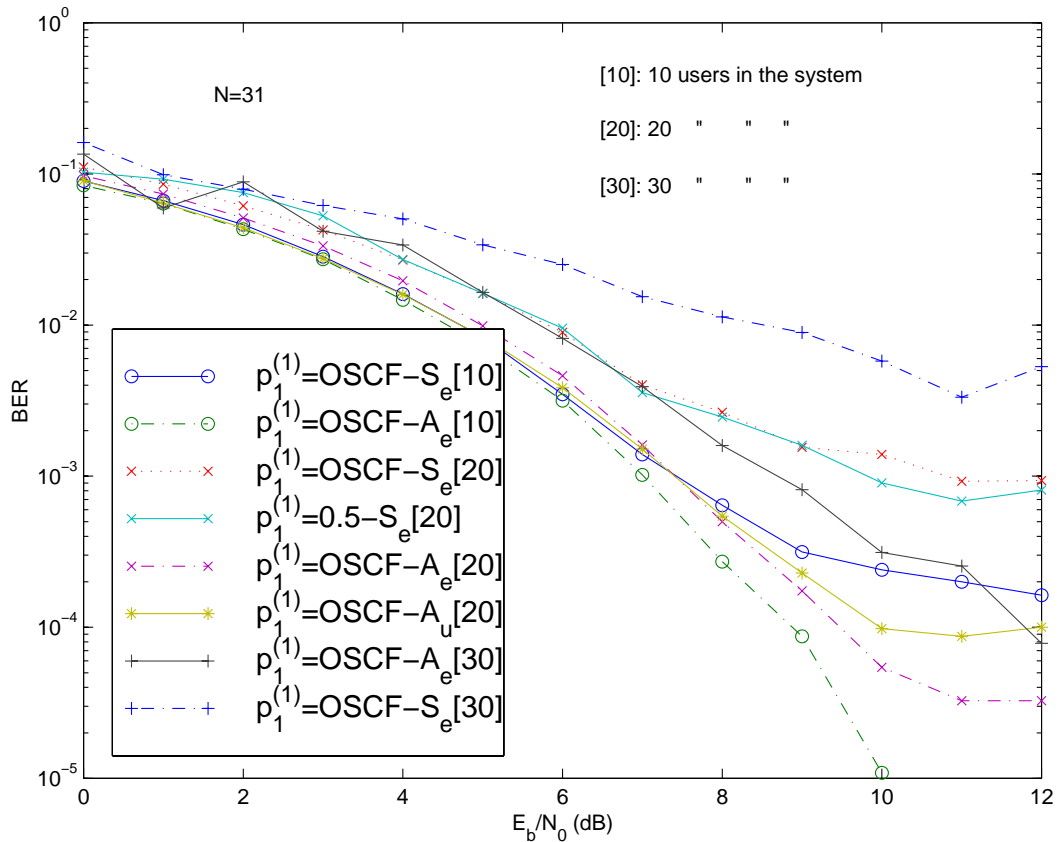


Figure 5.12: Desired user's BER as a function of its E_b/N_0 with 10, 20 or 30 users in the system, respectively.

To study the performance of an iterative coded system using PIC, a rate 1/2 convolutional code with a constraint length 3 is used. The BER of the desired user

vs. E_b/N_0 is presented in Fig. 5.13 for a coded system having 10 users and using two stages of PIC. Along with the above notations, the terms “uncoded” and “coded” refer respectively, to the uncoded and the coded systems and “Optimal SCF+0.25” refers to the value of SCF, which is 0.25 more than the optimal SCF calculated for the uncoded synchronous case. By comparing the plots, it is clear that a sub-optimal choice of SCF degrades BER performance considerably. The optimal SCF for an uncoded system performs quite poorly in the coded system. Some performance gain may be achieved by using a higher value of SCF than the optimal value from the uncoded system, because the signal fidelity out of the MAP decoder is higher than that out of initial matched filter.

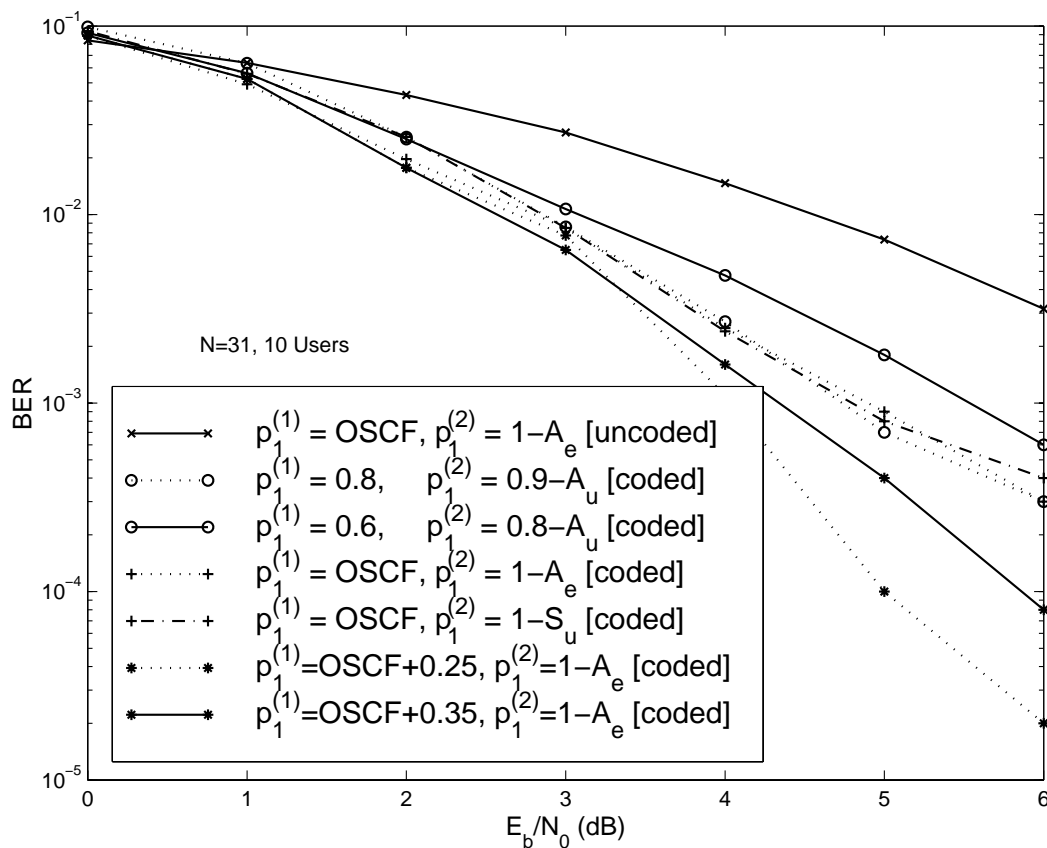


Figure 5.13: Desired user’s BER versus its E_b/N_0 considering 10 users in the coded system.

5.3.5 Section Summary

Our simulation results demonstrate the BER performance of the desired user under various scenarios. These results show that a well-chosen SCF improves the IC capability considerably and that the choice of SCF is more sensitive for a coded system than for an uncoded one. Although the optimized choice of the SCF for the synchronous system works well in an asynchronous system if the system is uncoded and moderately loaded, it results in unsatisfactory performance in other scenarios: coded system, heavily loaded system and near-far environment. On the other hand, the optimized value of the SCF for the synchronous system is stable and sub-optimal in asynchronous and near-far system when the system loading is low. In light to moderately loaded systems without coding, the BER in IC is stable for small changes of the optimal SCF. Values in the range of 0.5 to 0.7 for the SCF can be used without severe degradation of the BER. Since the cancellation of weak signals does not improve the performance significantly, selective interference cancellation can be used. For the coded system, we can use the OSCF for the uncoded system with an incremental value, which depends on the choice of codes.

As a final observation, we note that the BER performance is independent of whether the MAP decoder output is soft or hard. Fig. 5.14 shows the BER of the desired user as a function of its E_b/N_0 considering 10 users in the coded system for hard and soft estimation of the signal amplitude. This verifies that the BER performance is dominated by the bias of the amplitude estimation, not by the symbol estimation fidelity. This is significant because we do not have a linear (soft) symbol estimate available at the output of the error correction decoder.

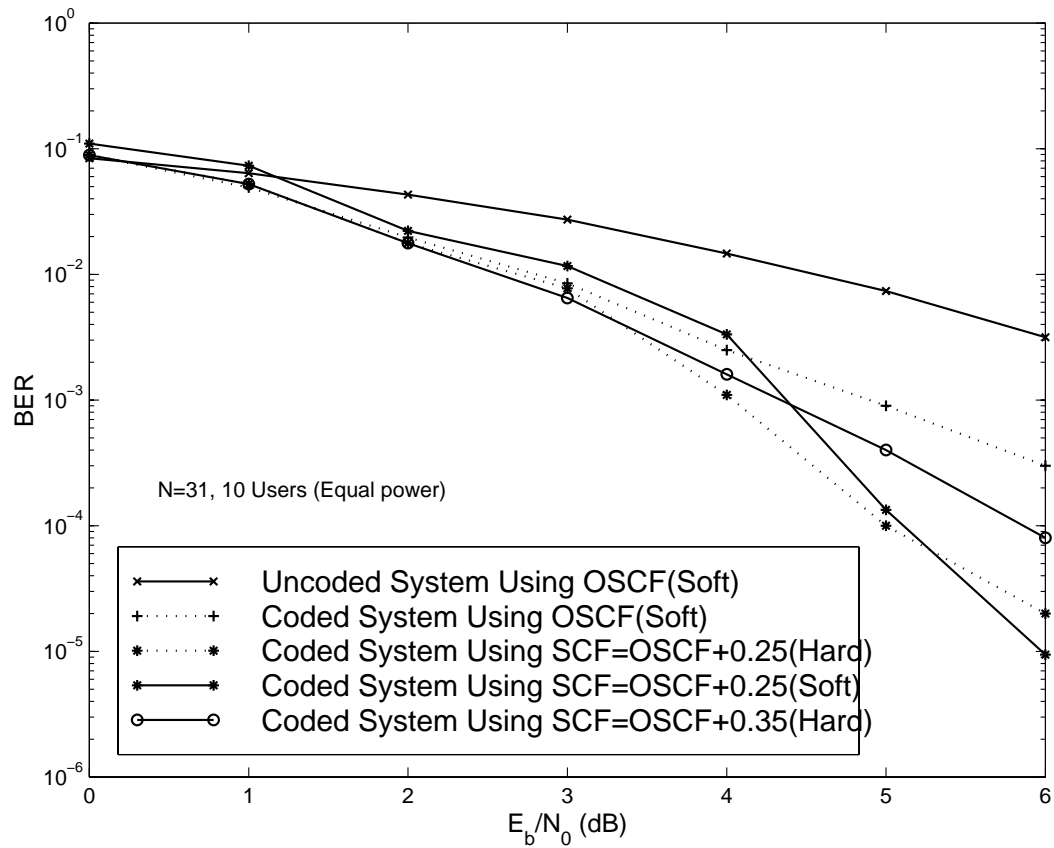


Figure 5.14: Desired user's BER versus E_b/N_0 considering 10 users in the coded system for hard and soft estimation of the signal amplitude.

Chapter 6

Decoder-Assisted Frame Synchronization for Coded Systems

6.1 Motivation and Problem Definition

The word *synchronization* is typically used to define the process of attaining and maintaining the time concurrence of the corresponding events in the transmitted and received signal or sequence. Synchronization generally occurs in two stages, acquisition (attaining) and tracking (maintaining). In acquisition, an attempt is made to align the signals within some degrees of tolerance. Once it is determined that the sequences have been aligned properly, the tracking mode is entered, which maintains the alignment with the received signal. Acquisition is often considered as the most difficult aspect of the synchronization. In packet radio system, the output of the demodulator must be sampled periodically in order to extract the transmitted information symbol. Since the propagation delay of the packet is unknown, at least three types of synchronizations are needed to be achieved before decoding of the information symbols. They are presented in order of their occurrences.

- **Carrier Synchronization:** For coherent demodulation, the phase agreement must exist between the incoming signal and its local replica at the receiver. This is required to bring the signal to the base band. Carrier synchronization brings the phases in coherence.
- **Symbol Synchronization:** When the receiver generates a symbol clock signal which is identical in phase and frequency to the timing of the incoming signal

clock, symbol synchronization occurs. This determines the duration of the information signal, which is a prerequisite for sampling of signals to extract the information.

- **Frame Synchronization:** When the receiver generates a frame clock signal locally, which is identical in the phase and frequency to the timing of the incoming signal, frame synchronization occurs. The start of the data block for continuous transmission or the frame for packet radio transmission is needed to estimate for a successful decoding process.

The studies of previous chapters have been conducted under the implicit assumption of perfect receiver synchronization. In the previous chapter, we analytically showed how soft-information can be exchanged between PIC stage and decoding stage of the receiver to achieve near-optimal performance in DS-CDMA system for packet radio applications. The use of concatenated convolutional codes in conjunction with iterative decoding, popularly known as turbo coding, has enabled communications at previously unachievable signal-to-noise ratios. These developments have resulted in the corresponding problem that the steady-state performance of a coded multi-user or turbo-coded system may exceed the ability of the system to achieve initial synchronization.

In this chapter, we are particularly concerned with the problem of frame synchronization. In circuit switched cellular systems, where overhead is not a significant issue, synchronization may be achieved through the use of a pilot signal. However, for packet-based communications systems such as wireless local area networks or military packet radio, frame synchronization must be performed on each received packet. One alternative for improving the synchronization performance of a packet radio system is to increase the header length, thereby improving the signal-to-noise ratio. The drawback of this approach is the resulting increase in overhead, which may partially nullify the performance improvement obtained through turbo-coding. An alternative solution is to employ the error-correction capability of the decoder to assist in the frame synchronization operation. Throughout this chapter we will answer the following question: can the decoder performance, which we optimized in the previous chapters using iterative decoding, assist and improve the frame synchronization operation?

This chapter proposes a novel frame synchronization scheme for convolutionally encoded data packets. Rather than placing in a separate header, the sync bits are

placed in a mid-amble and encoded as part of the data sequence, using the error correction encoder to resolve time ambiguities. The scheme is based on the principle that an error in trellis termination may result in decoding a wrong information bit sequence while the starting portion of the sequence can be decoded as error free. This technique requires fewer bits for frame synchronization. This frame synchronization technique is then extended for synchronization of turbo code. The performance improvement over conventional synchronization techniques is explored via simulation.

Most of the conventional synchronization techniques were derived assuming continuous transmission or traditional packets with pre-amble. The continuous transmission can be either synchronous or asynchronous. In the latter case, a known symbol sequence to startup bit timing and carrier synchronization is followed by the frame synchronization word. Packet frame synchronization is a special case of continuous frame synchronization, which is the subject of our study. The conventional frame synchronization scheme for continuous transmission synchronizes the data frames and the packet frame synchronization scheme is a one shot problem of the conventional frame synchronization scheme for continuous transmission. The packet frame synchronization technique may determine the location of the packet in a time-slot or the delay of the packet in a sporadic transmission of packets. Our goal is to present a brief overview of the relevant frame synchronization techniques using standard methods, which will eventually build the foundation of our proposed scheme, next, we will present several frame synchronization techniques, and compare the performance of those techniques with the state-of-the-art frame synchronization techniques.

6.2 State-of-the-Art

Frame synchronization is essential for reliable digital communications in a packet radio environment. Simply put, this is the task of knowing where the frame starts. It is of little use to the information sink in a communications system if the information sequence is even one symbol off; therefore, frame synchronization is a ‘hit’ and ‘miss’ problem. Frame synchronization is an estimation problem of frame start position using, but need not, a known sync word (SW) inserted into the data to be transmitted. This technique is referred to as the marker concept [80]. Since the objective is to determine the discrete starting bit position of the frame, this is a detection problem where the received signal window is the random output and the frame starting position

is the cause. The maximum a posteriori principle (MAP) can be used to determine this starting position by minimizing a cost function such as false probability of the frame synchronization. Special hardware and software are usually employed at the transmitter and the receiver to accomplish frame synchronization. The most widely used method for frame synchronization is to append a known SW onto the packet header, and then select the frame starting position which minimizes some distance metric between the SW and received signal. The optimal way to search for the SW is to evaluate a likelihood function that minimizes the probability of incorrect synchronization [81].

The author of [81] has derived several frame synchronization rules using maximum-likelihood (ML) estimation for BPSK modulation in an AWGN channel, including optimal ML rule, and high signal-to-noise ratio (SNR) and low SNR approximations to the optimal rule. In [82], the author shows that high SNR approximation to the optimal rule is near optimal for practical low SNR values, and its implementation is similar to the simple correlation rule; in contrast, the low SNR approximation to the optimal rule fails for moderate or high SNR. Similar observations are reported in [83] for M-ary phase modulation with coherent and noncoherent detection. This paper derives analytical performance bounds for frame synchronization in synchronous transmission in terms of random data limit. As in reference [81], they also have established the fact that high SNR approximation of the ML rule outperforms the correlation rule with little additional implementation expense. Similar results were obtained for the time invariant channel with intersymbol interference (ISI) [84]. In [85], the author extended this work to the case of flat fading where channel state information entered the ML decision rule and obtained similar results. In all the above-mentioned works, one common fact is that a SW pattern is embedded in random information data symbols. In [86], a frame synchronization technique is proposed that makes use of the terminating bits of the convolutionally-encoded data to augment the SW. In this chapter, we show that by inclusion of a coded mid-amble sequence, it is possible to eliminate the need for a SW header entirely in a coded system.

The appearance of the SW pattern in the random data sequence can degrade the performance of synchronization. An upper bound of this degradation in a noiseless case is obtained in [82]. One way of solving this problem is to choose the SW and data symbols from separate alphabets, but this will increase the complexity of the synchronization process. Another way to minimize this problem is to use a SW, which does not appear in the data sequence. For asynchronous packet transmission,

carrier and bit synchronization should be performed prior to frame synchronization. In this case, each packet starts with a pre-amble, which consists of a *bit sync* sequence followed by SW. In [87], the optimum SW with regard to various bit sync sequences when employing the correlation rule was found by computer search. The information contained in the bit sync sequence is used in a two stage frame synchronization in [88].

The SW can be integrated with the data sequence in the pre-amble, post-amble or mid-amble. The SW can also be distributed throughout the pre-amble, post-amble and mid-amble. Usually, the SW is embedded in the pre-amble in the belief that synchronization must occur before reception of the ensuing data. However, as storage capabilities increase, it is increasingly useful to view reception of an entire packet as a single operation, encompassing synchronization, demodulation and decoding. These operations may be performed in parallel, sharing the information in the process.

Channel coding is an essential component in digital communication systems for low BER performance. The SW can be transmitted with the coded bits as uncoded or coded sequence. Our approach exploits the power of the error correction code to improve the synchronization performance. We introduce the technique here for use with convolutional codes with the belief that it can be extended to more powerful coding schemes. The remainder of the chapter is organized as follows. The standard frame synchronization model is presented in Section 6.3. Section 6.4 presents our proposed scheme for synchronization and is followed by the simulation results in Section 6.5. Using the proposed scheme of frame synchronization and list synchronization concept, we introduce several alternative architectures of improved frame synchronization in Section 6.6 and Section 6.7; next, we apply the soft frame synchronization idea to turbo synchronization in Section 6.8. Section 6.9 describes the frame synchronization technique for time-division multiple-access channel. Finally, conclusions and possible improvements of these proposed schemes are given in Section 6.10.

6.3 Standard Frame Synchronization Techniques

6.3.1 Basics of Frame Synchronization

Traditionally, there have been two ways to estimate the frame start position. The first way is to perform a ‘sliding’ evaluation of a correlation function that is the correlation between a portion of the received signal and the SW sequence, or more

accurately to calculate a likelihood function $L(\mu)$ over the time μ ; then accept that μ as the estimated frame starting position $\hat{\mu}$ for which the correlation function or $L(\mu)$ crosses a threshold value for the first time. This approach is relatively easy to implement. The second way is to calculate the $L(\mu)$ for every position of the received signal vector, and take the μ for which $L(\mu)$ is maximum. Since this frame synchronization technique is a parameter estimation problem for a known distribution of the received signal, we will first describe the maximum likelihood (ML) estimation theory in perspective.

The basic parameter estimation theory is described in [89], where the author derives the best estimator under the assumption that the distribution of a sample set $\{z_1, z_2, \dots, z_n\}$ is known. The estimator evaluates a likelihood function $L(\mu|\mathbf{z})$, which is the probability, $P(\mu|\mathbf{z})$, for a given sample set $\{z_1, z_2, \dots, z_n\}$ of n samples that are independent and identically distributed (i.i.d.) according to a cumulative probability distribution function $F(z_1, z_2, \dots, z_n|\mu)$ with pdf $f(z_1, z_2, \dots, z_n|\mu)$. Here μ is the parameter to be estimated for the sample set $\{z_1, z_2, \dots, z_n\}$, and μ can be either a deterministic quantity, $\mu \in \{\text{Re}\}$, or a random variable with known a priori probability. In former case, the best estimator is the ML estimator and in the latter case, that is the maximum a posteriori (MAP) estimator. From mixed Bayes rule,

$$P(\mu|\mathbf{z}) = f(\mathbf{z}|\mu) \cdot \frac{P(\mu)}{f(\mathbf{z})}. \quad (6.1)$$

So, the likelihood function $L(\mu|\mathbf{z}) = cf(\mathbf{z}|\mu)$, where c is a constant. Note that the ML estimator makes the most likely observation. In practice $c = 1$, because it does not play any role to the maximization. The ML estimator can be written as:

$$\begin{aligned} L_{ML}(\mu|\mathbf{z}) &= \arg \left\{ \max_{\mu} [f(z_1, z_2, \dots, z_n|\mu)] \right\} \\ &= \arg \left\{ \max_{\mu} \left[\prod_{i=1}^n f(z_i|\mu) \right] \right\}. \end{aligned} \quad (6.2)$$

We are interested in the exponential family of pdf. Then,

$$f(\mathbf{z}|\mu) = ce^{-J(\mu)}. \quad (6.3)$$

In our case, μ is a parameter of location or discrete time and $z = \mu + r$, where, r is the residual. Hence, $f(\mathbf{z}|\mu) = f(\mathbf{r}|\mu)$. If we take the logarithm, the likelihood function of (6.2) becomes

$$L_{ML}(\mu|\mathbf{z}) = \arg \left\{ \min_{\mu} [J(\mu)] \right\}$$

$$= \arg \left\{ \min_{\mu} \left[\sum_{i=1}^n -\ln f(r_i) \right] \right\}, \quad (6.4)$$

since ‘ln’ is a monotonic function. If we assume Gaussian distribution with $f(\mathbf{r}) = N(0, 1)$, (6.4) becomes

$$\begin{aligned} L_{ML}(\mu|\mathbf{z}) &= \arg \left\{ \min_{\mu} \left[\sum_{i=1}^n -\ln f(r_i) \right] \right\} \\ &= \arg \left\{ \min_{\mu} \left[\frac{1}{2} \sum_{i=1}^n r_i^2 \right] \right\}. \end{aligned} \quad (6.5)$$

For our derivation, let us assume that μ and β are two statistically independent random variables. Then the pdf $f(\mathbf{z}|\mu)$ can be obtained by integrating over all possible β 's and is given by

$$f(\mathbf{z}|\mu) = \sum_{\forall\beta} f(\mathbf{z}|\mu, \beta) \cdot P(\beta). \quad (6.6)$$

6.3.2 Single-Frame Synchronization

Frame synchronization is a parameter detection problem where the unknown parameter is the frame starting position [81]. We consider frame synchronization for the case of an AWGN channel with BPSK modulation. We assume that the data is random, independently distributed and perfect symbol timing is already achieved. The data is transmitted in a stream of N -symbol frames, of which L symbols comprise the known SW $\mathbf{s} = (s_0, s_1, \dots, s_{L-1}) \in \{1, -1\}^L$, and the remaining $(N - L)$ symbols represent data sequence $\mathbf{d} = (d_L, d_{L+1}, \dots, d_{N-1}) \in \{1, -1\}^{(N-L)}$. The complex baseband received signal, sampled at symbol intervals $t = kT$, is given by

$$r_k = a_k + n_k, \quad (6.7)$$

where $\{a_k\}$ denotes the transmitted encoded bit sequence and $\{n_k\}$ are samples of AWGN with two-sided power spectral density $N_0/2$. Here k is an integer, T is the symbol period and we assume that symbol and phase synchronizations have been achieved. The receiver operates on the sequence $\mathbf{r} = (r_0, r_1, \dots, r_{N-1})$ of N demodulated symbols. The frame synchronization problem is to estimate the relative delay $\hat{\mu} \in [0, M - 1]$ of the arriving packet, where M is the number of resolvable delays. This relative delay can be any of the M positions with equal probability without a priori information about the position. The ML estimate of μ under the Gaussian

assumption is the minimum error probability synchronizer and is given by

$$\hat{\mu} = \arg \left\{ \max_{\hat{\mu} \in [0, M-1]} [f(\mathbf{r}|\hat{\mu})] \right\}, \quad (6.8)$$

where $f(\mathbf{r}|\mu)$ is the conditional *pdf* of \mathbf{r} given μ .

The MAP approach requires that a frame synchronization must choose $\hat{\mu}$ that maximizes the conditional probability $P(\hat{\mu}|\mathbf{r})$ [81]. Here, \mathbf{r} is an N dimensional received vector, where $r_i = x_i + n_i$. Assuming that all $\hat{\mu}$ are equally likely, this corresponds to a ML rule where we maximize $f(\mathbf{r}|\hat{\mu})$. According to (6.6), we can write

$$\begin{aligned} f(\mathbf{r}|\mu) &= \sum_{\forall \mathbf{d}} f(\mathbf{r}|\mu, \mathbf{d}) \cdot P(\mathbf{d}) \\ &= \frac{1}{(\pi N_0)^N} \prod_{i=0}^{L-1} \exp \left[-\frac{\|r_{i+\mu} - S_i\|^2}{N_0} \right] \sum_{\forall \mathbf{d}} P(\mathbf{d}) \prod_{i=L}^{N-1} \exp \left[-\frac{\|r_{i+\mu} - d_i\|^2}{N_0} \right]. \end{aligned} \quad (6.9)$$

The first product takes an account of the Euclidian distance between the SW and the portion of the sequence \mathbf{r} where the SW is expected to occur, had $\hat{\mu} = \mu$. The second product shows the distance between any observation data sequence \mathbf{d} and the corresponding signal in \mathbf{r} . Following the derivation by Massey [81], this can be written as

$$L(\mu|\mathbf{r}) = \sum_{i=0}^{L-1} r_{i+\mu} \cdot S_i - \frac{N_0}{2} \sum_{i=0}^{L-1} \ln \{ \cosh(\sqrt{E_s} r_{i+\mu} / N_0) \}, \quad (6.10)$$

where E_s is the energy of the BPSK symbol set. The value of $\hat{\mu}$ that maximizes $L(\mu|r)$, will make the best choice for μ . The first term in (6.10) corresponds to the soft correlation rule between the SW and the data sequence. The value of the correlation term at any position μ resembles the similarity of the replicated SW with the noise corrupted data sub-sequence of length L starting at μ . In reference [83], *Lui* derived the ML value of $L(\mu)$ for M-ary signal and is given by

$$L(\mu|\mathbf{r}) = \sum_{i=0}^{L-1} r_{i+\mu} \cdot S_i - \frac{N_0}{2} \sum_{i=0}^{L-1} \ln \sum_{j=0}^{M-1} \exp \left[\frac{2}{N_0} \left\{ \langle r_{i+\mu}, W_j \rangle - \frac{\|W_j\|^2}{2} \right\} \right], \quad (6.11)$$

where, W_i is the energy associated with M-ary symbol set and $\langle \cdot, \cdot \rangle$ denotes the inner product.

For high SNR, the function $f(\mathbf{r}|\mu)$ can be expressed as [81]

$$f(\mathbf{r}|\mu) = \sum_{i=0}^{L-1} S_i \cdot r_{\mu+i} - \sum_{i=0}^{L-1} |r_{\mu+i}|, \quad (6.12)$$

where (r_1, r_2, \dots, r_N) indicates the received signal sequence.

In [85], Robertson derived the ML rule of frame synchronization for flat fading where channel state information enters the ML decision rule. According to [85], the likelihood function for high SNR is given by

$$L_H(\mu) = \sum_{i=0}^{L-1} S_i \cdot a_{\mu+i} r_{\mu+i} - \sum_{i=0}^{L-1} |a_{\mu+i} r_{\mu+i}|, \quad (6.13)$$

where a_i is the fading coefficient assuming coherent demodulation.

For packet transmission, the data is packed into frames. For spontaneous transmission of the data, the actual information frame is preceded by a pre-amble sequence, which is composed of a *bit sync* sequence for carrier and phase synchronization and a SW for frame synchronization. After a few bits delay with respect to the delay of packet start, symbol and carrier synchronization will be accurately acquired. Fig. 6.1 shows the frame synchronization window. The window contains a complete frame synchronization word. The starting point of the sync window can be measured from received power. The possible synchronization point can be derived from ML estimation or by using equation (6.12).

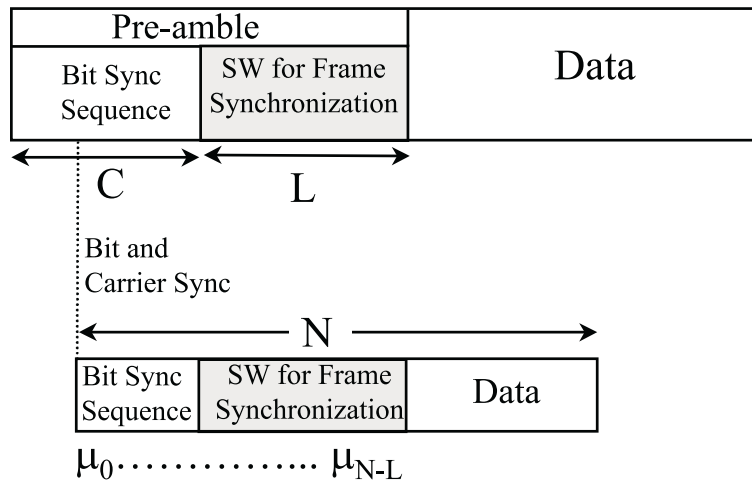


Figure 6.1: Synchronization window for carrier and frame synchronization.

6.3.3 Multiple-Frame Synchronization

In a single-frame synchronization technique, the estimation of the starting position of a periodically inserted frame synchronization sequence depends on one frame length

observation. Multiple frames of channel observations can be used for this purpose, and this scheme is called multiple frame synchronization. Here, individual SW word starting position can be obtained using significant observations for m successive frames. The majority decision decides on the majority of the m independent frame estimates as the sync pattern starting position. For individual frame synchronization, high SNR rule or ML rule can be used. Let us assume that P_s is the probability of correct synchronization for an individual frame rule and P_m is the probability of the multiple frame synchronization considering m frame. Then,

$$P_m = \sum_{[i=\frac{m}{2}]+1}^m \binom{m}{i} P_s^i (1 - P_s)^{m-i}. \quad (6.14)$$

6.3.4 The Choice of the Sync Word

Classically, Barker codes have been used for packet frame synchronization in communication systems. These real sequences have ideal auto-correlation functions (ACFs) in that the side-lobes of the even and odd periodic and aperiodic ACFs are bounded by ± 1 . There are no Barker sequences longer than 13. Neglecting their inverses, there are only two Barker sequences of any given length, one of which is the time-reversed version of the other. It is the aperiodic ACF properties that are of interest when the sequences are used for synchronization purposes, as the sequence will be surrounded by actual data. As a result, only the central point of the ACF is guaranteed. Any other point of the ACF depends upon the combined effect of side-lobes, actual data and noise. These factors may cause the ACF of any other point to exceed that of the central point and result in false synchronization. In other words, the correlation term in (6.12) protects synchronization locally, and the energy term in (6.12) protects synchronization globally in the packet.

6.3.5 Frame Synchronization of Coded Packet

One assumption of the ML rule is that all observation data sequences are equally likely. This allows us to eliminate the sum over \mathbf{d} in (6.9), and construct a computable correction term; however, when the data is coded, this term can not be eliminated because the probabilities of all the sequences are not equal. Depending on the encoder structure, some sequences may occur more often than the others. The second part of

(6.9) is needed to evaluate for each \mathbf{d} sequence,

$$P(\mathbf{d}) \prod_{i=L}^{N-1} \exp \left[-\frac{\|r_{i+\mu} - d_i\|^2}{N_0} \right]. \quad (6.15)$$

The observed data window, $r_{L+\mu}, r_{L+\mu+1}, \dots, r_{N-1+\mu}$ is a function of μ and the value of (6.15) will depend on μ . The contribution of the term in (6.15) will be small when the expected data sequence \mathbf{d} is more different than the observed data sequence $r_{L+\mu}, r_{L+\mu+1}, \dots, r_{N-1+\mu}$, i.e., a larger Euclidian distance. Conversely, if $r_{L+\mu}, r_{L+\mu+1}, \dots, r_{N-1+\mu}$ is close to any \mathbf{d} , then (6.15) will be larger. The MAP decoder chooses this \mathbf{d} for a given value of \mathbf{r} and μ . An optimal receiver will calculate (6.9) for all \mathbf{d} sequences and μ [90]. As a result, the integration of the frame synchronization and decoding becomes a joint detection problem, where the number of decoders needed is N . In fact, if we use N number of decoders, each for every μ position, we do not need any SW. In practice, the combination of several stages of synchronization is used where, the final stage is a decoder.

One such approach, proposed in [91], is a generalized synchronizer – concatenated synchronizer, which is composed of a list synchronizer, and either a more reliable frame synchronizer or a decoding unit. The list synchronizer supplies a few best frame starting positions to the second unit, which selects the correct position from the list. Basically, the only modification to a standard frame synchronizer is the replacement of the ML searching unit by a unit that finds the x largest $L(\mu)$'s. This unit evaluates (6.9) for all N positions of μ by assuming equal probability of the data sequence and keeps x positions corresponding to x largest $L(\mu)$. These can be kept as a sorted list that is continuously updated as the $L(\mu)$'s are evaluated. If the stage following the list synchronizer is able to detect immediately a correct sync (e.g. decoder), the synchronizer can start by supplying that position, which is corresponding to the highest $L(\mu)$. In case of a sync failure, the next position corresponding to the second highest $L(\mu)$ is supplied, and this process can be continued up to an assigned number of times. If this finally leads to no correct sync, then a sync failure has occurred. The list synchronization technique improves the performance of a standard synchronizer with the expense of the additional stages of processing. Fig. 6.2 shows the optimal likelihood function for the coded case where, in the first stage the data is assumed equally distributed ; in the second stage, the decoder evaluates the energy term expressed in (6.15) for all distributions of \mathbf{d} , and takes the frame starting position for which this energy term has maximum value.

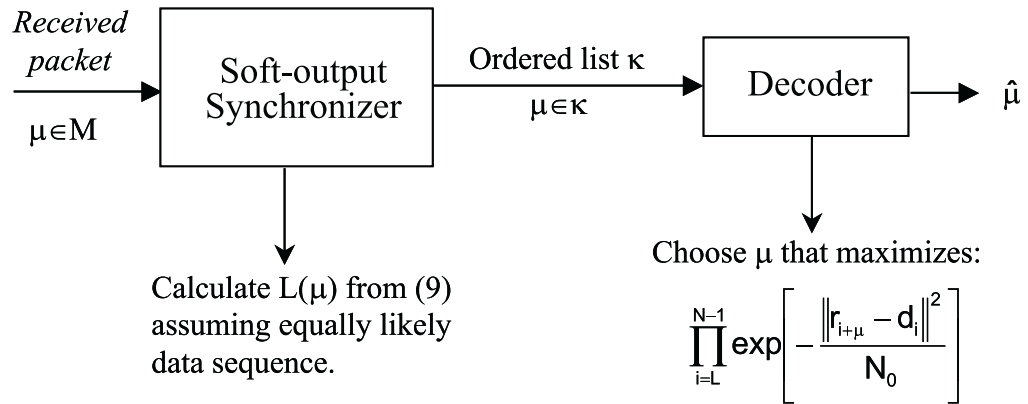


Figure 6.2: List synchronizer to compensate for the dependency of the coded data bits.

6.3.6 Preamble-less Packet Communication

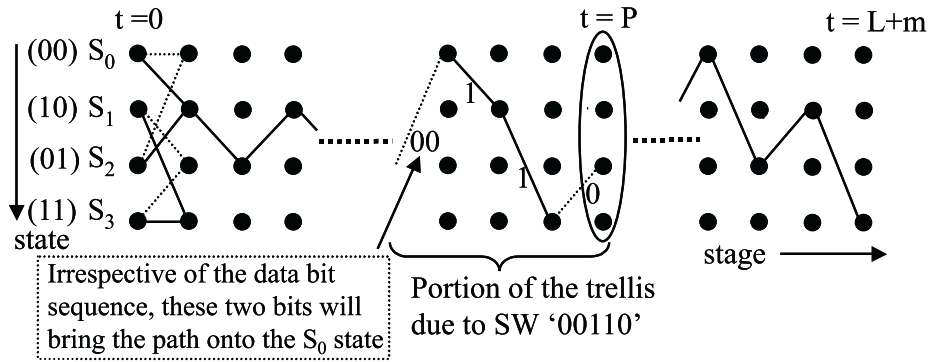
Traditionally a packet used to be consisted of a pre-amble, and was followed by a SW for frame synchronization and data. After a packet had been received, the carrier phase and symbol time was obtained; this used to be followed by the frame synchronization for packet starting position. Finally, the data was demodulated and decoded. Basically, packets were treated as if it were a long continuous stream of data. As a result, the overhead of a packet was considerable, and this was a constraint for a shorter packet transmission. The development of block-oriented packet processing algorithms assisted the idea of the new packet structure, called preamble-less packet. This packet is sampled and stored prior to processing. The efficient block oriented synchronization techniques for symbol timing, carrier estimation and frame synchronization determine a preamble-less packet. In a preamble-less packet, the only overhead is the SW, which can be embedded in the data. The packet is sampled at a sufficiently high rate and stored in a memory. Various processing stages are now invoked, such as coarse frequency offset estimation using FFT techniques and symbol timing offset estimation using digital square and filtering [92]. Interpolation and decimation methods are used to translate into different sample rates. These operations, which are efficient due to the advancement of the DSP, exclude the need for an extra pre-amble. The fine carrier timing and phase estimation are obtained using more signal processing techniques. Before decoding, the frame synchronization is obtained using SW, though this SW may not be mandatory. The synchronization and decoding operation can be done jointly.

6.4 Proposed Scheme

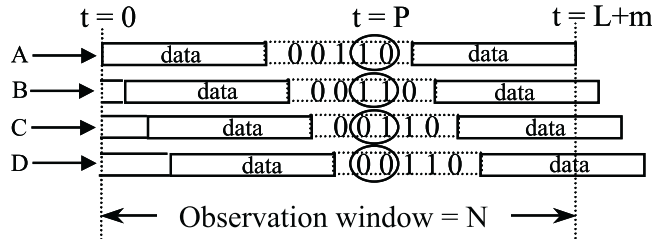
Error correction coding is an integral part of digital communication systems. For low SNR, convolutional coding is often chosen for error protection. A convolutional code can be described by its trellis, which represents the possible states of the encoder and the allowable transitions between states. The soft-decision Viterbi Algorithm (VA) can be used to determine optimally the most likely path through the trellis. Fig. 6.3(a) shows a trellis diagram for decoding a rate $1/2$, constraint length 3 convolutional code, where L and m denote information bit sequence length and memory of the encoder, respectively. The trellis has four states and $(L + m + 1)$ stages, starting from time $t = 0$ and terminating at time $t = L + m$. Our objective is to exploit the distance properties of the error correction code for frame synchronization. We assume that carrier synchronization and symbol timing are already achieved, but the frame synchronization is yet to be determined.

Fig. 6.3(b) shows observation windows of one packet-length, which arrive at the receiver with different delays. In the block diagram, Packets A, B, C and D have 0-3 information bits delay respectively. The SW ‘00110’ is embedded in the mid-amble of the packet before encoding. Fig. 6.3(a) also shows the trellis segment with the surviving path due to SW, which is a part of the trellis for the whole observation window. The starting ‘00’ bits of the SW force the trellis into the state S_0 and the subsequent ‘110’ bits guide the path through states S_1 , S_3 and S_2 successively. This portion of the trellis path is independent of the bit sequences in the observation window. These four distinct states can distinguish between up to 4 distinct delays of the packets. If we observe the state at $t = P$ for packet delays of 0, 1, 2 and 3 information bits, respectively as shown in Fig. 6.3(b), we can recognize a one-to-one correspondence between the state of the convolutional encoder at time P and the relative delay of the received vector.

Since the starting position of a packet is yet to be determined, we can not relate any bit position in the observation window with that of a packet, but the state of the Viterbi decoder can be used to determine the packet starting position. Note that the trellis can terminate at any of the states due to an arbitrary delay of the packet. Even if we always start in state S_0 at time $L + m$ to determine the state at $t = P$, a wrong information bit sequence may be decoded, but the trellis will eventually merge back to the correct state after a sufficient number of stages [93]. The correct state at time $t = P$ can be decoded successfully if the distance from the termination stage to $t = P$



(a) Trellis representation of a 4 state convolutional encoder. The trellis terminates in an arbitrary state, depending on the arbitrary delay of the observation window.



(b) At the transmitter, SW '00110' is embedded in the mid-
amble of a packet and at the receiver, 4 observation
windows A, B, C and D arrive with 0-3 bits delay respectively.

Figure 6.3: Trellis diagram of the proposed synchronization scheme; Packet arrivals at the receiver for different delays are also shown for the proposed scheme of frame synchronization.

is sufficient. Based on this principle, our goal is to determine the state of the decoder at time $t = P$ for the AWGN channel. We observe the state at $t = P$ and compare that with the actual state it should be on, which can be obtained from the encoder structure. If they match, this is a successful event; otherwise, the event results in a false acquisition. The '00110' SW is capable of resolving 4 distinct information bit (8 coded bit) delays using a rate 1/2 and constrain length 3 code. This SW length requirement and the number of distinct delays that can be resolved depend on the number of states of the encoder.

Up to this point, we have assumed that the delayed packet aligns with the start of a stage in the code trellis. This would always occur if QPSK modulation and a rate 1/2 code were used. However, for the case of BPSK modulation, there are two code

symbols for each trellis stage. As a result, a delay of an odd number of coded symbols would result in a received packet that is offset from the assumed trellis. Generally, the decoder of the convolutional codes is robust to this out-of-sync situation named *offset sync* - the misalignment of the received symbols to the trellis-branch, where no additional information is needed with the transmitted symbols; the decoder output will have large error rate when the packet is not aligned. Any form of error indicator can resolve this offset sync problem. One method can be monitoring the rates at which the path metrics are increasing. The way to implement this method is through the use of two decoders, offset from each other by a single coded bit [90]. After decoding a fraction of the frame, the decoder with larger metric associated with its best path will indicate the information bit aligned packet. As a result, for the example above, the proposed technique is able to resolve $M = 8$ total bits of delay.

Another method is to use the merging properties of the trellis; when the information miss-aligned packet is received, the surviving paths in the trellis merge much more slowly than when the information bit aligned packet is received. We applied the first method in our simulation study.

This technique can be extended to include alternative decoding algorithms for determining the state at time P . The MAP algorithm [73] minimizes the symbol error probability while obtaining precise estimates of a posteriori probability of each state transition and information bit, respectively, given the received signal vector. This algorithm requires forward and backward recursions and is therefore suitable for packet oriented processing. In this algorithm, the terms $\alpha(S_i[P])$ and $\beta(S_i[P])$ denote the probability of the forward and backward recursion for state S_i at $t = P$, respectively, [73]. It is simple to prove that for a given received bit vector \mathbf{r} , the probability to be in a state S_i at $t = P$ is given by

$$P(S_i[P]|\mathbf{r}) = \alpha(S_i[P]) \times \beta(S_i[P]) \times P(\mathbf{r}). \quad (6.16)$$

The largest value of $P(S_i[P]|\mathbf{r})$, $\forall i$ can determine the surviving state at $t = P$. In this manner, the same principle can be applied to synchronization of the turbo codes.

6.4.1 Motivation of the Coded SW

The main incentive for adding SW before encoding is to take advantages of the powerful decoding schemes for the coded system, where the decoder can reduce the number of errors for SW searching. These advantages of the coded SW scheme are obtained

from the cost of the rate penalty for the selection of the SW length. The uncoded SW scheme has the advantage that for a given code rate R , information sequence length I and frame length N that is the packet length at input of the channel, the length of the SW L^{Unc} can be chosen to be

$$L^{Unc} = N - I/R, \quad (6.17)$$

whereas the length of the SW L^{Coded} for the coded SW system can be

$$L^{Coded} = R.N - I = R.L^{Unc}. \quad (6.18)$$

As a result, the coded SW scheme suffers from the rate penalty. The advantages of the coded SW scheme is obviously some form of coding gain from the decoding scheme. The frame synchronization is needed to be established at the beginning of a transmission session and occasionally the synchronization is lost. Since the SW is intertwined with the information bit sequences and both the positions and values of these bits are known when the receiver is in sync mode of operation, this also can help the decoding performance.

The decoder-assisted synchronization scheme proposed in Section 6.4 depends on the decoder performance. Let us assume that P_b is the bit-error probability under perfect frame synchronization and P_{sn} is the synchronization failure probability. Thus, the bit-error probability P_{bT} under both perfect and false synchronization can be written as

$$P_{bT} \simeq P_b(1 - P_{sn}) + 0.5P_{sn}. \quad (6.19)$$

Let us assume that $P_{sn} \approx P_b$; then,

$$P_{bT} \simeq 1.5P_b. \quad (6.20)$$

6.5 Simulation Results

To compare the performance of the proposed scheme with that of the uncoded ML decision rule, we simulated the system using Monte Carlo methods. We considered a system where packets were transmitted through an AWGN channel with BPSK modulation. Fig. 6.4 shows flow charts of simulations for both techniques. For the proposed scheme, the uncoded packet size is 45 bits long including the SW '00110'; after encoding with a rate 1/2 and constraint length 3 convolutional code, the transmitted packet size to the channel is 94 bits long. We assume that the delay is a

uniformly distributed random variable in the range of $[0 - 7]$ coded bits. We calculated the probability of false acquisition ($P(Acq_{false})$) as a function of the system E_b/N_0 . For our example $t = 25$, $L + m = 47$ and the observation window is 94 bits long.

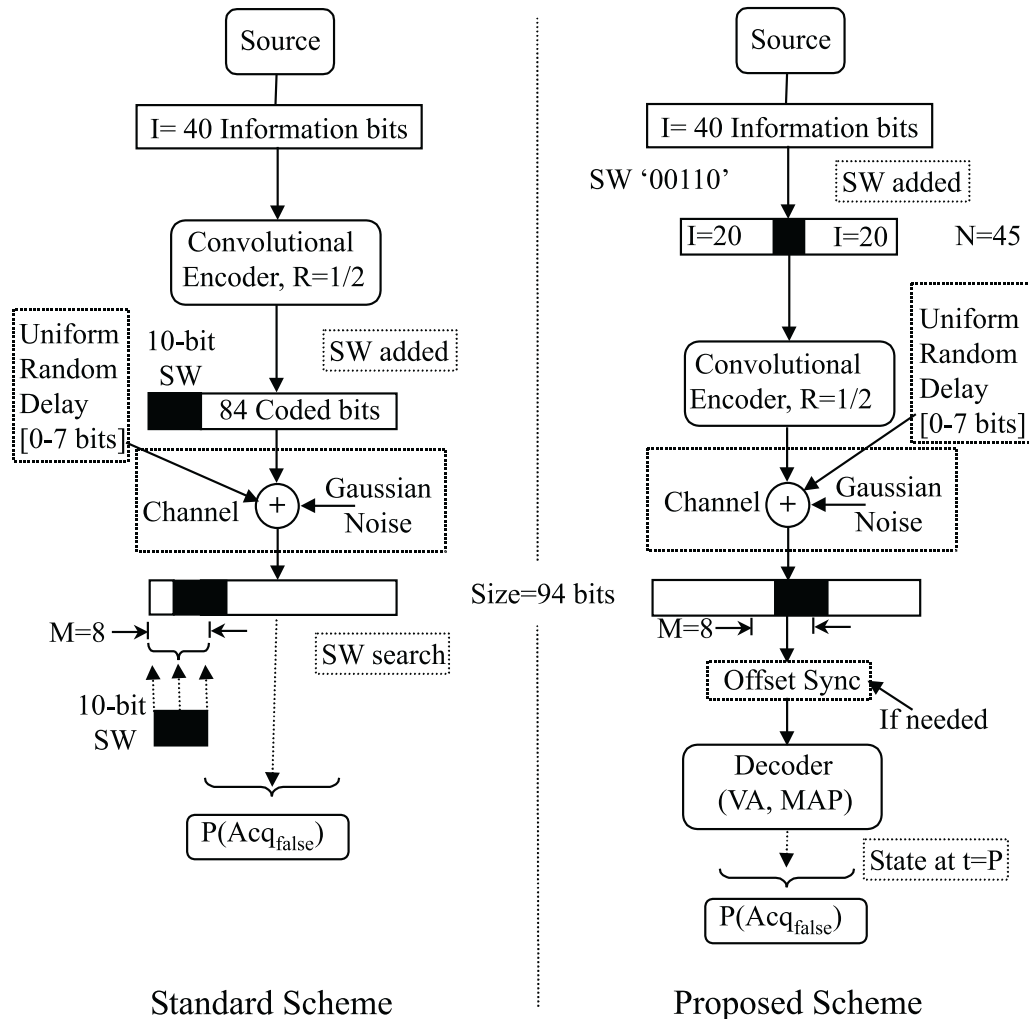


Figure 6.4: Flow charts for Monte Carlo simulation method to obtain the probability of false synchronization.

For an equivalent comparison with the standard ML synchronization, we assume that the transmitted packet size to the channel is 94 bits long including the 10-bit SW '101110000' taken from [94]. This SW has the minimum partial auto-correlation property. We calculated the $P(Acq_{false})$ of a packet from (6.12) for the ML frame synchronization. Since the SW and data bits are from the same binary alphabet, this estimation of acquisition suffers from the appearance of SW in a random data

sequence, as does our proposed scheme. So we calculated the optimum decision rule for frame synchronization excluding this repetition effect. This means that if the argument of the right hand side of (6.12) is maximum for more than one position of the SW including the correct position, we consider that the acquisition is achieved. In practice, this repetition phenomenon is avoided by employing data constraint on the random input information bit sequence.

Fig. 6.5 shows the performance of the system as a function of E_b/N_0 . The term “10-bit SW” refers to a 94 bits long packet including the header, where the header contains 10-bit uncoded SW. The terms “Proposed Scheme (VA)” and “Proposed Scheme (MAP)” refer to our proposed technique using VA algorithm and MAP algorithm, respectively. Both algorithms show similar performance, and the proposed scheme for frame synchronization provides significantly better performance than the widely used ML decision rule for reasonably high E_b/N_0 of the system. Note that the delay was considered as an integer multiple of one information bit period for the proposed scheme in Fig. 6.5.

The probability of false acquisition as a function of E_b/N_0 of the system for various packet sizes using the proposed scheme is depicted in Fig. 6.6. The performance is nearly identical for various packet sizes. One reason is that if the distance of the observation stage $t = P$ is far enough from the last stage of the trellis, its stability is independent of that distance. Still, mid-amble should be the best position for SW because mid-amble is the least vulnerable position of the packet. Since the performance is similar for various packet sizes, we can infer from the plots that the performance is insensitive of the SW positions near mid-amble. This proposed scheme should be useful for shorter packets, where bandwidth overhead is the main limitation in frame synchronization. Shorter packets are used when small amounts of data are to be transmitted, or data only arrives sporadically or a low latency is required.

The flowchart of the proposed scheme has a block entitled ‘offset sync’ that aligns the received symbols to the branch of the trellis using two decoders. As a result, the proposed scheme can resolve up to 8 coded bits delay in two stages. We assume that the delay is a uniformly distributed random variable in the range of $[0 - 7]$ coded bits. In the first stage, both decoders output the metric associated with its best path at time $t = Q$, where $Q \leq$ the uncoded packet length. The decoder with the larger metric will indicate the information bit aligned packet. Then, we can recognize a one-to-one correspondence between the state of the convolutional encoder at time P and the relative delay of the received vector in the same way mentioned earlier. Fig.

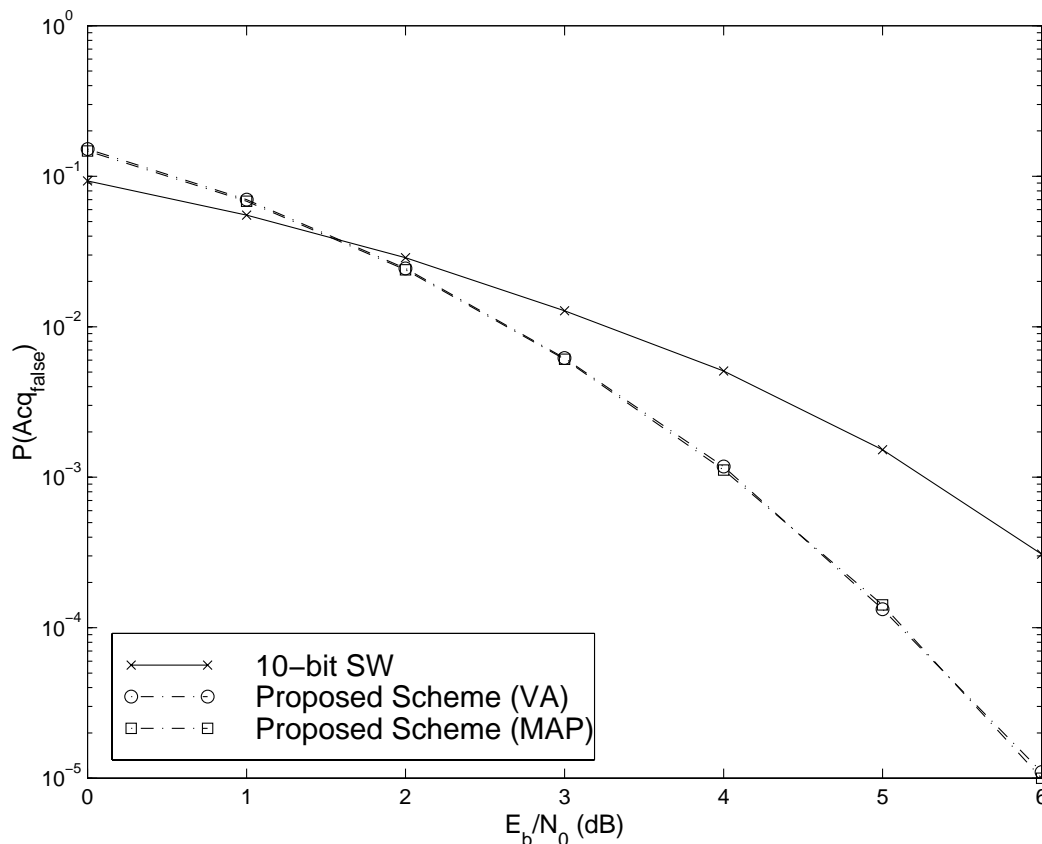


Figure 6.5: Probability of false acquisition versus $\frac{E_b}{N_0}$ of the system using various synchronization schemes.

6.7 shows the synchronization performance by combining these two stages. Note that for $Q \geq 45$, the probability of false alignment of the received symbols to the branch of the trellis is very low and this is independent of the packet length.

We can resolve more distinct delays of the packet using higher constraint length code, and this also requires longer SW at the mid-amble. For example, using rate 1/2 and constraint length 4 code, we can resolve up to 16 distinct delays of the packet. This will require 10-bit SW ‘0001011100’. So the number of resolvable delays is proportional to the constraint length of the code.

We also evaluated the synchronization performance of the system for flat fading channel. Fig. 6.8 shows the performance of the synchronizer using different schemes. By comparing the plots of the flat fading channel of Fig. 6.8 to those of Fig. 6.5 for AWGN channel, the false synchronization rates of the standard and the proposed methods follow the similar pattern. The crossover points for the AWGN channel

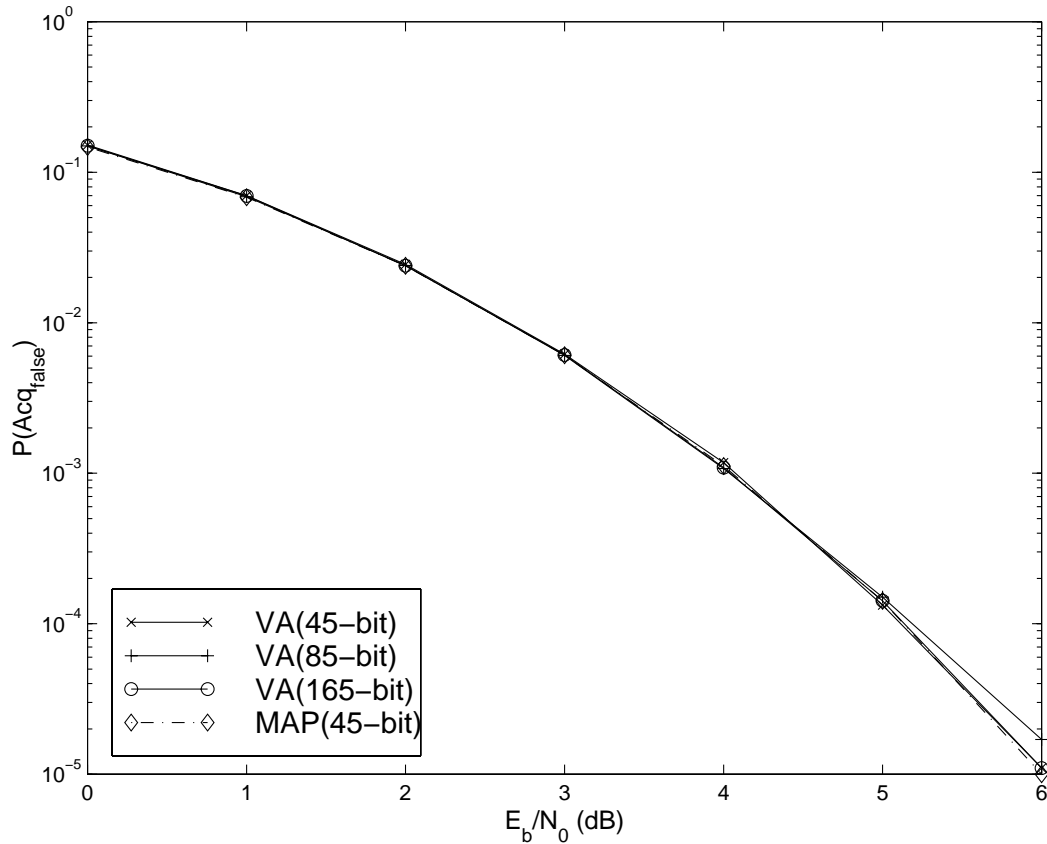


Figure 6.6: Probability of false acquisition as a function of $\frac{E_b}{N_0}$ of the system for various packet sizes using the proposed scheme.

and flat fading channels are at 1.7 and 4.8 E_b/N_0 , respectively. The performance improvement using the proposed scheme is higher in the fading channel.

6.6 Soft-Synchronization of Frame

So far we have evaluated the performance of the hard synchronization only, where the frame synchronizer estimates a packet starting position by calculating the ML function or estimating the ML state of the Viterbi algorithm. Once the decision about the frame synchronization is made, no other information is saved; if the decision is wrong, false synchronization occurs. In soft-synchronization of frame, a decoder follows the soft-output frame synchronizer (list-synchronizer) and these two units jointly estimate the packet starting position. Instead of estimating the packet starting position, the soft-output frame synchronizer produces an ordered list of few κ best estimates

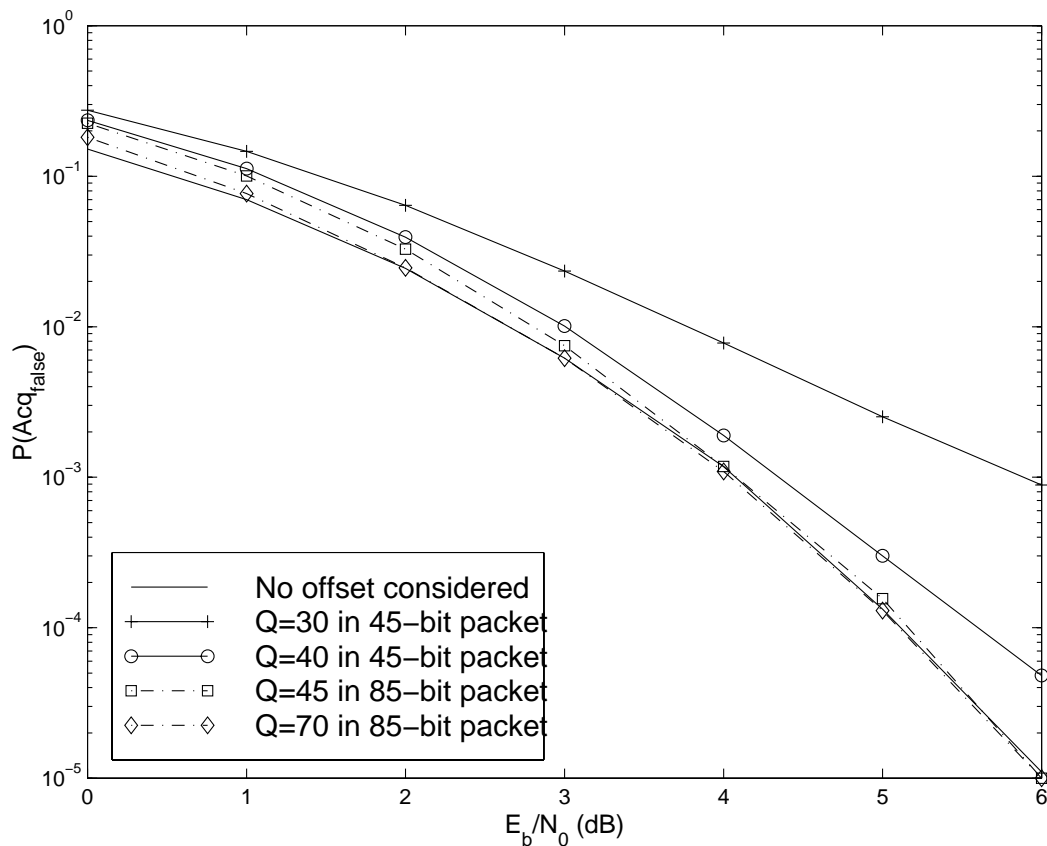


Figure 6.7: Probability of false acquisition vs. $\frac{E_b}{N_0}$ for different values of Q , which is described in the text.

of frame starting positions, depending on the probability of the states in the trellis at the observation stage $t = P$. The decoder first accepts the packet starting position corresponding to the highest probability of the states and calculates the path metrics; then, it makes the final decision about the frame starting position the same way it makes decision about *node synchronization* we discussed previously. If the decoder recognizes a false synchronization, it accepts the packet starting position corresponding to the next highest probability of the states and reevaluates path metrics. This operation can be continued until the decoder recognizes a correct packet starting position. Fig. 6.9 shows this scheme using a flowchart. Without the use of any SW that results in no need of a soft-output synchronizer, the decoder alone can obtain synchronization by evaluating the metrics for every position of the packet, but with the expense of N decoding operations.

We evaluate the frame synchronization performance using Monte Carlo methods considering soft-synchronization we just discussed for our convolutionally- encoded

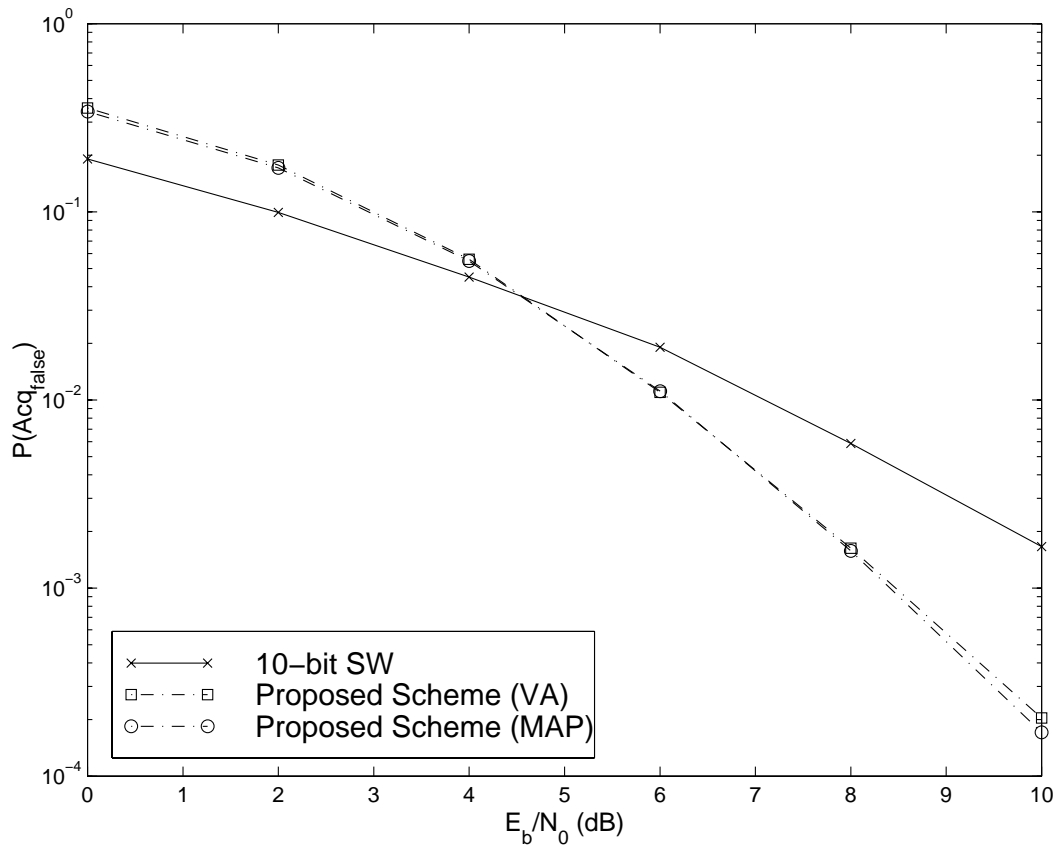


Figure 6.8: Probability of false acquisition vs. $\frac{E_b}{N_0}$ of the system for flat fading channel.

system in AWGN channel. Note that after correct frame synchronization, the receiver needs to decode the transmitted information bit sequence anyway. In our simulation, we assume that if the decoder finds a false synchronization considering the most probable packet starting position, it simply considers the second most probable position. Since the decoder only needs to decode a fraction of the frame to make a decision whether it should continue decoding or not, the complexity of this soft-synchronization scheme stays almost same as in the hard synchronization scheme. The performance of this soft-synchronization scheme along with the plots of Fig. 6.5 is presented in Fig. 6.10. These plots show that this soft-estimation of the packet starting position significantly improves the synchronization performance with a little increase in the receiver complexity.

Next section uses the concept of iterative estimations (concatenated-synchronization) for improved synchronization, where the first synchronizer generates a soft estimate and the second synchronizer makes a hard decision. Three different architectures of

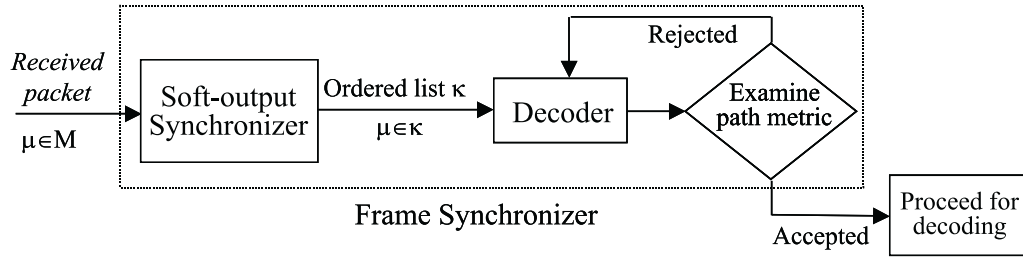


Figure 6.9: Block diagram of a concatenated frame synchronizer.

frame synchronization based on the concatenated-synchronization principle are presented and the performance of these schemes are investigated via simulation.

6.7 Concatenated Synchronizers

The decoder-aided synchronization scheme can be employed jointly with other frame synchronization and decoding schemes. In [88] it is shown that decoding operation can aid the frame synchronization operation in a coded system. Soft and iterative estimates can be passed between synchronization modules to enhance the overall synchronization performance. We present several frame synchronization architectures using the list-synchronization concept.

Let us assume that $P_{sn1}(\kappa)$ is the probability that the frame starting position is not in the list provided by the first synchronizer; thus, the probability that the frame starting position is in the list is $[1 - P_{sn1}(\kappa)]$ and this probability increases monotonically with the list-length κ . Let us also assume that the probability of incorrect frame starting decision of the second synchronizer is P_{sn2} , when the list provided by the first synchronizer contains the correct starting position. Note that these two synchronization stages are independent; so, the probability of the synchronization failure can be written as

$$\begin{aligned}
 P_{snT} &= [1 - (1 - P_{sn1}(\kappa))(1 - P_{sn2})] \\
 &\simeq [P_{sn1}(\kappa) + P_{sn2}].
 \end{aligned}
 \tag{6.21}$$

So, in order to have a very-low probability of synchronization failure, both $P_{sn1}(\kappa)$ and P_{sn2} should be very low. The probability $P_{sn1}(\kappa)$ can be kept very low for sufficiently higher value of the κ , and is comparatively easier to achieve; however, the probability P_{sn2} is also needed to be very low, and this requires a more reliable

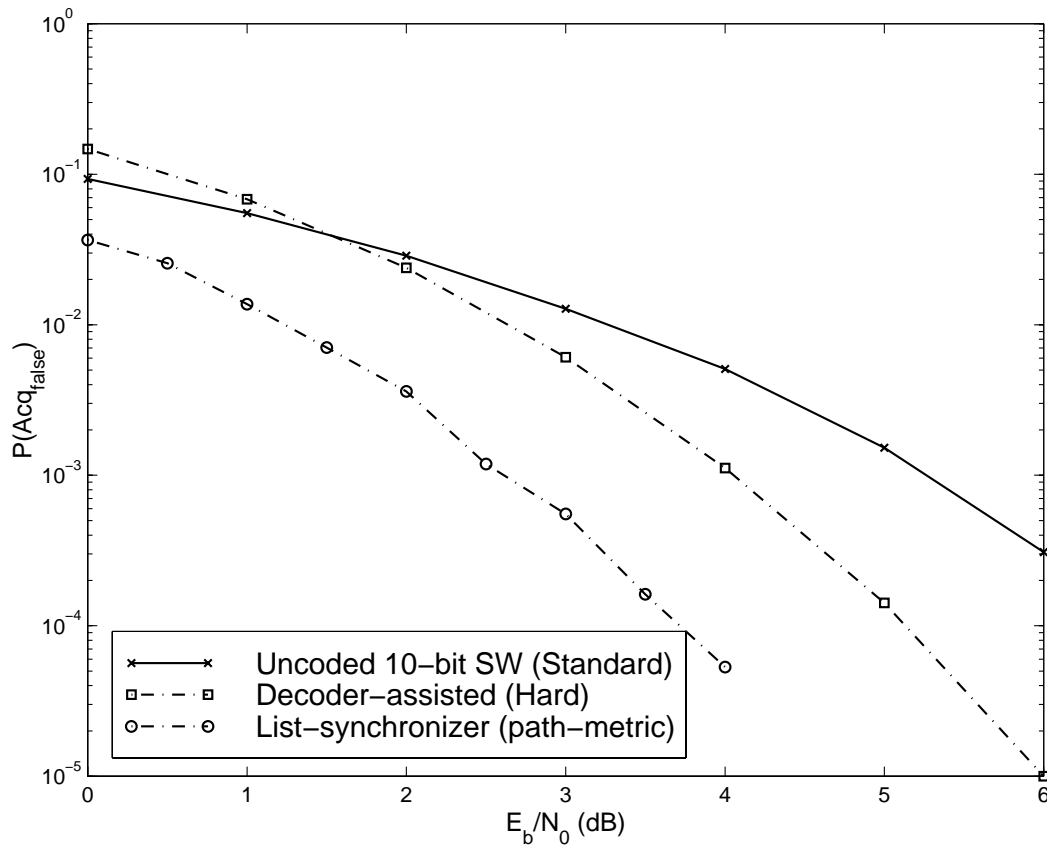


Figure 6.10: Synchronization failure rate vs. $\frac{E_b}{N_0}$ of the system using convolutional encoding, where soft synchronization is employed.

frame synchronizer in the second stage. So, the first synchronizer can be a simple one, such as standard synchronizer based on (6.12), where synchronizer performance can be compensated by the list-length κ .

6.7.1 Scheme for Estimating Longer Packet Delays

Fig. 6.11 shows a concatenated-synchronization technique for resolving any time ambiguity of the packet. Note that the decoder-assisted scheme discussed above can resolve only $M = 8$ time ambiguities. Here, we assume that the time delay can be up to N bits, where N is the packet length. The first module is a conventional frame synchronizer and the SW ‘110101’ is 6-bit long; next paragraph will explain about the selection of this SW. This module outputs a list of estimated starting positions of the packet, in descending order of likelihood. The last block is the decoder-assisted synchronizer we proposed in Section 6.4, which takes the most probable packet starting

position from the ordered list and verifies the positions of the mid-amble bits using a one-to-one correspondence with state of the decoder. If these bits are correct, the receiver proceeds to the decoding stage. Note that the complexity of this synchronization scheme is the same as the conventional synchronization technique using a 6-bit SW because the last verification stage can be considered as the decoding operation. If the estimated mid-amble bits are not correct, this unit rejects the delay estimate and proceeds to the next most likely estimate on the ordered list. These cycles of operations can be continued until the correct mid-amble bits are obtained, or a designated number of iterations. After exhausting all iterations, if a correct mid-amble bit can not be obtained, we consider it as a failure event.

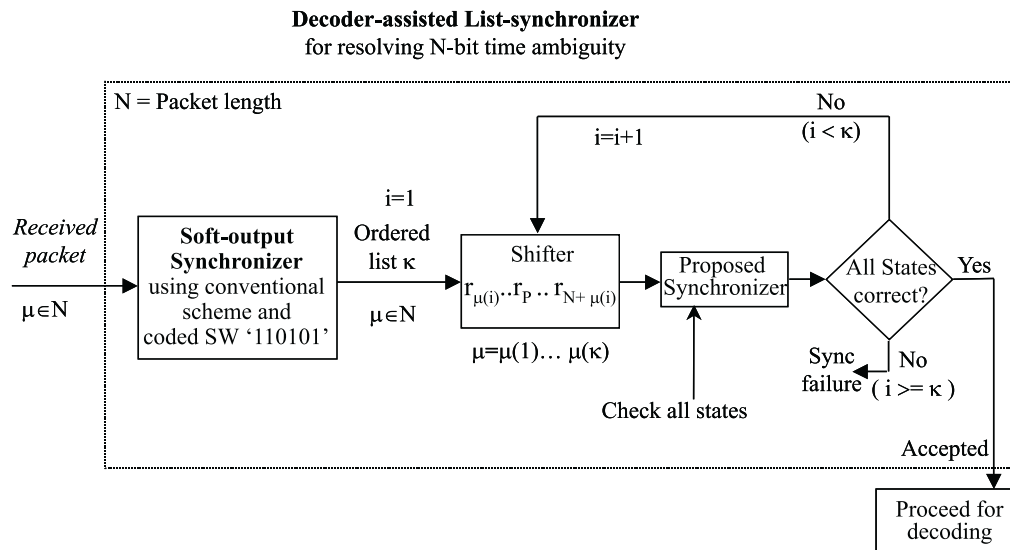
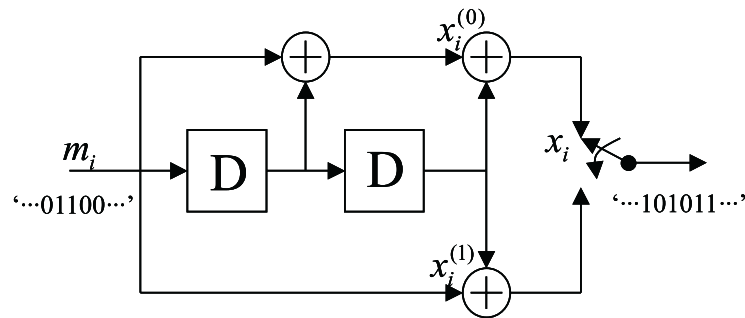


Figure 6.11: List synchronizer for resolving any time ambiguity of the packet.

Fig. 6.12(a) shows the schematic diagram of a rate 1/2 and constraint length 3 convolutional encoder. Here, m_i is an uncoded bit at time i of an input word composed of an information word and the SW; we consider only the SW part, which is the mid-amble of the packet. The terms ' $x_i^{(0)}$ ' and ' $x_i^{(1)}$ ' represent the two constituent coded bits respectively due to an uncoded bit at the input to the encoder. Fig. 6.12(b) shows the register contents, states of the encoder and the coded output bits due to the uncoded SW '01100'. The notation '*' in the table of Fig. 6.12(b) denotes that the coded bit is unknown; that is, the coded bit is dependent on the preceding or following information bits. It is clear from the tables that the 6 coded bits '110101' due to the uncoded SW '00110' are independent of the information bits. This coded

6-bit word ‘110101’ can be considered as a known SW for a standard synchronization technique before the decoding stage. Note that the 6-bit coded SW ‘110101’ due to the uncoded SW ‘00110’ of the mid-amble is always known to the receiver, but the decoder-assisted scheme of Section 6.4 does not need any information about the coded SW. On the other hand, this 6-bit coded SW ‘110101’ is an additional information for a standard synchronizer, which can consider the coded SW as known. One drawback of this SW is that it does not guarantee the best partial auto-correlation function as does the Barker code.



(a) Rate 1/2, constraint length 3 convolutional encoder

Uncoded SW	Register content	State	Coded SW
0	0 * *	* *	* *
0	0 0 *	0 *	* *
1	1 0 0	0 0	1 1
1	1 1 0	1 0	0 1
0	0 1 1	1 1	0 1
*	* 0 1	0 1	* *

$x_i^{(0)} \quad x_i^{(1)}$

(b) Encoder input, output, state and register content due to the SW ‘00110’

Figure 6.12: Schematic diagram showing the independent coded SW due to a uncoded SW in the mid-amble.

The performance of the proposed scheme of Fig. 6.11 was compared with that of the uncoded ML decision rule using Monte Carlo simulations. The uncoded packet size is 45 bits including the SW ‘00110’; so after encoding with a rate 1/2 and constraint length 3 convolutional code, the transmitted packet size is 94 bits. We simulated for the probability of false acquisition ($P(Acq_{false})$) as a function of the system

E_b/N_0 . For an equivalent comparison with the standard ML synchronization, we assume that the transmitted packet size is 94 bits long including the 10-bit uncoded SW ‘1101110000’ taken from [94]. Equation (6.12) was used for resolving N time ambiguities. Fig. 6.13 shows the performance of the system. The term “Unc. 10-bit SW (repetition)” refers to a 94 bit long packet including the header for standard ML scheme, where the header contains 10-bit uncoded SW and the word ‘repetition’ means that the SW may appear in the transmitted data. The term ‘List-synchronizer (n iter)’ refers to the scheme shown in Fig. 6.11, where the ‘Shifter’ operates on the received signal N times to consider all possible packet delays. The performance improves significantly due to the above mentioned concatenated synchronization scheme. The plots also show a trade-off between the performance and the complexity. Note that the coded SW ‘00110’ may be embedded in any location in the packet. If this SW is placed at the end of a packet, a portion of the SW also can act as the termination bits, thereby reducing overhead. When we consider the two uncoded bits as required for the purpose of trellis termination, this reduces the equivalent redundancy due to the frame synchronization to three uncoded or six coded bits.

6.7.2 Scheme for Estimating Shorter Packet Delays

Often times, ambiguities are only a few bits, and in reference [95], the decoder-assisted scheme of Section 6.4 was shown suitable to resolve these few bits delay. The performance of this scheme can be further improved by resolving the 6-bit coded SW ‘110101’ discussed in the previous section, with almost no increase in computational complexity. Fig. 6.14 presents a flowchart of this cascading technique, where the second stage takes the ordered list of the estimated packet delays from the first stage and makes a final decision. As we discussed before, there are numerous ways to apply the ‘standard scheme’ in the second stage; in our simulation, we used (6.12) to calculate the metric assuming the estimated delay obtained from the first stage. If the estimated delay from the first stage is verified at the second stage, this is the final estimated delay; otherwise, the next most probable estimated delay from the first stage is accepted.

Fig. 6.15 shows synchronization performance as a function of the input $\frac{E_b}{N_0}$ of the system. The terms ‘Uncoded 10-bit SW(Standard)’, ‘Decoder-assisted(Hard)’ and ‘List-synchronizer(Standard)’ refer to the standard ML scheme, the decoder-assisted scheme of Section 6.4 and the list-synchronization scheme of Fig. 6.14 for resolving

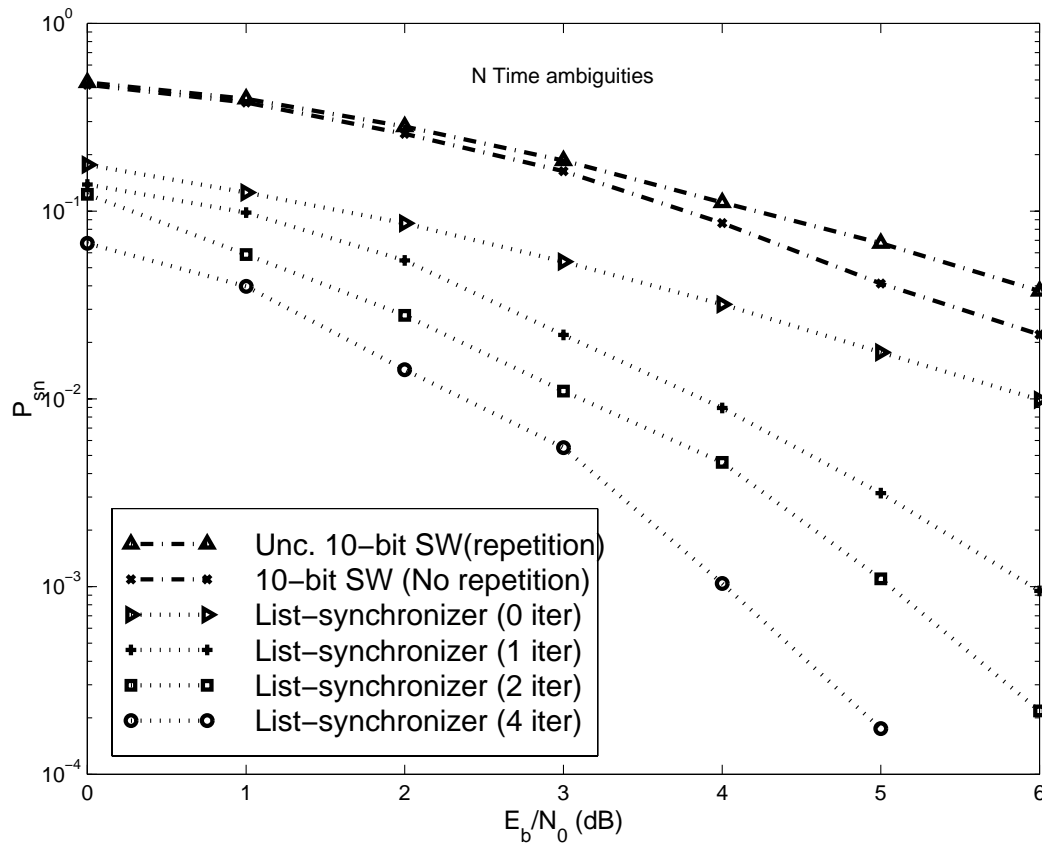


Figure 6.13: Synchronization failure rate vs. $\frac{E_b}{N_0}$ of the system using the standard ML schemes and the list-synchronization scheme, respectively.

up to 8 coded bit delay, respectively. The term ‘List-synchronizer(path-metric)’ denotes the list-synchronization scheme of Fig. 6.14, where in the second stage we use a decoder to make a final decision of the delay. This technique shows the best performance in expense of the additional computational complexity. Our list-synchronizer improves the performance over the decoder-assisted scheme of Section 6.4 with little additional complexity.

6.7.3 Scheme for Estimating Shorter or Longer Packet Delays

If the packet delay is more than eight coded bits, the above concatenated-synchronization scheme of Fig. 6.14 will fail. Although the alternate choice is the technique of Fig. 6.11, the complexity of this scheme will be a wastage for shorter packet delays. This problem can be solved with the alternate architecture proposed in Fig. 6.16; here,

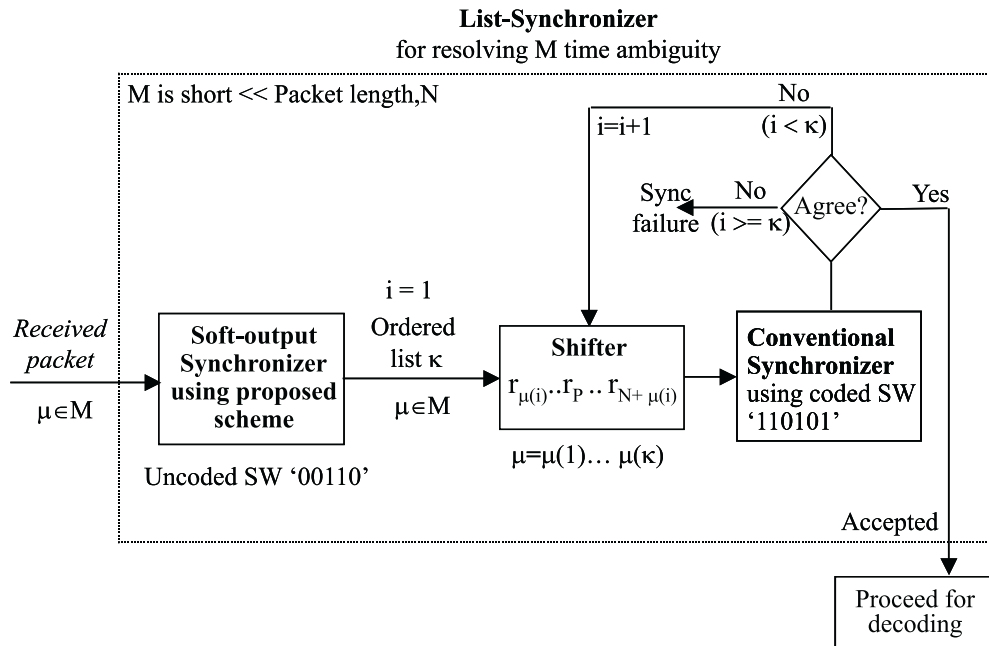


Figure 6.14: List synchronizer for resolving shorter packet delays.

the synchronizer is equivalent to the synchronizer presented in Fig. 6.14 for a shorter packet delay, but can now resolve larger packet delays. If the packet delay is more than 8 bits, the synchronization window can move every 8 bits to resolve another 8 bits delay. Since the mid-amble is more vulnerable to errors within a range from the packet end positions, the entire packet is needed to shift in order to avoid instability of the decoder-assisted scheme after a few steps.

6.7.4 Derivation of the Likelihood Function in a Coded System

The received packet is composed of several possibly known sequences and the actual data sequence. The starting symbol sequence and the ending symbol sequence can be two of the few known sequences; for the example of our rate 1/2 and constraint length 3 code, the terminating or the starting coded-bit sequences can be one of the four sequences '0000', '1100', '1011' and '0111'. The next coded-bit sequence following the starting sequence of packet is the data sequence and is followed by the 6-bit coded SW '110101'. Then, we have the data sequence and the packet termination sequence. In [86], a frame synchronization technique is proposed that makes use of the terminating

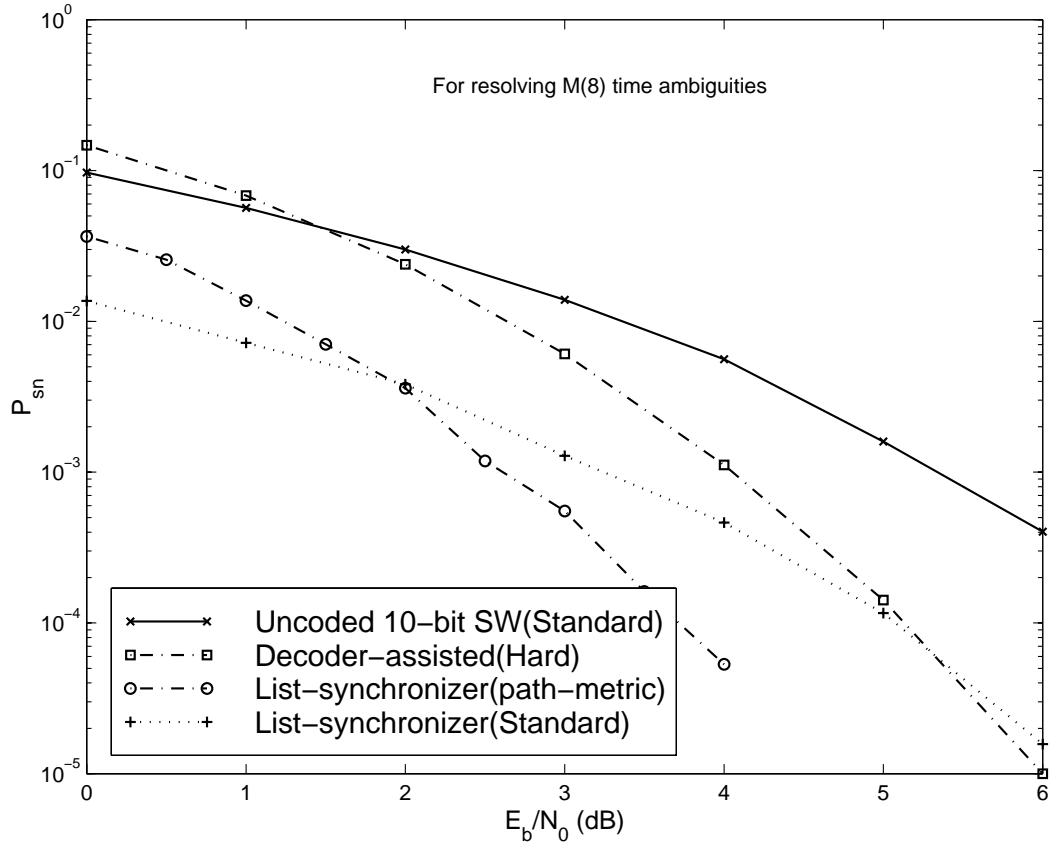


Figure 6.15: Synchronization failure rate against $\frac{E_b}{N_0}$ of the system using various schemes for resolving up to 8 coded bit delay .

bits of the convolutionally-encoded data to augment the SW. Considering all these components, the general pdf function can be written as

$$\begin{aligned}
 f(\mathbf{r}|\mu) &= \sum_{\forall \mathbf{d}} f(\mathbf{r}|\mu, \mathbf{d}) \cdot P(\mathbf{d}) \tag{6.22} \\
 &= \frac{1}{(\pi N_0)^N} \sum_{\forall \mathbf{d}} P(\mathbf{d}) \prod_{i=0}^{nm-1} \exp \left[-\frac{\|r_{i+\mu} - s_i\|^2}{N_0} \right] \\
 &\times \prod_{i=nm}^{N_1-1} \exp \left[-\frac{\|r_{i+\mu} - d_i\|^2}{N_0} \right] \prod_{i=N_1}^{N_2-1} \exp \left[-\frac{\|r_{i+\mu} - S_i\|^2}{N_0} \right] \\
 &\times \prod_{i=N_2}^{N-nm-1} \exp \left[-\frac{\|r_{i+\mu} - d_i\|^2}{N_0} \right] \prod_{i=N-nm}^{N-1} \exp \left[-\frac{\|r_{i+\mu} - t_i\|^2}{N_0} \right],
 \end{aligned}$$

where, n , m , s_i , t_i , N_1 and N_2 denote the rate, memory of the encoder, trellis opening sequence, trellis termination sequence, the data sequence before the SW and the data sequence after the SW, respectively.

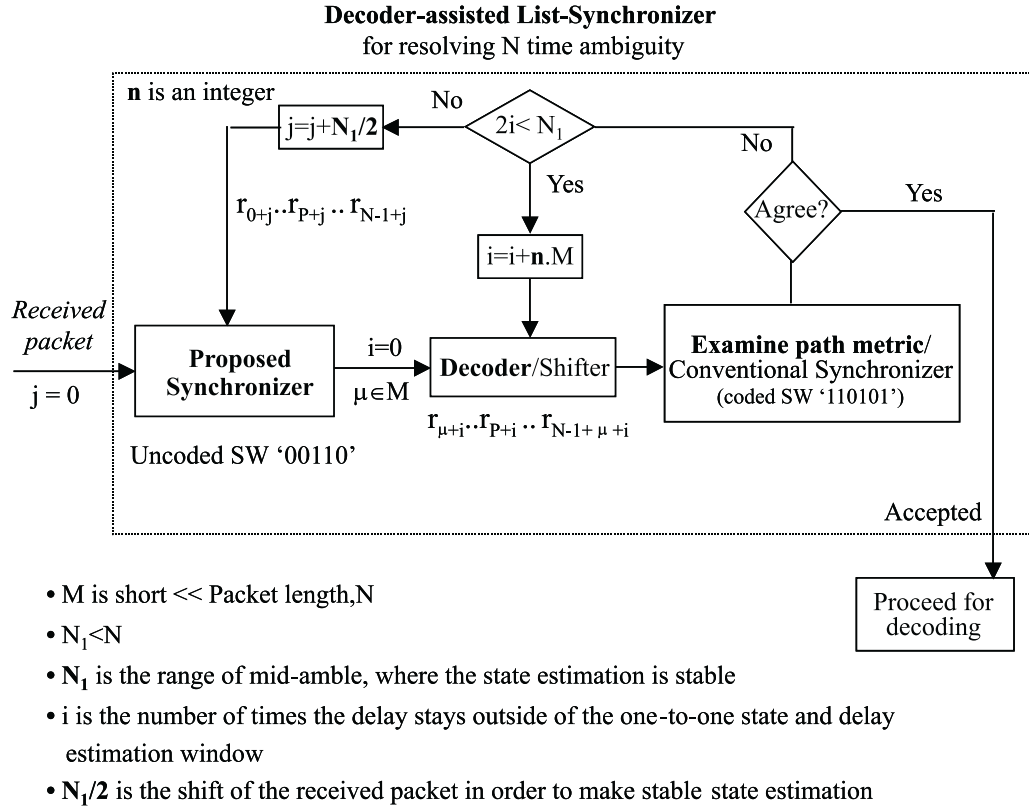


Figure 6.16: Frame synchronizer for estimating shorter packet delay, which is capable of resolving any packet delay.

Following the similar derivations presented in the previous sections, assuming the independence of the coded-data sequence although those are not, and applying the technique derived in [86] for the terminating-bit sequence, the following result can be obtained for the likelihood function for high SNR approximation

$$\begin{aligned}
 L_H(\mu) &= \sum_{i=0}^{nm-1} \left[\langle r_{i+\mu}, \hat{s}_i - W_j \rangle + \frac{\|W_j\|^2 - \|\hat{s}_i\|^2}{2} \right] \\
 &\times \sum_{i=N-nm}^{N-1} \left[\langle r_{i+\mu}, \hat{t}_i - W_j \rangle + \frac{\|W_j\|^2 - \|\hat{t}_i\|^2}{2} \right] \\
 &\times \sum_{i=N_1}^{N_2-1} \left[\langle r_{i+\mu}, S_i - W_j \rangle + \frac{\|W_j\|^2}{2} \right],
 \end{aligned} \tag{6.23}$$

where, W_i is the energy associated with M-ary symbol set, and \hat{t}_i and \hat{s}_i are the terms with the best correlation property among the four sequences. The above expression can be used for improved standard method of the synchronization technique.

6.7.5 Section Summary

In this section, we proposed three different schemes to estimate the delays of arriving packets. The decoder-assisted technique outperforms the standard ML technique and the concatenated-synchronizers achieve significant performance improvement over the stand-alone decoder-assisted scheme. Since the storage capability is improving, the decoder-assisted scheme for frame synchronization can be integrated with the decoding process.

6.8 Turbo Synchronization

Presently reliable communications at very low SNR and signal-to-interference ratio (SIR) are possible due to advancements in receiver design, such as turbo coding and multiuser detection. This link level improvement is made possible by assuming perfect synchronization of the packets. As the SNR requirement decreases, the synchronization of the packet becomes increasingly difficult. The standard way of performing frame synchronization is to embed an uncoded SW in the header of the packet. Our proposed scheme for convolutionally encoded data packets, in which SW is embedded in the mid-amble and coded along with information bits can be used for turbo synchronization (frame synchronization in turbo decoding). The aim of this technique is fast frame synchronization of packets at low SNR, especially to recover lost synchronization. In this case, we need not consider the whole packet for a possible packet starting position. We showed that our proposed scheme outperforms the standard ML frame synchronization scheme for resolving relatively shorter delays of the packet using convolutional code. We believe that this technique offers a new way of performing ‘*soft*’ frame synchronization for packet transmissions at low SNR .

In [96], a turbo synchronization technique is proposed, where the constituent decoder pair is involved for turbo synchronization without the requirement of any SW. This scheme is applicable in any packet radio system, where convolutional type decoding is necessary. The author also optimized the synchronization time by sharing the synchronization task between two decoders at a certain ratio. In his scheme, decoder 1 carries on the major task, since decoder 2 has to wait until the whole packet transmission for any decision because of the interleaver. Since our proposed scheme in Section 6.4 is suitable for shorter packet delays, any other scheme in conjunction to our scheme can be used to resolve longer packet delays.

We can extend the soft frame synchronization concept to turbo synchronization using the ‘Soft-output Synchronizer’ and the ‘Decoder 1’ shown in Fig. 6.17. The ‘Frame Synchronizer’ is responsible for turbo synchronization, where the ‘Soft-output Synchronizer’ produces initial soft estimations of the frame starting position. Decoding of the packet starts after ‘Decoder 1’ decides on the frame start position. For our convolutional code example, the SW ‘00110’ was embedded in the mid-amble of the packet before encoding, where the starting ‘00’ bits of the SW force the trellis into the state S_0 and the next ‘110’ bits guide the path through states S_1 , S_3 and S_2 successively. Since the code must be systematic for turbo decoding, the starting ‘00’ bits of the SW will not merge the trellis into the state S_0 anymore. During encoding, these initial two bits can be adaptively inserted to force the trellis to S_0 state by monitoring the state of the trellis. This will not add any extra complexity in the encoder, rather than encoding the SW in a different way. The sequence ‘100’ will guide the trellis through states S_2 , S_3 and S_1 successively. As a result, the uncoded SW is ‘* * 100’, where ‘*’ means that the bits are unknown.

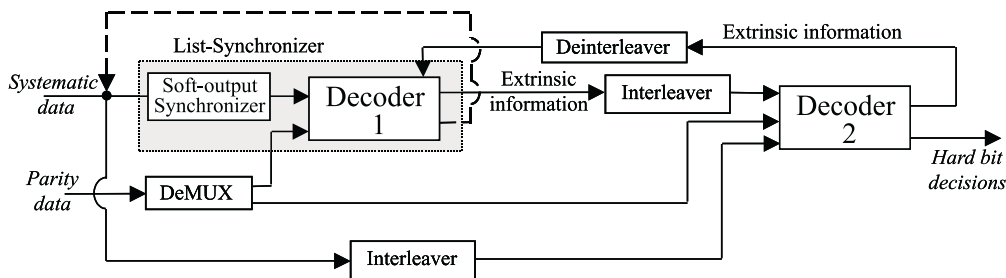


Figure 6.17: Block diagram of a turbo-decoder assisted list-synchronizer .

We simulated the system using Monte Carlo Method. We considered a rate $1/2$, constraint length 3 turbo code, where even-odd bit puncturing was used to increase the rate from $1/3$. Note that the performance of rate $1/3$ turbo code is the same as illustrated in Fig. 6.10 because they are equivalent as far as synchronization is concerned. Fig. 6.18 plots the performance of the turbo synchronization for the system. We assume that the node synchronization for BPSK system can be resolved using two positions of the coded bit sequence as we described above. As expected, the synchronization performance degrades due to puncturing, but soft-synchronization of frame helps the performance significantly.

Generally, a turbo decoder provides an improved a posteriori estimation of the

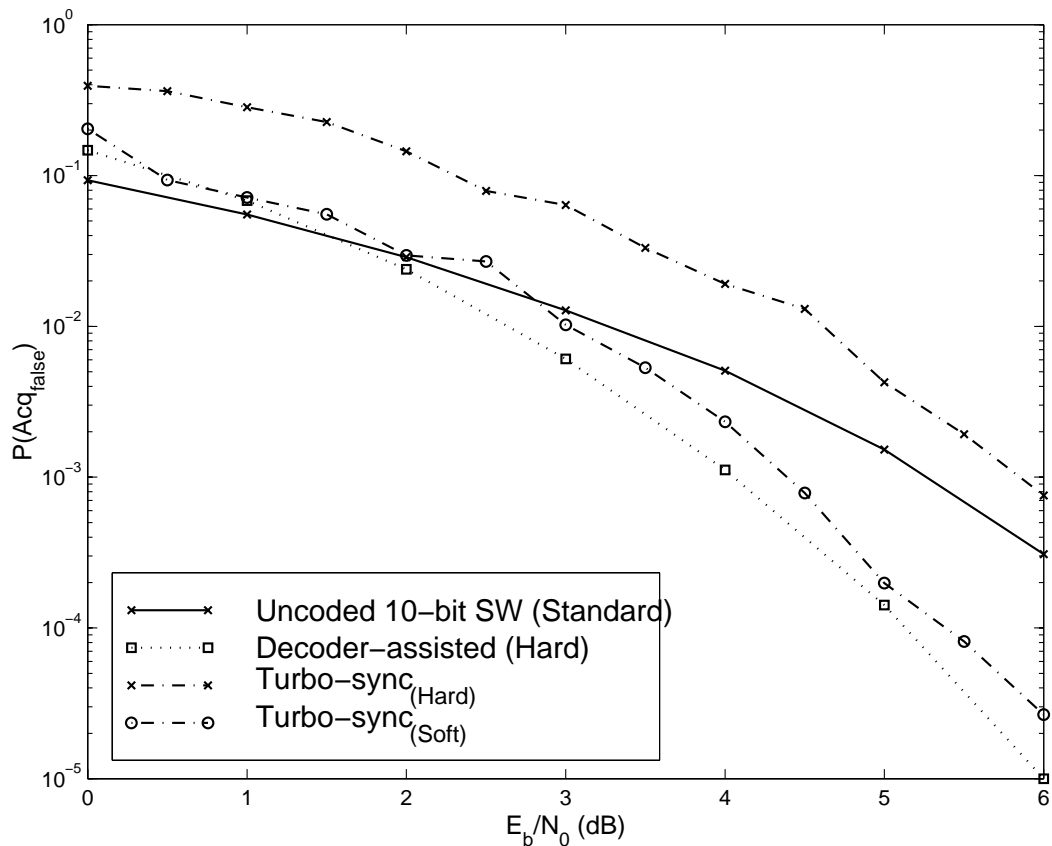


Figure 6.18: Comparison of the turbo synchronization performance considering hard and soft estimation of the synchronizer.

transmitted symbol after each iteration. Let us consider a list-synchronization technique, where the first decoder is a simple standard synchronizer based on (6.12) and second synchronizer is a turbo decoder. The synchronization performance can be improved significantly using this turbo decoding principle. For our purpose, the frame starting position is yet to be known. From the potential list of the packet starting positions provided by the first synchronizer, if one of two constituent decoders selects a wrong packet starting position, estimates the a posteriori probability of transmitted data or packet delay, and passes that probability to the other decoder, the second synchronizer (turbo decoder) will simply fail; because the a posteriori probability is incorrect and becomes the a priori probability for the other decoder input. However, if the second synchronizer selects the correct frame starting position from the list, which is yet to be determined, the probability of the correct estimation of the frame starting positions increases with each successive iteration. Note that the synchronization

process is not complete yet because the decoder needs to assure whether the selected frame starting position from the list is correct or not. An extrapolation module can be deployed. Based on these methodology, we propose three different architectures of frame synchronization for resolving any packet delays, which is presented as follows.

Fig. 6.19 depicts the flow diagram of a turbo-decoder assisted frame synchronizer; the first block is a standard synchronizer based on (6.12) and is followed by the turbo decoder. The last module is the CRC check for error detection, and this block extrapolates whether the synchronization is correct or false. The SW is an uncoded Barker sequence and can be inserted at any position in the packet or can be distributed throughout the packet, although coded SW also can be used. The turbo decoder completes n iterations before making any final decision. If the list length κ contains the correct frame starting position, the synchronization failure rate is equal to the BER performance of the turbo decoder provided that the CRC check determines errors perfectly. A similar principle is presented in [90] for convolutional coded system. One drawback of this technique is that in addition to the SW, CRC bits are overhead which decreases the bandwidth efficiency. To overcome this overhead due to CRC bit, a SDR technique for stopping of turbo decoding is presented in [97].

Another method of turbo-decoder assisted frame synchronization is presented in Fig. 6.20; the first block is a standard synchronizer based on (6.12) and is followed by the turbo decoder. Instead of using another extrapolation device, the turbo decoder estimates the $P(s_0, s_1, \dots, s_{L-1} | \mathbf{r})$ for every frame starting position provided by the first synchronizer and takes the position corresponding to the highest probability. In terms of synchronization failure rate, this technique shows similar performance to the technique presented in Fig. 6.19 provided CRC check module works error free; that is, if the turbo decoder selects the correct frame starting position from the list, which is yet to be determined, in both cases, the turbo decoder estimates either LLR of the SW or LLR of the information packet. In the earlier case, a decision device makes the information bit estimation from LLR; in the latter case, a simple calculation can determine $P(s_0, s_1, \dots, s_{L-1} | \mathbf{r})$ from LLR values. Since, the earlier technique uses the information of the whole packet, it may perform marginally better. The main disadvantage of the scheme in 6.20 over the earlier scheme is that it requires κ decoding operations (DO) of the turbo decoder, whereas the scheme of Fig. 6.19 goes through the list successively and the number of decoding operation is bounded by $1 \leq DO \leq \kappa$. In addition, empirical studies showed that the uncoded SW outperforms the coded SW for the standard synchronizer based on (6.12); however,

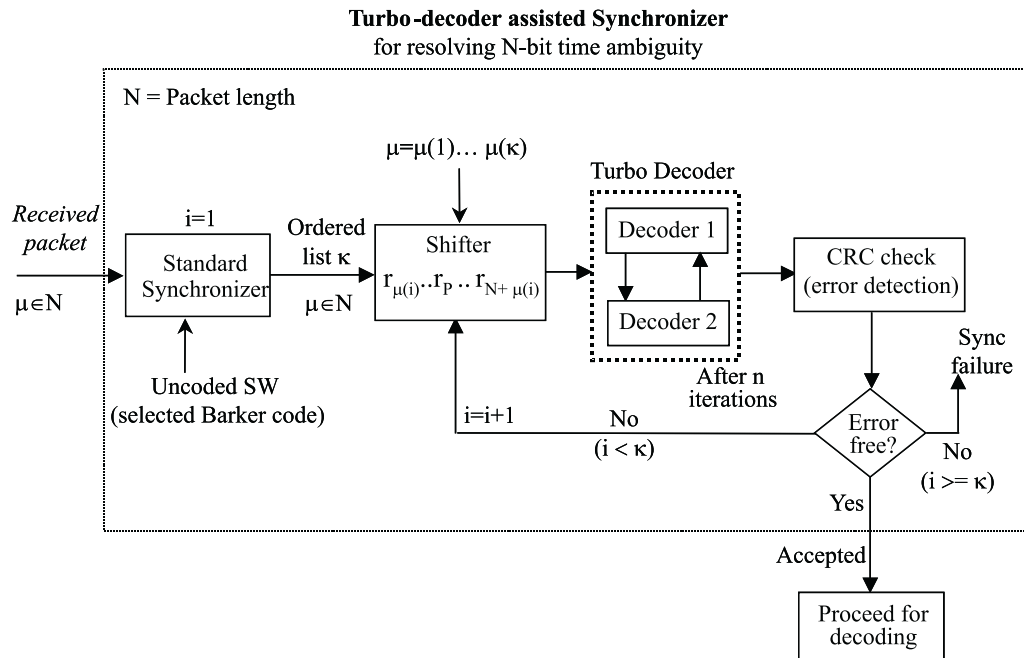


Figure 6.19: Block diagram of a turbo-decoder assisted list-synchronizer; the first module is a standard synchronizer, which resolves uncoded SW (Barker code) embedded in the pre-amble of the packet, and is followed by the turbo decoder and CRC error detection code word, which accepts an error free packet starting position from the list supplied by the first module.

the SW must be added before encoding for the scheme of 6.20.

Fig. 6.21 shows the flow diagram of a turbo-decoder assisted frame synchronizer using our proposed scheme of Section 6.4; the first block is a standard synchronizer based on (6.12) and is followed by the turbo decoder. The SW '110101' or '11001' (punctured) is 6-bit long; the reasons of selection of this particular SW are discussed in the next paragraph. The first synchronizer provides a list of potential frame starting positions, in descending order of likelihood. The following block is a shifter, which simply shifts the received packet data positions according to the list provided by the first synchronizer. The next block is a turbo-decoder type synchronizer; that is, decoding principle is the same as that of a turbo decoder, where decoder 1 generates a posteriori information of the transmitted packet bits (information bits and the SW) and decoder 2 accepts that probability as a priori probability and makes a successive estimation about the same transmitted packet. The only difference is that after the final iteration, the decoder outputs state informations from time $t = P - 3$ to $t = P$. Before decoding, the turbo decoder takes the most probable frame starting

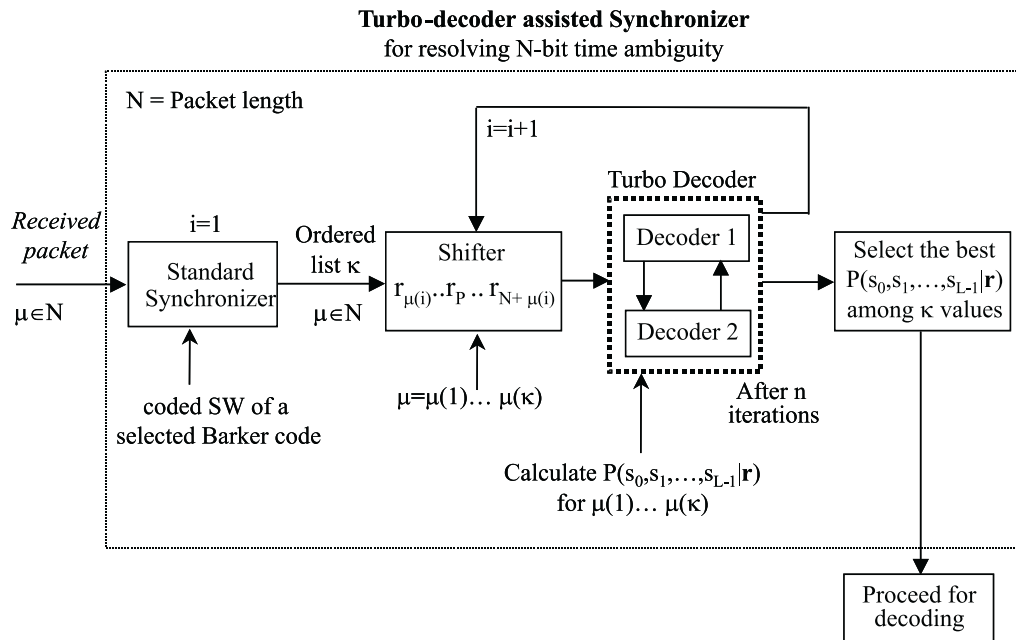


Figure 6.20: Block diagram of a turbo-decoder assisted list-synchronizer; the first module is a standard synchronizer, which resolves coded SW embedded in the preamble of the packet (due to uncoded Barker code), and is followed by the turbo decoder, which calculates the best probable packet starting position from the list supplied by the first module.

position from the list and makes a shift of the received data packet such that the SW aligns with the anticipated position in a mid-amble. As a result, the turbo decoder functions as an iterative decoder, which is the same as the previous two schemes; as well as, it also acts as an extrapolator, which eliminates any need of a packet overhead such as CRC. These states are compared with the anticipated states and if they agree, the receiver proceeds to the decoding stage. Note that the complexity of this synchronization scheme is the same as the conventional synchronization technique using a 6-bit SW because the last verification stage can be considered as the decoding operation. If the estimated mid-amble bits are not correct, this unit rejects the delay estimate and proceeds to the next most likely estimate on the ordered list. These cycles of operations can be continued until the correct mid-amble bits are obtained, or a designated number of iterations are considered. A synchronization failure occurs after exhausting all iterations.

The soft-synchronization schemes in the previous sections are applicable for turbo synchronization. Fig. 6.22(a) shows the schematic diagram of a rate 1/2, constraint

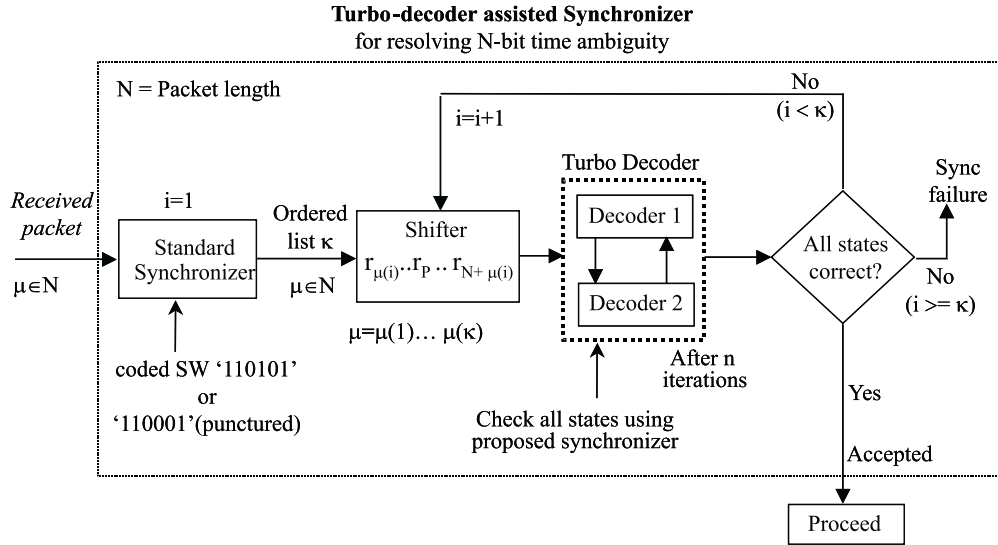
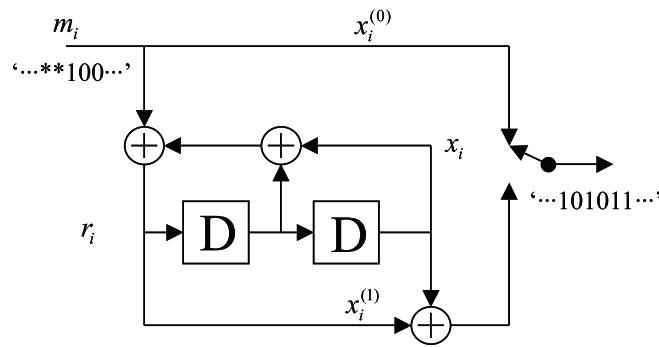


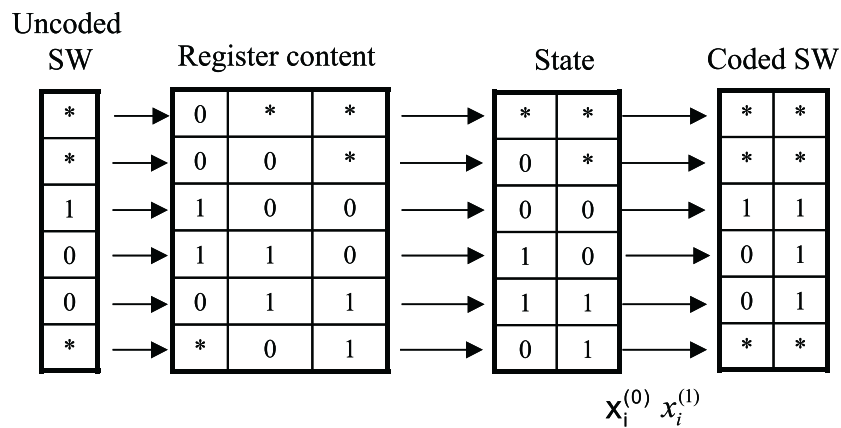
Figure 6.21: Block diagram of a turbo-decoder assisted list-synchronizer; the first module is a standard synchronizer, which resolves the coded SW embedded in a mid-amble, and is followed by the proposed synchronizer described in Section 6.4.

length 3 recursive convolutional encoder. Here, m_i is an uncoded bit at time i of an input word composed of an information word and the SW. We consider only the SW part, which is the mid-amble of the packet. The terms $x_i^{(0)}$ and $x_i^{(1)}$ represent two constituent coded bits consecutively due to an uncoded bit at the input to the encoder, where $x_i^{(0)}$ is the information bit itself. Fig. 6.22(b) shows the register contents, states of the encoder and the coded output bits due to the uncoded SW $* * 100'$. The notation $*$ in the table of Fig. 6.22(b) denotes that the coded bit is unknown, which means that the coded bit is dependent on the information bits. It is clear from the tables that the 6 coded bits $'110101'$ due to the uncoded SW $* * 100'$ are independent of the information bits. This coded 6-bit word $'110101'$ can be considered as a known SW for a standard synchronization technique before the decoding stage. Note that the 6-bit coded SW $'110101'$ due to the uncoded SW $* * 100'$ of the mid-amble is always known to the receiver, but the decoder-assisted scheme of Section 6.4 does not need any information about the coded SW. On the other hand, this 6-bit coded SW $'110101'$ is an additional information for a standard synchronizer, which can consider the coded SW as known.

The performance of the proposed scheme of Fig. 6.21 was compared with that of the uncoded ML decision rule using Monte Carlo simulations. The uncoded packet size is 45 bits including the SW $* * 100'$. We simulated the synchronization failure



(a) Rate $\frac{1}{2}$, constraint length 3 recursive systematic convolutional encoder



(b) Encoder input, output, state and register content due to the SW ‘**100’

Figure 6.22: Schematic diagram showing the independent coded SW due to uncoded SW in the mid-amble.

rate P_{sn} as a function of the system E_b/N_0 . For an equivalent comparison with the standard ML synchronization, we assume that the transmitted packet size is 99 bits long including the 15-bit uncoded SW. Fig. 6.23 shows the performance of the system. The term “ $i = n, k = m$ ” denotes that the list length is k and the iteration of the turbo decoder is n . The performance improves significantly; the plots also show a trade-off between the performance and the complexity.

An additional module can be added to the Fig. 6.21 at the very last stage of synchronization, which is an “extrapolator”. This extrapolator can be a source encoder; it also can gather information from the previous data and can make a decision from multiple frame observations. The corresponding block diagram is presented in Fig. 6.24.

The other feature is that our proposed synchronization scheme can be coherently

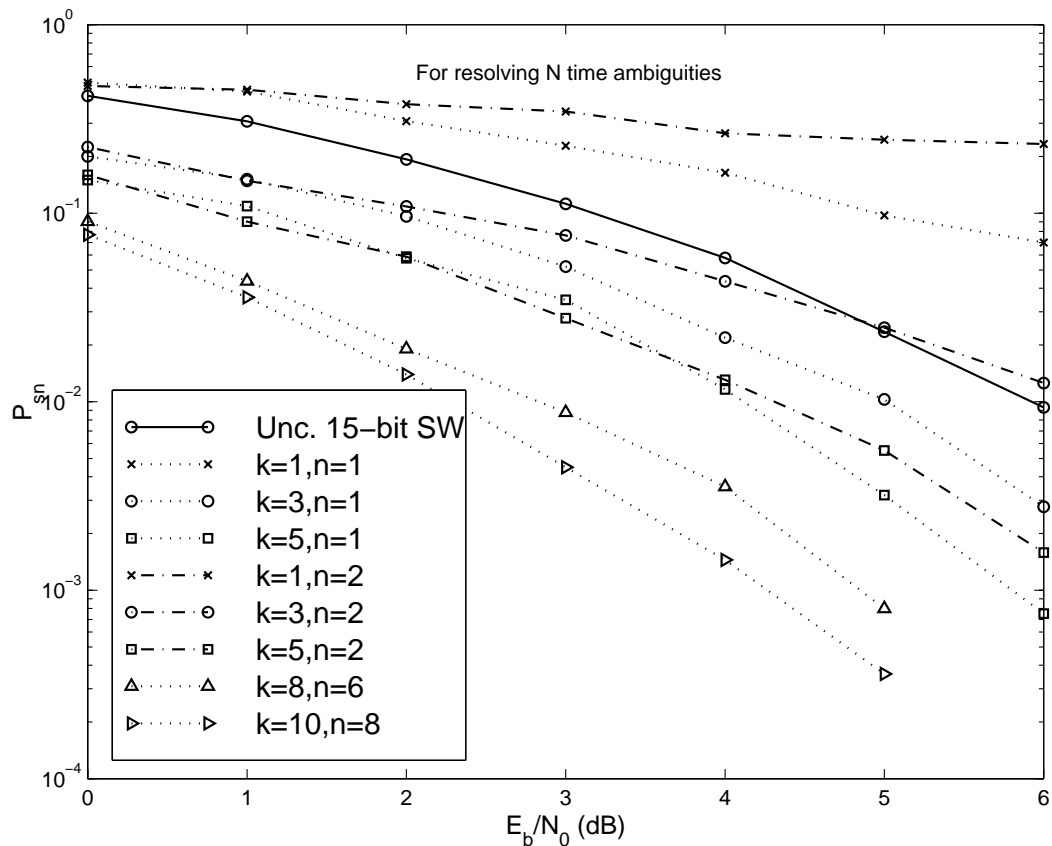


Figure 6.23: Simulated frame failure rate against the E_b/N_0 of the system for the turbo-decoder assisted list-synchronizer shown in Fig. 6.21 .

installed with other schemes and be switched to the scheme described in [96], depending on the time ambiguities or the modulation method. Secondly, the structure of the synchronization algorithm follows the same steps as the decoding algorithm almost to the end, since one algorithm estimates the information bits and the other estimates the state of the trellis. The same decoder can be used for turbo synchronization with little modification. In fact, the computational complexity in the synchronization mode is less than that in the decoding mode. So our proposed scheme does not add any extra hardware for the decoder. Another feature is that if synchronization is lost during decoding, this scheme will have better performance to bring it back because of the better a priori estimation of the coded bits in the packet. In other words, the synchronization performance will improve with the decoding performance after every iteration. This is also true for the scheme described in [96].

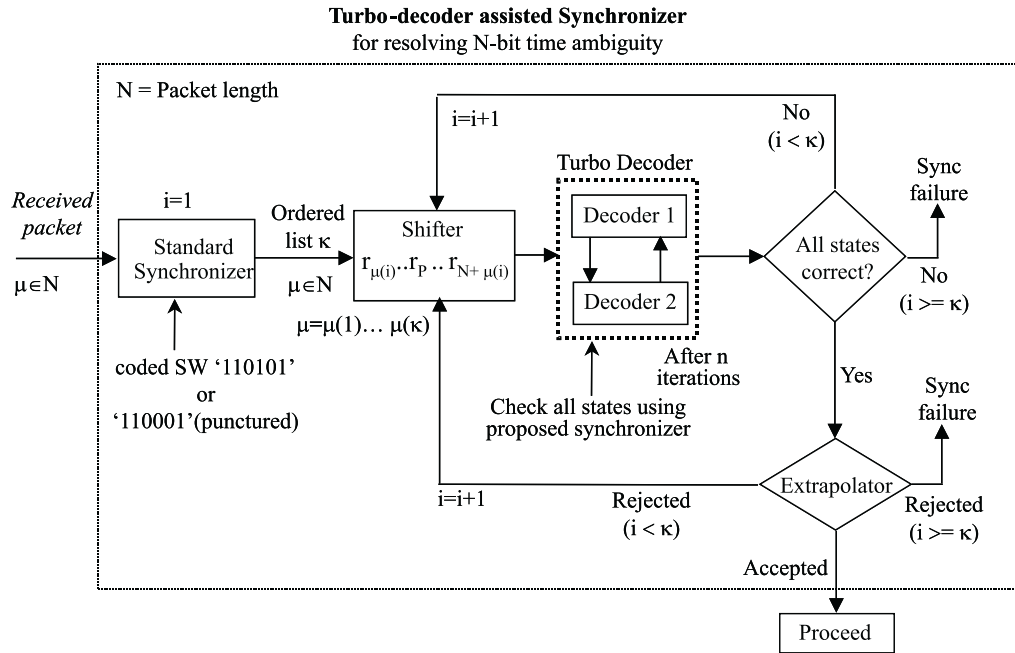


Figure 6.24: Block diagram of a turbo-decoder assisted list-synchronizer; the first module is a standard synchronizer, which resolves the coded SW embedded in a mid-amble, and is followed by the proposed synchronizer described in Section 6.4. The final module is an extrapolator, which verifies the synchronization output: for example, a source coder, a decoder, CRC decoder or the last module of Fig. 6.20.

6.9 Packet Synchronization for TDMA

Packets are used for transmitting data for two main reasons: a more efficient way of transmitting bursty data traffic, and for the need by several users to share a common channel. The packet transmission is characterized by the access protocols such as TDMA, FDMA and CDMA. TDMA random access protocol can be roughly classified into three main categories; fixed TDMA and reservation protocol, ALOHA protocol and slotted-ALOHA protocol. If the collisions are ignored, the TDMA and slotted-ALOHA protocol become equivalent. For TDMA, packet arrives in the designated time slot and for ALOHA, packet arrives in random manner. The receiver can detect the presence of a packet by evaluating the energy continuously and comparing the energy with a threshold value. Furthermore, the ALOHA and the TDMA protocol have the same characteristics for the frame synchronization purpose. Thus, an artificial window can be placed for the newly acquired packet prior to subsequent processing. The assumption is that the packet can not extend beyond the boundaries of the slot.

The model of packet synchronization for TDMA or ALOHA protocol is similar to the continuous frame synchronization or frame synchronization for CDMA or FDMA protocol. The only difference is that the packet occupies a portion of the slot. As a result, the remaining portion of the slot does not contain any signal except the channel noise. So, the standard frame synchronization adds an additional term related to the thermal noise, but the influence of this additional term is less significant [90].

6.10 Chapter Summary

We systematically presented the state-of-art techniques of packet frame synchronization, which eventually led to the development and evaluate the performance of our proposed scheme. We proposed a simple technique for enhancing the frame synchronization of shorter coded packets through integration of decoding and synchronization operations. For shorter packets and smaller constraint lengths, significant improvement is possible. As coding techniques improve, the SNR requirements for reliable data communications may surpass the ability to achieve frame synchronization using conventional techniques. This integrated approach may represent a solution to this problem. We believe that this scheme will enhance the quest of performing decoding and synchronization using a single unit.

Chapter 7

Summary and Future Work

7.1 Summary

The potential use of packet radio communications is not limited to military applications or bursty data traffic any more; there is serious interest in the use of packet radio communications in distributed wireless networks for voice, data and video. Presently, the commercial applications of packet radio communications for the above purposes are available; Internet is becoming another means for voice communications using packet radio, and Metricom, a wireless service provider, is offering wireless services named Richocet using packet radio. In our research, we proposed that DS-CDMA can be used for peer-to-peer packet radio network, where an efficient receiver is important to overcome the shortcoming of DS-CDMA technique - the near-far problem. The final part of our dissertation is the associated challenge and advantage of designing an efficient receiver using error-correction technique and iterative decoding : the required improved frame synchronization using the power of the decoding technique; this frame synchronization technique is the prerequisite for an efficient decoding scheme. In short, the research was divided into three parts, where the goal was to design an efficient receiver for DS-CDMA packet radio systems. The first part was the IC and modeling of a peer-to-peer system. The second part was integration of coding with this IC techniques, and the third and final one was packet synchronization using the decoding techniques.

The work reported herein has examined several problems associated with the use of multiuser detection and decoding to enhance the performance of DS-CDMA in a packet radio environment. Chapters 2 and 3 of this dissertation introduced the readers

to spread spectrum and multiple access techniques. Chapter 2 compares DS-SS to FH-SS to justify our opt for DS-CDMA in peer-to-peer packet radio network. Next, the necessary information about the peer-to-peer packet radio network is presented. Chapter 3 showed that multiuser detection is a viable technology for overcoming the near-far problem. Several relevant receivers are presented from the literature, including the receiver structures considered later in this work.

The primary original contributions of this dissertation are described in Chapters 4 through 6. The first major contribution has been the study of multiuser detection within a packet radio environment. Aspects of this contribution include:

- Development of a model for packet radio networks for DS-CDMA.
- Exploration of the plausibility of using a multiuser receiver to alleviate the near-far problem for DS-SS packet radio networks. The techniques considered include parallel multistage interference cancellation and successive interference cancellation [98].
- A comparative study of the above mentioned multiuser receivers based on selective parallel or successive interference cancellation techniques with a single-user adaptive receiver in a common peer-to-peer packet communication environments is presented in the second part of Chapter 4 [99].

The second part of our work is summarized as follows.

- A scheme is proposed for the integration of parallel interference cancellation (PIC) with forward error control coding in a multiuser receiver for DS-CDMA systems. This integrated approach is compared with a partitioned approach, where the final stage output of PIC is followed by decoding using a soft-input Viterbi algorithm (VA) [100].
- Optimization of the partial cancellation factor for optimizing the combined performance of interference cancellation and coding is studied for various system conditions. These include both synchronous and asynchronous CDMA systems, having equal or unequal signal powers [101].

Chapter 6 proposed a novel decoder-assisted frame synchronization technique for convolutionally coded and turbo coded packet radio systems. This chapter presented numerous architectures for frame synchronizations and evaluated the performance of

these synchronizers for various scenarios. These schemes showed better performance than the conventional scheme using the power of the error-correction code; furthermore, this technique suggested that synchronization and decoding operation could be performed simultaneously. Since the proposed schemes of frame synchronization are applicable for any convolutional type coded system, the technique is adaptable to various forms of decoding techniques. Some of our contributions are listed below.

- We reviewed the state-of-art synchronization techniques.
- We proposed a decoder-assisted synchronization scheme for convolutional code and evaluated the performance of the scheme via simulation [95].
- Based on the proposed scheme, we introduced several list-synchronization architectures to obtain improved synchronization performance [102].
- We applied the proposed schemes of frame synchronization for convolutional to turbo synchronization [103], [104].

Fig. 7.1 presents a block diagram of our original contributions in this research effort. Although the goal of our study is to design an efficient receiver for packet radio using DS-CDMA, the bulk of the research can be used for other wireless communications systems as well; for example, frame synchronization technique is applicable for any coded digital communications systems.

7.2 Recommendation for Future Work

The three problem areas explored in Chapters 4 through 6 can be extended in many directions.

The work in Chapter 4 represents the initial stages of a research topic in its crude beginnings. This work can be expanded and combined with many other issues for the peer-to-peer packet radio networks. Some of these topics include:

- The study in Chapter 4 can be extended to various practical channel environments.
- Since the PIC may not be enough for severe interference-limited environments, a distributed power control can be combined with this interference cancellation technique.

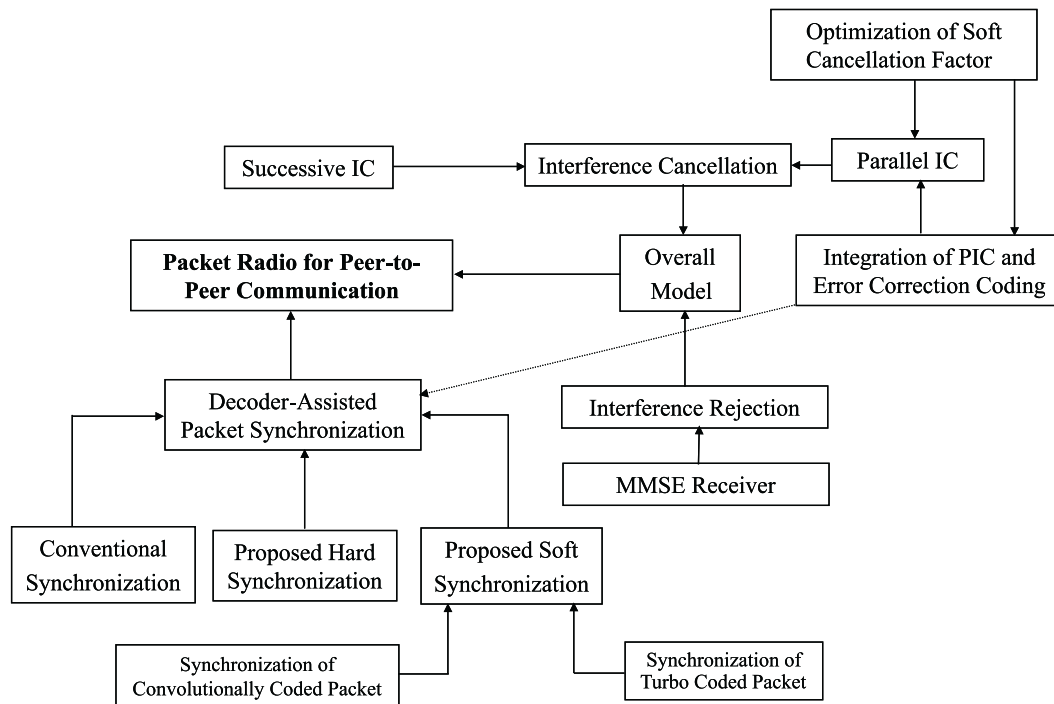


Figure 7.1: Illustration of the main contributions of the work.

- The adaptive single-user receiver is suitable for out-of-cell interference rejection. Successive and parallel cancellation can be concatenated for multirate system; their combination can be used for multirate peer-to-peer network.
- The interference cancellation technique can be combined with adaptive antenna array, and the optimization of this combined scheme is a challenging issue.

The work described in Chapter 5 is among the first to consider full integration of multiuser detection and decoding using log-likelihood ratios to pass soft-decision information. Topics that can be explored in the future are listed below:

- The derivation of an analytical tractable approximation for the optimal soft-cancellation factor of a coded system is still a challenge. There are several issues involved to solve this problem; the most important one is the complexity of the receiver. The derivation of the bit-by-bit soft-cancellation factor from the log-likelihood ratio of the previous stage might be possible. Further investigation on this issue is required.

- Integrated scheme of coded multiuser detection does not outperform the partitioned approach significantly. Improved use of extrinsic decoder information could be considered along with more powerful error correction codes.
- The work of the dissertation has considered only BPSK coherent modulation. Expanding this work to other modulations such as QPSK and DQPSK would be a useful development.
- The interference cancellation technique can be combined with transmit diversity or space-time processing/coding.

In Chapter 6, we proposed a novel decoder-assisted frame synchronization technique; we believe this scheme will be the basis of numerous developments on this topic. Following is a list of recommendation for future work.

- Other modulation schemes and channel environments can be considered for the proposed frame synchronization schemes.
- Performance evaluations of these schemes were based on simulation studies; theoretical bounds of the performance need to be investigated.
- The implementation complexity of these schemes need to be evaluated for the development.
- We assumed that the channel was known for frame synchronization study. The channel estimation can be performed by sending the known header bits, where frame synchronization is assumed perfect [105]. The same SW can be used for both channel estimation and frame synchronization.
- Higher constraint length code and more practical packet length can be considered for further exploration of our simulation study; we believe that the improvement of our proposed scheme will be more significant in those cases.

Appendix A

Abbreviation

ACF	auto-correlation probability
APP	<i>a posteriori</i> probability
AWGN	additive white Gaussian noise
BER	bit error rate
BPSK	binary phase shift keying (modulation)
CDMA	code-division multiple-access
CDPD	cellular digital packet data
CHRT-LAR	chip-rate linear adaptive receiver
CH-SS	chirped spread-spectrum
CRC	cyclic redundancy check (code)
CSMA	carrier sensing multiple-access
DO	decoding operations
DQPSK	differential quadratic phase shift keying (modulation)
DS	direct sequence
DS-CDMA	direct sequence code-division multiple-access
DSP	digital signal processing
DS-SS	direct-sequence spread-spectrum
FDMA	frequency-division multiple-access
FEC	forward error correction
FER	frame error rate
FFT	fast Fourier transform
FH	frequency hopping
FH-SS	frequency-hopping spread-spectrum

GSM	global system for mobile communications
HD-SIC	hard-decision successive interference cancellation
IC	interference cancellation
i.i.d.	independent and identically distributed
IS-95	interim standard 95
LAN	local area network
LAR	linear adaptive receiver
LLR	log-likelihood ratio
LMMS	linear minimum mean-square error
LMS	least mean-square error
MAI	multiple-access interference
MAP	maximum <i>a posteriori</i>
MC	multi-carrier
MF	matched filter
MIMO	multi-input multi-output
ML	most likelihood, maximum likelihood
MLSE	maximum-likelihood sequence estimation
MMSE	minimum mean-square error
MSE	mean-square error
MUD	multiuser detector
NLMS	normalized least mean-square error
OSCF	optimal soft-cancellation factor
pdf	probability density function
PG	processing gain
PIC	parallel interference cancellation
PL	path loss
PN	pseudo-noise
QPSK	quadratic phase shift keying (modulation)
RLS	recursive least-square
RSC	recursive systematic convolutional (code)
SCF	soft-cancellation factor
SDMA	space-division multiple-access
SDR	sign difference ratio
SD-SIC	soft-decision successive interference cancellation

SIC	successive interference cancellation
SIR	signal-to-interference ratio
SISO	soft-input soft-output, single-input single-output
SNR	signal-to-noise ratio
SOVA	soft-output Viterbi algorithm
SW	sync word
TCB	time complexity per bit
TDMA	time-division multiple-access
TE	transverse electric
TH	time hopping
TH-SS	time-hopping spread-spectrum
TM	transverse magnetic
T-R	transmitter-receiver
VA	Viterbi algorithm
w.r.t.	with respect to

Appendix B

A Postdetection Approach for Interference Cancellation and Soft Cancellation Factor

This appendix shows the postdetection methods for PIC in coded system performing parallel interference cancellation. An optimization rule for soft cancellation factor for iterative detection of coded system is derived. The received signal to the matched filter receiver can be written as

$$r(t) = \sum_{k=1}^K \sqrt{P_k} d_k a_k(t - \tau_k) e^{j\phi_k} + n(t). \quad (\text{B.1})$$

For convenience we assume that the system is synchronous and only consider the first bit of the coded bit sequence. Then, the received signal to the matched filter receiver can be expressed as

$$r(t) = \sum_{k=1}^K \sqrt{P_k} d_k a_k(t) e^{j\phi_k} + n(t), \quad (\text{B.2})$$

with the normalized received vector \mathbf{r} with components

$$r_k \triangleq \frac{1}{\sqrt{T}} \int_0^T r(t) a_k(t) dt; \quad k = 1, 2, \dots, K \quad (\text{B.3})$$

and the normalized AWGN vector \mathbf{n} with components

$$n_k \triangleq \frac{1}{\sqrt{T}} \int_0^T n(t) a_k(t) dt; \quad k = 1, 2, \dots, K. \quad (\text{B.4})$$

The components of the PN correlation matrix, \mathbf{R} are

$$\begin{aligned}\rho_{kl} &\triangleq \frac{1}{T} \int_0^T a_k(t)a_l(t)dt; & k, l = 1, 2, \dots, K \\ &= \sum_{m=1}^N \acute{a}_{km}\acute{a}_{lm}(t); & k, l = 1, 2, \dots, K\end{aligned}\quad (\text{B.5})$$

where $\acute{a}_{km} = \frac{a_{km}}{\sqrt{N}}$ and $a = \{a_{kl}\}$ is the normalized user $K \times N$ PN code matrix. Here, N is the processing gain of the CDMA system. The variance of the normalized noise component, σ^2 is given by

$$E\{|n_k|^2\} = \frac{N_0}{T} \int_0^T a_k^2(t) = N_0; \quad k = 1, 2, \dots, K \quad (\text{B.6})$$

and the conditional cross-corelation is

$$E\{n_k n_l^* | \rho_{kl}\} = N_0 \rho_{kl}; \quad k, l = 1, 2, \dots, K \quad (\text{B.7})$$

where the cross-corelation matrix $\mathbf{R} \triangleq \mathbf{a}\mathbf{a}^T$. Let us assume that the *zero*th bit interval of the code vector is $\mathbf{d}_0 \in \{d_{10}, d_{20}, \dots, d_{K0}\}$, the complex carrier phase matrix

$$\mathbf{\Phi} \triangleq \begin{bmatrix} e^{j\phi_1} & 0 & \cdot & \cdot & 0 \\ 0 & e^{j\phi_2} & 0 & \cdot & \cdot \\ \cdot & 0 & \cdot & \cdot & \cdot \\ \cdot & \cdot & \cdot & \cdot & \cdot \\ 0 & 0 & \cdot & \cdot & e^{j\phi_K} \end{bmatrix} \quad (\text{B.8})$$

and the SNR matrix

$$\mathbf{B} \triangleq \begin{bmatrix} \sqrt{\frac{2E_{b1}}{N_0}} & 0 & \cdot & \cdot & 0 \\ 0 & \sqrt{\frac{2E_{b2}}{N_0}} & 0 & \cdot & \cdot \\ \cdot & 0 & \cdot & \cdot & \cdot \\ \cdot & \cdot & \cdot & \cdot & \cdot \\ 0 & 0 & \cdot & \cdot & \sqrt{\frac{2E_{bK}}{N_0}} \end{bmatrix} \quad (\text{B.9})$$

with $E_{bk} \triangleq P_k T$. Equation (B.2) can be written in vector form as given by

$$\mathbf{y} = \mathbf{a}\mathbf{a}^T \mathbf{\Phi} \mathbf{B} \mathbf{d}_0 + \mathbf{a}\eta \quad (\text{B.10})$$

where $\mathbf{y} = r/\sqrt{\frac{N_0}{2}}$ is the normalized received vector, $\eta = N_k/\sqrt{\frac{N_0}{2N}}$ and $N_k = \frac{1}{\sqrt{T}} \int_{(i-1)T}^{iT} n(t)dt$. The optimum decision rule of \mathbf{d}_0 for a given $r(t)$ can be found

by maximizing the distance

$$\begin{aligned}
x^2 &= \int_0^T \left| r(t) - \sum_{k=1}^K \sqrt{P_k} d_{k0} a_k(t) e^{j\phi_k} \right|^2 dt \\
&= \int_0^T |r(t)|^2 dt - 2\text{Re} \left\{ \int_0^T r(t) \sum_{k=1}^K \sqrt{P_k} d_{k0} a_k(t) e^{-j\phi_k} dt \right\} \\
&+ \int_0^T \left[\sum_{k=1}^K \sqrt{P_k} d_{k0} a_k(t) e^{j\phi_k} \right] \left[\sum_{l=1}^K \sqrt{P_l} d_{l0} a_l(t) e^{-j\phi_l} \right] dt. \tag{B.11}
\end{aligned}$$

By dropping the terms upon which the optimization is independent and expressing in vector form, we can write the above distance in the following form:

$$\Omega = \Re \left\{ \mathbf{d}_0^\top \mathbf{B} \Phi^* \mathbf{y} \right\} - \frac{1}{2} \mathbf{d}_0^\top \mathbf{B} \Phi \mathbf{R} \Phi^* \mathbf{B} \mathbf{d}_0. \tag{B.12}$$

Because of the symmetry of the \mathbf{R} matrix, we can rewrite the above equation as follows,

$$\Omega = \Re \left\{ \mathbf{d}_0^\top \mathbf{B} \Phi^* \mathbf{y} \right\} - \frac{1}{2} \mathbf{d}_0^\top \mathbf{B} \Phi^* \mathbf{R} \Phi \mathbf{B} \mathbf{d}_0. \tag{B.13}$$

The above equation determines the optimal decoding for all users that was proposed by Verdu [17] and the computational complexity of this scheme is not practical. For parallel interference cancellation, we assume that user 1 is the user of interest and other users are interferers toward user 1. For that, we can choose d_{10} that maximizes

$$\begin{aligned}
\Omega &= \Re \left\{ \sqrt{\frac{2E_{b1}}{N_0}} d_{10} y_1 e^{-j\phi_1} - \frac{1}{2} d_{10} \sqrt{\frac{2E_{b1}}{N_0}} \sum_{k=2}^K \sqrt{\frac{2E_{bk}}{N_0}} d_{k0} \rho_{1k} e^{j(\phi_k - \phi_1)} \right. \\
&\quad \left. - \frac{1}{2} d_{10} \sqrt{\frac{2E_{b1}}{N_0}} \sum_{k=2}^K \sqrt{\frac{2E_{bk}}{N_0}} d_{k0} \rho_{k1} e^{j(\phi_k - \phi_1)} \right\}. \tag{B.14}
\end{aligned}$$

Since \mathbf{R} is a symmetric matrix, the scaled version of this expression can be rewritten as

$$\Omega_1 = \Re \left\{ d_{10} e^{-j\phi_1} \left[y_1 - \sum_{k=2}^K \sqrt{\frac{2E_{bk}}{N_0}} d_{k0} \rho_{k1} e^{j\phi_k} \right] \right\}. \tag{B.15}$$

If $d_{10} \in \{1, -1\}$, the decision rule based on the above equation can be formulated as a comparison of $\Omega_1|_{d_{10}=1}$ with a zero threshold, or equivalently

$$\hat{d}_{10} = \text{sgn}\{\Omega_1\} = \text{sgn} \left[\Re \left\{ e^{-j\phi_1} \left(y_1 - \sum_{k=2}^K \sqrt{\frac{2E_{bk}}{N_0}} d_{k0} \rho_{k1} e^{j\phi_k} \right) \right\} \right]. \tag{B.16}$$

Note that we do not have the exact value of d_{k0} , instead we have an estimate of it. If we have q stages of interference cancellation, then the coded bit estimation after q stages of interference cancellation can be written as

$$\hat{d}_{10}(q) = \text{sgn} \left[\Re \left\{ e^{-j\phi_1} \left(y_1 - \sum_{k=2}^K \sqrt{\frac{2E_{bk}}{N_0}} \hat{d}_{k0}(q-1) \rho_{k1} e^{j\phi_k} \right) \right\} \right]. \quad (\text{B.17})$$

Note that $\hat{d}_{k0}(0)$ is the MF output before first stage of interference cancellation. The above equation can be expressed in a generalized vector form for all users as

$$\hat{\mathbf{d}}_0(q) = \text{sgn} \left[\Re \left\{ \mathbf{\Phi}^* \left(\mathbf{y} - (\mathbf{a}\mathbf{a}^T - \mathbf{I})\mathbf{\Phi}\mathbf{B}\hat{\mathbf{d}}_0(q-1) \right) \right\} \right], \quad (\text{B.18})$$

where \mathbf{I} is a $K \times K$ identity matrix. In stead of zero threshold, any general decision statistics can be used and the above equation can be generalized as a function of the decision statistics as

$$f\{\tilde{\mathbf{d}}_0(q)\} = f \left[\Re \left\{ \mathbf{\Phi}^* \left(\mathbf{y} - (\mathbf{a}\mathbf{a}^T - \mathbf{I})\mathbf{\Phi}\mathbf{B}\tilde{\mathbf{d}}_0(q-1) \right) \right\} \right], \quad (\text{B.19})$$

where $\tilde{\mathbf{d}}_0(q)$ is the vector of tentative soft decisions of coded bits at the q th stage of iteration.

B.1 Interference Cancellation Based on the Joint Observation of the Received Signal and the Tentative Decision Statistics in the Previous Stage

Interference cancellation suffers from biased estimation of the decision statistics and the fidelity of the transmitted coded bits, which is not high in the first stage of cancellation. So, partial cancellation is appropriate instead of cancelling the full magnitude of the estimated interference. Our objective is to establish a relationship between this partial cancellation factor and the likelihood ratio from the log-MAP decoder, if we use an iterative decoding integrated with parallel interference cancellation. Now, consider y_1 , which is the first component of the normalized received signal vector and from equation (B.10), we can write

$$e^{-j\phi_1} y_1 = \sqrt{\frac{2E_{b1}}{N_0}} d_{10} + \sum_{k=2}^K \sqrt{\frac{2E_{bk}}{N_0}} d_{10} e^{j(\phi_k - \phi_1)} \rho_{k1} + n_1 e^{-j\phi_1}. \quad (\text{B.20})$$

Taking the real part we have

$$Y_1 = \sqrt{\frac{2E_{b1}}{N_0}}d_{10} + I_1 + W_1. \quad (\text{B.21})$$

Here, I_1 is the real part of the interferences towards user 1 from all other users and W_1 is a Gaussian noise with variance σ_1^2 . Now, let us consider the tentative decision at the q th stage of user 1 using equations (B.19) and (B.20), and after a few steps we can write

$$\begin{aligned} \tilde{d}_{10}(q-1) &= \Re \left\{ e^{-j\phi_1} y_1 + \sum_{k=2}^K \sqrt{\frac{2E_{bk}}{N_0}} \hat{d}_{10}(q-2) e^{j(\phi_k - \phi_1)} \rho_{k1} \right\} \\ &= \sqrt{\frac{2E_{b1}}{N_0}} d_{10} + \Re \left\{ \sum_{k=2}^K \sqrt{\frac{2E_{bk}}{N_0}} (d_{10} - \hat{d}_{10}(q-2)) e^{j(\phi_k - \phi_1)} \rho_{k1} \right\} + W_1 \\ &= \sqrt{\frac{2E_{b1}}{N_0}} d_{10} + W_2(q-1). \end{aligned} \quad (\text{B.22})$$

Here, $W_2(q-1)$, with variance σ_{2k}^2 , is the summation of the Gaussian noise variable W_1 and the residual interference after $(q-2)$ interference cancellation stages, which is assumed to be Gaussian also. Obviously, W_1 and $W_2(q-1)$ are correlated and let us assume that their correlation coefficient is ρ_k . Now by observing Y_1 and $\tilde{d}_{10}(q-1)$, the maximum likelihood estimation about d_{10} can be obtained where the conditional probability density function of the observations is given by

$$\begin{aligned} Pr(Y_1, \tilde{d}_{10}(q-1) | d_{10}, I_1) &= \frac{1}{2\pi\sigma_1\sigma_{2k}\sqrt{1-\rho_k^2}} \times \\ \exp \left[\right. &\left. \left\{ \frac{\sigma_{2k}^2 (Y_1 - \sqrt{\frac{2E_{b1}}{N_0}}d_{10} - I_1)^2 + \sigma_1^2 (\tilde{d}_{10}(q-1) - \sqrt{\frac{2E_{b1}}{N_0}}d_{10})^2}{2\sigma_1^2\sigma_{2k}^2(1-\rho_k^2)} \right. \right. \\ &\left. \left. - \frac{2\rho_k\sigma_1\sigma_{2k} (Y_1 - \sqrt{\frac{2E_{b1}}{N_0}}d_{10} - I_1) (\tilde{d}_{10}(q-1) - \sqrt{\frac{2E_{b1}}{N_0}}d_{10})}{2\sigma_1^2\sigma_{2k}^2(1-\rho_k^2)} \right\} \right]. \end{aligned} \quad (\text{B.23})$$

In fact, instead of I_1 we have estimate of I_1 and is given by

$$\hat{I}_1(q) = \Re \left[\sum_{k=2}^K \sqrt{\frac{2E_{bk}}{N_0}} d_{10} e^{j(\phi_k - \phi_1)} \rho_{k1} \right]. \quad (\text{B.24})$$

After sum steps of calculation and dropping the terms that do not depend on d_{10} , we can write the above equation as

$$\begin{aligned} Pr(Y_1, \tilde{d}_{10}(q-1) | d_{10}, \hat{I}_1(q)) &= D \exp \left[\sqrt{\frac{2E_{bk}}{N_0}} d_{10} \left\{ \frac{(\sigma_{2k}^2 - \rho_k\sigma_1\sigma_{2k})(Y_1 - \hat{I}_1(q))}{\sigma_1^2\sigma_{2k}^2(1-\rho_k^2)} \right. \right. \\ &\quad \left. \left. + \frac{(\sigma_1^2 - \rho_k\sigma_1\sigma_{2k})\tilde{d}_{10}(q-1)}{\sigma_1^2\sigma_{2k}^2(1-\rho_k^2)} \right\} \right] \end{aligned} \quad (\text{B.25})$$

where D is a constant. Let us assume a normalized term to make the coefficients of $Y_1 - \hat{I}_1(q)$ and $\tilde{d}_{10}(q-1)$ in the above equation sum to unity,

$$c_k \triangleq \frac{\sigma_{2k}^2 - \rho_k \sigma_1 \sigma_{2k}}{\sigma_1^2 + \sigma_{2k}^2 - 2\rho_k \sigma_1 \sigma_{2k}}, \quad (\text{B.26})$$

and the above equation can be expressed as

$$Pr\left(Y_1, \tilde{d}_{10}(q-1) | d_{10}, \hat{I}_1(q)\right) = D \exp(d_{10} \alpha_k \beta_k), \quad (\text{B.27})$$

where

$$\alpha_k \triangleq \sqrt{\frac{2E_{b1}}{N_0}} \left(\frac{\sigma_1^2 + \sigma_{2k}^2 - 2\rho_k \sigma_1 \sigma_{2k}}{\sigma_1^2 \sigma_{2k}^2 (1 - \rho_k^2)} \right), \quad \beta_k \triangleq c_k (Y_1 - \hat{I}_1(q)) + (1 - c_k) (\tilde{d}_{10}(q-1)) \quad (\text{B.28})$$

The estimation of d_{10} can be expressed as

$$E \left\{ d_{10} | Y_1, \tilde{d}_{10}(q-1), \hat{I}_1(q) \right\} = (1) Pr \left(1 | Y_1, \tilde{d}_{10}(q-1), \hat{I}_1(q) \right) \\ + (-1) Pr \left(-1 | Y_1, \tilde{d}_{10}(q-1), \hat{I}_1(q) \right), \quad (\text{B.29})$$

where $Pr \left(d_{10} | Y_1, \tilde{d}_{10}(q-1), \hat{I}_1(q) \right)$ is the a posteriori probability of user 1 coded bit in the *zereth* transmission interval given the observations and interference.

Using the Bay's rule, and after some simplification we can write

$$E \left\{ d_{10} | Y_1, \tilde{d}_{10}(q-1), \hat{I}_1(q) \right\} = \frac{\Lambda(1)m(1) - \Lambda(-1)m(-1)}{\Lambda(1)m(1) + \Lambda(-1)m(-1)}, \quad (\text{B.30})$$

where the above equation is evaluated assuming $d_{10} \in \{1, -1\}$ and

$$\Lambda(d_{10}) = Pr \left(d_{10} | Y_1, \tilde{d}_{10}(q-1), \hat{I}_1(q) \right) \quad \text{and} \quad m(d_{10}) = Pr(d_{10}, \hat{I}_1(q)). \quad (\text{B.31})$$

From equation (B.27) for the evaluation of $\Lambda(d_{10})$ we have that

$$\Lambda(d_{10}) = D \exp(d_{10} \alpha_k \beta_k). \quad (\text{B.32})$$

From the equiprobable properties of the data streams, we can write $m(1) = m(-1)$.

Hence, equation (B.30) becomes

$$E \left\{ d_{10} | Y_1, \tilde{d}_{10}(q-1), \hat{I}_1(q) \right\} = \frac{\Lambda(1) - \Lambda(-1)}{\Lambda(1) + \Lambda(-1)} = \hat{d}_{10}. \quad (\text{B.33})$$

By substituting equation (B.32) into equation (B.33), we have the estimation about coded bit as

$$\hat{d}_{10}(q) = \frac{D \exp(\alpha_k \beta_k) - D \exp(-\alpha_k \beta_k)}{D \exp(\alpha_k \beta_k) + D \exp(-\alpha_k \beta_k)} = \tanh(\alpha_k \beta_k). \quad (\text{B.34})$$

Bibliography

- [1] C. E. Shannon, "Communication in the presence of noise," *IRE*, vol. 37, pp. 10–21, January 1949.
- [2] L. W. Couch II, *Digital and Analog communication Systems*. Englewood Cliffs, NJ: Prentice Hall, Inc., 5th ed., 1998.
- [3] J. L. Massey, *Towards an Information Theory of Spread-Spectrum Systems*. Kluwer Academic Publishers, 1995.
- [4] R. A. Scholtz, "The spread spectrum concept," *IEEE Trans. Commun.*, vol. 25, no. 8, pp. 748–755, 1977.
- [5] R. C. Dixon, *Spread Spectrum Systems with Commercial Applications*. John Wiley & Sons, 3rd ed., 1994.
- [6] R. E. Ziemer and R. L. Peterson, *Introduction to Digital Communication*. New York: Macmillan Publishing Company, 1992.
- [7] M. K. Simon, J. K. Omura, R. A. Scholtz, and B. K. Levitt, *Spread Spectrum Communications Handbook*. McGraw Hill, 1994.
- [8] A. Viterbi, *CDMA : Principles of Spread Spectrum Communication*. Addison-Wesley Pub. Co., 1995.
- [9] R. Cameron and B. D. Woerner, "Performance analysis of CDMA with imperfect power control," *IEEE Trans. Commun.*, vol. 44, pp. 777–781, July 1996.
- [10] J. H. Gass and M. B. Pursley, "A comparison of slow frequency hop and direct sequence spread-spectrum communications over frequency-selective fading channel," *IEEE Trans. Commun.*, vol. 47, pp. 732–741, May 1999.

- [11] T. S. Rappaport, *Wireless Communications: Principles and Practice*. Englewood Cliffs, NJ: Prentice Hall, Inc., 1996.
- [12] D. J. Goodman, *Wireless Personal Communications Systems*. Addison-Wesley, 1997.
- [13] G. Durgin, T. S. Rappaport, and H. Xu, "Measurements and models for radio path loss and penetration loss in and around homes and trees at 5.85 ghz," *IEEE Trans. Commun.*, vol. 46, pp. 1484–1496, November 1998.
- [14] R. H. Clarke, "A statistical theory of mobile radio reception," *Bell Systems Technical Journal*, vol. 47, pp. 957–1000, 1968.
- [15] S. Verdu, *Optimum Multi-user Signal Detection*. PhD thesis, Univ. Illinois, Urbana-Champaign, 1984.
- [16] G. D. Forney, "Maximum-likelihood sequence estimation of digital sequences in the presence of intersymbol interference," vol. IT-18, pp. 363–378, May 1972.
- [17] S. Verdu, "Minimum probability of error for asynchronous gaussian multiple access channels," *IEEE Transactions on Information Theory*, vol. IT-32, pp. 85–96, Jan. 1986.
- [18] R. Lupas and S. Verdu, "Near-far resistance of multiuser detectors in asynchronous channel," *IEEE Trans. Commun.*, vol. 38, pp. 496–508, April 1990.
- [19] K. S. Schneider, "Optimum detection of code division multiplexed signals," *IEEE Transactions on Aerospace and Electronic Systems*, vol. AES-15, Jan. 1979.
- [20] R. Kohno, M. Hatori, and H. Imai, "Cancellation techniques of co-channel interference in asynchronous spread spectrum multiple access systems," *Electronics and Communications in Japan*, vol. 66-A, no. 5, pp. 20–29, 1983.
- [21] R. Lupas and S. Verdu, "Linear multiuser detectors for synchronous code-division multiple-access channels," *IEEE Transactions on Information Theory*, vol. 35, pp. 123–136, January 1989.
- [22] Z. Xie, R. Short, and C. Rushforth, "A family of suboptimum detectors for coherent multiuser communications," *IEEE Journal on Selected Areas in Communications*, vol. 8, pp. 683–690, May 1990.

- [23] S. Moshavi, "Multi-user detection for DS-CDMA communications," *IEEE Communications Magazine*, pp. 124–136, Oct. 1996.
- [24] A. Duel-Hallen, "Decorrelating decision-feedback multiuser detector for synchronous code-division multiple-access channel," *IEEE Transactions on Communications*, vol. 41, pp. 285–290, Feb. 1993.
- [25] Z. Xie, C. Rushforth, and R. Short, "Multiuser signal detection using sequential decoding," *IEEE Transactions on Communications*, vol. 38, pp. 578–583, May 1990.
- [26] S. Verdu, *Multiuser Detection*. Cambridge Press, 1998.
- [27] S. Haykin, *Adaptive Filter Theory*. New Jersey: Prentice Hall, 1996.
- [28] M. L. Honig, U. Madhow, and S. Verdu, "Blind adaptive multiuser detection," *IEEE Transactions on Information Theory*, vol. 41, pp. 944–960, July 1995.
- [29] S. L. Miller, "Training analysis of adaptive interference suppression for direct sequence code-division multiple access," *IEEE Trans. Commun.*, vol. 44, pp. 488–495, Apr. 1996.
- [30] A. J. Viterbi, "Very low rate convolutional codes for maximum theoretical performance of spread-spectrum multiple-access channels," *IEEE Journal on Selected Areas in Communications*, vol. 8, pp. 641–649, May 1990.
- [31] P. Patel and J. Holtzman, "Analysis of a simple successive interference cancellation scheme in a DS/CDMA system," *IEEE Journal on Selected Areas in Communications*, vol. 12, pp. 796–807, June 1994.
- [32] P. Dent, B. Gudmundson, and M. Ewerbring, "CDMA-IC: A novel code division multiple access scheme based on interference cancellation," in *Proc., IEEE PIMRC*, pp. 98–102, 1992. Boston, MA.
- [33] M. Ewerbring, B. Gudmundson, G. Larsson, and P. Teder, "CDMA with interference cancellation: A technique for high capacity wireless systems," in *Proc., IEEE Int. Conf. on Commun.*, pp. 1901–1906, 1993.
- [34] M. K. Varanasi and B. Aazhang, "Multistage detection in asynchronous code-division multiple access communications," *IEEE Transactions on Communications*, vol. 38, pp. 509–519, Apr. 1990.

- [35] R. Kohno, H. Imai, M. Hatori, and S. Pasupathy, "An adaptive canceller of cochannel interference for spread-spectrum multiple-access communication networks in a power line," *IEEE Journal on Selected Areas in Communications*, vol. 8, pp. 691–699, May 1990.
- [36] R. M. Buehrer, *The Application of Multiuser Detection to Cellular CDMA*. PhD thesis, Virginia Polytechnic Institute and State University, 1996.
- [37] A. Kaul, "An adaptive multistage interference cancellation receiver for CDMA," Master's thesis, Virginia Polytechnic Institute and State University, March 1995.
- [38] R. A. Cameron, *Fixed Point Implementation of a Multistage Receiver*. PhD thesis, Virginia Polytechnic Institute and State University, Jan. 1997.
- [39] A. Kaul and B. D. Woerner, "Analytic limits on the performance of adaptive multistage interference cancellation for CDMA," *Electronics Letters*, vol. 30, pp. 2093–94, December 1994.
- [40] R. K. Morrow and J. S. Lehnert, "Bit-to-bit error dependence in slotted DS/SSMA packet systems with random signature sequences," *IEEE Trans. Commun.*, vol. 37, pp. 1052–1061, Oct. 1989.
- [41] J. M. Holtzman, "A simple, accurate method to calculate spread spectrum multiple access error probabilities," *IEEE Trans. Commun.*, vol. 40, pp. 461–464, March 1992.
- [42] J. C. Liberti, *Analysis of CDMA Cellular Radio Systems Employing Adaptive Antennas*. PhD thesis, Virginia Polytechnic Institute and State University, 1995.
- [43] P. Agashe, "Selective cancellation of multipath and multicell interference in CDMA," Master's thesis, Virginia Polytechnic Institute and State University, December 1995.
- [44] P. Agashe and B. D. Woerner, "Analysis of interference cancellation for multicellular CDMA environment," in *Proc., IEEE PIMRC*, September 27-29 1995. Toronto, Canada.

- [45] S. Striglis, A. Kaul, N. Yang, and B. D. Woerner, "A multistage RAKE receiver for improved capacity of CDMA systems," in *IEEE Vehicular Technology Conference*, pp. 789–793, June 1994.
- [46] M. J. Juntti, B. Aazhang, and J. O. Lilleberg, "Iterative implementation of linear multiuser detection for dynamic asynchronous CDMA systems," *IEEE Trans. Commun.*, vol. 46, pp. 503–508, Apr. 1998.
- [47] S. Das, J. Cavallaro, and B. Aazhang, "Computationally efficient multiuser detectors," in *Proc., IEEE PIMRC*, (Helsinki, Finland), pp. 62–67, september 1997.
- [48] S. Verdu, "Adaptive multiuser detection," in *IEEE International Symposium on Spread Spectrum Techniques and Applications*, pp. 43–50, July 1994.
- [49] R. Buehrer, N. Correal, and B. Woerner, "A comparison of multiuser receivers for cellular CDMA," *IEEE Global Telecommunications Conference*, pp. 1571–1577, Nov. 1996.
- [50] M. B. Pursley, "The role of spread spectrum in packet radio network," *Proc. IEEE*, vol. 75, pp. 116–134, jan 1987.
- [51] J. H. Gass and M. B. Pursley, "Tradeoffs between frequency-hop and direct sequence signaling for frequency selective fading channels," in *Proc., IEEE MILCOM*, pp. 70–74, oct 1996.
- [52] D. Torrieri, "Future army mobile multiple-access communications," in *Proc., IEEE MILCOM*, pp. 650–654, nov 1997.
- [53] J. M. Holtzman, "DS/CDMA successive interference cancellation," in *Proc., IEEE Int. Symp. on Spread Spectrum Techniques and Applications*, (Oulu, Finland), pp. 69–76, July 1994.
- [54] M. J. Feuerstein, K. L. Blackard, T. S. Rappaport, and S. Y. Seidel, "Path loss, delay spread and outage models as function of antenna height for micro cellular system design," *IEEE Trans. Veh. Tech.*, vol. 43, pp. 211–221, August 1994.
- [55] N. S. Correal, R. M. Buehrer, and B. D. Woerner, "Improved CDMA performance through bias reduction for parallel interference cancellation," in *IEEE*

- International Symposium on Personal, Indoors and Mobile Radio Communications*, pp. 565–569, 1997.
- [56] D. Divsalar and M. Simon, “Improved CDMA performance using parallel interference cancellation,” Tech. Rep. 95-21, JPL, Oct. 1995.
- [57] P. G. Renucci and B. D. Woerner, “Optimization of soft interference cancellation for DS-CDMA,” *IEE Electronics Letters*, vol. 34, pp. 731–733, April 1998.
- [58] F. V. der Wijk, G. Janssen, and R. Prasad, “Groupwise successive interference cancellation in a DS/CDMA system,” in *Proc., IEEE PIMRC*, pp. 742–746, July 1995.
- [59] U. Madhow and M. L. Honig, “MMSE interference suppression for direct-sequence spread-spectrum CDMA,” *IEEE Trans. Commun.*, vol. 42, pp. 3178–3168, dec 1994.
- [60] T. Miyajima and K. Yamanaka, “Prefiltering for LMS based adaptive receivers in DS/CDMA communications,” *IEICE Transactions on Fundamentals of Electronics, Communications*, vol. E80-A, dec 1997.
- [61] E. Strom and S. Miller, “Optimum complexity reduction of minimum mean square error DS-CDMA receivers,” in *Proc., IEEE Veh. Tech. Conf.*, pp. 568–72, 1994.
- [62] M. L. Honig, U. Madhow, and S. Verdu, “Blind adaptive multiuser detection,” *IEEE Trans. Inform. Theory*, vol. 41, pp. 944–960, July 1995.
- [63] A. J. Viterbi, “Spread spectrum communications-myths and realities,” *IEEE Commun. Magazine*, pp. 11–18, 1979.
- [64] A. Park, R. M. Buehrer, and B. D. Woerner, “Throughput performance of an FHMA system with variable rate coding,” in *Proc., IEEE MILCOM*, (San Diego, CA), November 1995.
- [65] A. Goldsmith, “Joint source/channel coding for wireless channels,” in *Proc., IEEE Veh. Tech. Conf.*, vol. 2, pp. 614–618, 1995.
- [66] C. Berrou, A. Glavieux, and P. Thitimasjshima, “Near Shanon limit error-correcting coding and decoding: Turbo-codes(1),” in *Proc., IEEE Int. Conf. on Commun.*, (Geneva, Switzerland), pp. 1740–1745, May 1993.

- [67] S. Wicker, *Error Control Systems for Digital Communications and Storage*. Englewood Cliffs, NJ: Prentice Hall, Inc., 1995.
- [68] E. Dahlman, B. Gudmundson, M. Nilsson, and J. Skold, "UMTS and IMT-2000 based on wideband CDMA," *IEEE Commun. Magazine*, sep 1998.
- [69] R. Giallorenzi and S. Wilson, "Multistage decision feedback and trellis-based multiuser receivers for convolutionally coded CDMA systems," tech. rep., University of Virginia, Communication Systems Lab., Dept. of Electrical Engg., May 1993. UVA/538341/EE93/102.
- [70] J. Lilleberg and W. Haifeng, "Novel iterative multi-user receiver for asynchronous CDMA systems in Rayleigh fading channels," in *Proc., IEEE PIMRC*, pp. 208–212, September 1998.
- [71] T. Giallorenzi and S. Wilson, "Multiuser ML sequence estimator for convolutionally coded asynchronous DS-CDMA systems," *IEEE Transactions on Communications*, vol. 44, pp. 997–1008, Aug. 1996.
- [72] G. D. Forney, "The viterbi algorithm," *Proc. IEEE*, pp. 268–278, March 1973.
- [73] L. Bahl, J. Cocke, F. Jelinek, and J. Raviv, "Optimal decoding of linear codes for minimizing symbol error rate," *IEEE Trans. Inform. Theory*, vol. 20, pp. 284–287, March 1974.
- [74] P. Robertson, P. Hoeher, and E. Villebrun, "Optimal and sub-optimal maximum a posteriori suitable for turbo decoding," *European Trans. on Telecommun.*, vol. 8, pp. 119–125, March/April 1997.
- [75] M. Fossorier, F. Burkert, S. Lin, and J. Hagenauer, "On the equivalence between SOVA and max-log-MAP algorithm," *IEEE Commun. Letters*, vol. 2, pp. 137–139, May 1998.
- [76] M. Valenti, *Iterative Detection and Decoding for Wireless Communications*. PhD thesis, Virginia Polytechnic Institute and State University, July 1999.
- [77] D. Divsalar, M. Simon, and D. Raphaeli, "Improved parallel interference cancellation for CDMA," *IEEE Trans. Commun.*, vol. 46, pp. 258–268, Feb. 1998.

- [78] G. Xue, J. Weng, T. Le-Ngoc, and S. Tahar, "Adaptive multistage parallel interference cancellation for CDMA over multipath fading channels," in *Proc., IEEE Veh. Tech. Conf.*, (Houston, TX), May 1999.
- [79] J. Hagenauer, "Forward error correcting for CDMA systems," in *Proc., IEEE Int. Symp. on Spread Spectrum Techniques and Applications*, (Mainz, Germany), pp. 566–569, September 1996.
- [80] R. H. Barker, *Group synchronization of binary digital systems*. London: Butterworth, 1953.
- [81] J. L. Massey, "Optimum frame synchronization," *IEEE Trans. Commun.*, vol. 20, pp. 115–119, April 1972.
- [82] P. T. Neilson, "Some optimum and suboptimum frame synchronizers for binary data in gaussian noise," *IEEE Trans. Commun.*, pp. 770–772, June 1973.
- [83] G. L. Lui and H. H. Tan, "Frame synchronization for gaussian channels," *IEEE Trans. Commun.*, vol. 35, pp. 818–829, aug 1987.
- [84] B. Moon and S. Soliman, "ML frame synchronization for gaussian channel with ISI," in *Proc., IEEE Int. Conf. on Commun.*, pp. 1698–1702, june 1991.
- [85] P. Robertson, "Maximum likelihood frame synchronization for flat fading channels," in *Proc., IEEE Int. Conf. on Commun.*, vol. 3, (Chicago, IL, USA), pp. 1426–1430, June 1992.
- [86] P. Robertson, "Improving frame synchronization when using convolutional codes," in *Proc., IEEE GLOBECOM*, pp. 1606–1611, December 1993.
- [87] P. Driessen, "Binary frame synchronization sequences for packet radio," *Electronics Letters*, vol. 3, pp. 1190–1191, October 1987.
- [88] S. Schaub and A. Hansson, "Frame synchronization for spontaneous transmission," in *Proc., IEEE GLOBECOM*, pp. 617–622, 1990.
- [89] Fisher, "On the mathematical foundations of theoretical statistics," *Philos. Trans. Royal Society, London*, pp. 309–368, 1922.
- [90] P. Robertson, *Optimal frame synchronization for continuous and packet data transmission*. PhD thesis, VDI-Verlag, Germany, 1995.

- [91] P. Robertson, "A generalized frame synchronizer," in *Proc., IEEE GLOBECOM*, pp. 365–369, December 1992.
- [92] M. Oerder and H. Meyr, "Digital filter and square timing recovery," *IEEE Trans. Commun.*, vol. 36, pp. 605–612, May 1988.
- [93] J. Hagenauer, "A Viterbi algorithm with soft-decision outputs and its application," in *Proc., IEEE GLOBECOM*, pp. 1680–1686, November 1989.
- [94] R. Scholtz, "Frame synchronization techniques," *IEEE Trans. Commun.*, vol. 28, pp. 1327–37, August.
- [95] M. M. K. Howlader and B. D. Woerner, "Frame synchronization of convolutionally encoded sequences for packet transmission," in *Proc., IEEE Int. Conf. on Commun.*, pp. 317–321, June 2000.
- [96] S. S. Pietrobon, "Efficient implementation of continuous MAP decoders and a synchronization technique for turbo decoders," *Proc., International Symposium On Information Theory And Its Applications*, pp. 586–589, September 1996.
- [97] Y. Wu, *Implementation of Parallel and Serial Concatenated Convolutional Codes*. PhD thesis, Virginia Polytechnic Institute and State University, April 2000.
- [98] M. M. K. Howlader and B. D. Woerner, "Direct-sequence spread-spectrum with multiuser detection for peer-to-peer packet radio," in *Proc., IEEE MILCOM*, vol. 3, (Boston, MA), pp. 762–766, October 1998.
- [99] M. M. K. Howlader and B. D. Woerner, "Adaptive single-user and multiuser receivers for asynchronous DS-CDMA in peer-to-peer packet radio networks," in *Proc., IEEE MILCOM*, (Atlantic City, New Jersey), p. pp. 34.2, October 1999.
- [100] M. M. K. Howlader and B. D. Woerner, "Iterative interference cancellation and decoding for DS-CDMA systems," in *Proc., IEEE Veh. Tech. Conf.*, (Amsterdam, The Netherlands), pp. 1815–1819, September 1999.
- [101] M. M. K. Howlader and B. D. Woerner, "Iterative interference cancellation and decoding using a soft cancellation factor for DS-CDMA," in *Proc., IEEE Veh. Tech. Conf.*, (Tokeyo, Japan), pp. 2076–280, 2000.

- [102] M. M. K. Howlader and B. D. Woerner, "Decoder-assisted frame synchronization of convolutionally encoded packet transmission," in *Proc., IEEE MILCOM*, (Los Angeles, CA), October 2000.
- [103] M. M. K. Howlader and B. D. Woerner, "Fast frame synchronization of convolutionally coded sequences for packet transmission and turbo synchronization," in *Proc., IEEE Veh. Tech. Conf.*, (Boston, MA), September 2000.
- [104] M. M. K. Howlader, Y. Wu, and B. D. Woerner, "Decoder-assisted frame synchronization for turbo coded systems," in *Proc., 2nd International Symposium on Turbo Codes and Related Topics Conference*, (organized by ENST, Brest, France), September 2000.
- [105] M. C. Valenti and B. D. Woerner, "Refined channel estimation for coherent detection of turbo codes over flat-fading channels," *Electronics Letters*, vol. 34, pp. 1648–1650, Aug. 1998.

Vita

M. Mostofa K. Howlader received his B.S. degree in Electrical & Electronics Engineering from Bangladesh University of Engineering and Technology (BUET) in 1991, and the M.S. degree in Electrical Engineering from University of New Orleans, LA in 1994, where he was involved with optical communication, photonic information processing, and beamforming . From August 1994 to July 1996 he worked at School of Optics/CREOL, University of Central Florida, where he was a graduate research fellow.

In March 1997, he joined the Mobile and Portable Radio Research Group (MPRG) at Virginia Tech, where he has been pursuing his Ph.D. degree. His research interests include wireless communication systems, spread spectrum communications, information theory and channel coding. He has co-authored 11 journal papers and 14 conference papers jointly with his thesis advisors in the area of wireless communications, beamforming and optical communication.